THE INVERSION OF GEOMAGNETIC DATA

by

David McNeil Summers

Thesis presented for the degree of Doctor of Philosophy of the University of Edinburgh in the Faculty of Science.

1976

How deep do we dig, and for how coarse gold!
And what other touchstone have we of our gold
but comparison, whether we be as happy as others,
or as ourselves at other times?

John Donne (1624)

ABSTRACT

The inference of electrical conductivity at some depth within the Earth from a finite set of surface induction data is a non-unique problem in the sense that a range of conductivity distributions may conceivably give rise to such data. Interpreting surface data requires some form of generalized inversion procedure which can characterize the space of models which comprises this non-uniqueness. In this thesis we discuss the application of the generalized linear inverse formalism of Backus and Gilbert (1967, 1968, 1970) to the induction problem, and particular attention is directed to its application to the magnetotelluric response of a half-space with a one-dimensional conductivity distribution. This inverse problem finds very simple expression analytically. Thus the magnetotelluric problem is particularly suitable for studying (by synthetic example) the inverse induction problem.

The inverse formalism of Backus and Gilbert is easily discretized to accommodate models parameterized as horizontal strata. Under this discretization the relevant Fréchet kernels are generated from well-known recursion formulae. The formalism requires a quasi-linear representation of a non-linear relationship between surface data and the model, and for simple cases it is possible to inspect some higher-order terms associated

with this linearization. This can indicate some parts of the model space where the linearization loses validity.

Some theoretical discussion is made of the uniqueness of the induction problem for discretized models. An instructive way of visualizing the impedance at the surface of a stratified conductor is offered.

In order to locate acceptable models from reasonable guessed models, the least-squares inverse procedure (Backus and Gilbert, 1967) is applied to synthetic sets of magnetotelluric data. Since this optimization problem generally results in a system of equations both underdetermined and overconstrained, the iterative procedure often requires to be stabilized. The method of ranking and winnowing (Gilbert, 1971) is employed to effect such a stabilization. The procedure is applied to some experimental sets of data with a particular view to discovering the implication of phase data when it is added to a set of amplitude data.

The model resolution -- as defined by Backus and Gilbert (1968) -- attached to a set of induction data is studied for some synthetic cases. Some comparison is made (in terms of model resolution) between magnetotelluric data represented as amplitude and phase, and then as real and imaginary parts of the complex surface impedance. Study is also made of the implication of error to the resolution of magnetotelluric data. The inverse theory of Backus and Gilbert (1970) for erroneous

data is described and various illustrations of the trade-off relationship between error and resolution of localized averages of the conductivity are presented.

Various suggestions are offered about the directions in which this work could proceed.

DECLARATION

I hereby declare that the work presented in this thesis is my own unless otherwise stated in the text, and that the thesis has been composed by myself.

ACKNOWLEDGEMENTS

I should like to thank the Geophysics Department of Edinburgh University for giving me the opportunity to work in that congenial environment. Gratitude is expressed to Dr. B. A. Hobbs, my supervisor, for suggesting the topic of research, and for his encouragement throughout the work. Dr. Jane Sik has helped me to make the necessary adjustments to my faulty English in the typescript stage of this thesis. I express thanks as well to Mr. A. G. Jones for helpful discussions and for his permission to look at some of his magnetotelluric data. Mr. David Hall is thanked for his various kindnesses.

Some of the impetus for this thesis emanates from the work of Prof. Schmucker (Gottingen University). He has been the author of sound advice at various stages and it is fitting that he be acknowledged here.

I have been supported financially by a NERC post-graduate studentship for the first two years of this research. Since January 1976 I have been supported by a University of Edinburgh post-graduate studentship. Gratitude is expressed to the awarding bodies concerned.

Mrs. Pat Scrutton has typed this thesis -- a feat for which I am very grateful.

CONTENTS

LIST OF FIGURES

* indicates the Figure appears on stated page.

CHAPTER 1

INTRODUCTION

1.1 Preliminary Remarks

There exists a class of geophysical problems which concern themselves with the inference of internal Earth structure from a set of measurements made at the Earth's surface. This inference problem can be described as an 'inverse problem', since mathematically it can be posed as a problem of discovering a governing equation from knowledge of the solution to that equation on a closed boundary (i.e. on the Earth's surface). We shall be interested here in studying the inference of models for the Earth's electrical conductivity from measured surface values of the time-varying component of the geomagnetic field. Before entering into discussion of this inverse problem, a few general remarks of a somewhat philosophical nature will be directed towards the matter of finding models.

Modelling is strictly the simulation of natural structures (or natural processes) in a form which is adjustable. A simulation, or model, can be made to conform to evident reality by adjustment of a set of variables -- this set is called the space of model variables, or model space. Once a working model has been constructed, one can use trial and error methods to make

the model more 'realistic'. Alternatively one can systematize the problem of improving a model by posing it as an optimization problem. Also one can seek to find direct equations or mappings which will indicate adequate models. Whatever the mechanics of the modelling procedure, implicit in the design of any model there are arbitrary constraints. Of course, there are also constraints which are not arbitrary since they are determined by physical law. But in addition to these, there is also a class of constraints associated with the way in which the space of model parameters is ordered: that is, by considerations of geometry, efficiency, or mathematical convenience. Indeed, the 'material' out of which one constructs a model must itself be intrinsically constraining.

For a model to be revealing, proper account must be taken of the arbitrary constraints within which one is allowing the model to vary. By way of historical illustration of this point, one might recall the great variety of pre-Copernican models which were proposed for the Earth. Differing in many respects, they form a strong consensus on the question of the Earth's shape. With the considerable advantage of hindsight, we can now recognize that those early geophysicists burdened their models with an unfortunate (and arbitrary) constraint. As a consequence, their models reveal less about the natural structure of the Earth than they do about the

preconceptions of their era. Always in one's mind must be the uncomfortable question: how can a given model reflect personal bias -- or more innocently reflect bias which is random, or structural, but nevertheless arbitrary.

A. T. Price (1973) provides some cautionary advice: "One of the dangers we have to guard against is that of including some feature in our Earth model, for mathematical convenience or simplicity, and then drawing inferences from the results of our mathematical solution about some feature in the real Earth, whereas this stems only from the particular model we have chosen."

Viewed in this cautious manner, modelling may seem a rather unattractive method of inferring Earth structure. Is there another way? Naively one can ask whether an equation or formula can be devised which would map our surface observations directly into an acceptable model. Such a mapping would have particular power if it possessed the property of uniqueness: we would then insert our surface data into the formula, and the formula would simply supply us with the conductivity distribution within the Earth. As we shall see (from a result by Bailey (1970)), even if such a mapping exists, uniqueness need not be expected unless our surface data satisfy rather stringent conditions. Practically, we can expect a direct mapping to supply one of a family of possible models which are acceptable. Direct mappings have the

advantage that any bias which appears in the resulting model must be impersonal and intrinsic to the mathematics.

It has been the particular insight of Backus and Gilbert (1967, 1968, 1970) that the inverse problem in its totality must involve not only the discovery of acceptable models, but also the characterization of the space of acceptable models. To this end they have developed a language with which to address the total inverse problem; the theory, called Generalized Inverse Theory, has found alternative formulation by Lanczos (1961) and others. This Generalized Inverse formulation is a theory designed to deal with the inference of models from a finite set of surface data -- as such it is an extension of modelling procedures which have been used previously. And, as a modelling procedure, the cautionary advice of Professor Price must still be borne in mind.

Perhaps from induction data one can achieve only the most ambiguous notion of the general distribution of conductivity over the upper eight hundred or so kilometers of the Earth. Or, on a more local scale, perhaps inductive soundings may be acceptably explained by so many distinct conductivity structures that, in a word, our data resolves nothing about the conductivity structure in the Earth.

Of course, this is to speculate rather bleakly. But if uncomfortable possibilities are to be meaningfully dispelled, one must learn to use a quantative language

with which to discuss resolution. Also, one must try to explore, qualitatively and systematically, the space of acceptable models associated with a given data set. One must seek to learn from our knowledge of the physics and mathematics of induction phenomena (and from an understanding of the total inverse problem) how one might improve the resolving power of our data. In this respect one may look profitably to the work of Parker (1970) for the direction in which we should proceed.

1.2 The 'Forward Problem' and the 'Inverse Problem'

Since the terms 'inverse problem' and 'inversion procedure' have come to assume a variety of meanings in geophysical literature, we shall here offer a brief formal explanation of the sense in which we shall use these expressions. We are interested to acquire some knowledge of a distribution of physical parameters in a (Cartesian or curvilinear) space V enclosed by a boundary ∂V, by measuring the surface effects on ∂V of physical processes taking place inside V.

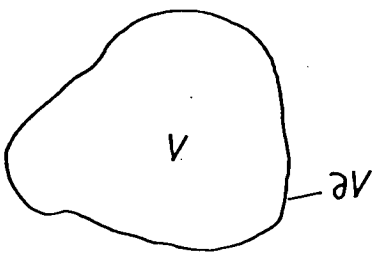

To approach this problem we can formulate two types of mathematical procedure. If the physical parameters are

assumed to be known, one can set up the differential equation which describes the physical processes, and solve the resulting boundary value problem for the measurable effect on the surface ∂V. This is called the forward problem, and is a familiar pursuit of theoretical geophysicists. Expressed in crude terms, one can consider physical law as an 'operator' operating on the physical parameters defined in V (as well as any other relevant physical variables which might enter the problem). This maps these variables onto a space of responses defined on the surface ∂V. Symbolically we can write:

$$M : \begin{bmatrix}\text{physical parameters} \\ \text{in } V\end{bmatrix} \longrightarrow \begin{bmatrix}\text{surface response} \\ \text{on } \partial V\end{bmatrix}$$

The mapping will generally be unique, since a given specified physical situation will give rise to a single surface response. (If this were not the case one would be entering the realm of stochastic processes). For the induction problem the forward problem consists of solving Maxwell's equations in a given geometry and for a specified distribution of conductivity. One solves for electromagnetic fields at the surface ∂V, or for some derivative of these fields, or perhaps some ratio of these fields. Some details of this problem are discussed in Chapter 3. It will be noted that in an important sense the 'forward' induction problem is linear: if ψ_1 is a solution to Maxwell's equations, and ψ_2 is an independent solution to Maxwell's equations, then the superposition of

$\psi_1 + \psi_2$ is also a solution to Maxwell's equations. Thus the solution to the forward problem is said to be linear. The mapping, for the induction problem, can be described

$$M : \quad P (V , s) \longrightarrow \mathcal{C}(\partial V)$$

This is to say that a collection of real parameters associated with the space V and source, s, are mapped onto a (complex) space of responses defined over the boundary ∂V.

How the forward mapping can be used to infer knowledge of the Earth's interior will be described in the following Section.

Broadly speaking the inverse problem concerns itself with the operator M^{-1}:

$$M^{-1} : \quad \mathcal{C}(\partial V) \longrightarrow P (V , s)$$

With the knowledge of the surface response on ∂V, one seeks an operator which will map this response into the set of physical parameters defined in V (and <u>very</u> generally, also into those parameters associated with the source, s). Such a mapping, if it exists, may well not possess the property of uniqueness: a given response might be explicable in terms of a variety of physical variables. Even if the forward mapping, M, is linear in the sense we have discussed, it does not follow that the inverse mapping is in any sense linear. Indeed for a wide class of geophysical problems the inverse mapping is

decidedly non-linear in the following sense: if a variable distribution P_1 gives rise to the response ψ_1 and the distribution P_2 gives rise to the response ψ_2, then it may not be true that $P_1 + P_2$ gives rise to the response $\psi_1 + \psi_2$.

In general, to pursue the inverse problem, a rather intimate knowledge of the forward problem is required. In particular, one commonly requires some knowledge of the partial derivatives of the response with respect to all the chosen model parameters (either explicitly or in the form of some kernel).

1.3 Direct Modelling

In 1889 Schuster, acting upon a suggestion of Gauss, performed a spherical harmonic analysis of the time-varying component of the geomagnetic field, considering specifically daily variations. He was able to show that the larger part of this field was of external origin (an origin since understood to be ionospheric) and the smaller part was consistent with that expected from current induced in the Earth by the external part of the field. Schuster relied upon Maxwell's general formulation (1873) of the electromagnetic forward problem, and Lamb's (1883) solution to the problem of induction in a uniformly conducting sphere. Chapman (1919) made a quantative analysis of quiet-day variations, and by obtaining amplitude ratios of the internal to external parts of the

field, and from the phase difference between these components, he was able to propose a model of the Earth's conductivity consisting of an inner sphere of radius 0.96 a (a is the Earth's radius) and conductivity 0.036 $ohm^{-1}m^{-1}$. This conducting sphere is overlain by a non-conductor of depth (approximately) 240 km. This was found, by trial and error, to be an acceptable model in the sense that it gave rise to a theoretical response in reasonable agreement with the analysed data. The set of models from which Chapman had to find an acceptable model was arbitrarily constrained to be that set of models consisting of non-conducting upper layer and a conducting inner sphere of radius q a ($q < 1$) and conductivity σ. Thus the matter of finding an acceptable model involved the adjustment of two parameters, q and σ. This first attempt to infer the conductivity distribution of the Earth has proved very influential in subsequent research. Price (1970) has pointed out that the constraint imposed in the two-parameter modelling undertaken by Chapman was an expedient for achieving mathematical simplicity.

Investigations subsequent to Chapman's have shown that as one considers less and less constrained models, there emerges an increasingly wide family of acceptable models. Chapman and Price (1930) studied the inductive response of the Earth to aperiodic variations, such as those associated with sudden commencement magnetic storms. Again performing spherical analysis, and applying trial

and error methods to the constrained two-parameter model previously considered by Chapman, they found an acceptable model to consist of an inner sphere of radius 0.94 a with conductivity 0.44 $ohm^{-1}m^{-1}$. This conductivity is an order of magnitude greater than was previously obtained by Chapman (1919) for the different sources associated with variations of daily periodicity. Sudden commencement storms are characteristically impulses with a time-width of a few hours, and a recovery time of several days. Chapman and Price showed that they penetrated to greater depth in the Earth than daily variations. They concluded that the higher conductivity associated with analyses of sudden commencement storm data indicated greater conductivity at depth. Of course, a model consistent with all data was sought. The discrepancy between the models obtained from periodic data with those obtained from aperiodic data has its explanation in the manner in which the space of conceivable models is constrained.

To make the model space less constrained, Lahiri and Price (1939) examined the forward problem for a family of conductivity distributions given by

$$\sigma(r) = \kappa\left(\frac{r}{\mathcal{A}}\right)^{-m} \qquad (1.3.1)$$

where $\mathcal{A} = q\,a$, $q < 1$, and m is any real number. κ is a real constant. In this way a set of continuous distributions could be investigated which were specified by three discrete parameters (κ, q, m). An attempt was

made to search out a model in this class which would satisfy both periodic daily variation data, and sudden commencement storm data. Lahiri and Price were not successful but found that, if a thin conducting layer were included at the Earth's surface, a range of acceptable conductivity profiles could be found (by trial and error) which would satisfy the complete data set. In Fig. 1-1 models 'd' and 'e' are an illustration of such profiles. The models (now including the surface layer) consist of four adjustable parameters; even so the specific structure of equation (1.3.1) may effectively exclude a wider set of acceptable models.

Since this pioneering work by Chapman, Price, Lahiri, and others, there have been many other attempts to infer the global conductivity distribution from wider ranges of variation fields (Rikitake, 1950, 1966; Price and Wilkins, 1963; Yukutake, 1959; etc.). Price (1970) has pointed out that much of the work subsequent to Lahiri and Price (1939) has been based on the same parameterization of the model, i.e. equation (1.3.1). Of course, this parameterization is arbitrary. Most of the models proposed since Lahiri and Price resemble the models of Fig. 1-1 in the sense that they all indicate a sharp increase in conductivity between 400 km and 800 km from the Earth's surface. Despite this common feature, there is a wide range of models achieved from these analyses, as is shown in Fig. 1-2.

FIG. 1-1 The models of Lahiri and Price. The conductivity distributions 'a', 'b', and 'c' satisfy daily variation data. Models 'd' and 'e' satisfy daily variation and storm (Dst) data; these latter have a conducting layer at the surface. (Diagram after Lahiri and Price (1939)).

FIG. 1-2 Some more recent models for the Earth's conductivity. The model 'M', the MacDonald-Price model, is determined from a composite data set of magnetic variation data, and the main geomagnetic field diffusion data. Model 'Y' (Yukatake (1959)) is determined exclusively from main field diffusion. Model 'R' is determined from an analysis of various magnetic variations by Rikitake (1966). Figure after Rikitake, 1966.

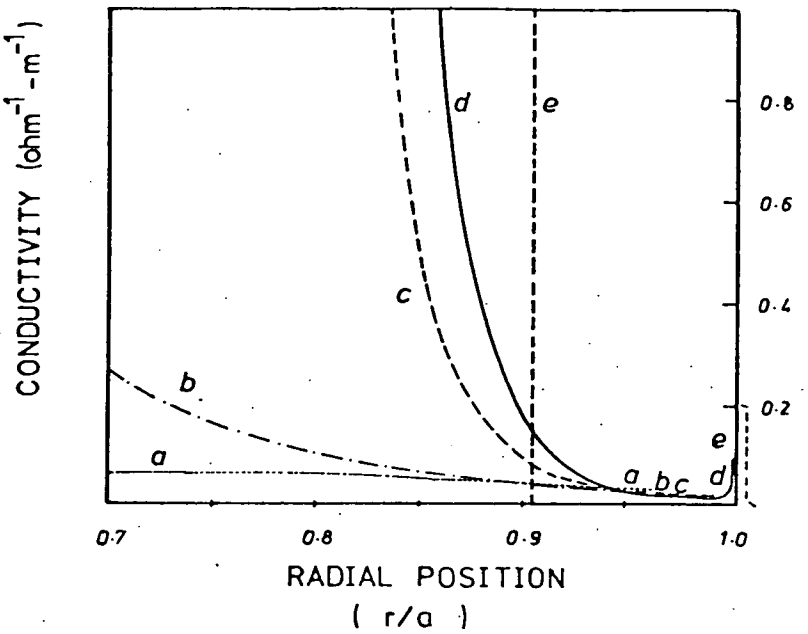
CONDUCTIVITY (ohm^{-1}-m^{-1})
0·8
0·6
0·4
0·2
d
e
c
b
a
e
a b c d
0·7
0·8
0·9
1·0
RADIAL POSITION
(r/a)

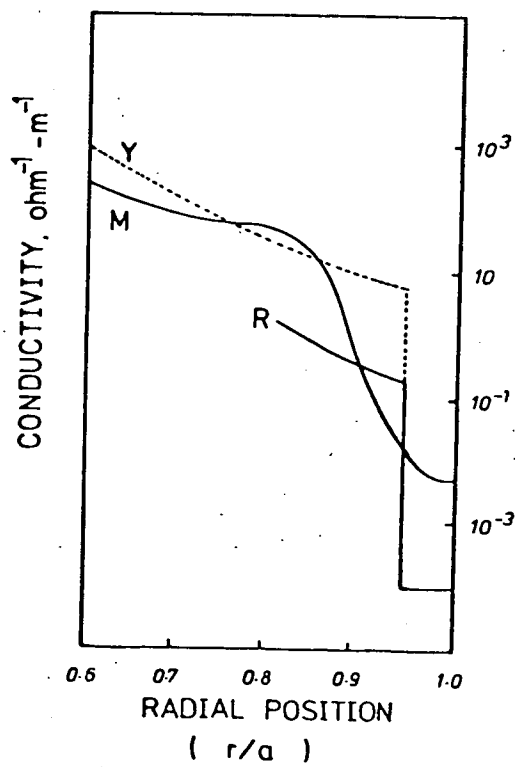
CONDUCTIVITY, ohm^{-1}-m^{-1}
10^{3}
10
10^{-1}
10^{-3}
Y
M
R
0·6
0·7
0·8
0·9
1·0
RADIAL POSITION
(r/a)

A recent analysis of periodic daily variation data, that of Banks (1969), does not rely on the four-parameter model family studied by Lahiri and Price. Banks generated his theoretical surface response from a set of concentric layers. By trial and error Banks then inferred the distribution indicated in Fig. 1-3. Again one observes the steep rise in conductivity at a depth of some 400 km (0.94 a).

Price (1970, 1973) raises questions concerning the common feature of all the proposed models to date -- the steep rise in conductivity at 400 km. Price asks whether there is conclusive geomagnetic evidence for this (so-called) 'discontinuity'; or can it be a pre-supposition (innocently originating from the two-layer models of Chapman (1919) and Chapman and Price (1930)) which enters subjectively into our choice of models? Recent geothermal speculation and seismic models of the mantle may so subtly condition our search for plausible models, that the unifying feature of Figs. 1-1, 1-2, and 1-3 may itself be unrelated to magnetic evidence. Price does add that, personally, he believes the 'discontinuity' to be real.

We see from the beginning, a variety of global models were found to be consistent with geomagnetic data. Exactly what factors can contribute to this observed variety? Of course data collection has improved over the years, and harmonic analyses of data have become more

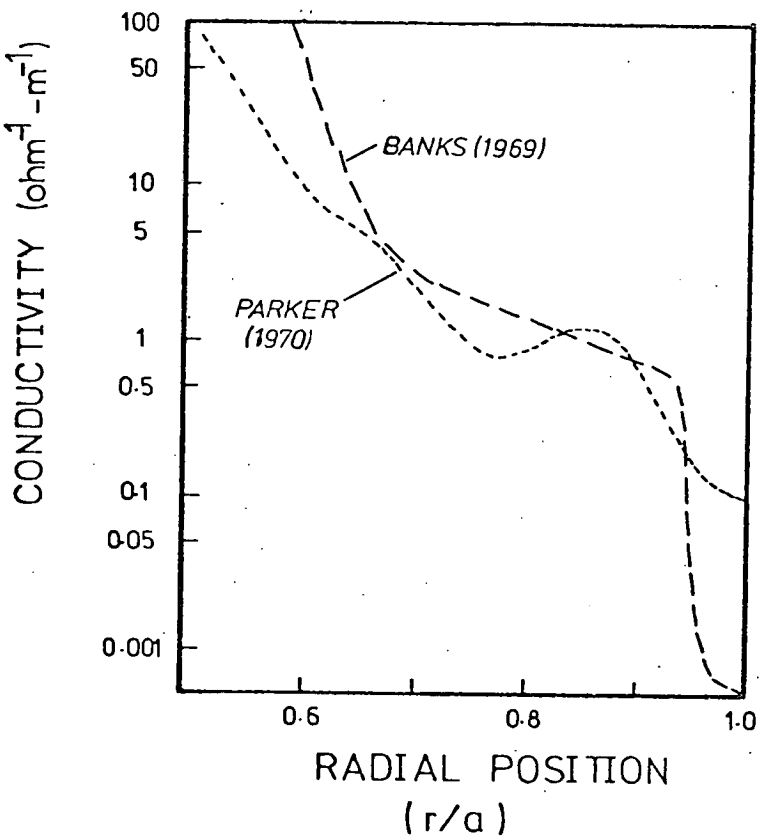

FIG. 1-3 Conductivity models determined from daily variation observatory data published and analysed by Banks (1969). The dashed line is the model of Banks. The dotted line indicates the model suggested by Parker (1970) in his application of Backus-Gilbert inversion to Banks' data.

sophisticated. But considerable differences of opinion still seem to exist, especially concerning the matter of attributing experimental and statistical error to response estimates. Presumptions about the source harmonics associated with particular variations may yet be proven incorrect or misleading. And surface structure -- particularly the oceans -- may significantly influence daily variation data (as Chapman and Whithead (1923) have predicted). But all these considerations arise from an imperfect understanding of the data. There is an equally fundamental question related to the range of non-uniqueness to be expected from perfectly understood data. To address the question of what exactly geomagnetic evidence can infer (independently of all other evidence or speculation) one needs to characterize the space of acceptable conductivity models and to develop some quantitative notion of the resolving power of geomagnetic data. But these ideas are related to the inverse problem which will be discussed later.

With the advent of computers the trial and error methods for finding acceptable models can be systematized. The problem of personal bias entering into the modelling problem can be mitigated by the process of selecting models randomly, then testing these models against some preset criteria of acceptability. The procedure, often called the 'Monte Carlo Procedure', has been applied to the global induction problem by Anderssen (1968, 1970)

but only for storm time data. If the selection of trial models is truly unbiased and sufficiently thorough, representative elements of the space of acceptable models may be isolated. In fact, to improve the efficiency of the search for models, some a priori bounds are usually constructed, within which the search for models is limited. It should be noted that Monte Carlo procedures (as in all modelling procedures) are still constrained by the chosen parameterization of the model.

To investigate near-surface conductivity structure, Cagnaird (1953) introduced a method of single-station prospecting in which the conductivity distribution is inferred from measurements of the total tangential electric field at the surface of the Earth along with the orthogonal total tangential magnetic field. In fact, for the magnetotelluric method as it is called, one uses a response

$$\rho_a = \frac{1}{\omega \mu} \left| \frac{E_x}{H_y} \right|^2 \qquad (1.3.2)$$

where ω is the frequency (in rad-sec^{-1}), μ the permeability, E_x is the x-component of the electric (or 'telluric') field and H_y denotes the orthogonal magnetic component. A Cartesian half-space has been assumed, with the z-direction taken to point downwards into the Earth. The response ρ_a is called the apparent resistivity; which, along with the phase ϕ (where $\phi = \arg (E_x/H_y)$) constitutes the surface response from which the

conductivity may be inferred. The nature of magnetotelluric response is described in more detail in Chapter 3. The method, originally developed in analogy with plane-wave theory, has application for those frequencies which are sufficiently high that the Earth's curvature can be ignored, and a plane half-space approximates the Earth (Srivastava, 1966). A further requirement is associated with the spatial extent of the inducing source (Wait, 1953; Price, 1962) -- the spatial extent of the source must be greater than the penetration depth of the field. The magnetotelluric method has been widely used to study near-surface conductivity (Srivastava, Douglass, and Ward, 1965; Swift, 1967; Caner and Auld, 1968; Patrick and Bostick, 1969; Reddy and Rankin, 1971, 1972, 1973; Madden, 1972; Vozoff, 1972; and others). Reviews of the method may be found in Hermance (1973), and more recently in Porstendorfer (1976) in which the considerable work accomplished by Soviet researchers is described.

Price (1970) has pointed out a similar feature of many models inferred from magnetotelluric data -- a high conductivity zone (~ 0.01 ohm^{-1}m^{-1}) situated at some 50 km from the Earth's surface.

It must be expected that magnetotelluric data will be strongly influenced by the near-surface inhomogeneities in the Earth's conductivity. It will not be surprising that surface measurements of ρ_a can show strong anisotropy. The interpretation (by trial and error) of data arising

from two- and three-dimensional conductivity structures, requires the solution of a much less tractable forward problem. Solution of these problems usually requires purely numerical techniques, such as finite element methods (Coggan, 1971; Reddy and Rankin, 1973; etc.) or finite difference methods (Jones and Price, 1970; Jones, 1971). If the one-dimensional global problem is subject to arbitrary parameter constraint, the two- and three-dimensional problem is vulnerable to such constraint in a much more exaggerated and complicated way. Often, to come to some primitive understanding of anisotropic magnetotelluric data, one presupposes a 'strike' -- that is to say, a vertical fault in proximity to the magnetometer station. Such a model (like the concentric spheres of Chapman (1919)) imposes an enormous constraint on one's understanding of surface data, and restricts the space of models from which to choose acceptable models. The practice of assuming vertical faults below or in proximity to the magnetometer station often arises not so much from physical considerations, as from the necessity (in the absence of a clear physical and mathematical understanding of two- and three-dimensional induction problems) to confine oneself to simple models.

A word must be said about 'simple models'. The case of the one-dimensional two-layer sphere is easily formulated since there are relatively few boundary conditions to be matched. However from an <u>inverse</u> point

of view, such a model is very highly structured. When one asks if a set of surface data can infer such a model, one may be demanding high resolving power of one's data. Such localized parameterizations may lead one to ask completely unprofitable questions such as: 'what is the depth of the discontinuity?', when in fact one's data may at best be able to suggest only the most obscure notion of the actual conductivity in the Earth. Similar difficulties arise in the more 'complicated' model of a vertical fault. A vertical discontinuity may be conceptually simple to visualize and discuss -- but mathematically it is not really a simple model, and certainly from an inverse point of view, it is very localized and structured. It is conceivable that to resolve such a structure would require data of enormous accuracy and extent, data which itself would need to demonstrate great 'structure'. A vertical fault perhaps should be viewed as an extreme parameterization, and an attempt to infer such a structure might well lead to unprofitable questions.

Of course, without a clear idea of the resolving power of geomagnetic data, it is difficult to assess the suitability of any given parameterization in this respect. But this brings us again to the question of the inverse problem.

1.4 Approximate Inversion

Three general categories of inverse induction problem can be described: approximate inversion, exact inversion, and heuristic (linearized) inversion. In this Section we shall discuss two approximate inversion schemes.

It would be very desirable if one could use a simple technique to infer the conductivity distribution of the Earth directly from surface data. Because of the evident non-uniqueness of the inverse problem such a mapping alone would not be a complete solution, but would serve as an indication of where some useful models might lie. In Section 1.5 it will be seen that such a mapping may be difficult to find unless one's data satisfy strict conditions. However a very useful insight of Schmucker (1970) (and rather later of Kuckes (1973a, 1973b)) yields a technique for determining an approximate conductivity structure directly from a set of surface data.

The method depends upon an understanding of the problem of the two-layer conductor. A non-conducting slab is assumed to overlay a good conductor. Schmucker determines an approximate response formula for the case where the depth of penetration in the underlying substratum is small compared with the spatial wavelength of the variation. This response can be written

$$c = h + \frac{1}{2}\delta - \frac{i}{2}\delta \qquad (1.4.1)$$

where h is the depth to the good conductor; δ is the

skin-depth of the conducting layer, and $i = \sqrt{-1}$. For magnetotelluric data, the response c is defined by

$$c = - \frac{i}{\omega \mu} (E_x/H_y) \qquad (1.4.2)$$

Comparison between (1.4.1) and (1.4.2) will show that in an inverse sense knowledge of the surface response E_x/H_y (for models which happen to conform to the conditions of the approximation) can determine uniquely the two quantities on the right hand side of equation (1.4.1); these are namely,

$$h = (\omega \mu)^{-1} \{ Im(E_x/H_y) - Re(E_x/H_y) \} \qquad (1.4.3)$$

and

$$\delta = (\omega \mu)^{-1} \{ 2Re(E_x/H_y) \} \qquad (1.4.4)$$

The real part of c is related to the imaginary part of E_x/H_y, and can be identified with the mean depth to the internal eddy currents. The imaginary part of c (inferred from the real part of E_x/H_y) indicates (with δ) the conductivity at that depth. Thus if one were to know a priori that the Earth consisted of a poor conductor overlaying a very good conductor, one could infer from the complex response directly the depth to the conductor and its conductivity. The physical idea of inferring the mean depth of the current distribution has application even in an Earth which were not two-layered. If one (conceptually) considers the conductivity of the bottom layer to be infinite, then E_x/H_y would be purely imaginary

(the phase of c in equation (1.4.1) would be $\pi/2$), and the depth h*, defined by

$$h^* = h + \frac{1}{2}\delta \,, \qquad (1.4.5)$$

determined from experimental data and equation (1.4.3) would take on the significance of the depth of the perfect substitute conductor. As such, this depth would represent the geometric centre of the current distribution. If j(z) were the current density at depth z, then Weideldt (1972) shows formally

$$h^* = \int_0^h z \, \mathrm{Re}\{j(z)\} \, dz \Big/ \int_0^h \mathrm{Re}\{j(z)\} \, dz \qquad (1.4.6)$$

This equation can be interpreted as the depth to the 'centre of gravity' of the real part of the induced current distribution. The ambient conductivity at depth h* can be inferred from (1.4.4) for the particular frequency ω. The approximate inversion of Schmucker can be performed individually on elements of a data set, and thus a set of model pairs (σ^*, h*) can be built up for the various frequencies represented in the data set. This produces a conductivity distribution which is particularly reliable if the distribution of conductivity in the Earth monotonically increases with depth -- a condition which one cannot know a priori of course.

A somewhat similar idea has been exploited by Jady (1974a)for global harmonic problems. He has considered the case of a poorly conducting slab of conductivity σ,

overlaying a perfectly conducting sphere situated at radial position q (i.e. the radial distance from the centre of the Earth normalized with respect to the Earth's radius). In a manner similar to the analysis leading to Schmucker's technique, knowledge of the real and imaginary parts of the surface response (for given frequency and harmonic) can lead to a unique solution for the depth q of the inner sphere, and for the conductivity of the slab. From variational principles, an expression is obtained

$$\sigma = \frac{\mathrm{Im}\left[R_\ell^{m*} \frac{d}{dr} R_\ell^m \right]_{r=1}}{\omega \mu a^2 \int_q^1 r^2 |R_\ell^m|^2 \, dr} \qquad (1.4.7)$$

where R_ℓ^m is the radial part of the separated solution to the spherical Sturm-Liouville equation. The position q can be inferred independently of (1.4.7) directly from the surface response. Relying on the assumption that first order changes in the eigenfunction R_ℓ^m give rise only to second-order changes in the model distribution σ, an iterative procedure can be initiated by assuming a conductivity $\sigma^{(0)}$, calculating the theoretical response R_ℓ^m, and performing the calculation of (1.4.7) to yield the first iterate $\sigma^{(1)}$. Such a procedure was found by Jady to be rapidly convergent. This effectively systematized the problem of improving the Chapman (1919) Earth model in a manner which may be instructive from an inverse point of view. For different individual frequencies, and different harmonics, one can construct model 'pairs'

(q, σ), and a collection of such models for a given set of data might indicate the region of the model space where compatible solutions lie. Of course, it has already been noted that treating such highly constrained models leads to difficulty when one comes to find models consistent with <u>all</u> data. Jady has extended his procedure to treat multilayer conductors (still overlaying a perfect conductor). For N such layers, a system of equations is obtained:

$$\mathrm{Im}\left(R_\ell^{m*} \frac{d}{dr} R_\ell^m\right)_{r=1} \omega^{-1}\mu^{-1}a^{-2}$$

$$= \sigma_1 \int_{r_1}^{1} r^2 |R_\ell^m|^2 dr + \sigma_2 \int_{r_2}^{r_1} r^2 |R_\ell^m| dr + \ldots + \sigma_N \int_{q}^{r_{N-1}} r^2 |R_\ell^m|^2 dr \qquad (1.4.8)$$

for each ω. If the coefficients of σ_i

$$\int_{r_1}^{1} r^2 |R_\ell^m|^2 dr \qquad \text{etc.}$$

are considered to be independent of conductivity, the system of equations implied by (1.4.8) for N frequencies will be linear in the σ_i's, and can be solved. The new σ_i's will constitute the first iterate in an iterative procedure. It is not clear whether the layer depths $(r_1, r_2, r_3, \ldots, r_{N-1})$ can be uniquely determined from the response as was the case for the two-layer problem. However it would seem from example that the depths are chosen arbitrarily (Jady, 1974a). Within this same

formalism Jady has sought to discuss the effect of error on model estimates, and has developed a test for the consistency of data pairs (Jady, 1974b).

1.5 Exact Inversions

An exact inversion procedure is one which utilizes a mapping from the surface data directly into the model space. The study of such procedures is particularly valuable since they shed considerable light onto the problem of uniqueness in the inverse problem. In fact, both of the exact procedures which have been developed to deal with the inverse induction problem -- that of Bailey (1970) and the inverse Sturm-Liouville problem studied by Weideldt (1970, 1972) -- establish rigorous conditions for such procedures to yield a unique solution.

Bailey, for the global problem, separates fields into parts of internal and external origin at some arbitrary radius $r = \rho a$ within the Earth. Thus

$$\frac{\ell(\ell+1)}{\rho} R_\ell^m = \ell e_\ell^m - (\ell+1)\, i_\ell^m$$
$$\frac{1}{\rho}\frac{\partial}{\partial \rho}(\rho R_\ell^m) = e_\ell^m + i_\ell^m \qquad (1.5.1)$$

where R_ℓ^m is defined in the previous Section. In order to develop a relationship between conductivity and a modified response function defined in Fourier ω-space, Bailey uses the fact that the linearity of Maxwell's equations implies that the internal part i_ℓ^m is linearly related to e_ℓ^m. (The response is in fact the solution to an equation

developed by Eckhardt (1963) for the forward problem.) Bailey used the causal nature of the response to derive an inverse formulation. We do not introduce any of Bailey's analysis here, but state his derived condition for uniqueness to the exact inverse formalism. The condition which must be satisfied is that the response be known for a complete range of frequencies $0 \leq \omega \leq \infty$. Of course, such complete knowledge is not available from experimental data, reflecting as they do a finite set of frequencies. Bailey has developed an algorithm to deal with experimental data: he supplies the extreme branches of the response curve by using asymptotic techniques and gaps in the response curve by interpolation. However, it seems the solution is strongly affected by scatter in the data. The inversion of data generated (synthetically) from discontinuous models, shows that the algorithm tends to isolate smoothed conductivity distributions (Bailey, 1973). In view of the implied non-uniqueness to be associated with a finite set of data, the use of asymptotic techniques may serve to restrict one's view of the space of acceptable models.

Weideldt (1972) performed an inverse Sturm-Liouville analysis, analogous to that of Gel'fand and Levitan (1955) which was developed originally to infer scattering potentials in quantum mechanics. Weideldt's work is very illuminating concerning many aspects of both forward and inverse induction problems. The conditions for

uniqueness for solutions of this exact procedure are the same as Bailey's -- one must have complete knowledge over all frequencies of a spectral function, which is related closely to the response function. Weideldt introduces methods to uniquely infer conductivity distributions from experimental data (suitably completed and smoothed). However, he admits that finding one element in a family of possible models does not constitute a solution to the 'total' inversion problem.

1.6 Heuristic Linear Inversion

In the previous Sections, the fundamental problems associated with finding acceptable Earth models have been discussed. Forward modelling techniques can be biased, and because of the non-uniqueness of the problem, individual models which are obtained can give an incomplete impression of the total space of acceptable models. Also, direct inversion procedures seem to require rather too much of typical experimental data, both in terms of frequency range, and in terms of the smoothness of the data. Even in circumstances where the data set may be completed and smoothed, and a solution found, this solution may be an individual element of a space of solutions of considerable diversity. Furthermore, exact inversion techniques take no account of experimental error.

Clearly, it would be an advantage over the informed

guesswork of direct modelling to have a systematic process for improving a proposed model. It would be a powerful advantage if, within this same framework, one could also address questions about the consistency of data, or the resolvability of models, about uniqueness or about errors. Generalized linear inverse theory seems to have provided geophysicists with such a framework. The theory has found two formulations: that of Lanczos (1961) described by Wiggins (1972) and Jackson (1972), in which the model parameters are expressed discretely; and the formulation developed by Backus and Gilbert (1967, 1968, 1970) in which the model parameters are taken to be distributions. Both formalisms are equivalent (Wiggins, 1972) and both have become widely practised.

Parker (1970), in a venturesome work, applied generalized linear inverse theory to global electromagnetic induction data (the data accumulated by Banks (1969)), and since then a number of authors have followed his example: among them Hobbs (1972), Ward et al. (1974), Jupp and Vozoff (1975), Larsen (1975). Some authors are already considering two- and three-dimensional models (Weideldt, 1975) and some are treating models with anisotropic conductivity parameters (Abramovici et al., 1976).

The generalized inversion theory as formulated by Backus and Gilbert involves two useful procedures. If one is given a model which is 'close' to an exactly

fitting model (close in the least-squares sense), one may move iteratively towards the exactly fitting model. If one has found a model which exactly fits the data, one can describe quantitively the power of the data to resolve the model at various points along the model profile. This resolving power will be related to the distribution and quantity of data; also it can be expressed as a function of the experimental error of the surface data.

It must be pointed out that the generalized inversion theory is a linear one, depending as it does on the theory of linear operators. The mathematical outline of the theory is presented in Chapter 2. We present here, for purposes of an introductory discussion, some basic aspects of that formalism.

a. Finding an acceptable model

Model-fitting associated with induction data is often posed as a non-linear least-squares optimization problem. Typically, a Taylor expansion in the model space (here expressed in terms of M model parameters, m_j) is made of a set of surface responses y_i, so that

$$y_i = y_i^0 + \sum_{j=1}^{M} A_{ij}\, \delta m_j + 0\,|\delta m_j|^2 \qquad (1.6.1)$$

where $\underline{\underline{A}}$ is the matrix whose elements consist of partial derivatives of y_i with respect to m_j, i.e.

$$A_{ij} = \partial y_i / \partial m_j$$

Linearizing (1.6.1), one can proceed to minimize the sum

of the squares of data residuals,

$$\sum_i (y_i - y_i^0)^2$$

If we define the ith component of a vector $\delta \underline{y}$ to be $y_i - y_i^0$, and the jth component of a vector $\delta \underline{m}$ as δm_j, then the minimization of data residuals gives rise to the solution for the increment $\delta \underline{m}$ in

$$\delta \underline{m} = (\underline{\underline{A}}^T \underline{\underline{A}})^{-1} \underline{\underline{A}}^T \delta \underline{y} \qquad (1.6.2)$$

In a non-linear problem, the addition of the perturbation $\delta \underline{m}$ to the current model vector $\underline{m}$, yields a new improved model $\underline{m} + \delta \underline{m}$ from which a new improved (i.e. diminished) data residual can be computed. Repeated application of this procedure constitutes an iterative procedure which may or may not be convergent.

The problem thus expressed can be unstable for several reasons. The instability can arise from an inadequate linearization of equation (1.6.1). Marquardt (1963) supplies a more elaborate algorithm to deal with non-linear problems, based on the searching out of the maximum neighbourhood of the starting model in which the first term of the Taylor expansion (1.6.1) is valid. The data residual is constrained to decrease in consecutive iterations. A number of researchers have performed model-fitting in this way, among them Wu (1968) and Patrick and Bostick (1969) for the magnetotelluric problem.

In addition to the instability which may arise from the non-linearity of the problem, there is another fundamental problem to be associated with equation (1.6.2). If one has parameterized the model space too intricately for the resolution power of the data, then the problem is said to be underdetermined. This is to say, the information contained in the data is not sufficient to resolve some of the parameters in the set $\{m_j\}$. This underdeterminacy leads to the matrix $\underline{\underline{A}}\,\underline{\underline{A}}^T$ becoming singular and hence its inverse $(\underline{\underline{A}}\,\underline{\underline{A}}^T)^{-1}$ will not exist. An attempt to evaluate the inverse of a nearly singular matrix can give rise to very great numerical instability entering into the iterative procedure. This in turn can lead to great perturbations δm_j, which may violate the conditions under which the Taylor expansion (1.6.1) was formed. Of course, one cannot know in advance what model parameterization will be appropriate (i.e. we cannot know how to make a singular matrix $\underline{\underline{A}}$ non-singular by adjustment of $\{m_j\}$). On the other hand, if one makes the model too crude for the information in the data, one may be over-constraining the problem. In this case the full information available from the data is not exploited. Most of the Marquardt least-squares procedures carried out successfully have been in overconstrained situations (two- and three-layer half spaces, for example).

It is to deal with the general problem of under-determined systems that generalized inverse theory has

been developed. Backus and Gilbert (1967) parameterize the model in a manner almost guaranteed to give rise to an underdetermined problem: a vector Earth model $\underline{m} = (m_1, m_2, m_3, \ldots, m_M)$, the components of which are real-valued piecewise continuous functions of radius r (or depth z). This space is recognizably Hilbert space, upon which one can define the inner product as

$$\langle \underline{m}, \underline{m}' \rangle = \int_0^a \{ m_1(r)m_1'(r) + m_2(r)m_2'(r) + \ldots \} \, dr \tag{1.6.3}$$

and the norm $\| \underline{m} \| = \langle \underline{m}, \underline{m} \rangle^{\frac{1}{2}}$. If γ_i indicates an element of the data set, and is defined in terms of a functional g_i, by

$$\gamma_i = g_i(\underline{m}) \tag{1.6.4}$$

then the functional equivalent to (1.6.1) is

$$g_i(\underline{m}) - g_i(\underline{m} + \delta \underline{m}) = \langle \underline{G}_i, \delta \underline{m} \rangle + 0 \| \delta m \|^2 \tag{1.6.5}$$

where $\underline{G}_i$ is a kernel which is also a member of the Hilbert space containing the $m_i(r)$'s. Again an optimization problem can be posed; however it is the particular insight of Backus and Gilbert to exploit the non-uniqueness of this problem. They formulate the problem as one of finding the model $\underline{m}$ closest to a starting model $\underline{m}^0$. (The model $\underline{m}$ is constrained to satisfy the data.) Thus one clearly is finding an optimal model which is closest to the starting model. One develops a matrix solution similar to (1.6.2)

$$\underset{\sim}{\nu} = \underset{\approx}{\Gamma}^{-1} \underline{\Delta g} \qquad (1.6.6)$$

where $\underset{\sim}{\nu}$ is a set of Lagrange multipliers, $\Gamma_{ij} = \langle \underline{G}_i, \underline{G}_j \rangle$ and $\underline{\Delta g}$ is defined $\Delta g_i \equiv \gamma_i - g_i(\underline{m}^0)$. The model perturbation is hence given by

$$\delta \underline{m} = \sum_i \nu_i \underline{G}_i \qquad (1.6.7)$$

The iterative procedure is initiated by recalculating Δg_i using $\underline{m} + \delta \underline{m}$. Stability can be introduced to the system if $\underset{\approx}{\Gamma}$ is decomposed by similarity transformation into a form

$$\underset{\approx}{\Gamma} = \underset{\approx}{B} \underset{\approx}{\Gamma}' \underset{\approx}{B}^T$$

where $\underset{\approx}{\Gamma}'$ is now diagonal. If the columns of matrix $\underset{\approx}{B}$ contain the eigenvectors of $\underset{\approx}{\Gamma}$, then the diagonal elements of $\underset{\approx}{\Gamma}'$ will be the corresponding eigenvalues of $\underset{\approx}{\Gamma}$. By excluding those eigenvalues near zero (which tend to make $\underset{\approx}{\Gamma}$ singular), one can impose stability on the system. In fact, one can exclude sufficient eigenvalues to meet more stringent pre-set criteria. For example, one can make the same constraint as suggested by Marquardt: that of restricting $\delta \underline{m}$ in a given iteration in such a way that the data residual does not increase at that iteration. Thus instability can be smoothed whether that instability arises from the quality of the linearization, or from the singularity of $\underset{\approx}{\Gamma}$, or from both factors. Excluding eigenvalues effectively excludes certain linear combinations of the data from the procedure. Thereby

a degree of information is lost. The resolution of the data may also be degraded by this procedure, in exchange for a stable convergent process.

b. Resolution

Once one has isolated particular solutions to the inverse problem, one tries to characterize the space of acceptable solutions (Backus and Gilbert, 1968, 1970). For linear problems one can write a response γ_i as

$$\gamma_i = \int m(r)\, G_i(r)\, dr \qquad (1.6.9)$$

this is to say, as a weighted average of the model distribution m(r). In fact, one can construct a further weighted average of the model by forming a linear combination of the surface data:

$$\sum a_i \gamma_i = \int m(r) \left[\sum a_i G_i(r) \right] dr \qquad (1.6.10)$$

If the $G_i(r)$'s form a complete set, any possible average of the model distribution which can be evaluated from combinations of data elements, can be constructed by choice of the N-tuple $\{a_i\}$. If the N-tuple is chosen so that the kernel

$$\sum a_i G_i(r)$$

resembles a delta-function centred at $r = r_0$ (i.e. the function is zero everywhere except at $r = r_0$, where it is infinite), then the average which (1.6.10) represents is a local average of the model at r_0, i.e.

$$\sum a_i \gamma_i = \langle m(r) \rangle_{r_0} \qquad (1.6.11)$$

How 'localized' this average will really be, will depend upon the width of the delta-like function which has been achieved. The actual task of constructing a delta like function is posed by Backus and Gilbert (1968) as an optimization problem. One seeks to minimize the area under the kernel $\sum a_i G_i(r)$ away from $r = r_0$; the area under the distribution is constrained to satisfy a unimodular condition

$$\int \sum a_i G_i(r)\, dr = 1$$

If the optimum kernel which is achieved is broad, and rather unlike a delta-function, then the local average $\langle m(r) \rangle_{r_0}$ determined with this kernel is said to have a long resolving length, since the average draws upon the model distribution over a long range of depth. In such a case one can conclude that the data poorly resolves the model. On the other hand if the kernel is a sharp spike, the local average which is achieved from (1.6.11) is truly localized, and one can conclude that the model distribution is well resolved at that depth. By way of making the matter of resolution quantitative, Backus and Gilbert introduce the spread of the kernel defined by

$$s = \int J(r, r_0) \left[\sum a_i G_i(r) \right]^2 dr$$

as a measure of the area beneath the kernel for $r \neq r_0$. The function $J(r, r_0)$ is an arbitrary function which is

zero at $r = r_0$, and whose modulus increases monotonically away from $r = r_0$. If the spread is large, then resolution is poor. If the spread is very small, then the resolution is good. The spread is directly related to the width of the delta-like distribution, and to the geometrical centre of the distribution. In fact, it is the spread which one seeks to minimize (by optimally choosing the N-tuple $\underline{a}$) in order to construct a delta-like function out of the space $\{G_i(r)\}$.

For non-linear responses, the situation is significantly more complicated, since one must admit that the space formed by the kernels $\{G_i(r)\}$ is itself model-dependent. Furthermore, the equation (1.6.9) cannot be true. Thus the local average, which is achieved from a linear combination of kernels as they appear in equation (1.6.5), is fashioned out of a subspace of the space of all acceptable models; the subspace is called the space of G-acceptable models. The significance of this restriction to the general theory has been a matter of some concern (Sabatier, 1974; Anderssen, 1975).

If the data is erroneous, error can be reflected by the local average represented by equation (1.6.11). Backus and Gilbert (1970) show that there is a trade-off relationship between resolution and such model error: if one wishes to improve the resolution of the model at a given depth, one can do so by increasing the error which can be attached to the model local average. They present

a scheme which facilitates the algebraic problem of performing this dual optimization of model resolution and model error.

The details of Generalized Inversion Theory are outlined in the following Chapter.

c. Using linear inversion to examine data

As we have mentioned previously, Parker (1970) performed a Backus Gilbert inversion of data published by Banks (1969), and determined a model (described by Parker as an element of a family of such models) which satisfies the data within one standard deviation. This model is indicated in Fig. 1-3 along side Banks' model which we have discussed previously. Parker also determines a set of local averages, together with resolution lengths and error estimates to be associated with each local average. In this way he is able to address quantitively some of the questions raised by Price (1970) concerning the nature of the suspected 'discontinuity' at 400 km depth. For example, Parker claims that the levelling off of conductivity at the inner side of the 'discontinuity' (at 0.7 $ohm^{-1}m^{-1}$) occurs rather deeper than had been previously suggested -- namely at some 500 km depth instead of 400 km. Parker also suggests that the resolution is poor at this depth, but the flattening out of the profile is still barely resolvable. Parker's model differs from that of Banks significantly at the

surface. Again, Parker explains that near-surface resolution is poor, but any discrepancy below a depth of 0.96 a should be resolvable from the data.

Having developed a language designed to discuss resolution, error, and consistency of data, one can, with synthetic data (i.e. data generated theoretically from chosen models) use inversion theory to examine how one might improve the quality and resolving power of a data set.

Parker seeks to see specifically how the data set of Banks might be improved. The suggestion he offers to an experimental researcher is that he strive for more accurate estimates of the response function. A modest improvement in the error will yield significant improvement in the resolving power at depth. (Incidentally, one might bear in mind that Parker describes an experimental error of 2% as attainable ...) Furthermore, it seems that inclusion of accurate phase estimates may improve resolution at the surface. Parker's examination of how modifications to the data set can improve resolution, was confined to adjustments in the accuracy and to the inclusion of phase. His examination was not systematic; it is interesting to speculate whether such examinations can be put on a systematic basis by posing them as optimization problems. One can try to find how the data set can be improved by extension of the range of frequency and quantity of data. It would seem that many

questions can be asked of the data (in relation to a given space of G-acceptable models) which might greatly contribute to an improved strategy at the data gathering and data analysis stage.

Parker (1972) shows how some questions concerning the consistency of data pairs can be posed systematically from the language of generalized inversion. Apart from these contributions, it would seem little attempt has been made to exploit the language in this way.

Concerning the actual model Parker proposes -- it has aroused a certain amount of controversy. Anderssen (1975) has complained that the linearization may be misleading. Both Parker himself (1972) and Jady (1974b) have expressed doubts concerning the consistency of the Banks data. The current state of geothermal studies suggests that the conductivity inferred by Parker is rather too high (Duba, 1976), and the Parker conductivity at the Earth's surface is rather higher than that suggested by most magnetotelluric studies. The Banks data was collected from a global distribution of observatories, and Parker examines 28 daily variation responses without phase. One might recall the suggestion of Chapman and Whitehead (1923) that daily variation may be significantly affected by ocean edge effect if the observatory happens to be coastal; obviously the inclusion of magnetic storm data might supply a more promising data set for inversion, and work by a number of

researchers is proceeding in this direction (Schmucker, 1976). However, including storm data tends to increase the integrated conductivity at the surface, so Parker's model may become even more conductive with the inclusion of storm data!

1.7 Work Covered in This Thesis

Having attempted in this Introduction to establish the context for the linearized inversion problem, and to describe how inversion formalisms may be of use to achieve a more thorough understanding of geomagnetic data, in Chapter 2 we proceed to outline the principles of general linear inversion.

In Chapter 3 we describe some of those aspects of the forward problem which enter into the application of inversion theory to electromagnetic induction responses associated with conductivity distributions which are one-dimensional. In particular, various expressions of the response functional are described. The remaining part of the thesis concentrates upon the inversion of the magnetotelluric response of a multi-layered half-space. The problem of how one might effect the linearization is considered. The technique which is finally adopted is to discretize the functional, and to employ differential calculus to the resulting function (of 2M-1 discrete model parameters including depth parameters) in order to determine a Fréchet kernel, $G_i(r)$. The linearization is

examined in somewhat close detail for the two-layer conductor, but extension of the analysis to multilayered conductors is trivial. For the two-layer halfspace an attempt is made to ascertain those parts of the model space which give rise to the intrusion of higher-order terms in (1.6.5). An examination is made of the paths of convergence in a least-squares procedure for an underdetermined problem, and this shows how the higher order terms can introduce instability into the process. The beneficial effect of ranking and winnowing is also demonstrated in this example.

In Chapter 4, uniqueness is discussed for systems of discretely ordered model parameters entering the inverse Sturm-Liouville problem. The discussion draws heavily upon the work of Barcilon (1974) and Weideldt (1972). The nature of the inductive response as a continued fraction is illustrated. The response is also portrayed graphically as a combination of the discrete set of conductivity parameters: a combination with non-linear, complex coefficients. The graphs which result (in complex space) are given a simple energy interpretation. An analogy is suggested from circuit theory.

In Chapter 5 the least-squares inverse problem is examined in more detail for magnetotelluric data. The stabilizing effect of ranking and winnowing data is demonstrated. A magnetotelluric data set which is of demonstrable one-dimensional character (i.e. is isotropic)

recorded and analysed by Jones (1976) is inverted, and various acceptable model solutions are generated. The effect of including phase information into the least-squares procedure is examined. Also, a data set which has been examined by Fournier (1968) and Weideldt (1972) is re-examined with the generalized inverse scheme presented in this thesis.

The resolution associated with error-free magneto-telluric data is considered in Chapter 6. The effect of including phase on the resolution parameters is demonst-rated. A comparison is made (in terms of resolution) between the use of the real and imaginary parts of the response, and the amplitude and phase of the response.

In Chapter 7 the complication of erroneous data is introduced into the problem. The geometrical discussion of Backus and Gilbert (1970) is described. The application of their general theory is made to the induction problem, considering first absolute error, then the rather more complicated (but more appropriate for induction data) relative error. Some examples are displayed.

In Chapter 8 some general conclusions for the thesis are summarized, indicating the direction future work might go.

CHAPTER 2

GENERALIZED LINEAR INVERSE FORMULATIONS

2.1 Some Preliminary Remarks

Within the context of geophysical problems, the general inverse problem which interests us is that of inferring a model distribution (or alternatively a set of discrete model parameters) for the interior of the Earth, by making a set of measurements at the Earth's surface. We express this surface 'response' of the Earth as a functional of the form

$$\phi[m] = \int_V F(m(\underline{r}),\underline{r})\, d^3\underline{r} \qquad (2.1.1)$$

where square brackets denote a functional; m(r) is the model distribution which is a function of position within the Earth, and $d^3\underline{r}$ denotes an increment of volume. If a model is spherically symmetric, this symmetry can be exploited to transform the functional (2.1.1) into a scalar form

$$\phi[m] = \int_0^a F(m(r),r)\, dr \qquad (2.1.2)$$

where r is the (scalar) radial position, and 'a' is the radius of the spherical Earth. As we have seen in the previous Chapter, such a functional can be approximated by dividing the interval (0,a) into M subintervals separated by the points

$$0, r_1, r_2, \ \cdots\ , r_{n-1}, r_n, r_{n+1}, \ \cdots\ , a.$$

Equation (2.1.2) becomes

$$g(m_1, m_2, \ldots m_M) = \sum_{j=1}^{M} F(m_1, m_2, \ldots; h_1, h_2, \ldots)\, h_j \tag{2.1.3}$$

where $m_j = m(r_j)$, and $h_j = r_j - r_{j-1}$. To study in a variational sense such functionals as (2.1.2), one can employ analytic procedures and differential calculus to the discretely ordered function (2.1.3), and then discover the implication of such analysis for the functional $\phi[m]$.

If the ith surface response measurement is denoted by γ_i, we can write following (2.1.2) the functional relationship between γ_i and m by

$$\gamma_i = g_i[m(r)] \tag{2.1.4}$$

or alternatively by a function of M model variables,

$$\gamma_i = g_i(m_1, m_2, \ \cdots\ , m_M) \tag{2.1.5}$$

If g_i is linear, a possible expression for (2.1.4) is

$$\gamma_i = \int_0^a m(r)\, f(r)\, dr \tag{2.1.6}$$

and similarly, for the discrete case of equation (2.1.5), we may be able to write

$$\gamma_i = A_{ij} m_j \tag{2.1.7}$$

This latter equation can be written in tensor notation as

$$\underline{\gamma} = \underline{\underline{A}} \cdot \underline{m}$$

The variational problem based on the functional (2.1.6) or the (linear) operator (2.1.7) is easily expressed by either

$$\delta\gamma_i = \int_0^a \delta m(r)\, f(r)\, dr \qquad (2.1.8)$$

or

$$\delta\gamma_i = A_{ij}\, \delta m_j \qquad (2.1.9)$$

Two geophysical examples of such purely linear functionals are those associated with the mass, $\mathcal{M}$, of the Earth, if the Earth is taken to have spherically symmetric mass density, $\rho_m(r)$, and radius a:

$$\mathcal{M} = 4\pi \int_0^a r^2 \rho_m(r)\, dr \ ,$$

and the moment of inertia, $\mathcal{I}$, of a similar Earth:

$$\mathcal{I} = \frac{8\pi}{3} \int_0^a \rho_m(r)\, r^4\, dr$$

In addition to these relatively simple linear problems, there has been a wider class of linear inverse problems, that of isostatic Earth data, treated by Dorman and Lewis (1970, 1973).

In view of the complexity of most geophysical problems, it might be no surprise that most functionals appearing in geophysical contexts are <u>non-linear</u>, and if a linear variational formalism is to be developed, such functionals must be cast into quasi-linear form. In this present Chapter we examine two widely-accepted

formulations of this approach: Generalized Linear Inverse Theory developed by Lanczos (1961) and described by Wiggins (1972) and Jackson (1971): in this formulation the model parameters are discretely defined. Another approach is the method of Backus and Gilbert (1967, 1968, 1970) in which the models are taken to be piecewise continuous functions of depth. Both procedures have found fairly widespread use and Table 2.1 contains a brief list of some of the notable non-linear inverse problems which have been studied to date.

2.2 The Formalism of Backus and Gilbert

a. Notation

We follow the notation and method developed by Backus and Gilbert in their papers of 1967, 1968, and 1970. Apart from a brief discussion, we do not introduce the complication that is presented to the formalism by experimental error in the surface data. For the most part the modifications to the theory required to treat erroneous data are discussed in Chapter 7. The inverse problem is posed as one of finding a vector Earth model $\underline{m}$, $\underline{m} = \left\{ m_1(r), m_2(r), \ldots , m_M(r) \right\}$, whose components consist of real-valued, piece-wise continuous functions of radius r (or, in the case of Cartesian geometry, functions of the depth from the surface, z). The space of all conceivable models, $\mathcal{M}$, is considered as an infinite-

Surface Response	Model parameter(s)	Authors (date)	Type of Inversion
Normal modes of free oscillation	density, $\rho_m(r)$ elastic moduli, κ, μ, shear velocity, v_s compressional velocity, v_p dissipation, Q	Backus & Gilbert (1967,1968,1970) Gilbert & Dziewonski (1975) Wiggins (1972)	B-G B-G Lancz.
Electromagnetic induction in Earth	electrical conductivity, $\sigma(r)$	Parker (1970) Sims et al (1970) Ward et al (1974)	B-G Lancz. Lancz.
Gravity anomaly	mass density, $\rho_m(r)$	Parker & Heustis (1974)	B-G
Magnetic anomaly	magnetic susceptibility, μ_m	Courtillot et al (1975)	Lancz./ B-G
Seismic travel-times	shear velocities, v_s compressional velocities, v_p	Kennett (1976)	B-G

TABLE 2.1

dimensional linear space on which the inner product is defined

$$\langle \underline{m},\underline{m}' \rangle = \int \{ m_1 m_1' + m_2 m_2' + \ldots + m_M m_M' \} \, dr \qquad (2.2.1)$$

and the norm is defined by $\| \underline{m} \| \equiv \langle \underline{m} , \underline{m} \rangle^{\frac{1}{2}}$. It should be borne in mind that the model parameters are to be expressed in dimensionless units. The model $\underline{m}$ is to be inferred from a finite set of N surface measurements, γ_i, and the model is related to this data set by a set of generally non-linear functionals, $\mathcal{G}$, whose elements g_i are defined by

$$\gamma_i = g_i[\underline{m}] \qquad (2.2.2)$$

Equation (2.2.2) constitutes a set of N restrictions to be imposed on an infinite-dimensional model space. The set of models which falls within these constraints are termed 'acceptable models' and this set is also infinite-dimensional.

The question relevant to the inverse problem as it has been stated is: how does a small change $\delta\underline{m}$ in the model affect the surface data we might measure? With a view to stating this question mathematically we define Fréchet differentiable functionals to be that class of functionals which, for a given model perturbation $\delta\underline{m}$, satisfy

$$g_i[\underline{m}] - g_i[\underline{m}+\delta\underline{m}] = \langle \underline{G}_i , \delta\underline{m} \rangle + 0 \, \|\delta\underline{m}\|^2 \qquad (2.2.3)$$

where the function $\underline{G}_i = (G_i^{m1}(r), G_i^{m2}(r), \ldots, G_i^{mM}(r))$, with $i \in \{1, 2, \ldots, N\}$. The subscript i denotes the index associated with the ith element of the N-dimensional data set; the literal superscript denotes the component of $\underline{G}_i$ associated with the jth model parameter, $m_j(r)$. The vector $\underline{G}_i$ is called the Fréchet kernel (sometimes also called the 'data kernel' in the literature) and it is itself a member of $\mathcal{M}$. To first order in the perturbation $\|\delta \underline{m}\|$, we have

$$g_i[\underline{m}] - g_i[\underline{m}+\delta\underline{m}] = \langle \underline{G}_i, \delta \underline{m} \rangle \qquad (2.2.4)$$

For non-linear functionals, the Fréchet kernel $\underline{G}_i$ may also be a function of the model as well as the radius. It can be deduced that equation (2.2.3) is the functional equivalent of a Taylor expansion. Accepting the approximation of equation (2.2.4) is essentially a linearization of such an expansion, it must be remembered that Backus and Gilbert inversion is applicable to the class of Fréchet-differentiable functionals, and before one accepts the results of linear analysis, one must decide whether the functional being studied belongs to this class. For example, Wiggins (1972) has suggested that the Fréchet kernels associated with free-oscillation data and surface wave data are 'slowly-varying' functions of the model. In contrast, the Fréchet kernels associated with seismic body-waves are 'rapidly-varying' with respect to change in model parameters.

The Backus-Gilbert approach involves two useful procedures. Firstly, one makes a judicious guess for a model; that is, one makes a guess which is sufficiently close to a model exactly satisfying the data. Then, with knowledge of the Fréchet kernel, one can approach systematically 'closer' to this exact solution. One means 'closer' in a least-squares sense of minimizing the sum of the squares of the residuals formed by subtracting a theoretical response for a guessed model from the actual measured response.

The second procedure allows us to understand the quality of resolution associated with a given set of data and a given acceptable model. Although the set of acceptable models constitutes an infinite set, it may be that the elements of this set differ from each other by fine structure which a given finite data set cannot well resolve. In fact, this local non-uniqueness may be exploited to give some idea of the degree to which a given set of data can resolve a given model. Limitations of the procedure arise when one faces the problem of separating the ambiguities due to the inherent inadequacy of the data, and the ambiguities which may arise from the discounting of non-linear effects in equation (2.2.4).

b. The least-squares procedure

The least-squares procedure is described by Backus and Gilbert (1967). If a model $\underline{m}_0$ is guessed to be a

model which fits the data to some observed degree of approximation, one can seek to improve this guess by minimizing the quantity $\| \underline{m} - \underline{m}_0 \|^2$, where $\underline{m}$ is an element of $\mathcal{M}_E$, the space of models which exactly satisfy equation (2.2.2). Thus the minimization is subject to side-constraints that the models explored satisfy the data. The problem is formulated as a standard variational problem. We form the function U

$$U = \| \underline{m} - \underline{m}_0 \|^2 - \sum \nu_i (g_i[\underline{m}] - \gamma_i) \qquad (2.2.5)$$

where $\{\nu_i\}$ constitutes a set of N Lagrange multipliers. We take the variation of U,

$$\delta U = 2(\underline{m} - \underline{m}_0) . \delta \underline{m} - \sum \nu_i \, \underline{G}_i . \delta \underline{m} \qquad (2.2.6)$$

-- where the dot indicates the scalar product between the vectors $\underline{G}_i$ and $\delta \underline{m}$. Equation (2.2.6) can be expressed in our previously established notation as

$$\delta U = 2 \langle \underline{m} - \underline{m}_0, \delta \underline{m} \rangle - \sum \nu_i \langle \underline{G}_i , \delta \underline{m} \rangle \qquad (2.2.7)$$

For a stationary solution, we set $\delta U = 0$ and redefine the Lagrange multipliers to obtain

$$\langle (\underline{m} - \underline{m}_0 - \sum \nu_i \, \underline{G}_i), \delta \underline{m} \rangle = 0 \qquad (2.2.8)$$

Since we consider the components of $\delta \underline{m}$ to be linearly independent of each other (otherwise we could eliminate some from the parameterization) we can conclude

$$\underline{m} = \underline{m}_0 + \sum \nu_i \, \underline{G}_i \qquad (2.2.9)$$

This equation implies that if our stationary solution is a

minimum, an acceptable model is more exactly given by equation (2.2.9). However, we must yet identify the N-tuple of Lagrange multipliers $\{\nu_i\}$. To do this, one appeals to the definition of Fréchet differentiability, letting the perturbation be represented by $\underline{m} - \underline{m}_0$, thus

$$g_j[\underline{m}] - g_j[\underline{m}_0] = \langle \underline{G}_j, m-\underline{m}_0 \rangle \qquad (2.2.10)$$

Eliminating $\underline{m}$ from this equation (with the aid of equation (2.2.9)) we obtain for the residual $\gamma_j - g_j(\underline{m}_0)$:

$$\gamma_j - g_j[\underline{m}_0] = \langle \underline{G}_j, \sum \nu_i \underline{G}_i \rangle = \sum \nu_i \langle \underline{G}_i, \underline{G}_j \rangle \qquad (2.2.11)$$

We can express this equation in operator notation by defining the i-j th element of the matrix $\underline{\underline{\Gamma}}$ by $\Gamma_{ij} = \langle \underline{G}_i , \underline{G}_j \rangle$; the jth element of the residual vector is defined

$$\Delta g_j \equiv \gamma_j - g_j[\underline{m}_0]$$

and finally the N-tuple $\{\nu_i\}$ is expressed as a vector $\underline{\nu}$, so we have

$$\Delta \underline{g} = \underline{\underline{\Gamma}}\ \underline{\nu} \qquad (2.2.12)$$

The elements of $\Delta \underline{g}$ are the differences between the data computed from a guessed model, $\underline{m}_0$, and the actual measured data. If $\underline{\underline{\Gamma}}$ is identified for a particular set of data functionals (and, in the case of non-linear data, for the particular model $\underline{m}_0$ since the $\underline{G}_i$'s in the matrix are model-dependent) then the set of multipliers $\underline{\nu}$ can in principle be found. The matrix called the inner-product matrix, is symmetric and positive definite. It may,

however, be ill-conditioned, i.e. nearly singular; but in well-conditioned situations, the inverse $\underline{\underline{\Gamma}}^{-1}$ can be found directly (for example, using Gauss elimination on a computer), thus $\underset{\sim}{\gamma}$ can be discovered from

$$\underset{\sim}{\gamma} = \underline{\underline{\Gamma}}^{-1} . \underline{\Delta g} \qquad (2.2.13)$$

Hence the improved model $\underline{m}$ can be found from equation (2.2.9).

If the problem were linear, the least squares problem would be solved by the discovery of $\underline{m}$ from (2.2.9). In the non-linear problem we use the 'closer' model computed from (2.2.9) as a new starting model in what is to become the next iteration of an iterative least-squares procedure. Since the Fréchet-kernel may be dependent on the model, $\underline{\underline{\Gamma}}$ must be recomputed during each iteration of the procedure. If the original initial guess was sufficiently close to an exactly acceptable model, successive iterations should converge.

c. Resolution

If we have found by the foregoing procedure an exactly fitting model, this in itself is not completely satisfying since the solution to the variation problem is fundamentally non-unique. That is, the space of acceptable models is infinite. At this stage, it should be emphasized, we are not even considering the scatter and uncertainty associated with erroneous real data. For an exactly determined set of data there is an infinity of

models which can satisfy equation (2.2.2). Having found one such model does not complete the inverse problem -- one would like to learn something about the space of acceptable models.

We shall formally separate 'non-uniqueness' into two categories: the first which is quasi-linear in a precisely defined sense; the second is associated with acceptable models not falling into the first category. For non-linear problems, the space of acceptable models falling into the first category may itself be a subspace of the total space of acceptable models. Models in the second category can be described as 'globally distinct models' and they arise out of the non-linearity of the functional space $\mathcal{G}$. Backus-Gilbert formalism is powerless to address the contribution this latter set might make to the overall non-uniqueness of $\mathcal{M}_E$.

One could have observed in equation (2.2.8) there can exist a non-zero model $\underline{m}_\perp$ satisfying $\langle \underline{m}_\perp, \delta\underline{m} \rangle = 0$; in this case one could write for (2.2.9)

$$\underline{m} = \underline{m}_0 + \sum \nu_i \underline{G}_i + \beta \underline{m}_\perp \qquad (2.2.14)$$

where β is an arbitrary small parameter which, because of (2.2.8) does not explicitly enter the variational least-squares problem which has been discussed. We might note as well that (2.2.9) implies $\langle \underline{m}_\perp, \underline{G}_i \rangle = 0$. By selecting various values of β in (2.2.14), a family of N-tuples $\{\nu_i\}$ can be constructed which, to a first-order degree

in β encompass a degree of non-uniqueness in a solution set $\underline{m}$. The coefficients $\{\nu_i\}$ are determined by the single parameter β, and can be written with functional dependence $\{\nu_i(\beta)\}$ as can the model itself, $m(\beta)$. If β is changed to $\beta + \delta\beta$ a model $m(\beta)$ is changed to $m(\beta + \delta\beta)$ and if $m(\beta)$ is an exactly acceptable model, $m(\beta + \delta\beta)$ is also an exact solution to (2.2.2). Thus β generates a one-parameter family of exact solutions, and the curve in the model space satisfies

$$\underline{m}(\beta) = \underline{m}^0 + \beta \underline{m}_\perp + 0(\beta^2)$$

where $\underline{m}^0$ is the solution to (2.2.2) if $\beta = 0$. This is the solution represented by equation (2.2.9) which results from the least-squares procedure. The Backus-Gilbert procedure isolates a one-parameter family of exact solutions; and the non-uniqueness associated with this family (as long as β is small and $0(\beta^2) \approx 0$) can be explored. If we define $\mathcal{G}$ as the linear space formed by the set of N independent Fréchet kernels $\{\underline{G}_1, \underline{G}_2, \ldots\ldots, \underline{G}_N\}$, then we define the model curve $m(\beta)$ to be a space of $\mathcal{G}$-acceptable models.

This brings us to the second very valuable procedure developed by Backus and Gilbert (1968, 1970). They derived a procedure to assess quantatively the degree to which a given acceptable model can be resolved by the data. In the case of linear functionals the set of acceptable models is infinite, however if one confines

oneself to models which are $\mathcal{G}$-close (in the sense of the previous discussion) then one can actually exploit the local non-uniqueness to obtain some quantative idea of the ability of a given data set to resolve a model. In fact, for linear functionals, one can construct a model average entirely out of the surface data, together with a resolving length to be associated each local average.

One must be cautious when one applies the theory to non-linear problems, since non-uniqueness may arise from outside the range of $\mathcal{G}$-acceptable models around which one is constructing a local average.

We imagine our space of data functionals to consist of linearly-independent measurements; that is to say one measurement does not imply another. In what follows, one should make it clear that one is momentarily dealing with linear functionals. Thus, if we express equation (2.2.2) as an integral operator (such as 2.1.2)), we can write for scalar model m,

$$\gamma_i = \int m\, G_i\, dr \qquad (2.2.15)$$

and can think of our datum γ_i as some surface average of m(r), where G_i is a weighting function. If the N G_i's are indeed linearly independent, they form a complete space and a collection of averages of the form of equation (2.2.15) can be constructed by using linear combinations of the G_i's as new weighting functions. The value of such a 'surface average' will necessarily be equal to the

same linear combination formed out of the surface data. One such possible average of the model can be expressed as

$$\sum a_i \gamma_i = \int m(r) \sum a_i G_i(r)\, dr \qquad (2.2.16)$$

We define the linear combination of the Fréchet kernels as an 'averaging kernel', $A(r) \equiv \sum a_i G_i(r)$. In view of the scope for constructing advantageous and meaningful averages of the model, one possible approach would be to seek an average which would itself signify a 'local average' of the model at some depth, say r_0. Such an average would be formed out of the encompassment of the data. We should like to form a local average $\langle m \rangle_{r_0}$ by seeking a function $A(r,r_0)$ such that

$$\langle m \rangle_{r_0} = \int m(r)\, A(r,r_0)\, dr \qquad (2.2.17)$$

where $\langle m \rangle_{r_0}$ indicates a model average centred at some depth r_0. Such an averaging kernel would have to resemble the Dirac-delta function centred at r_0, i.e. $A(r,r_0) \approx \delta(r-r_0)$. If $A(r,r_0)$ were such a delta-function then

$$\langle m \rangle_{r_0} = \sum a_i \gamma_i \qquad (2.2.18)$$

Thus for linear functions one has in this procedure a method whereby one can construct a local average of the model (an average centred at r_0) out of the surface data set. The success of this procedure depends upon one's ability to find an optimum set of coefficients $\{a_i\}$ which will give to the linear combination $A(r,r_0)$ the appearance

of a delta-function, $\delta(r - r_0)$. That is, one hopes for a weighting function with a sharp peak at $r = r_0$, and enclosing a very small area beneath the curve where $r \neq r_0$, i.e. nearly zero side-bands to the distribution. We also ask that the function $A(r,r_0)$ resemble the delta-function in that it be unimodular, that is

$$\int A(r,r_0)\, dr = 1 \qquad (2.2.19)$$

The matter of finding the optimum $A(r,r_0)$ can be posed as a variational problem in a number of different ways. For example, one can seek to minimize directly the quantity

$$D_1(r_0) = \int |\delta(r-r_0) - A(r,r_0)|^2\, dr \qquad (2.2.20)$$

and the min $\{D_1(r_0)\}$ will thus be a measure of the closeness of $A(r,r_0)$ to the delta-function. An unfortunate aspect of this formulation of the problem, is that min $\{D_1(r_0)\}$ cannot be evaluated explicitly (Oldenburg, 1976a)since the integral of the square of the delta function is not defined. However Gilbert (1973) offers a non-rigorous argument around the problem.

Backus and Gilbert offer an alternative approach to the essential minimization required for equation (2.2.17). The area enclosed by the side-bands associated with a delta-like weighting function is generally called the 'spread' of the distribution; clearly some freedom in defining such a quantity for a delta-like function is possible, but it can be expressed in approximate fashion by a functional of the form

$$s\,[A;r_0] = \int J(r,r_0)(A(r,r_0))^2\,dr \qquad (2.2.21)$$

where $J(r,r_0)$ can be chosen to be any function satisfying the two conditions that $J(r_0,r_0) = 0$, and that $J(r,r_0)$ increases monotonically as $|r - r_0|$ increases. Such a function will weight heavily the 'side wings' of a distribution and exclude the area adjacent to the point $r = r_0$. Thus to find a delta-like function we try to minimize the spread, at the same time insisting that the distribution be unimodular. The variational approach is to form V,

$$V = \int J(r,r_0)(A(r,r_0))^2 dr - \lambda\left[\int A(r,r_0)dr - 1\right] \qquad (2.2.22)$$

Forming the variational derivative with respect to the parameter a_j we have

$$\frac{\delta V}{\delta a_j} = 2\int J(r,r_0)\sum a_i G_i(r)G_j(r)dr - \lambda\int G_j(r)dr \qquad (2.2.23)$$

and the variation with respect to the parameter λ,

$$\frac{\delta V}{\delta \lambda} = \sum a_i \int G_i(r)\,dr - 1 \qquad (2.2.24)$$

For a stationary solution we set $\delta V/\delta a_j = 0$ for each parameter a_j, and $\delta V/\delta\lambda = 0$. We make the following compact definitions

$$\underline{a} = (a_1, a_2, \ldots, a_N)^T \qquad (2.2.25)$$

and

$$\underline{b} = (b_1, b_2, \ldots, b_N)^T$$

where

$$b_i = \int G_i(r)\, dr$$

The matrix S is defined with elements

$$S_{ij} = \int J(r,r_0)\, G_i(r)\, G_j(r)\, dr$$

Finally we set $\lambda = \lambda/2$. Thus equations (2.2.23) and (2.2.24) for a stationary solution imply

$$\underline{\underline{S}} \cdot \underline{a} = \lambda\, \underline{b} \qquad (2.2.26)$$

together with the implication of the unimodular condition

$$\underline{a} \cdot \underline{b} = 1$$

Solving these N + 1 equations for the N a_i's and the parameter λ we find

$$\underline{a} = \underline{\underline{S}}^{-1} \cdot \underline{b} \;/\; \underline{b} \cdot \underline{\underline{S}}^{-1} \cdot \underline{b} \qquad (2.2.27)$$

The optimal vector $\underline{a}$ may depend very much on the choice of $J(r,r_0)$, i.e. on the way one defines the spread of the distribution. Backus and Gilbert (1968) outline a variety of 'delta-ness criteria'; this involves choosing a variety of $J(r,r_0)$ including inverted box-cars centred at r_0. An equivalent expression for equation (2.2.22) which is analogous to the expression (2.2.20) is (from Oldenberg (1976a)).

$$D_2(r_0) = 12 \int \left| H(r-r_0) - \int A(r',r_0)dr' \right|^2 dr \qquad (2.2.28)$$

where $H(r-r_0)$ is a Heaviside step-function. Condition (2.2.20) can be called the first Dirichelet condition, and

condition (2.2.28) the second Dirichelet condition. The factor 12 in this condition is chosen so that a box-car shaped averaging kernel of width ℓ and height $1/\ell$ implies $D_2(r_0) = \ell$. The Backus-Gilbert 1970 paper concentrates on the simple delta-ness criteria which arise when one chooses $J(r,r_0) = (r-r_0)^2$. In this case spread is defined (again, including the conventional factor 12)

$$s[A;r_0] = 12 \int (r-r_0)^2 A(r,r_0)\, dr \qquad (2.2.29)$$

The centre of the distribution $A(r,r_0)$ is defined

$$c(A) = \int r\, A(r,r_0)^2\, dr \,/\, \int A(r,r_0)^2\, dr \qquad (2.2.30)$$

This is the point from which the spread from r_0 is least. In fact this spread from the centre c(A) is called the width, $w(A) = s[A;c]$. Hence it can be deduced that the spread at r_0 is

$$s[A;r] = w(A) + 12(r_0-c(A))^2 \int A(r,r_0)^2 dr \qquad (2.2.31)$$

where it can be seen that the spread consists of a contribution from the width of the distribution, and a contribution from the displacement of the centre c(A) from r_0. If, upon inspection of the optimum averaging kernel $A(r,r_0)$, it is indeed found to be delta-like, i.e. $s[A;r_0] \ll 1$, then

$$\int m(r)\, A(r,r_0)\, dr$$

would constitute a local average of the m(r) over an interval of length w(A) and centred at c(A). If however

$s[A;r_0]$ is not much less than one and the averaging kernel is broad, and if r_0 is severely displaced from c(A), then one must conclude that the given set of data cannot well determine the model at that depth. If $s[A;r_0] \ll 1$ we say that the set of data functionals $\mathcal{G}$ is mean decisive. If $s[A;r_0]$ is not much less than 1, we say $\mathcal{G}$ is mean indecisive.

Choosing as Backus and Gilbert do, $J(r,r_0) = (r-r_0)^2$, and including the factor 12 in front of definition (2.2.29), we make the following additional definitions

$$S_{ij}^{(0)} = 12 \int G_i(r)G_j(r)\, dr$$

$$S_{ij}^{(1)} = 12 \int r\, G_i(r)G_j(r)\, dr \qquad (2.2.32)$$

$$S_{ij}^{(2)} = 12 \int r^2\, G_i(r)G_j(r)\, dr$$

With these we see that

$$S_{ij}(r_0) = r_0^2 S_{ij}^{(0)} - 2r_0 S_{ij}^{(1)} + S_{ij}^{(2)}$$

$$S(r_0,A) = \underline{a}\cdot\underline{\underline{S}}\cdot\underline{a}$$

$$c(A) = \underline{a}\cdot\underline{\underline{S}}^{(1)}\cdot\underline{a} \;/\; \underline{a}\cdot\underline{\underline{S}}^{(0)}\cdot\underline{a} \qquad (2.2.33)$$

$$w(A) = \underline{a}\cdot\underline{\underline{S}}^{(2)}\cdot\underline{a} - (\underline{a}\cdot\underline{\underline{S}}^{(1)}\cdot\underline{a})^2 \;/\; \underline{a}\cdot\underline{\underline{S}}^{(0)}\cdot\underline{a}$$

Of course equation (2.2.14) is <u>untrue</u> if the functional g_i is non-linear. Thus it cannot be possible to construct a local average $\langle m \rangle_{r_0}$ directly out of the surface data $\{\gamma_i\}$ such as was accomplished in equation (2.2.18) for the linear case. However if one has a model

which one believes to be close to an exactly fitting model, then one can construct the model-dependent N-tuple $\{q_i\}$ where

$$q_i = \int m(r)\, G_i(r)\, dr \qquad (2.2.34)$$

and proceed with the analysis as previously. The local average will be given by

$$\langle m \rangle_{r_0} = \sum{}' a_i\, q_i \qquad (2.2.35)$$

instead of (2.2.18). Thus for non-linear problems the possibility of globally distinct solutions which do not contribute to $\langle m \rangle_{r_0}$ may render the local average rather less informative. The local average is itself constructed out of the space of $\mathcal{G}$-acceptable models as previously defined. The extent to which the set of $\mathcal{G}$-acceptable models approximates the total space of acceptable models is the extent of the efficacy of the theory. If two models m and m' are both $\mathcal{G}$-acceptable, they both satisfy

$$g_i(m) = g_i(m') + \int (m-m')\, G_i(r)\, dr + 0\|m-m'\|^2 ,$$

from the assumption of Fréchet differentiability. Since they both give rise to the same measured surface response, i.e. $g_i(m) = g_i(m')$, then

$$\int (m-m')\, G_i(r)\, dr = 0\|m-m'\|^2$$

Thus two model averages such as (2.2.34) constructed for m and m' will be the same to first order in $|m-m'|$ since

$$\sum a_i q_i' = \sum a_i q_i + O\|m-m'\|^2$$

Thus the space of $\mathcal{G}$-acceptable models share the same resolution characteristics (2.2.33) etc. The significance which can be attached to an average formed in this way must be conditioned by the possibility of acceptable models falling outside of $\mathcal{G}$-acceptability.

d. Experimental error

We here discuss briefly the fundamental aspects of including experimental error in the inversion formalism, preferring to leave a rather more geometrical discussion until Chapter 7. If one can attribute to a set of surface data $\{\gamma_i\}$ a corresponding set of error estimates, then this uncertainty in the data can contribute to the non-uniqueness of acceptable models. In fact Backus and Gilbert have shown that this error can be reflected in the resolution characteristics of a space of -acceptable models by introducing a further resolution characteristic: that of the error attached to a local average of the model, $\langle m \rangle_{r_0}$. From equation (2.2.18) it can be seen that error in γ_i, i.e. $\Delta\gamma_i = \gamma_i - \gamma_{exact}$ can be reflected in the local average by

$$\Delta \langle m \rangle_{r_0} = \sum a_i \Delta\gamma_i \qquad (2.2.36)$$

This suggests that the error in the surface data could be projected onto the model space. If m satisfies the erroneous data and model m_E satisfies the exact data (both

m_E and $\langle m_E \rangle_{r_0}$ are unknown of course), can one use knowledge of $\{\Delta\gamma_i\}$ to construct knowledge of the error in m_E, or more meaningfully of $\Delta\langle m_E\rangle$? Since

$$\Delta\langle m_E\rangle = \sum a_i \int (m-m_E)\, G_i(r)\, dr$$

and since we can write $\Delta\gamma_i = \gamma_i - \gamma_i^E$, then if m and m_E are $\mathcal{G}$-near

$$\Delta\gamma_i = \int (m-m_E)\, G_i(r)\, dr$$

We can infer from this relationship that error in the data is related to error in the model in a linear way, as long as one is confined to $\mathcal{G}$-close models. The experimental error is expressed in a N x N covariance matrix $\underline{\underline{E}}$ whose elements are

$$E_{ij} = \overline{\Delta\gamma_i\, \Delta\gamma_j} \qquad (2.2.37)$$

where the bar denotes the expectation value. Expressing the error in (2.2.36) in terms of this matrix, we can write

$$\varepsilon^2 = \sum a_i a_j E_{ij} \qquad (2.2.38)$$

where ε^2 is the square of the variance of the model average, i.e. $\varepsilon = \Delta\langle m_E\rangle_{r_0}$. The variance ε is the error committed by evaluating our model average using equation (2.2.18). We shall consider the covariance matrix $\underline{\underline{E}}$ to be symmetric, positive definite and in the case of statistically independent error estimates for our data, the matrix is diagonal.

Introducing the idea of error in the model local average also introduces a new degree of freedom in seeking optimum averaging kernels. We could, for example, seek to minimize the spread as before, however our variance would be given by substituting our optimum $\{a_i\}$ into equation (2.2.38). On the other hand, one could seek to minimize the error as expressed by equation (2.2.38) and in this case our spread would be determined by substituting the resulting $\{a_i\}$ into equation (2.2.33). Thus a useful approach might be to select a threshold spread, s_t, such that spreads s, $s < s_t$, are thought to be useful; for each s in this set we could inspect the associated error ε and perhaps find some optimum combination of spread and error.

For models varying over orders of magnitude, error in the model is most meaningfully represented by relative error, which for purposes of the Backus-Gilbert formalism is defined, as one might expect from the definition (2.2.38) and equation (2.2.35),

$$\varepsilon^2 = \sum a_i a_j E_{ij} / [\sum a_i q_i]^2 \qquad (2.2.39)$$

Backus and Gilbert show, largely by arguments made understandable by geometrical illustration, that the error $\varepsilon^2(A)$ is a monotonically increasing function of spread s(A). The problem of minimizing the error ε^2 for a range of spreads $s < s_t$ is expressed (analogously to equation (2.2.26)) as

$$(\underline{\underline{S}} + \alpha \underline{\underline{E}}) \cdot \underline{a} = \lambda \underline{b}$$

$$\underline{a} \cdot \underline{\underline{S}} \cdot \underline{a} = s \qquad (2.2.40)$$

$$\underline{b} \cdot \underline{a} = 1$$

where α and λ are scalar unknowns, and $\underline{a}$ is a vector unknown which can be uniquely determined for a chosen $s < s_t$. In fact, Backus and Gilbert demonstrate (relying strongly on their geometrical approach to the analysis) that the variable α is uniquely determined by s, and the problem is reduced to familiar form by choosing α as an independent variable (rather than s). Choosing $\alpha = w \tan\theta$, and defining $\underline{\underline{W}} = \underline{\underline{S}} \cos\theta + w \underline{\underline{E}} \sin\theta$, and $\lambda = \beta(\theta) \sec\theta$, then

$$\underline{\underline{W}}(\theta) \cdot \underline{a} = \beta \underline{b}$$

$$\underline{b} \cdot \underline{a} = 1 \qquad (2.2.41)$$

$$s = \underline{a} \cdot \underline{\underline{S}} \cdot \underline{a}$$

Solving for $\underline{a}(\theta)$, one determines $s = \underline{a}(\theta) \cdot \underline{\underline{E}}\ \underline{a}(\theta)$ and $\varepsilon^2(\theta) = \underline{a}(\theta) \cdot \underline{\underline{E}} \cdot \underline{a}(\theta)$ by varying θ between $0 \leq \theta \leq \frac{\pi}{2}$. In this range of θ one ranges between the pair $(\varepsilon^2_{max}, s_{min})$ for $\theta = 0$ (the value achieved by equation (2.2.18) previously) and the pair $(\varepsilon^2_{min}, s_{max})$ when $\theta = \frac{\pi}{2}$. The scalar w is a factor which can be chosen at will: it affects the convenience of parameterization in terms of θ; it however does not affect the shape of the curve of spread as a function of error.

This curve of spread as a function of error (or vice

versa) is called the trade-off curve, and Backus and Gilbert demonstrate this curve is continuous.

e. Ranking and winnowing

Gilbert (1971) introduced a very helpful sequel to the General Theory by observing that, if the Fréchet kernels were orthogonal, the formalism assumed a more simple form since the inner product matrix would become diagonal. The matter of orthogonalizing a set of linearly independent functions such as the N-tuple of Fréchet kernels, can be accomplished by standard techniques such as the Gramm-Schmidt technique. In the foregoing we use the prime to denote quantities which have been transformed into such an orthogonal frame.

One requires to find a matrix which diagonalizes the inner-product matrix, and this is achieved by a similarity transformation $\underline{\underline{T}}$ which is applied to $\underline{\underline{\Gamma}}$:

$$\underline{\underline{T}} \cdot \underline{\underline{\Gamma}} \cdot \underline{\underline{T}}^T = \underline{\underline{\Gamma}}' \qquad (2.2.42)$$

Here $\underline{\underline{\Gamma}}'$ is diagonal. The original matrix problem of equation (2.2.12) is similarly transformed from $\underline{\underline{\Gamma}} \cdot \underline{\nu} = \underline{\Delta g}$ into

$$\underline{\underline{T}}^T \cdot \underline{\underline{\Gamma}}' \cdot \underline{\underline{T}}\, \underline{\nu} = \underline{\Delta g}$$

or

$$\underline{\underline{\Gamma}}' \cdot \underline{\nu}' = \underline{\Delta g}' \qquad (2.2.43)$$

where $\underline{\nu}' = \underline{\underline{T}} \cdot \underline{\nu}$ and $\underline{\Delta g}' = \underline{\underline{T}} \cdot \underline{\Delta g}$. A possible orthogonal

transformation $\underline{\underline{T}}$ can be constructed out of the eigenvectors of the matrix $\underline{\underline{\Gamma}}$: the columns of $\underline{\underline{T}}$ will consist of these eigenvectors, and the diagonal elements of $\underline{\underline{\Gamma}}'$ will then be the corresponding eigenvalues of $\underline{\underline{\Gamma}}$, i.e. the set $\{\xi\}_i$. The solution to (2.2.43) in this case will be

$$\underline{\nu}' = \underline{\underline{\Gamma}}^{-1} \underline{\Delta g}'$$

or written in scalar form

$$\nu_j = \Delta g_j / \xi_j$$

Diagonalizing the inner product matrix is equivalent to orthogonalizing the N Fréchet kernels, and the orthogonal N-tuple of Fréchet kernels can be expressed as $G'_i(r)$, where $G'_i(r) = T_{ij} G_j(r)$. The model perturbation arising for a given iteration in the least-squares formalism (equation (2.2.9)) can now be expressed

$$\delta m = \sum_i \nu'_i G'_i(r)$$

$$= \sum_i \Delta g'_i G'_i(r) / \xi_i \qquad (2.2.44)$$

Also $\|\delta m\|^2$ can be expressed as

$$\|\delta m\|^2 = \sum_{ij} \nu'_i \nu'_j \int G'_i(r) G'_j(r)\, dr$$

$$= \sum_i \nu'^2_i / \xi_i \qquad (2.2.45)$$

If $\underline{\underline{\Gamma}}$ is poorly conditioned or nearly singular, some of its eigenvalues will be close to zero, thus making the perturbation (2.2.44) very large -- this in turn rendering

the iteration scheme unstable. Having orthogonalized the problem, however, one can choose to exclude near zero eigenvalues from equation (2.2.43) and thereby truncate the sums (2.2.44) or (2.2.45) to satisfy some preset stability criteria. One could for example insist that the sum of the squares of the residual decrease in subsequent iterations. With this application in mind it is advantageous to construct the transformation $\underline{\underline{T}}$ in such a way that the moduli of $\{\zeta_1, \zeta_2, \ldots, \zeta_N\}$ are ranked in descending order of magnitude. Truncation of (2.2.45) to achieve stability would then imply the exclusion of small eigenvalues in (2.2.43). Gilbert calls this procedure 'winnowing' and it has the effect of discarding various pieces of transformed data, $\Delta g'_i$, from a given iteration. Since the transformed data are linear combinations of the original data, winnowing will imply some loss of information but it could be argued that it is information which is anyway inaccessible.

Another advantage of this procedure is the simplification offered to the matrix equation (2.2.41) by diagonalizing the matrix $\underline{\underline{S}}$. The vector equation transforms to the scalar equations

$$a_i = b_i/(s_i \cos\theta + w_i \sin\theta) \qquad (2.2.46)$$

and

$$\lambda = 1 \Big/ \sum_i \frac{b_i^2}{s_i \cos\theta + w_i \sin\theta} \qquad (2.2.47)$$

We have assumed $\underline{\underline{E}}$ to be diagonal already in our discussion. However, should the covariance matrix not be diagonal (and the elements of the data set $\{\gamma_i\}$ not be statistically independent) Gilbert (1971) presents a scheme to diagonalize both $\underline{\underline{E}}$ and $\underline{\underline{\Gamma}}$ simultaneously

2.3 The Lanczos Formulation

An alternative approach to the inversion of geophysical data is that developed by Lanczos (1961). We briefly include here a description of this method which is based upon Jackson's (1972) analysis of the Lanczos problem, and we use Jackson's notation in what follows. Our intention is that of making a complete discussion of the inversion problem, and to give some perspective to the concepts of Backus and Gilbert. Jackson poses the inverse problem as one of inferring a set of M unknown discrete model parameters $\{x_j\}$ from a set of N surface measurements $\{y_i\}$. If the data and model are related to each other by a linear operator, $\underline{\underline{A}}$, one can write the relationship directly as

$$\underline{y} = \underline{\underline{A}} \cdot \underline{x} \qquad (2.3.1)$$

If the functional is non-linear, one can make a Taylor expansion of each datum with respect to each model parameter about some model $\{x_j^0\}$,

$$y_i = A_i(x_j^0) + \left[\frac{\partial A_i}{\partial x_j}\right]_{x_j^0} \Delta x_j + \ldots \qquad (2.3.2)$$

Assuming Δx_j is sufficiently small, and assuming the higher-order contributions to (2.3.2) can be neglected, we can write this expansion to first order as

$$y_i = A_{ij} x_j \tag{2.3.3}$$

where we redefine y_i, m_j, and A_{ij} to conform to the previous notation of equation (2.3.1) by

$$y_i = y_i - A_i(x_j^0)$$

$$x_j = \Delta x_j$$

$$A_{ij} = \partial A_i / \partial x_j \Big]_{x_j^0}$$

The N x M matrix $\underline{\underline{A}}$ is called the Jacobian matrix of the data functional. If we operate on equation (2.3.3) by a M x N inverse matrix $\underline{\underline{H}}$, we can construct a theoretical model vector $\hat{\underline{x}}$ given by

$$\hat{\underline{x}} = \underline{\underline{H}} \cdot \underline{\underline{A}} \cdot \underline{x} = \underline{\underline{H}} \cdot \underline{y} \tag{2.3.4}$$

To construct a satisfactory inverse operator $\underline{\underline{H}}$, requires that $\underline{\underline{A}}$ be well-conditioned and non-singular, and this in turn may suggest conditions required of the data set or of the model parameterization. In general the operators $\underline{\underline{A}}$ appearing in geophysical problems are not necessarily well-conditioned, and the problem of constructing an inverse $\underline{\underline{H}}$ assumes fundamental significance. We consider an operator $\underline{\underline{H}}$ to constitute a 'good inverse' if it satisfies the following criteria:

a.) If we operate on the left of each term in

equation (2.3.3) by $\underline{\underline{A}}$ we obtain

$$\underline{\underline{A}} \cdot \hat{\underline{x}} = \underline{\underline{A}} \cdot \underline{\underline{H}} \cdot \underline{y}$$

and if the operator $\underline{\underline{A}}\,\underline{\underline{H}} = \underline{\underline{I}}_N$, i.e. the N x N identity matrix, then the inferred model $\hat{\underline{x}}$ satisfies the data $\underline{y}$. Therefore the closeness of $\underline{\underline{A}}\,\underline{\underline{H}}$ to $\underline{\underline{I}}_N$ is an indication of the degree to which the model $\hat{\underline{x}}$ fits the data.

b.) From equation (2.3.4) if $\underline{\underline{H}}\,\underline{\underline{A}} = \underline{\underline{I}}_M$, the M x M identity matrix, then $\hat{\underline{x}} \cong \underline{x}$, i.e. the inferred model $\hat{\underline{x}}$ approximates the exact model $\underline{x}$. Of course if $\underline{\underline{H}} \cdot \underline{\underline{A}}$ is not exactly an identity $\underline{\underline{I}}_M$, each $\hat{x}_i$ is effectively a linear combination of the x_j's, the coefficients of this combination hopefully centred around the diagonal of $\underline{\underline{H}} \cdot \underline{\underline{A}}$. Thus closeness to the identity matrix of $\underline{\underline{H}} \cdot \underline{\underline{A}}$ can be considered a measure of the resolution with which surface data functionals can infer the model $\hat{\underline{x}}$.

c.) The uncertainties in $\hat{\underline{x}}$ must be sufficiently small, i.e.

$$\text{var}\,(\hat{x}_k) = \sum_{i=1}^{N} H_{ki}^{\,2}\,(\text{var}\; y_i)$$

(where var (y_i) is the statistical uncertainty attached to the surface data) must be small.

We now recall the transformation suggested in Section 2.2.d whereby the Fréchet kernels are made orthogonal and the inner product matrix as a consequence becomes diagonal with its N non-zero entries being the eigenvalues associated with $\underset{\sim}{\Gamma}$. To pursue the same idea in connection with equation (2.3.3), a more general inverse technique is required since $\underline{\underline{A}}$ is not square. Lanczos (1961) defines two eigenvectors associated with $\underline{\underline{A}}$ such that

$$\underline{\underline{A}} \cdot \underline{v}_j = \lambda_{(j)} \cdot u_j$$

and (2.3.5)

$$\underline{\underline{A}}^T \underline{u}_i = \lambda_{(i)} \underline{v}_i$$

and these imply

$$\underline{\underline{A}}^T \underline{\underline{A}} \underline{v}_j = \lambda^2_{(j)} \underline{v}_j$$

and (2.3.6)

$$\underline{\underline{A}} \underline{\underline{A}}^T \underline{u}_j = \lambda^2_{(i)} \underline{u}_i$$

It will be assumed (as in Section 2.2.d) that the eigenvalues are ranked in descending order of magnitude. Lanczos proves that there exists an integer p $\leq$ min M,N such that $\lambda_{(i)} = \lambda_{(j)}$, i = j, and i,j $\leq$ p, and $\lambda_{(i)} = 0$, $\lambda_{(j)} = 0$ if i,j $>$ p. Thus equations (2.3.6) possess p non-zero eigenvalues in common. The matrix $\underline{\underline{A}}$ is factored

$$\underline{\underline{A}} = \underline{\underline{U}} \, \underline{\underline{\Lambda}} \, \underline{\underline{V}}^T \qquad (2.3.7)$$

where $\underline{\underline{\Lambda}}$ is a p x p diagonal matrix of eigenvalues; the columns of $\underline{\underline{U}}$ consist of the eigenvectors $\underline{u}_i$ (corresponding

to non-zero eigenvalues) and has dimension N x p; the columns of $\underline{\underline{V}}$ similarly consist of the p eigenvectors $\underline{v}_j$ (corresponding to non-zero eigenvalues) and has dimension M x p.

Jackson complements the matrix equation (2.3.7) by defining the matrix of eigenvectors $\underline{u}_i$, $p < i \leq N$ corresponding to zero eigenvalues: $\underline{\underline{U}}_0$. Similarly $\underline{\underline{V}}_0$ is constructed from eigenvectors $\underline{v}_j$ corresponding to zero eigenvalues, and he observes the following relationships

$$\underline{\underline{U}}^T \underline{\underline{U}} = \underline{\underline{I}}_p \qquad \underline{\underline{V}}^T \underline{\underline{V}} = \underline{\underline{I}}_p$$

$$\underline{\underline{U}}_0^T \underline{\underline{U}}_0 = \underline{\underline{I}}_{N-p} \qquad \underline{\underline{V}}_0^T \underline{\underline{V}}_0 = \underline{\underline{I}}_{M-p} \qquad \text{and} \qquad (2.3.8)$$

$$\underline{\underline{U}}^T \underline{\underline{U}}_0 = 0 \qquad \underline{\underline{V}}^T \underline{\underline{V}}_0 = 0$$

$$\underline{\underline{U}}_0^T \underline{\underline{U}} = 0 \qquad \underline{\underline{V}}_0^T \underline{\underline{V}} = 0$$

He also observes that the set of N eigenvectors $\{\underline{u}_i\}$ is complete, and they can be used as a basis set in order to expand $\underline{y}$ as a linear combination of eigenvectors, i.e.

$$\underline{y} = \sum_{K=1}^{N} \beta_K \underline{u}_K$$

If the terms of this linear combination are separated into those eigenvectors in $\underline{\underline{U}}$, and those in $\underline{\underline{U}}_0$, one can write this as

$$\underline{y} = \underline{\underline{U}}\,\underline{\beta} + \underline{\underline{U}}_0\,\underline{\beta} \qquad (2.3.9)$$

where $\underline{\beta}_0 = \underline{\underline{U}}_0^T \underline{y}$, $\underline{\beta} = \underline{\underline{U}}^T \underline{y}$. Similarly, the model $\underline{x}$ can be expressed as a linear combination of the $\underline{v}_i$'s:

$$\underline{x} = \underline{\underline{V}}\,\underline{\alpha} + \underline{\underline{V}}_0\,\underline{\alpha}_0 \qquad (2.3.10)$$

If we consider $\underline{\underline{A}}$, $\underline{y}$, and $\underline{x}$ as are represented in (2.3.1) for the moment, the classical 'least-squares' problem is that of minimizing a data residual defined by $\underset{\sim}{\xi}_r = \underline{\underline{A}}\,\underline{x} - \underline{y}$. Our decomposition of $\underline{\underline{A}}$ in this case would imply for the square of the residual

$$|\underline{\xi}_r \underline{\xi}_r^T| = |\underset{\approx}{\Lambda}\,\underline{\alpha} - \underline{\beta}|^2 + |\underline{\beta}_0|^2 \qquad (2.3.11)$$

We note that this is <u>not</u> the residual involved in the procedure of Section 2.2.b. The least square of the data residual $|\xi_r|^2$ is thus achieved when $\underline{\beta} = \underset{\approx}{\Lambda}\,\underline{\alpha}$, with an error of $|\beta_0|^2$. Three cases can be isolated, depending upon the dimension of $\underset{\approx}{\Lambda}$.

If $p < N$, the solution will only be an exact solution if $\underline{\beta}_0 = 0$, i.e. if $\underline{\underline{U}}_0^T\,\underline{y} = 0$, and the operator $\underline{\underline{U}}_0^T$ annihilates the data. This implies that the system will only admit an exact solution if the vectors $\underline{u}_i$ and $\underline{y}$ are mutually perpendicular for $i = p+1 \ldots, N$. Jackson describes this system as overconstrained: the situation can, for example, arise if the model parameterization is too restrictive, or if the data admits inconsistencies.

Since $\underline{\alpha}_0$ does not appear in the classical least-squares solution equation (2.3.11), it may be chosen at will. The arbitrariness of the vector $\underline{\alpha}_0$ implies some degree of non-uniqueness in the solution to the least-squares problem, since from equation (2.3.10) an arbitrary $\underline{\alpha}_0$ lends a range of arbitrariness to $\underline{x}$. Jackson calls

this the underdetermined case; it may arise if the parameterization of the model contains too many degrees of freedom for the size of the corresponding data set.

Finally, if p < M and p < N, then there may not be admitted an exact solution to the classical least-squares problem. However, there still may exist an infinity of models satisfying equation (2.3.11). This implies a system both overconstrained and underdetermined.

We return now to the $\underline{\underline{A}}$, $\underline{y}$, and $\underline{x}$ as they are defined for equation (2.3.3). The generalized inverse as derived by Lanczos, which is associated with equation (2.3.3) is

$$\underline{\underline{H}}(L) = \underline{\underline{V}}\ \underline{\underline{\Lambda}}^{-1}\ \underline{\underline{U}}^{T} \qquad (2.3.12)$$

which is analogous to equation (2.3.4); we infer a model $\hat{\underline{x}}(L)$

$$\hat{\underline{x}}(L) = \underline{\underline{V}}\ \underline{\underline{\Lambda}}^{-1}\ \underline{\underline{U}}^{T}\ \underline{y} \qquad (2.3.13)$$

Jackson shows that this inverse supplies a least-squares solution which minimizes

$$|\underline{x}|^2 = |\underline{\underline{\Lambda}}^{-1}\underline{\beta}| + |\underline{\alpha}_0|^2 \qquad (2.3.14)$$

since $\underline{\alpha}_0 = \underline{\underline{V}}_0^{T}\ \hat{\underline{x}}(L) = 0$, and $\underline{\alpha} = \underline{\underline{V}}^{T}\ \hat{\underline{x}}(L) = \underline{\underline{\Lambda}}^{-1}\underline{\beta}$. If $\underline{x}$ is the model perturbation in an iterative scheme, the generalized Lanczos inverse minimizes this perturbation by finding a solution for which $\underline{\alpha}_0 = 0$. The vector $\underline{\alpha}_0$ is closely related to the normal model vector $\underline{m}_\perp$ which appears in equation (2.2.14).

For an overconstrained problem, Jackson proves that the solution to the classical least-squares problem (2.3.11) is identical to that achieved for (2.3.14); for the more general case of an overconstrained and underdetermined problem, the Lanczos inverse always exists, whereas the inverse to the classical problem may not always exist. For the purely overconstrained problem, the solution $\underline{\hat{x}}$ is expressible as

$$\underline{\hat{x}} = [\underline{\underline{A}}^T \underline{\underline{A}}]^{-1} \underline{\underline{A}}^T \underline{y}$$

however if the system is also underdetermined, the matrix $\underline{\underline{A}}^T\underline{\underline{A}}$ will be singular, so a solution satisfying the least-squares criterion that (2.3.11) be a minimum may not exist; however one can still discover a solution $\underline{\hat{x}}_{(L)}$ which minimizes the Lanczos least-squares criterion (2.2.14).

At the outset of this Section, we outlined criteria for a 'good inverse', $\underline{\underline{H}}$. The Lanczos inverse satisfies these criteria since we define the resolution matrix, $\underline{\underline{R}}$, as

$$\underline{\underline{R}} = \underline{\underline{H}}_{(L)} \underline{\underline{A}} = \underline{\underline{V}} \underline{\underline{\Lambda}}^{-1} \underline{\underline{U}}^T \underline{\underline{U}} \underline{\underline{\Lambda}} \underline{\underline{V}}^T = \underline{\underline{V}} \underline{\underline{V}}^T \qquad (2.3.15)$$

and it is optimized by $\underline{\hat{x}}_{(L)}$ since each row, r_k, is optimally close to the row of a corresponding M x M identity matrix $\underline{\underline{I}}_M$. The information density matrix $\underline{\underline{S}}$ is defined

$$\underline{\underline{S}} = \underline{\underline{A}} \cdot \underline{\underline{H}}_{(L)} = \underline{\underline{U}}\ \underline{\underline{U}}^T \qquad (2.3.16)$$

it is also optimum in the same sense that each row s_k is optimally close to the corresponding row of an N x N identity matrix $\underline{\underline{I}}_N$.

Analogous to the discussion of Section 2.2.d one can also construct a Lanczos inverse which minimizes

$$\underline{\varepsilon}_r^T \cdot \underline{\underline{F}} \cdot \underline{\varepsilon}_r$$

where $\underline{\underline{F}}$ is a covariance matrix identified with the experimental data. One can also seek to minimize $\underline{\varepsilon}_r^T \cdot \underline{\underline{F}} \cdot \underline{\varepsilon}_r$ <u>together</u> with $\underline{x} \cdot \underline{x}^T$.

The third criterion for a 'good inverse' states that the model variance should be small. This variance is defined by

$$\text{var } (\hat{x}_k) = \sum H_{ki}^2 \ (\text{var } y_i)$$

and using the Lanczos inverse from (2.3.12) and forming $\underline{\underline{H}}_{(L)}\ \underline{\underline{H}}_{(L)}^T$ we have

$$\text{var } (\hat{x}_{(L)_k}) = \sum_{j=1}^{p} \left(\frac{V_{kj}}{\lambda_j}\right)^2 \qquad (2.3.17)$$

for var $y_i = 1$. The smallest non-zero eigenvalues may make the variance unacceptably large, so one can truncate the sum so that

$$\sum_{j=1}^{q} \left(\frac{V_{kj}}{\lambda_j}\right)^2 < t_k \qquad q < p$$

where t_k is some threshold value for the variance. The effect of using some q smaller than p is to reduce the

number of eigenvectors in $\underline{\underline{U}}$ and $\underline{\underline{V}}$ and augment $\underline{\underline{U}}_0$ and $\underline{\underline{V}}_0$. This increases the constraints on the system, and increases the non-uniqueness, and thus effectively degrades resolution and information density in exchange for stability in an iterative scheme. The choice of q is thus a trade-off completely analogous to that associated with the ranking and winnowing procedures outlined in Section 2.2.e.

CHAPTER 3

THE ELECTROMAGNETIC INVERSE PROBLEM

3.1 Useful Aspects of the 'Forward Problem'

In order to apply the Backus-Gilbert generalized inversion procedure which has been outlined in the previous Chapter to a specific non-linear geophysical data functional, one must cast the variation of each datum into a form resembling equation (2.2.3). Since it is this equation which embodies the linearization associated with linear inverse theory, caution must be exercised and some effort made towards inspecting the possible implications of linearization to the inverse problem.

Thus, towards posing the inverse problem associated with the non-linear problem of inferring conductivity from the inductive response of a body, we examine here some aspects of the direct (or forward) problem which are of significance to the inverse problem. We mean by the 'forward' problem the solving for the response, given a conductivity model. The 'inverse problem' is of course the reverse of this procedure.

a. The model space for induction problems

We are concerned with the prospect of inferring the distribution of electrical conductivity within the earth from knowledge of its inductive response to external

current sources. One is tempted to ask what other electrical parameters, if any, might enter into the inductive response.

Electromagnetic phenomena can be represented in terms of the vector electric field (or electric intensity), $\underline{E}$, and the magnetic field vector, $\underline{H}$, which satisfy the Maxwell equations

$$\begin{aligned} \nabla \times \underline{E} &= -\partial \underline{B}/\partial t \\ \nabla \cdot \underline{B} &= 0 \\ \nabla \times \underline{H} &= \partial \underline{D}/\partial t + \underline{J} \\ \nabla \cdot \underline{D} &= \rho_c \end{aligned} \tag{3.1.1}$$

where ρ_c is charge density. These equations must be satisfied together with the constitutive relations (for an electrically isotropic medium):

$$\underline{D} = \varepsilon \underline{E} \quad , \quad \underline{B} = \mu \underline{H} \quad , \quad \underline{J} = \sigma \underline{E} \tag{3.1.2}$$

where ε is the electrical permittivity (SI units: farad-m^{-1}); μ is the magnetic susceptibility (SI units: henry-amp^{-1}); and σ is the electrical conductivity (SI units: ohm^{-1}-m^{-1}). We shall be restricting our attention to regions which exclude source currents and charges. Thus we may set $\rho_c = 0$ in Maxwell's equations and observe that the divergence of both $\underline{B}$ and $\underline{D}$ (and thus from (3.1.2) of both $\underline{H}$ and $\underline{E}$) vanishes. At this stage we see that the set (ε, μ, σ) comprises the only model parameters which enter into the governing equations.

Equations (3.1.1) and (3.1.2) are consistent with $\underline{E}$ and $\underline{H}$ satisfying the following wave-type equations:

$$\nabla^2 \underline{E} - \mu\varepsilon\, \partial^2 \underline{E}/\partial t^2 - \mu\sigma\, \partial \underline{E}/\partial t = 0 \qquad (3.1.3)$$

and for magnetic variations, the inhomogeneous equation

$$\nabla^2 \underline{H} - \mu\varepsilon\, \partial^2 \underline{H}/\partial t^2 - \mu\sigma\, \partial \underline{H}/\partial t = f(\sigma) \qquad (3.1.4)$$

where $f(\sigma) = \frac{1}{\sigma} \nabla\sigma \times \nabla \times \underline{H}$.

In view of the long periods associated with induction phenomena, two approximations may be made in Maxwell's equations. If the period of oscillation, T, of an electromagnetic source is such that $T \gg \varepsilon/\sigma$, then $\partial \underline{D}/\partial t \ll \underline{J}$, and displacement current, $\partial \underline{D}/\partial t$, can be neglected from Maxwell's equations. Even for very small conductivities, with $\sigma \sim 10^{-10}$ ohm^{-1}m^{-1}, the inequality is satisfied for periods greater than a few seconds. In the free-space region, $\sigma = 0$, however $\partial \underline{D}/\partial t$ can still be ignored if the period of oscillation of the source is large compared with the time taken by electromagnetic waves to traverse the free-space region one is considering. This follows from the coupled inequalities

$$|\partial \underline{D}/\partial t| \ll |\text{curl } \underline{H}| \qquad \text{if} \quad T \gg \sqrt{\mu\varepsilon}\, L$$

where L is the scale of the inducing field. This condition is satisfied for problems associated with global fields if $T \gg 0.03$ sec. These two approximations reduce equations (3.1.3) and (3.1.4) to the diffusion equations:

$$\nabla^2 \underline{E} - \mu\sigma\, \partial \underline{E}/\partial t = 0 \qquad (3.1.5)$$

and

$$\nabla^2 \underline{H} - \mu\sigma \partial \underline{H}/\partial t = f(\sigma) \qquad (3.1.6)$$

and we see that electrical permittivitity no longer appears in the equations describing inductive response.

At this stage we shall also invoke the conclusion of Tozer (1959) who deduces from physical and geological considerations that magnetic susceptibility does not vary appreciably within the earth, and that it has a value close to its free-space value, μ_0. If we set $\mu \equiv \mu_0$ in equations (3.1.5) and (3.1.6), we find these equations depend upon only one of the constitutive model parameters, namely σ. The solution to (3.1.5) and (3.1.6) will of course still be a function of source parameters and the frequency of the inducing source.

The forward problem is one of solving (3.1.5) and (3.1.6) subject to the boundary conditions which must be satisfied by the six components of the vector fields across the surface boundary and across boundaries internal to the surface. These conditions may be summarized as the continuity of components of $\underline{B}$ normal to an interface, and the continuity of components of $\underline{H}$ and $\underline{E}$ tangential to an interface. If we confine ourselves to models which are spherically symmetric (or to conductivity distributions which are functions only of depth, and not of lateral position) the governing equations are further simplified since $f(\sigma) = 0$ in (3.1.6).

In the analysis which follows we shall be considering exclusively time-harmonic variations of the form $\exp\{i\omega t\}$. This allows one to suppress the time dependence of the vector fields from the notation. We can write

$$\underline{H}(\underline{r},t) = \underline{H}(r,0)e^{i\omega t} = \underline{H}(r)$$

in an equation like (3.1.6) if we replace the $\partial/\partial t$ operator with multiplication by $i\omega$.

b. Representations of the field

The representation of the electromagnetic field in terms of three components of the vector $\underline{E}$ and the three components of $\underline{H}$ in equations (3.1.5) and (3.1.6) is not a unique representation. From Maxwell's equations (3.1.1) one observes that $\underline{H}$ can be represented by the curl of any vector $\underline{A}$, and the corresponding $\underline{E}$-field can be expressed as $\underline{E} = -\nabla\phi - i\omega\underline{A}$ (for time-harmonic sources) where ϕ is any scalar function. In fact a family of such vectors $\underline{A}_i$ can be discovered by applying any number of transformations (called the Gauge transformations) of the form

$$\underline{A}_i = \underline{A} - \nabla\psi_i$$

where the set $\{\psi_i\}$ consists of arbitrary scalar functions. Since a representation in terms of $\underline{A}$ (called the 'magnetic vector potential') and (the 'scalar potential') has this degree of arbitrariness, one can choose a vector potential to satisfy the modified Lorenz condition,

$$\nabla \cdot \underline{A} + \mu\sigma\phi = 0$$

whereupon $\underline{A}$ and ϕ both satisfy the diffusion equations

$$\begin{aligned} \nabla^2 \underline{A} - i\omega\mu\sigma \underline{A} &= 0 \\ \nabla^2 \phi - i\omega\mu\sigma\phi &= 0 \end{aligned} \tag{3.1.7}$$

The advantage of such a representation is that the field is now specified by four independent variables $(\underline{A}, \phi)$ rather than the six $(\underline{E}, \underline{H})$. The transformation has moved the problem away from the physical equations (3.1.1), but it may render the boundary-value problem associated with those equations more tractable.

There is another level of potential representation available since $\underline{A}$ and ϕ in (3.1.7) still enjoy some degree of arbitrariness. One can see this by observing that any $\underline{\Pi}$ and $\underline{\Gamma}$ such that

$$\begin{aligned} \phi &= -\nabla \cdot \underline{\Pi} \\ \underline{A} &= \nabla \times \underline{\Gamma} + \mu\sigma \underline{\Pi} \end{aligned} \tag{3.1.8}$$

(where the directions of $\underline{\Pi}$ and $\underline{\Gamma}$ are chosen at will) will satisfy (3.1.7). Electric and magnetic field vectors are transformed to this representation (called the Hertz vector representation) by

$$\begin{aligned} \underline{E} &= \nabla \times \nabla \times \underline{\Pi} - i\omega \nabla \times \underline{\Gamma} \\ \underline{H} &= \nabla \times \nabla \times \underline{\Gamma} + K \nabla \times \underline{\Pi} \end{aligned} \tag{3.1.9}$$

where $K = (i\omega\mu\sigma)^{\frac{1}{2}}$. It will be found, upon substitution of (3.1.8) into (3.1.7) that $\underline{\Pi}$ and $\underline{\Gamma}$ both satisfy the diffusion equation. Since their directions can be chosen

at will, for a given geometrical situation, a clever choice of this direction can further reduce the number of independent variables required to specify the field.

So far we have suggested that $\underline{E}$, $\underline{H}$, ϕ , $\underline{A}$, $\underline{\Pi}$, and $\underline{\Gamma}$ all satisfy the same equation; subject of course to different boundary conditions. A broad discussion of the general possibilities for higher potential representations may be found in Stratton (1941; Chapter 7). If ψ is a solution to the scalar diffusion equation, and $\underline{a}$ is any constant vector of unit length, then three independent solutions to the vector diffusion equation

$$\nabla^2 \underline{C} - i\omega\mu\sigma \underline{C} = 0$$

can be constructed from

$$\underline{L} = \nabla\psi \ , \quad \underline{M} = \nabla \times \underline{a}\psi \ , \quad \underline{N} = K^{-1}\nabla \times \underline{M} \qquad (3.1.10)$$

These fundamental vector solutions have the properties that $\underline{L}$ is irrotational; $\nabla \times \underline{L} = 0$; whereas $\underline{N}$ and $\underline{M}$ are solenoidal, $\nabla\cdot\underline{M} = 0$ and $\nabla\cdot\underline{N} = 0$. Since $\underline{a}$ is a constant vector, from vector identities we can deduce that $\underline{M} = \underline{L} \times \underline{a}$. Since $\nabla\cdot\underline{E} = 0$ and $\nabla\cdot\underline{H} = 0$, our induction problem is solenoidal, and $\underline{L}$ need not enter our fundamental solution set. The task of finding an appropriate $\underline{M}$ and $\underline{N}$ hinges on our finding an advantageous vector $\underline{a}$.

For example, if we are treating induction in a conducting half-space occupying $z > 0$ in an (x,y,z) Cartesian frame in which z is taken to be positive in the downwards direction and in which σ is taken to be

homogeneous in the x-y plane, a fortunate choice for the unit vector $\underline{a}$ might be $\underline{a} \equiv \hat{k}$, i.e. to lie along the z-direction. Then (3.1.9) can be expressed

$$\underline{E} = K\underline{N} - i\omega\underline{M}^{\dagger}$$
$$\underline{H} = K\underline{N}^{\dagger} + \mu\sigma\underline{M} \qquad (3.1.11)$$

where $\underline{N} = K^{-1} \nabla \times \underline{M}$ and $\underline{M} = \nabla \times \psi\hat{k}$, and $\underline{N} = K^{-1} \nabla \times \underline{M}^{\dagger}$, $\underline{M}^{\dagger} = \nabla \times \psi^{\dagger}\hat{k}$. The problem has been reduced to solving two differential equations (diffusion equations) for ψ and $\psi^{\dagger}$. We note a useful result of Weaver (1970) that <u>within</u> the conductor the boundary conditions associated with the induction in a half-space due to localized sources imply that $\underset{\sim}{\Pi}$ can be set to zero in equation (3.1.9). This implies $\underline{N}$ and $\underline{M}$ can be set to zero in (3.1.11) and the fields can be derived from the solution of a single scalar diffusion equation for $\psi^{\dagger}$.

Stratton shows that for the analogous problem of induction in a spherically symmetric conductor, choice of a <u>fixed</u> vector $\underline{a}$ to be $\hat{r}$ leads to the difficulty that, since $\hat{r}$ is not a constant vector (it can rotate), $\underline{M}$ and $\underline{N}$ need not always be perpendicular to $\underline{L}$, and $\underline{L} \times \hat{r}$ need not be always tangential to the surface of the sphere. One can construct a <u>non</u>-constant $\underline{a} = \underline{r}$, where $\underline{r}$ is the radial position vector, which does supply solenoidal $\underline{M}$ and $\underline{N}$. Thus for a strictly spherical problem, $\underline{E}$ (i.e. $\underline{M}$ in equation (3.1.10)) can be supplied by

$$\underline{E} = \nabla \times \psi \underline{r} \qquad (3.1.12)$$

and the problem reduces to the solution of a single scalar diffusion equation (in spherical coordinates) for ψ .

c. Solutions to the 'forward problem'

The direct problem of solving for the response for a given conductivity distribution has been the subject of much research. We very briefly indicate the nature of the various solutions, and where a more detailed analysis of the problem might be found in the literature.

The problem associated with induction in a spherical conductor involves solving for the potential ψ in equation (3.1.12). The diffusion equation in spherical coordinates is

$$\frac{1}{r^2}\frac{\partial}{\partial r}\left(r^2\frac{\partial \psi}{\partial r}\right) + \frac{1}{r^2 \sin\theta}\frac{\partial}{\partial \theta}\left(\sin\theta \frac{\partial \psi}{\partial \theta}\right) + \frac{1}{r^2 \sin^2\theta}\frac{\partial^2 \psi}{\partial \phi^2} + i\omega\mu\sigma\psi = 0 \qquad (3.1.13)$$

To solve this differential equation, one can seek to separate variables by a series expansion solution of the form

$$\psi = \sum_{\ell} \sum_{m} R_\ell^m(r) Y^m(\theta,\phi) \qquad (3.1.14)$$

Substituting (3.1.14) into (3.1.13), the diffusion equation decomposes into three equations: a radial equation (3.1.15)

$$\frac{d}{dr}\left(r \frac{d}{dr} R_\ell^m(r)\right) - (\ell(\ell+1) + i\omega\mu\sigma r^2) R_\ell^m(r) = 0$$

(this can be identified as a Sturm-Liouville type equation) and angular equations

$$\frac{d^2\Phi}{d\phi^2} + m^2\Phi = 0 \qquad (3.1.16)$$

and

$$\frac{d}{d\theta}\left(\sin\theta \ \frac{d\Theta}{d\theta}\right) + \left[\sin\theta \ \ell(\ell+1) - \frac{m^2}{\sin\theta}\right]\Theta = 0 \qquad (3.1.17)$$

where $Y_\ell^m = \Phi \cdot \Theta$. This latter can be identified as Legendres equation. It is interesting to observe that the model parameter $\sigma(r)$ only enters explicitly into the radial equation (3.1.15). This arises from the presumed spherical symmetry of the problem. Thus we may expect the inverse problem to be related strongly with equation (3.1.15). This problem has been analysed extensively in the literature (Lahiri and Price, 1939; Bailey, 1970; Parker, 1970).

For the half-space case, the solution to (3.1.11) is achieved by making a Fourier-space transform of ψ' , namely substituting

$$\psi' = \frac{1}{\sqrt{2\pi}} \iint P(\xi,\eta) e^{-i(\xi x+\eta y)} d\xi \, d\eta \qquad (3.1.18)$$

into equation (3.1.11). The resulting equation (in transform space) is

$$\frac{d^2P}{dz^2} - K^2P = 0 \qquad (3.1.19)$$

where $K^2 = \xi^2 + \eta^2 + i\omega\mu\sigma$. The Fourier components are

to be identified with the structure of the source; one solves the simple diffusion equation (3.1.19) for $P(\xi,\eta)$ and then Fourier transforms back into Cartesian x-y space -- this latter step effectively summing over the 'wave-numbers', K, associated with a given source structure. This has been the approach of Price (1952, 1962), Weaver (1970, 1973).

Particular mention should be made of the case where the source inducing currents in a half-space is uniform in the x-y plane. This 'non-local' source was presumed in the magnetotelluric theory developed by Cagnaird (1953), because at a single observation position on the earth, the spatial structure of the source is large compared with the depth of penetration of the fields. However Price (1962) showed that taking the limit from the spherical case (with uniform field) to the half-space case (i.e. the limit as radius $R \rightarrow \infty$) results in an indeterminate problem for the induced fields. The limit for tangential components of the induced field (or inducing field) tends to m/m+1, and this dependence of the field in a half-space on a spherical harmonic variable m, implies the separated fields cannot be determined uniquely (the choice of m is arbitrary in the context of a half-space).

The <u>total</u> fields however can easily be found. If one considers the $\underline{E}$ field of a uniform source to lie along the x-direction, i.e. $\underline{E}^s = (E_x,0,0)$, substitution into Maxwell's equations shows that one need only solve

$$\frac{\partial^2 E_x}{\partial z^2} - i\omega\mu\sigma E_x = 0 \qquad (3.1.20)$$

for E_x. The orthogonal component H_y can be found from (3.1.1).

d. Choice of response function

In Chapter 4 a specific inverse-oriented criterion for a suitable response function will be suggested. At this stage we outline the form of the response used in the various problems we have been discussing.

A spherical harmonic analysis of the global induction problem can yield for ψ appearing in (3.1.14) an expression of the form

$$\psi_\ell^m = a\left[\left(\frac{r}{a}\right)^\ell U_\ell^m + \left(\frac{a}{r}\right)^{\ell+1} V_\ell^m\right] P_\ell^m(\cos\theta)e^{im\phi} \qquad (3.1.21)$$

where U_ℓ^m and V_ℓ^m represent the coefficients associated with the decomposition of $R_\ell^m(r)$ into components of internal (V_ℓ^m) and external (U_ℓ^m) origin. It was such a separation of surface fields that Schuster (1889), Chapman (1919), and Lahiri and Price (1939) performed to analyse surface magnetic variation data. Thus a possible measure of the inductive response of the earth (for the (ℓ,m)-spherical harmonic of an inducing field) is to take the surface ratio of internal to external parts, S_ℓ^m, for tangential magnetic field components (following the notation of Schmucker, 1970)

$$S_\ell^m = V_\ell^m / U_\ell^m \qquad (3.1.22)$$

This is related to the same ratio for the radial magnetic field components by $-(\ell+1)V_\ell^m/\ell V_\ell^m$. One can also use as a response the surface ratio of magnetic radial to tangential variations:

$$H_{r/H_\theta} = \frac{\ell P_\ell^m}{dP_\ell^m/d\theta} \quad T_\ell^m$$

and (3.1.23)

$$H_{r/H} = \frac{\ell \sin\theta}{im} \quad T_\ell^m$$

where

$$T_\ell^m = \frac{1 - S_\ell^m (\ell+1)/\ell}{1 + S_\ell^m}$$

There is another, less direct, method of assessing the inductive response of a spherical conductor. Rather than separating R_ℓ^m into parts of internal and external origin, from equation (3.1.14) one can express the six field components in terms of R_ℓ^m and Y_ℓ^m to yield (from Srivastava, 1968):

$$\begin{aligned}
H_r &= -\frac{1}{r} R_\ell^m(r)\, \ell(\ell+1)\, Y_\ell^m(\theta,\phi) \\
H_\theta &= -\frac{1}{r}\frac{d}{dr}(r R_\ell^m(r))\frac{d}{d\theta} Y_\ell^m(\theta,\phi) \\
H_\phi &= -\frac{1}{r}\frac{d}{dr}(r R_\ell^m(r))\frac{d}{d\phi}\frac{Y_\ell^m(\theta,\phi)}{\sin\theta} \\
E_r &= 0 \\
E_\theta &= -i\omega R_\ell^m(r)\frac{d}{d\phi}\frac{Y_\ell^m(\theta,\phi)}{\sin\theta}
\end{aligned} \qquad (3.1.24)$$

$$E_\phi = i\omega R_\ell^m(r) \frac{d}{d\theta} Y_\ell^m(\theta,\phi)$$

If one forms the surface ratio of the orthogonal components of $\underline{E}$ and $\underline{H}$ one finds

$$\frac{E_\phi}{H_\theta} = - \frac{i\omega r R_\ell^m(0)}{\frac{d}{dr}(r R_\ell^m(r))_{r=0}}$$

and (3.1.25)

$$\frac{E_\theta}{H_\phi} = i\omega \frac{r R_\ell^m(0)}{\frac{d}{dr}(r R_\ell^m(r))_{r=0}}$$

Both these ratios depend solely on the radial function $R_\ell^m(r)$ which in turn depends on the parameter $\sigma(r)$. In fact the complex ratios (3.1.25) have (SI) units of ohms and are called (by analogy with wave propagation theory) the surface impedances.

For the problem of induction in a half-space due to a localized source (localized in the sense that its spatial extent is not negligible compared with its depth of penetration), separation of the field into its internal and external parts is still possible and the solution for $P(\xi,\eta)$ in (3.1.19) can be expressed in the form

$$P(\xi,\eta,z) = P^i(\xi,\eta)e^{-Kz} + P^s(\xi,\eta)e^{Kz} \qquad (3.1.26)$$

where $K^2 = \xi^2 + \eta^2$ and the surface ratio of internal to external parts of the field, $S(\xi,\eta) = P^i(\xi,\eta)/P^s(\xi,\eta)$ can be identified for a given conductivity distribution.

The separation of fields in this manner is not possible for the case involving uniform inducing fields. This is due to the indeterminacy of the problem of separating fields associated with infinitely extending fields. However one can still employ the impedance ratios of equation (3.1.25) which have no angular dependence. Thus, for uniform fields, one can use E_x/H_y and E_y/H_x as a suitable response. For strictly polarized fields these ratios can be written in the form

$$\frac{E_x}{H_y} = i\omega\mu \left[\frac{E_x}{\frac{d}{dz}E_x} \right]_{z=0} \tag{3.1.27}$$

Cagnaird (1953) employed a related response which he called the apparent resistivity, ρ_a, and which he defined as

$$\rho_a = \frac{1}{\omega\mu} \left| \frac{E_x}{H_y} \right|^2 \tag{3.1.28}$$

together with its phase,

$$\phi = \arg \frac{E_x}{H_y}$$

For the case of localized source fields, the surface impedance analogous to (3.1.27) is given by

$$\frac{\mathcal{F}\{E_x\}}{\mathcal{F}\{H_y\}} = i\omega\mu \left[\frac{P(\xi,\eta,0)}{\frac{d}{dz}P(\xi,\eta,z)} \right]_{z=0} \tag{3.1.29}$$

where $\mathcal{F}$ denotes the spatial Fourier transform of equation (3.1.18). Price (1962) shows this impedance ratio can be related to the separation components $P^i(\xi,\eta)$ and

$P^s(\xi,\eta)$ by

$$\frac{1}{i\omega\mu}\frac{\mathcal{F}\{E_x\}}{\mathcal{F}\{H_y\}} = -\frac{1}{i\omega\mu}\frac{\mathcal{F}\{E_y\}}{\mathcal{F}\{H_x\}} = \frac{P^s(\xi,\eta) + P^i(\xi,\eta)}{K(P^s(\xi,\eta) - P^i(\xi,\eta))} \qquad (3.1.30)$$

and this expression is analogous to the spherical harmonic separation coefficients U_ℓ^m and V_ℓ^m satisfying (from equation (3.1.23)) the relationship

$$\frac{1}{i\omega\mu}\frac{E}{H} = \frac{V_\ell^m - U_\ell^m \frac{\ell+1}{\ell}}{V_\ell^m + U_\ell^m} \qquad (3.1.31)$$

Thus there are really two types of response function commonly used: the ratio of separated field components arising from Fourier decomposition of the source field, and the surface impedance ratios. These two responses are closely related by equations (3.1.30) and (3.1.31) where field separation is mathematically possible. Bailey (1970) chooses V_ℓ^m/U_ℓ^m as the response function in his inversion approach, whereas Weideldt (1972) chooses a response of the form $\left[E(z)/\ \partial E(z)/\partial\ z\right]_{z=0}$, i.e. a response analogous to (3.1.27). Of course, one determining factor in the choice of response must be the experimental accuracy with which a response can be estimated. Banks (1969) puts forward such experimental arguments when explaining his preference for an impedance response of the form (3.1.31).

3.2 Linearizing the Induction Problem

a. Method of Parker

Linearizing a non-linear problem such as the inverse induction problem, obviously involves inherent risk. Sabatier (1974) has presented a mathematical (and somewhat synthetic) approach to assessing some of the possible ill-effects which can arise from a linearization. He has thus suggested that caution must accompany the conclusions formed from linearized procedures. In connection with the induction inverse problem, Anderssen (1975) has pointed out that little attention seems to have been paid to the possible contribution of higher order terms in an equation such as (2.2.3). He also (1974) presents specific reservations concerning the linearization of the electromagnetic problem as accomplished by Parker (1970).

In a Backus-Gilbert inversion of Banks' global induction data (from Banks (1969)), Parker chose as his model distribution a radially dependent conductivity in an earth with radius a. As a surface response he chose, for a given ith frequency ω, the quantity

$$V_i = \frac{1}{\ell(\ell+1)} \left\{ 1 + \frac{r}{R_\ell^m} \frac{dR_\ell^m}{dr} \right\}_{r=a} \qquad (3.2.1)$$

where $R_\ell^m(r)$ is the radial function which satisfies equation (3.1.15). One can see by comparison with

equation (3.1.25) that Parker's response is closely related to the surface impedance, since

$$V_i = \frac{i\omega\mu}{\ell(\ell+1)} \frac{H_\phi}{E_\theta}$$

and (3.2.2)

$$V_i = -\frac{i\omega\mu}{\ell(\ell+1)} \frac{H_\theta}{E_\phi}$$

Parker relates this response to the separation coefficients U_ℓ^m and V_ℓ^m appearing in equation (3.1.21) by the relationship

$$V_i = \frac{U_\ell^m + V_\ell^m}{\ell V_\ell^m - (\ell+1)V_\ell^m} \qquad (3.2.3)$$

which can be inferred from (3.1.31) directly. The reciprocal V_i^{-1} corresponds to the response function employed by Banks. By differentiating V_i with respect to r and by substitution into equation (3.1.15), Parker shows that V_i satisfies the first-order differential equation

$$\frac{dV_i}{dr} + \frac{\ell(\ell+1)V_i^2 - V_i - 1}{r} + \frac{i\omega\mu\sigma r}{\ell(\ell+1)} = 0 \qquad (3.2.4)$$

Forming the variation of V_i (with respect to a variation in model distribution $\sigma(r)$) one finds that

$$\frac{d}{dr}(\delta V_i) + \left(\frac{2\ell(\ell+1)V_i - 1}{r}\right)\delta V_i + \frac{(\ell+1)\ell(\delta V_i)^2}{r} + \frac{i\omega\mu r}{\ell(\ell+1)} = 0 \qquad (3.2.5)$$

and Parker effects the linearization of δV by neglecting

the third term in this equation. Anderssen has made the following two reservations of this procedure: a) it is not clear whether discarding the $(\delta V)^2$ - term in equation (3.2.5) is equivalent to discarding the terms of order δm^2 in an equation such as (2.2.3), and b) in any event it is not shown by Parker whether this discarded term is insignificant.

Parker obtains as his Fréchet kernel the function

$$G_i(\sigma,r) = \frac{i\omega\mu r^2}{\ell(\ell+1)} \frac{R_\ell^m(r)^2}{R_\ell^m(a)^2} \qquad (3.2.6)$$

by solving the linearized equation (3.2.5). However he discovered that, for the Banks' data at least, the Backus-Gilbert least-squares scheme was unable to converge. As Parker explains, in the case of real, scattered data, strict convergence would be very unlikely. The inverse problem is in general underdetermined, and the matrix equation (2.2.12) may be ill-conditioned even when one is treating perfect and consistent data. Parker was, however, able to find models which satisfied the data to within one standard deviation of the data (he did not elaborate concerning the method he employed to find these models).

There must be some ambiguity associated with discarding the δV^2 - term in equation (3.2.5). Assuming, for example, that V_i were related to the model distribution $\sigma(r)$ by a purely linear functional: can one take

the order-of-magnitude relationship

$$\delta V \sim \quad 0 \| \delta\sigma \|$$

to imply

$$(\delta V)^2 \sim \quad 0 \, \| \delta\sigma \|^2 \qquad ?$$

After all, if the functional is linear there do not exist terms of second order in $\delta\sigma$ associated with δV, yet one is identifying $(\delta V)^2$ as a term of precisely such order. In fact, if the variations are elements of a linear space, they <u>can</u> be treated in this way, that is, as variables in a linear algebra. In a non-linear problem, however, if one presumes linear characteristics of variations δV etc. <u>before</u> the linearization of the problem has been effected -- as is the case following equation (3.2.5) -- then the structure of the discarded terms is obscured. To avoid this difficulty in Section 3.2.b a more conventional approach to the linearization is considered.

Parsons (1972) suggests an alternative procedure for obtaining the Fréchet kernel of Parker. His procedure serves to illuminate some of the problems involved with taking the variation of the electromagnetic surface response. Briefly described, Parsons considers the Sturm-Liouville equation (3.1.15) for a particular conductivity distribution $\sigma_1(r)$,

$$\frac{d}{dr} r^2 \frac{d}{dr} R_1 - \left[i\omega\mu r^2 \sigma_1(r) + \ell(\ell+1) \right] R_1 = 0 \quad (3.2.7)$$

and then for a conductivity $\sigma_2(r)$, the similar equation for R_2 is written

$$\frac{d}{dr} r^2 \frac{d}{dr} R_2 - \left[i\omega\mu r^2 \sigma_2(r) + \ell(\ell+1) \right] R_2 = 0 \quad (3.2.8)$$

Multiplying (3.2.7) by R_2 and (3.2.8) by R_1 and integrating the difference between the resulting equations by parts, one obtains

$$\left[\frac{1}{R_2(a)} \frac{dR_2}{dr} - \frac{1}{R_1(a)} \frac{dR_1}{dr} \right]_{r=a}$$

$$= \frac{i\omega\mu}{a^2} \int_0^a r^2 \, \delta\sigma(r) \, \frac{R_1(r)R_2(r)}{R_1(a)R_2(a)} \, dr \quad (3.2.9)$$

where the induced electric and magnetic fields have been assumed, reasonably, to vanish towards the earth's centre. Thus $R_1(0) = 0$, $R_2(0) = 0$, and $dR_1/dr\big]_{r=0} = 0$, and $dR_2/dr\big]_{r=0} = 0$. If we recognize the left hand side of (3.2.9) as $\ell(\ell+1)\delta V_i/a$, then we have for the variation of Parker's response function

$$V_i = \frac{i\omega\mu}{\ell(\ell+1)a} \int_0^a \frac{R^2(r)\,\delta\sigma(r)}{R^2(a)} + \frac{R(r)\delta R(r)}{R^2(a)} \, dr \quad (3.2.10)$$

The first term in this integrand corresponds to Parker's Fréchet kernel (3.2.6). Parsons claims (without explanation) that the second term in this integrand is of order $\delta\sigma^2$ and then discards it. Before accepting this linearization one might ask whether this procedure is acceptable.

It might seem, for example, that the cross-multiplication of (3.2.7) and (3.2.8) and the eliminating of $R_1 R_2 \ell(\ell+1)$ is misleading, since it rather assumes that

one is eliminating common factors from two simultaneous equations. In fact, the two equations are not simultaneous. In taking a variation (as a derivative) one is not moving along the solution curve, but from one solution curve to another.

For example, an examination of the procedure shows that one would obtain exactly the same Fréchet kernel for the equation

$$\frac{d}{dr} r^2 \frac{d}{dr} R - i\omega\mu\sigma(r)r^2 R = 0$$

yet clearly the solution to (3.2.7) might be quite different to the solution to this equation, since (3.2.7) depends upon the harmonic 1. A family of curves $y = ax + b$ can be constructed by

$$y_1 = a_1 x + b$$

$$y_2 = a_2 x + b$$

etc.

If we take differences between these equations to form the variation δy, we will see that we are constraining the variation always such that y passes through $y(0) = b$. In the following Section we follow a procedure similar to Parsons', but without the implicit constraint we have just mentioned. Finally it must be remarked that (again) the discarded term in equation (3.2.10) is not clearly of second order in $\delta\sigma$.

What is required is an unambiguous demonstration that the kernel (3.2.6) comprises the linear part of the

variation and that the discarded terms are of order greater than or equal to $\|\delta\sigma\|^2$. We proceed towards this goal in the next Section.

b. Alternative expression of the Fréchet kernel

We offer an alternative method for determining the Fréchet kernel, equation (3.2.6). The method is reminiscent of some recent work of Jady (1974a). At this stage we wish to include the parallel problem of induction in a half-space occupying the $z > 0$ region of an (x,y,z) coordinate system, positive z downwards, by a uniform harmonic source. In this case the tangential electric field must satisfy the diffusion equation (3.1.20). As in the case of a spherical conductor, this equation is of the Sturm-Liouville type.

$$\frac{\partial}{\partial x} p(x) \frac{\partial}{\partial x} \psi(x) + q(x) \psi(x) + \lambda s(x) \sigma(x) \psi(x) = 0 \qquad (3.2.11)$$

If we multiply equation (3.2.11) by $\psi(x)$ and integrate over the region of interest ($0 \leq r \leq a$ for sphere of radius a and centre $r = 0$, or $0 \leq z \leq \infty$ for the half-space with $z = 0$ at the surface) we obtain

$$\left[\psi(x) \frac{\partial \psi}{\partial x}\right]_0^b - \int_0^b p(x) \left(\frac{\partial \psi}{\partial x}\right)^2 dx + \int_0^b q(x) \psi^2(x)\, dx = -\lambda \int_0^b s(x) \sigma(x) \psi^2(x)\, dx \qquad (3.2.12)$$

In the case of spherical conductors we have $b \equiv a$, $x \equiv r$ and $\psi \equiv R_\ell^m(r)$, and we make the following appropriate substitutions in equation (3.2.12): $q(r) = \ell(\ell+1)$, $p(r) = r^2$, $s(r) = r^2$ and $\lambda = -i\omega\mu$. We ask, reasonably, that the induced electric and magnetic fields vanish towards the earth's centre, so we may set $R_\ell^m(0) = 0$, and $\left[\partial R_\ell^m(r)/\partial r\right]_{r=0} = 0$. We obtain the following equation for V_i, the response function used by Parker:

$$V_i = \frac{1}{\ell(\ell+1)} + \frac{i\omega\mu}{\ell(\ell+1)a}\int_0^a \sigma(r) r^2 \mathcal{R}^2\, dr$$

$$+ \frac{1}{\ell(\ell+1)a}\int_0^a r^2(\mathcal{R}')^2\, dr + \frac{1}{a}\int_0^a \mathcal{R}^2\, dr \qquad (3.2.13)$$

where $\mathcal{R}(r) = R_\ell^m(r)/R_\ell^m(a)$, and $\mathcal{R}'(z) = \partial\mathcal{R}(r)/\partial r$.

We seek to find an expression for the variation δV_i in the form

$$\delta V_i = \int_0^a \delta\sigma(r)\left\{\frac{i\omega\mu r^2}{\ell(\ell+1)a}\mathcal{R}^2\right\} dr + \chi(\sigma,\omega) \qquad (3.2.14)$$

with χ a function which might admit any additional first-order contribution to δV_i. If $\chi \equiv 0$, the kernel (3.2.6) comprises entirely the first-order term.

For the half-space problem, we make the following substitutions in equation (3.2.12): $x \equiv z$, $b \equiv \infty$, $\psi = E_x$, with $q(z) = 0$, $p(z) = -1$, $s(z) = 1$, and $\lambda = -i\omega\mu$. Again asking that both electric and magnetic fields vanish as $z \to \infty$, and choosing our surface response

to be the ratio of tangential magnetic field, $H_y(0)$, to the orthogonal tangential component of the electric field, $E_x(0)$, we have

$$\gamma_i = H_y(0)/E_x(0)$$

$$= \int_0^\infty \sigma(z)\mathcal{E}^2(z)\,dz + \frac{1}{i\omega\mu}\int_0^\infty (\mathcal{E}'(z))^2\,dz \qquad (3.2.15)$$

where $\mathcal{E}(z)$ is the tangential electric field normalized with respect to the surface field, i.e. $\mathcal{E}(z) = E_x(z)/E_x(0)$, and $\mathcal{E}'(z) = \partial\mathcal{E}(z)/\partial z$.

We wish to find an expression for the variation $\delta\gamma_i$ in the form

$$\delta\gamma_i = \int_0^\infty \delta\sigma(z)\mathcal{E}^2(z)\,dz + \Upsilon(\sigma,\omega) \qquad (3.2.16)$$

where again the function Υ admits the possibility of additional first-order terms.

From Section 3.2.a, the half-space response, $H_y(0)/E_x(0)$ has been shown to be completely parallel to Parker's response, V_i, for the conducting sphere in the case of those frequencies where the Earth's curvature can be neglected. Also we have seen that Weideldt has supplied a set of transformation formulae which transforms the spherical problem to that of the half-space responding to uniform fields in cases where the Fourier variables associated with the source (i.e. the wave numbers) are independent of frequency. The geophysical applications which interest us are for frequencies such that the

Earth's curvature can be neglected ($T < 10^5$ s) and for time-harmonic inducing fields.

In view of this close relationship between spherical and half-space problems, in what follows we shall be content to restrict our attention to the somewhat less complicated half-space problem, believing our results to be directly applicable to corresponding spherical problems.

c. Homogeneous conductors

At this stage it might be advisable to test the validity of equations (3.2.13) and (3.2.14) for the most simple situation of a homogeneous conductor. Also we consider the conductor to vary in such a way that it remains homogeneous. This most simple case is the least interesting from the point of view of inversion, however it will give us the opportunity to inspect how the various terms in the integrands in equations (3.2.13), (3.2.14), (3.2.15), and (3.2.16) contribute to the variations δV_i and $\delta \gamma$.

For the case of a homogeneous half-space with conductivity σ, one can observe the following relationship to be true:

$$\mathcal{E}(z) = e^{-Kz} \tag{3.2.17}$$

and

$$\mathcal{E}'(z) = -K\, e^{-Kz} \tag{3.2.18}$$

where $K = (i\omega\mu\sigma)^{\frac{1}{2}}$. The surface response is

$$\gamma_i = K/i\omega\mu \tag{3.2.19}$$

To examine how each integral in (3.2.15) contributes to γ we substitute (3.2.17) and (3.2.18) into (3.2.15) in order to obtain

$$\gamma_i = \sigma\int_0^\infty \mathcal{E}^2(z)\,dz + \frac{K^2}{i\omega\mu}\int_0^\infty \mathcal{E}^2(z)\,dz$$

$$= \frac{\sigma}{2K} + \frac{\sigma}{2K} \equiv \frac{K}{i\omega\mu} \tag{3.2.20}$$

(This latter identity follows from the definition of K). It can thus be seen that each term in (3.2.15) contributes equally to γ for a uniform conductor. For the variation $\delta\gamma$ we can write

$$\delta\gamma_i = \int_0^\infty \delta\sigma\,\mathcal{E}^2(z)\,dz + \int_0^\infty \sigma\,\delta\left[\mathcal{E}^2(z)\right]dz$$

$$+ \frac{1}{i\omega\mu}\int_0^\infty K^2\,\delta\left[\mathcal{E}^2(z)\right]dz + \int_0^\infty \delta\sigma\,\mathcal{E}^2(z)\,dz \tag{3.2.21}$$

There is no ambiguity about taking the variation 'inside the integral sign', since γ is a function of the variable σ which is independent of z. If one performs the partial derivatives (with respect to σ) one can express this equation as

$$\delta\gamma_i = \int_0^\infty \delta\sigma\left\{2\mathcal{E}^2(z) + 2\sigma\frac{\partial}{\partial\sigma}\left[\mathcal{E}(z)^2\right]\right\}dz \tag{3.2.22}$$

Evaluating this second term on the right hand side of

(3.2.22), we have

$$2\sigma \frac{\partial}{\partial \sigma}\left[\mathcal{E}^2(z)\right] = -2Kz\,\mathcal{E}^2(z)$$

Thus our variation $\delta\gamma_i$ becomes

$$\delta\gamma_i = \delta\sigma \int_0^\infty \left[2 - 2Kz\right]\mathcal{E}^2(z)\,dz \qquad (3.2.23)$$

with the Fréchet kernel given by

$$\begin{aligned} G_i(\sigma,z) &= \left[2 - 2Kz\right]\mathcal{E}^2(z) \\ &= \left[2 - 2Kz\right] e^{-2Kz} \end{aligned} \qquad (3.2.24)$$

From the first integral on the right hand side of equation (3.2.23) the Fréchet kernel associated with the linearization as performed by Parker (1970) -- see equation (3.2.6) -- is

$$G_i(\sigma,z) = \mathcal{E}^2(z) = e^{-2Kz} \qquad (3.2.25)$$

In Fig. 3-1 we plot the real and imaginary parts of $G(\sigma,z)$ as defined by (3.2.24) and (3.2.25). In fact, the linearization associated with equation (2.2.3), i.e. the definition of Fréchet differentiability, is made to an equation involving the integral of $G_i(\sigma,z)$. Equation (3.2.22) can be written in the form

$$\delta\gamma_i = \delta\sigma \int_0^\infty \mathcal{E}^2(z)\,dz + \Upsilon(\sigma,\omega) \qquad (3.2.26)$$

with

$$\Upsilon(\sigma,\omega) = \delta\sigma \int_0^\infty \left[1 - 2Kz\right]\mathcal{E}^2(z)\,dz \qquad (3.2.27)$$

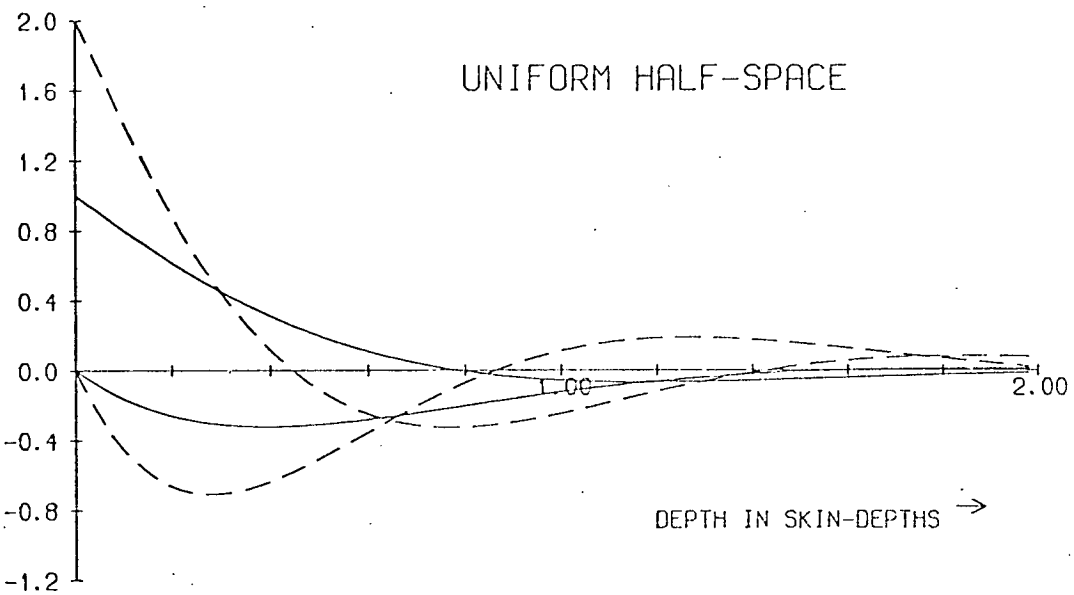

FIG. 3-1 The kernel $f(z) = \mathcal{E}^2(z)$ for a homogeneous half-space is indicated by the solid lines. The real part can be identified by $\mathrm{Re}\,\mathcal{E}^2(0) = 1$, and $\mathrm{Im}\,\mathcal{E}^2(0) = 0$. Also illustrated (by dashed lines) are the real and imaginary parts of the kernel $h(z) = (1 - 2 k z) \mathcal{E}^2(z)$. We note $\mathrm{Re}\, h(0) = 2$, and $\mathrm{Im}\, h(0) = 0$. The integration of both $f(z)$ and $h(z)$ over $(0 , \infty)$ gives the same result.

Upon performing this latter integration, it will be observed that $\Upsilon(\sigma,\omega) = 0$. Thus the Fréchet kernel developed by Parker (applied to the homogeneous half-space) is identical to that achieved by the method of Section 3.2.b. This is equivalent to the observation that integrating either function in Fig. 3-1 over the interval $(0,\infty)$ yields the same value for the integral. In particular

$$\mathrm{Re}\left\{\int_0^\infty e^{-2Kz}\,dz\right\} = \mathrm{Re}\left\{\int_0^\infty e^{-2Kz}\,(2 - 2Kz)\,dz\right\}$$

$$= 0.25$$

with the imaginary part having the same value.

Weideldt (1976) has supplied a useful way of evaluating the kernel for a uniform sphere. If one forms the variation of (3.2.13), one obtains

$$\delta V_i = \int_0^a \delta\sigma\left\{\frac{i\omega\mu r^2}{\ell(\ell+1)a}\mathcal{R}^2\right\}dr$$

$$+ \int_0^a \sigma\,\delta\left\{\frac{i\omega\mu r^2}{\ell(\ell+1)a}\mathcal{R}^2\right\} + \frac{1}{\ell(\ell+1)a}\int_0^a r^2\delta\{\mathcal{R}'^2\}\,dr + \frac{1}{a}\int_0^a \delta\mathcal{R}^2\,dr$$

where, because of the uniformity of σ, there is no ambiguity about bringing the variation inside the integrand. The 'functional' $g[\sigma]$ is in this case a function $g(\sigma)$ of the variable and differential calculus may now be used. Evaluating the variations in the last three integrals, one obtains

$$\delta V_i = \int_0^a \delta\sigma \left\{ \frac{i\omega\mu r^2}{\ell(\ell+1)a} \mathcal{R}^2 \right\} dr \qquad (3.2.28)$$

$$+ \int_0^a \delta\sigma \left\{ \frac{i\omega\mu r^2}{\ell(\ell+1)a} \right\} 2\mathcal{R}\delta\mathcal{R} dr + \frac{1}{\ell(\ell+1)a} \int_0^a r^2 2\mathcal{R}'(\delta\mathcal{R}')dr + \frac{1}{a} \int_0^a 2\mathcal{R}\delta\mathcal{R} dr$$

The third integral can be integrated by parts to yield

$$\frac{2}{\ell(\ell+1)a} \left[\left[\delta\mathcal{R} r^2 \mathcal{R}' \right]_0^a - \int_0^a (r^2\mathcal{R}')'\delta\mathcal{R} dr \right] = -\frac{2}{\ell(\ell+1)a} \int_0^a (r^2\mathcal{R}')'\delta\mathcal{R} dr \qquad (3.2.29)$$

substituting this result into (3.2.28) one can show (from (3.1.15) that the final three integrals in (3.2.28) collectively vanish. Thus for the homogeneous sphere, Parker's kernel is again achieved.

d. Discretizing the formalism

To ascertain the appropriateness of (3.2.6) as Fréchet kernel, one must examine the terms χ and Υ for the case of a continuous model distribution $\sigma(z)$. However, forming the variation of a functional requires care. Consider, for example, a functional such as (2.1.2):

$$\phi[m] = \int_0^a F(m(r), r)\, dr$$

If one wishes to determine the variation $\delta\phi$, i.e.

$$\delta\phi = \delta \int_0^a F(m(r), r)\, dr$$

one is not at liberty to write

$$\delta\phi = \int_0^a \delta F(m(r),r)\, dr$$

since the variation of a function F with respect to a distribution m(r) is not unambiguously defined. An acceptable approach toward evaluating this variational differential, $\delta\phi$, is described in Gel'fand and Fomin (1961). The strategy is to divide up the range of integration (0,a) into increments Δh_i over which the model has a constant value, m_i. This effectively transforms the functional into a function of M variables $\{m_i\}$. One can hence compute the total differential $\delta\phi$ using differential calculus and then take the result to the limit as $\Delta h_i \rightarrow 0$, $M \rightarrow \infty$. If this limit exists, the result $\delta\phi$ is defined as the variational differential of ϕ.

Our aim in the following section is to describe how the functional (3.2.15) can be discretized, and how the least-squares procedure described in Section 2.2.b can be expressed in discrete form. In Section 3.3 we return to the question of examining the linearization for a simple two-layer conductivity distribution.

We take the simple approach of discretizing the model distribution by restricting our attention to models of horizontally stratified layers. Furthermore, we constrain our variation such that the perturbed model remains horizontally stratified (or in the spherical case, concentrically stratified). This procedure, in the

context of generalized linear inverse theory, restricts the class of conceivable models and hence the class of acceptable models. In a particular situation of analyzing real data, one may overconstrain the problem by discretizing the conductivity distribution too coarsely for the data. The least-squares procedure described in Section 2.2.b will then provide a model $\underline{m}$ (closest to the starting model $\underline{m}_0$) which satisfies the data and falls within the class of M-layered models. If the discretization effectively overconstrains a problem, and if the problem treats a sufficient quantity of data, (and is otherwise well-posed) so that the problem is overdetermined -- then (as described in Section 2.3) the generalized inverse is identical to the classical least-squares inverse where the sum of the squares of the data residuals is minimized. Overconstraining the problem can possibly be useful for determining coarse features of models satisfying the data (to some preset degree of approximation). Since a set of constrained models will be a subset of $\mathcal{M}$, the effect of non-linearity on any such simple class of models and variations may prove indicative.

We wish to discretize the distribution $\sigma(z)$ so that we may specify the model by a model vector

$$\underline{\sigma} = (\sigma_1, \sigma_2, \sigma_3, \ldots; \; d_1, d_2, \ldots d_M)$$

where σ_j is the conductivity of the jth layer, $z_{j-1} \; z \; z_j$, with $z_0 = 0$ and $d_j = z_j - z_{j-1}$. We

illustrate the situation in Fig. 3-2.

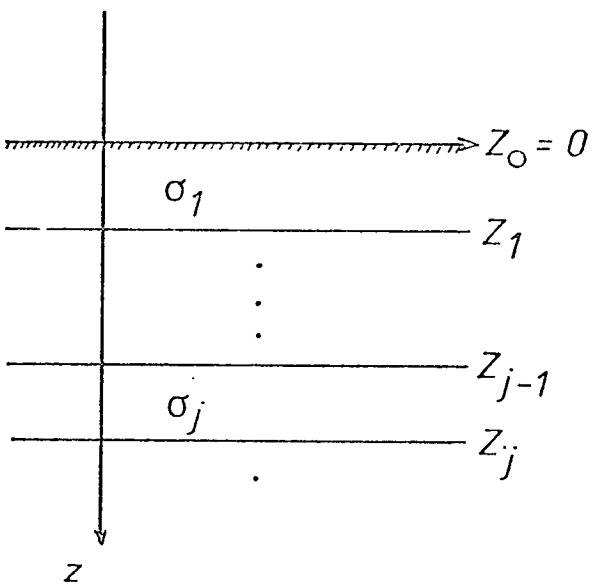

FIG. 3-2

An obvious way to achieve this discretization is to use a string of Heaviside step-functions (denoted by H(z)) such that

$$\sigma(z) = \sigma_1 H(z_1 - z) + \sum_{j=2}^{M-1} \sigma_j \{H(z - z_{j-1}) - H(z - z_j)\} + \sigma_M H(z - z_M) \tag{3.2.30}$$

for the case of M layers ($M \geq 2$). Substituting this expression into equation (3.2.15) effectively discretizes the response. The variation of the resulting function can then be taken. We can, of course, directly take the variation of $\sigma(z)$, and obtain

$$\delta\sigma(z) = H(z_1 - z)\,\delta\sigma_1 + \sum_{j=2}^{M-1} \delta\sigma_j \{H(z - z_{j-1}) - H(z - z_j)\}$$

$$+ H(z - z_M)\,\delta\sigma_M + \sum_{j=1}^{M} (\sigma_j - \sigma_{j+1})\,\delta(z - z_j)\,\delta d_j$$

(3.2.31)

where $\delta(z - z_j)$ is the Dirac delta-function centred at z_j. Of course this variation of generalized functions (such as Heaviside step-functions) cannot be performed in isolation from the integrands in which they appear. Consider for example, a function F defined by

$$F(\beta, a) = \int_0^a g(\beta, x) f(x) dx$$

where f(x) is any function, and g(x) is a generalized function. If we form the variation with respect to β,

$$\delta F = \int \delta g(\beta, x) f(x) dx$$

the variation $g(\beta, x)$ is well-defined only if f(x) is continuous over the range of integration. Of course if f(x) is discontinuous, at some finite collection of points, a limiting procedure must be employed. We defer this question until Section 3.3 where we address it within the context of a two-layer illustration of the present discretization.

The appropriate analytic expressions for $\mathcal{E}(z)$ have been developed by Srivastava (1966) and have been re-stated by Schmucker (1970) (whose notation we shall largely follow). The problem of solving for the

(normalized) field in a stratified half-space, is one of generating a function Q_ν for the νth layer $z_{\nu-1} \leq z \leq z_\nu$, where Q_ν is developed recursively starting with $Q_M = 1$ in the bottom semi-infinite layer and using the relation

$$Q_\nu = (K_{\nu+1}Q_{\nu+1} + K_\nu \tanh K_\nu d_\nu)/(K_\nu + K_{\nu+1}Q_{\nu+1} \tanh K_\nu d_\nu) \tag{3.2.32}$$

where $K_\nu = (i\omega\mu\sigma_\nu)^{\frac{1}{2}}$, and $d_\nu = z_\nu - z_{\nu-1}$. We note that, if the following function can be defined for the νth layer,

$$Q(z) = \{Q_\nu - \tanh K_\nu(z-z_{\nu-1})\}/\{1 - Q_\nu \tanh K_\nu(z-z_{\nu-1})\} \tag{3.2.33}$$

-- incidentally $Q(z)$ is a function which is discontinuous across interfaces in the conductor -- the expression for $\mathcal{E}'(z)$ in the νth layer is given by

$$\mathcal{E}'(z) = -K_\nu Q(z)\mathcal{E}(z) \tag{3.2.34}$$

Thus equation (3.2.16) can be written in the form

$$\gamma_i = \int_0^\infty \sigma(z)\mathcal{E}^2(z)\left[1 + Q(z)^2\right] dz \tag{3.2.35}$$

Substituting (3.2.30) into this equation shows we can express our surface response over an M-layered half-space by

$$\gamma_i = \sum_{j=1}^{M} \alpha_j \sigma_j \tag{3.2.36}$$

with the complex coefficients α_j given by

$$\alpha_j = \int_{z_{j-1}}^{z_j} \mathcal{E}^2(z) \left[1 + Q(z)^2 \right] dz \qquad (3.2.37)$$

that is to say, as a 'non-linear' combination of the discrete model parameters. We investigate this summation in greater detail in Section 4.3 of the following Chapter.

It is interesting to note that whereas $\mathcal{E}(z)$ is continuous across interfaces in the conductor, $Q(z)$ is not. However, the product $\sigma(z)\mathcal{E}(z)$ is discontinuous across such interfaces and $\sigma(z)\ Q(z)$ is continuous.

The least-squares problem described in Section 2.2.b can now be re-stated in terms of the parameters of (3.2.30). We wish to minimize $|\sigma - \sigma^0|^2$ subject to the constraint that the surface data be satisfied by the model and to our discretization constraint, that our model remain stratified. Equation (2.2.5) can be rewritten as

$$U = |\sigma - \sigma^0|^2 - \sum_i^N \nu_i \left[g_i(\sigma) - \gamma_i \right] \qquad (3.2.38)$$

and a stationary solution for this implies

$$\sum_j^M (\sigma_j - \sigma_j^0)\,\delta\sigma_j + \sum_j^M (z_j - z_j^0)\,\delta d_j - \sum_i^N \nu_i \int_0^\infty \sum_j^M \left\{ G_i^{(j)}\,\delta\sigma_j + G_i^{(dj)}\,\delta d_j \right\} = 0 \qquad (3.2.39)$$

In this equation the vector Fréchet kernel corresponding to the ith frequency is defined

$$\underline{G}_i = (G_i^{(1)}, G_i^{(2)}, \ldots G_i^{(d_1)}, G_i^{(d_2)}, \ldots G_i^{(d_{N-1})})$$

where the bracketed superscript corresponds to the discretized model parameter. We have not used the vector $\underline{G}_i$ in exactly the same sense suggested by Backus and Gilbert (1967) -- there they use $\underline{G}$ to denote a vector space of kernels associated with M linearly independent, stepwise continuous model distributions. Here we are using their notation to facilitate the discretization of their formalism, although we too are strictly considering a set of step-wise continuous distributions $\sigma(z)$. The distribution is the sum of these as defined in (3.2.30). Since we consider the perturbations $\delta\sigma_1$ etc. in equation (3.2.39) to be linearly independent, we can write equations analogous to (2.2.9) as

$$\sigma_j - \sigma_j^0 = \sum_{i=1}^{N} \nu_i \int_0^{\infty} G_i^{(j)}(z)\, dz \qquad (3.2.40)$$

and

$$z_j - z_j^0 = \sum_{i=1}^{N} \nu_i \int_0^{\infty} G_i^{(d_j)}(z)\, dz \qquad (3.2.41)$$

We recall at this point that our model parameters are to be measured in dimensionless units.

If we establish a (2M-1)-tuple $\{b_i^{(j)}\}$ denoted vectorally as $\underline{b}_i$ such that

$$\underline{b}_i = \int_0^{\infty} \underline{G}_i(z)\, dz \qquad (3.2.42)$$

we write (2.2.12) as

$$\Delta g_i = \left\langle \underline{G}_i, \sum_{k=1}^{N} \gamma_k \underline{b}_k \right\rangle = \sum_{k=1}^{N} \gamma_k \langle \underline{G}_i, \underline{b}_k \rangle \tag{3.2.43}$$

From the definition of the inner product (equation (2.2.1)) and observing that $\underline{b}_k$ is independent of z,

$$\Delta g_i = \sum' \gamma_k B_{ik} \tag{3.2.44}$$

with

$$B_{ik} = \underline{b}_i \cdot \underline{b}_k \tag{3.2.45}$$

where the dot indicates the scalar product of the two (2M-1)-dimensional vectors. Thus, under our discretization, the matter of evaluating the inner product matrix reduces to evaluating the matrix $\underline{\underline{B}}$, which, as can be seen from (3.2.45), is the sum of matrices

$$\underline{\underline{B}} = \underline{\underline{B}}^{(1)} + \underline{\underline{B}}^{(2)} + \ldots \underline{\underline{B}}^{(d_{N-1})} \tag{3.2.46}$$

The elements of these matrices are the products of i-values for a single element of the (2M-1)-tuple $\{b_i^{(j)}\}$. For example, for the σ_1-matrix,

$$\underline{\underline{B}}^{(1)} = \begin{bmatrix} b_1^{(1)} b_1^{(1)} & b_1^{(1)} b_2^{(1)} & b_1^{(1)} b_2^{(1)} & \cdots \\ b_2^{(1)} b_1^{(1)} & b_2^{(1)} b_2^{(1)} & b_2^{(1)} b_3^{(1)} & \cdots \\ \vdots & \vdots & & \\ & & & \\ & & b_N^{(1)} b_{N-1}^{(1)} & b_N^{(1)} b_N^{(1)} \end{bmatrix}$$

Since the discretization implies that $\underline{\underline{B}}$ be found rather than $\underline{\underline{\Gamma}}$ in equation (2.2.1), a considerable simplification to the problem has been achieved. We now require to evaluate the product of two integrated Fréchet kernels, rather than the integral of the product of two Fréchet kernels. To illustrate the discretization we next consider the most simple layered conducting half-space: that consisting of two layers.

3.3 The Two-Layer Half-Space

We now consider, in some detail, the constrained situation of a two-layer half-space parameterized by the vector $\underline{\sigma} = (\sigma_1, \sigma_2, d)$ where σ_1 and σ_2 are the conductivities of the first and second layers respectively, and d is the depth of the discontinuity. Figure 3-3 illustrates the model.

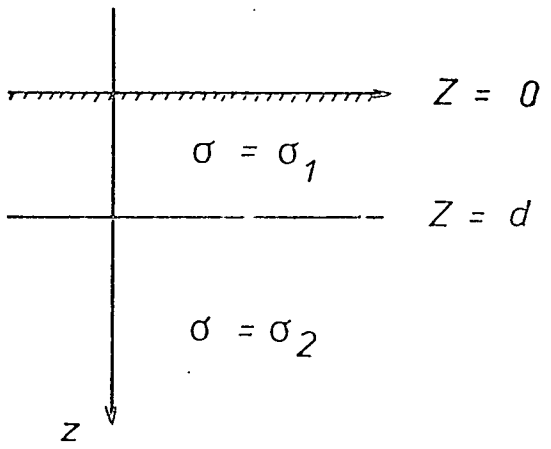

FIG. 3-3

Substituting the conductivity distribution

$$\sigma(z) = \sigma_1 H(d-z) + \sigma_2 H(z-d) \tag{3.3.1}$$

into equation (3.2.35), we have

$$\gamma_i = \sigma_1 \int_0^d [1 + Q^2(z)] \mathcal{E}^2(z)\, dz + 2\sigma_2 \int_d^\infty \mathcal{E}^2(z)\, dz \tag{3.3.2}$$

Having constructed γ_i, the variation $\delta\gamma_i$ (to first order) is expressible by components as follows:

$$\delta\sigma_1: \int_0^\infty [H(d-z)(1+Q(z)^2)\mathcal{E}^2(z) \tag{3.3.3a}$$

$$+\sigma_1 H(d-z)\frac{\partial}{\partial\sigma_1}[(1+Q(z)^2)\mathcal{E}^2(z)] + \sigma_2 H(z-d)\frac{\partial}{\partial\sigma_1}[(1+Q(z)^2)\mathcal{E}^2(z)]\, dz$$

$$\delta\sigma_2: \int_0^\infty [H(z-d)(1+Q(z)^2)\mathcal{E}^2(z) \tag{3.3.3b}$$

$$+\sigma_1 H(d-z)\frac{\partial}{\partial\sigma_2}[(1+Q^2(z))\mathcal{E}^2(z)] + \sigma_2 H(z-d)\frac{\partial}{\partial\sigma_2}[(1+Q^2(z))\mathcal{E}^2(z)]\, dz$$

$$\delta d: \int_0^\infty \Big[\sigma_1 \frac{\partial}{\partial d}\Big[(1+Q(z)^2)\mathcal{E}^2(z)H(d-z)\Big] + \sigma_2 \frac{\partial}{\partial d}\Big[(1+Q(z)^2)\mathcal{E}^2(z)H(z-d)\Big]\Big] dz$$

We refer to our observation in the previous Chapter that $\mathcal{E}(z)$ is continuous across the interface at $z = d$, and $Q(z)$ is <u>not</u> continuous. The presence of the Heaviside step-functions in the $\delta\sigma_1$- and $\delta\sigma_2$-components ensures that the integrations on $(0,\infty)$ do not involve 'integration across' the discontinuity $z = d$. However, care must be taken with the d-component, since one requires to perform the partial differentiation with respect to the parameter d appearing in a generalized function. Lighthill (1958, Chapter 2) indicates how we might proceed: we can write the δd-component as

$$\int_0^d \sigma_1 \frac{\partial}{\partial d}\Big[1+Q(z)^2\Big]\mathcal{E}^2(z)\, dz + \int_d^\infty \sigma_2 \frac{\partial}{\partial d}\Big[(1+Q(z))\mathcal{E}^2(z)\Big]\, dz + \int_0^\infty \Big[\sigma_1 - \sigma_2 + \sigma_1 Q^2(d-0) - \sigma_2 Q^2(d+0)\Big]\mathcal{E}^2(z)\delta(z-d)\, dz$$

Since $\mathcal{E}^2(z)\, Q^2(z)$ is continuous across $z = d$, we observe

$$\sigma_1 Q^2(d-0) = \sigma_2 Q^2(d+0)$$

and the δd-component is given by

$$\int_0^d \sigma_1 \frac{\partial}{\partial d}\Big[(1+Q(z)^2)\mathcal{E}^2(z)\Big]\, dz + 2\int_d^\infty \sigma_2 \frac{\partial}{\partial d}\mathcal{E}^2(z)\, dz + \int_0^\infty (\sigma_1 - \sigma_2)\mathcal{E}^2(z)\,\delta(z-d)\, dz \qquad (3.3.3c)$$

where we have set $Q(z) = 1$ in $z \geq d$. Expressing equations (3.3.3) in the form of equation (3.2.16), we may write

$$\delta\gamma_i = \left\{ \int_0^d \mathcal{E}^2(z)\, dz \right\} \delta\sigma_1 + \left\{ \int_d^\infty \mathcal{E}^2(z)\, dz \right\} \delta\sigma_2 + \left\{ (\sigma_1 - \sigma_2)\, \mathcal{E}^2(d) \right\} \delta d + \Upsilon(\sigma,\omega) \tag{3.3.4}$$

where the required expression for $\Upsilon(\sigma,\omega)$ can be inferred from equations (3.3.3). We may write $\Upsilon(\sigma,\omega)$ also in 'component form' by the expression $(\Upsilon^{(1)}, \Upsilon^{(2)}, \Upsilon^{(d)})$, the mth component of which is defined

$$\Upsilon^{(m)} = \int_0^\infty \left[\sigma_1 H(d-z) \frac{\partial p}{\partial m} + \sigma_2 H(z-d) \frac{\partial p}{\partial m} \right] dz \; ; \; m \in \{\sigma_1, \sigma_2, d\}$$

where $p = (1 + Q(z)^2)\, \mathcal{E}(z)^2$. Equation (3.3.4) will constitute a satisfactory Fréchet kernel if $\Upsilon^{(m)} \equiv 0$, for each m. Before considering whether error is afforded to equation (3.3.4) by neglecting Υ, we try to illustrate the integrands associated with equations (3.3.3).

We first ascertain that our present expressions (i.e. equations (3.3.3)) are consistent with our results for the homogeneous half-space discussed in Section 3.2.d. To do this we convert our two-layer half-space to a homogeneous conductor by setting $\sigma_1 = \sigma_2$ in equations (3.3.3), and observe how the kernel defined by equation (3.2.24) and illustrated by the dashed line in Fig. 3-1, decomposes into a $\delta\sigma_1$- and $\delta\sigma_2$-component. The

resulting expressions for the integrands, appearing in equations (3.3.3a) and (3.3.3b), are illustrated in Fig. 3-4 by the solid line and dotted line respectively. They are seen to be discontinuous across z = d, as one might expect. We treat the case where $\delta\sigma_1 = \delta\sigma_2$, since in this case if we <u>add</u> the two integrands of (3.3.3a) and (3.3.3b) we should arrive at the kernel (3.2.24). In fact this sum is performed numerically, and we plot it in Fig. 3-4: we see the sum of the two discontinuous integrands of (3.3.3a) and (3.3.3b) results in the continuous dashed curve -- and this curve is identical to the dashed curve in Fig. 3-1.

Having assured ourselves that our expressions (3.3.3) are consistent with our previous discussion in Section 3.2.d, we now attempt to illustrate the integrands of Υ for a particular conductivity constraint, σ_2/σ_1. This is done in the six illustrations Fig. 3-5. Before discussing this diagram, we make the following explanation: the depth variable, z, is measured dimensionlessly in the skin-depths of the surface conductor. If z' is the depth in metres, the depth z in Figure 3-5 is transformed by z = z'/s, where

$$s = \left(\frac{2}{\mu \omega \sigma} \right)^{\frac{1}{2}}$$

- all quantities are in SI units. Making such a transformation does not affect the $\delta\sigma_1$ and $\delta\sigma_2$ components if one also considers the conductivities to be normalized

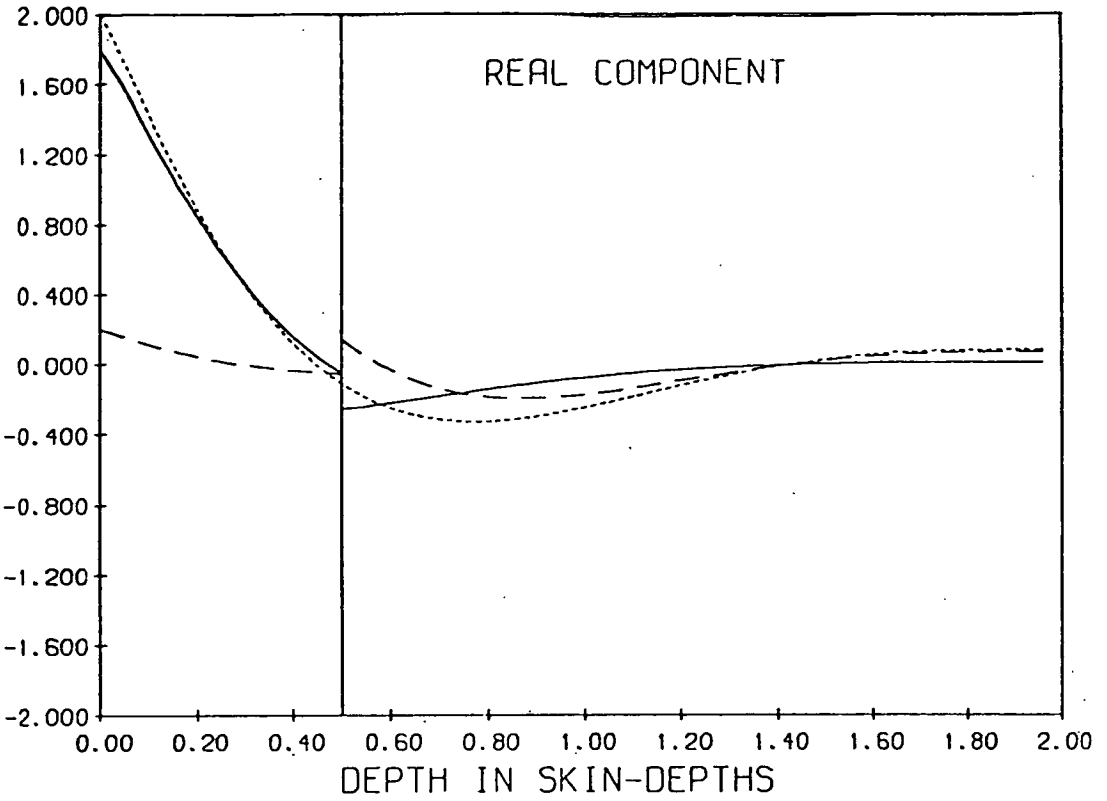
REAL COMPONENT
2.000
1.600
1.200
0.800
0.400
0.000
-0.400
-0.800
-1.200
-1.600
-2.000
0.00
0.20
0.40
0.60
0.80
1.00
1.20
1.40
1.60
1.80
2.00
DEPTH IN SKIN-DEPTHS

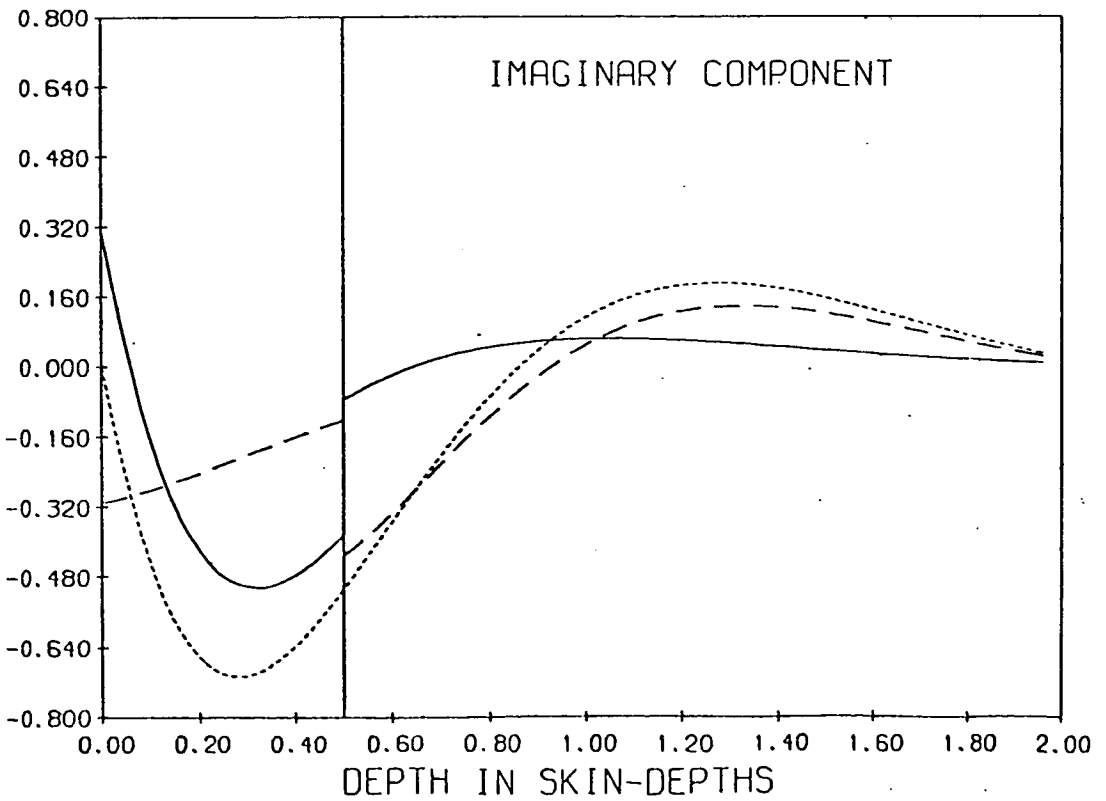
IMAGINARY COMPONENT
0.800
0.640
0.480
0.320
0.160
0.000
-0.160
-0.320
-0.480
-0.640
-0.800
0.00
0.20
0.40
0.60
0.80
1.00
1.20
1.40
1.60
1.80
2.00
DEPTH IN SKIN-DEPTHS

with respect to the conductivity of the top layer. Since $\mathcal{E}(z)$ and the integrands of (3.3.3a) and (3.3.3b) are dimensionless, such transformations do not alter these expressions; at the same time, such transformations render the model parameters dimensionless in a natural way. Of course, the integrals (as opposed to the integrands) still have units of 'depth' [m], and since the response Y_i is the reciprocal of impedance, we expect it to have dimensions of $[\text{ohm}^{-1}]$. The distribution $\sigma(z)$ -- and the perturbation $\delta\sigma(z)$ -- have units of $[\text{ohm}^{-1} - \text{m}^{-1}]$. The integrand of the δd-component (3.3.3c) is not dimensionless, but has dimension of $[\text{ohm}^{-1} - \text{m}^{-2}]$. Thus when regarding Figures 3-5, one should recall that the $\delta\sigma_1$- and $\delta\sigma_2$-integrands are naturally dimensionless and the curves represent kernels for any σ_1 and σ_2 satisfying the indicated conductivity ratio, e.g. $\sigma_2/\sigma_1 = 10$ in Fig. 3-5. On the other hand, the δd-curve has been rendered dimensionless by multiplying it by a quantity s/σ_1. This 'scale factor' will alter the magnitude of the δd-integrand curve for various values of ω or σ_1, however the shape of the curve will remain unaltered.

Another observation we should make is that the crucial linearization which is to be performed, i.e. the neglecting of Υ in (3.2.16), is a linearization effected to an equation containing the integral of the kernel $G_i(\sigma, z)$. Although examining the integrands of (3.3.3)

and comparing them to the integrands appearing in the $\delta\sigma_1$, $\delta\sigma_2$, δd-components of equation (3.3.4) is of interest, the real test of whether the integrands of (3.3.4) are to prove a satisfactory set of Fréchet kernels, must involve the evaluation of the integrals of Υ.

We plot in Fig. 3-5 the integrands of the components of equation (3.3.4), i.e. the Fréchet kernels, by the dashed lines. In addition to this we plot by solid lines the integrands appearing in the components of Υ. In this graphic way we pose the question of whether the kernels appearing explicitly in the integrals (3.3.4) form a set of suitable Fréchet kernels: if the net area enclosed by the integrands of Υ (the shaded region in Fig. 3-5) is zero, then $\Upsilon = 0$, and γ is Fréchet differentiable with kernel given by equation (3.3.4).

3.4 Linearization Error

a. Is there error of order $\delta\sigma$?

In the preceding Section we have taken some pains to state the question of the Fréchet differentiability of γ unambiguously. We have posed the question as one of ascertaining the significance (if any) of a quantity which is expressible analytically; and in Fig. 3-5 we have posed the same question as one of evaluating the area enclosed by the integrands of Υ. The intent has been

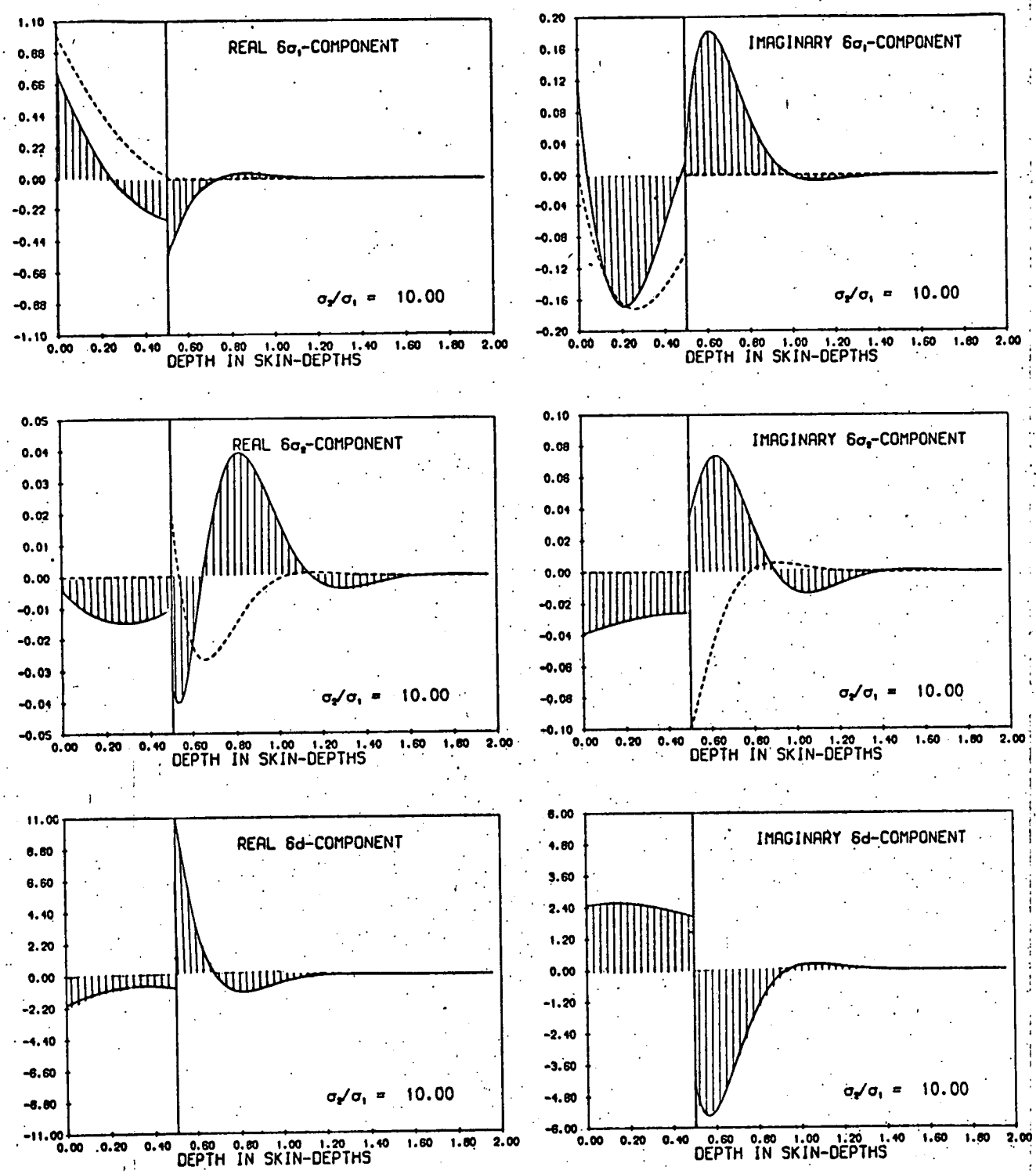

FIG. 3-5 — The dotted lines represent the kernel $f(z) = \ell^2(z)$ for the various components associated with a two-layer half-space. Also illustrated (by solid lines) are the corresponding components of the integrands of $\Upsilon(\sigma, \omega)$ in equation (3.3.4). If the integral over these integrands (in fact the shaded area) is zero, the kernel f(z) constitutes a Fréchet kernel exact first order in $\delta\sigma$.

to demonstrate unambiguously whether or not (3.3.4) constitutes an appropriate first-order kernel. If one can show that $\Upsilon = 0$, for arbitrary distributions $\sigma(z)$, then the linearization achieved by Parker (1970) is entirely satisfactory.

Equivalently, we can make the required demonstration in a rather simple manner. If γ is Fréchet-differentiable, and (3.3.4) constitutes appropriate first-order kernel, then for conductors of two layers, we have

$$\delta\gamma = \int_0^d \mathcal{E}^2(z)\, dz\ \delta\sigma_1 + \int_d^\infty \mathcal{E}^2(z)\, dz\ \delta\sigma_2 + (\sigma_1 - \sigma_2)\mathcal{E}^2(d)\,\delta d \tag{3.4.1}$$

as the first-order variation of γ. One has also a recursively defined expression for the surface impedance

$$\gamma = \left(\frac{\sigma_1}{i\omega\mu}\right)^{\frac{1}{2}} Q_1 \tag{3.4.2}$$

where Q_1 has been defined in Section 3.2.e. In this expression γ is defined as a function of the discrete set of model parameters $\{\sigma_j, d_j\}$ hence one can evaluate from (3.4.2) the partial derivatives $\partial\gamma/\partial\sigma_1$, $\partial\gamma/\partial\sigma_2$, $\partial\gamma/\partial d$, and these can be compared to the $\delta\sigma_1$-, $\delta\sigma_2$- and δd-coefficients of (3.4.1). It is a straightforward matter to show

$$\frac{\delta \gamma}{\delta \sigma_1} = \int_0^d \mathcal{E}^2(z)\, dz \qquad (3.4.3)$$

$$= \frac{d(K_2^2 - K_1^2)\ \mathrm{sech}^2 K_1 d}{(K_1 + K_2 \tanh K_1 d)^2} + \frac{\tanh K_1 d}{(K_1 + K_2 \tanh K_1 d)}$$

$$\frac{\delta \gamma}{\delta \sigma_2} = \int_d^\infty \mathcal{E}^2(z)\, dz = \frac{i\omega\mu\sigma_1\ \mathrm{sech}^2 K_1 d}{2K_2(K_1 + K_2 \tanh K_1 d)^2} \qquad (3.4.4)$$

$$\frac{\delta \gamma}{\delta d} = (\sigma_1 - \sigma_2)\mathcal{E}^2(d) = \frac{i\omega\mu\sigma_1(\sigma_1 - \sigma_2)\ \mathrm{sech}^2 K_1 d}{(K_1 + K_2 \tanh K_1 d)^2} \qquad (3.4.5)$$

We take these relationships to be the required demonstration that there is no first-order error, and that $\Upsilon = 0$. This latter equality can be demonstrated (more arduously) directly. The extension of this analysis to M-layered conductors is straightforward.

b. Error arising from $0\|\delta\sigma\|^2$

It has been our strategy to investigate the questions associated with the linearization of the inverse problem, by discretizing the functional, and then to use differential calculus to form the variation $\delta\gamma$. A similar strategy may be used to acquire some elementary view of the higher-order terms associated with the linearization of equation (2.2.3). If we regard the variation as expressed in (3.3.4) as the functional equivalent of a Taylor expansion, in the case of discretely expressed model parameters we can learn

something of the higher order contribution to the expansion by looking at second-order partial derivatives.

At this stage we follow Parker (1970) in seeking to consider the phase and amplitude of γ as data, rather than its real and imaginary parts. The necessary adjustment to equation (3.2.16) is straightforward since $\ln\gamma = \ln|\gamma| + i \arg\gamma$ and $\delta\gamma/\gamma = \delta(\ln\gamma)$.

Unlike Parker, we have not chosen to use $\ln\sigma$ as model parameter (instead of σ), nor have we chosen to minimize $\|\delta m/m\|^2$ (instead of $\|\delta m\|^2$) in equation (2.2.5). The question of whether $m(z) = \ln\sigma(z)$ results in a more suitable model parameter, in the sense that this transformation might afford some numerical advantage, can be discussed in the following illustration.

If $\ln\sigma$ is chosen as model parameter, equation (3.2.16) can be written, to first order in $\delta\sigma$,

$$\delta\gamma = \int_0^\infty \delta(\ln\sigma)\, G_i^\dagger \, dz = \int_0^\infty \frac{\delta\sigma}{\sigma} \cdot \sigma G_i \, dz \qquad (3.4.6)$$

where $G_i^\dagger$ is the Fréchet kernel associated with the parameter $\ln\sigma$: G_i is the kernel associated with the model parameter σ. Clearly $G_i^\dagger = \sigma(z)G_i(\sigma,z)$. Equation (3.2.38) is now written so that $|\delta\sigma/\sigma|^2$ is minimized (subject to constraints) rather than $|\delta\sigma|^2$. We have

$$U = \left|\frac{\sigma - \sigma_0}{\sigma_0}\right|^2 - \sum \nu_i (\gamma_i - g_i(\sigma)) \qquad (3.4.7)$$

A stationary solution for this is achieved by

$$\frac{\delta\sigma}{\sigma} = \sum \nu_i \sigma G_i(\sigma,z) \qquad (3.4.8)$$

Substituting (3.4.8) into (3.4.6) we obtain

$$\delta\gamma_j = \sum_i \nu_i \int_0^\infty \sigma(z)^2 G_i G_j \, dz \qquad (3.4.9)$$

For purposes of this illustration, we take the matrix $\langle G_i, G_j\sigma^2 \rangle$ to be diagonal (the diagonalization of the matrix can anyway be accomplished following the procedure described in Section 2.2.e) and deduce

$$\nu_j = \delta\gamma_j \left[\int_0^\infty \sigma^2 G_j^{\,2} \, dz \right]^{-1}$$

Substituting this result into equation (3.4.8), we obtain for the model perturbation

$$\frac{\delta\sigma}{\sigma} = \sum_j \frac{\sigma(z) G_j(\sigma,z) \, \delta\gamma_j}{\int_0^\infty \sigma^2(z) G_j^{\,2}(\sigma,z) \, dz} \qquad (3.4.10)$$

or, alternatively expressed,

$$\delta\sigma(z) = \sum_j \frac{\sigma(z)^2 G_j(\sigma,z) \, \delta\gamma_j}{\int_0^\infty \sigma^2(z) G_j^{\,2}(\sigma,z) \, dz} \qquad (3.4.11)$$

If the model distribution σ is independent of z, we obtain for $\delta\sigma$ the same perturbation as was achieved by minimizing $|\delta\sigma|^2$. One can interpret the denominator of (3.4.10) and (3.4.11) as the weighted average of $\sigma^2(z)$, with weighting function $G_i(\sigma, z)$. If, for $z = z_k$,

$\left| \int_0^\infty \sigma^2(z)\, G_j^{\,2}(\sigma,z)\, dz \right| \ll \sigma^2(z_k)$ one might expect the perturbation $\delta\sigma(z_k)$ from (3.4.10) to be somewhat greater than that achieved by minimizing $\|\delta\sigma\|^2$. On the other hand if $\left| \int_0^\infty \sigma^2(z)\, G_j^{\,2}(\sigma,z)\, dz \right| > \sigma^2(z_k)$ then the perturbation $\delta\sigma(z_k)$ will be less than that achieved by minimizing $\|\delta\sigma\|^2$. The question of whether it is advantageous to choose as model distribution $\ln\sigma$ instead of σ requires specific investigation for individual problems. For our magnetotelluric problem, we have chosen to use simply $m = \sigma(z)$.

The response function at the surface of a layered half-space is given by (3.4.2) as

$$\gamma_i = \left(\frac{\sigma_1}{i\omega\mu}\right)^{\frac{1}{2}} Q_1$$

where Q_1 and γ_1 are defined previously. We can now identify the $\delta\sigma_k$-coefficient of the expanded variation

$$\left[\frac{\delta\gamma_i}{\gamma_i}\right]_{\sigma_k} = \tfrac{1}{2}\kappa_{k1}\,\frac{\delta\sigma_1}{\sigma_1} + \frac{1}{Q_1}\left\{\frac{\partial Q_1}{\partial\sigma_k}\,\delta\sigma_k + \frac{1}{2}\sum_{j=1}^{M}\frac{\partial^2 Q_1}{\partial\sigma_j\partial\sigma_k}\,\delta\sigma_k\,\delta\sigma_j + \ldots\right. \qquad (3.4.12)$$

where κ_{k1} is a Kroeneker-delta. In order to observe the structure of the second-order terms, we try to identify the function $f_{jk}(\sigma,\omega)$ which satisfies

$$\frac{\partial^2 Q_1}{\partial\sigma_j\partial\sigma_k} = \frac{2}{\sigma_j}\, f_{jk}(\sigma,\omega)\,\frac{\partial Q_1}{\partial\sigma_k} \qquad (3.4.13)$$

If we set $\delta\sigma_j = \beta_j \sigma_j$, where β_j is the relative variation in σ_j , we may write the variation in (3.4.12) as

$$\left[\frac{\delta\gamma_i}{\gamma_i}\right]_{\sigma_k} = \frac{K_{k1}}{2}\frac{\delta\sigma_1}{\sigma_1} + \frac{1}{Q_1}\frac{\partial Q_1}{\partial\sigma_k}\left\{1 + \sum_j f_{jk}(\sigma,\omega)\beta_j\right\}\delta\sigma_k + \ldots \tag{3.4.14}$$

and consider the criterion for Fréchet differentiability for the kth parameter to be the condition

$$\left|\sum_j f_{jk}(\sigma,\omega)\beta_j\right| << 1 \tag{3.4.15}$$

If this condition is satisfied, equation (3.4.14) represents the $\delta\sigma_k$-component in a first-order equation such as (3.2.16) or (3.3.4). It will be noted that the criterion (3.4.15) will depend on the magnitude of β_j , and thus on $\delta\sigma_j$. For a given datum γ_i and a given distribution of conductivities, $\underline{\sigma}$, (3.4.15) could be satisfied if the collection of perturbations $\{\delta\sigma_j\}$ were sufficiently small. Of course in a least-squares procedure the magnitude of the elements of $\{\delta\sigma_j\}$ are determined from the solution to equations such as (3.2.43); whether (3.4.15) is satisfied will ultimately depend upon the stability of the process and on the size of the sum of the data residuals. If we start too far removed from an acceptable model, our data residual Δq will be large and our set of perturbations may be correspondingly large as the procedure attempts to move

(in the model space) to a more exactly fitting model. Thus the significance of higher-order terms is related to the perturbation size -- after all, these terms are of order $\delta\sigma^2$, and one must expect such terms to be related to the size of $\delta\sigma$. To understand the structure of these discarded terms we can try to contour

$$\left| \beta_j \, f_{jk}(\sigma, \omega) \right| \leq a$$

where a is suitably small so that (for each j and k) (3.4.15) is satisfied. It would be appropriate to contour this function over the model space for various values of perturbation size, i.e. various values of β_j. Thus if (3.4.15) is satisfied for a large β_j, we can infer that the linearization is quite acceptable. On the other hand if (3.4.15) is not satisfied ($|\beta_j f_{jk}(\sigma,\omega)| > a$) even for small β_j, we can conclude that the linearization is rather less acceptable.

Turning specifically to the two-layer case, we identify the following functions: for the $\delta\sigma_1$-component of the variation we have

$$f_{11}(\sigma, \omega) = -\frac{K_1}{2}\left\{ \frac{K_1 d}{\left[(K_1^2 - K_2^2)d - K_2\right]} + d \tanh K_1 d \right.$$

$$\left. - \frac{1}{S}\,(1 + K_2 d \, \mathrm{sech}^2 K_1 d) \right.$$

where $S = K_1 + K_2 \tanh K_1 d$. For the $\delta\sigma_2$-component we have

$$f_{22}(\sigma, \omega) = K_2 \tanh K_1 d \; / \; 2S$$

Two cross-terms are given by

$$f_{12}(\sigma,\omega) = \frac{K_1}{4}\left\{\frac{\left(\frac{\partial Q_1}{\partial K_1}\right)\tanh K_1 d + Q_1 d\,\mathrm{sech}^2 K_1 d}{(1 - Q_1 \tanh K_1 d)} + \frac{1}{S}(1 + K_2 d\,\mathrm{sech}^2 K_1 d)\right\}$$

and

$$f_{21}(\sigma,\omega) = \frac{K_2}{4}\left\{\frac{(2K_2 d + 1)}{\left[(K_1^2 - K_2^2)d - K_2\right]} - \frac{2}{S}\tanh K_1 d\right\}$$

Also we include the d-term,

$$f_{dd}(\sigma,\omega) = -\frac{2K_1 K_2\,\mathrm{sech}^2 K_1 d}{S}\left\{1 + \frac{Q_1 S \tanh K_1 d}{K_1^2 - Q_1 K_1 K_2\,\mathrm{sech}^2 K_1 d}\right\}$$

We try to illustrate the situation represented by the formulae for $f_{11}(\sigma,\omega)$, $f_{12}(\sigma,\omega)$, $f_{21}(\sigma,\omega)$, and $f_{dd}(\sigma,\omega)$ in Figures 3-6a - 3.6d respectively.

In order to examine the structure of the higher-order contribution we consider, for each j and ν, the region of the model space defined by the condition

$$\left|\beta_j f_{j\nu}(\sigma,\omega)\right| \leq 0.1 \qquad (3.4.16)$$

to be that in which linearization is acceptable. Of course, it is a linear combination of terms (represented by the summation in equation (3.4.15)), which must appear in any linearization criterion; and in this respect each condition (3.4.16) may be thought of as a

FIG. 3-6 Contours associated with higher order terms in a two-layer half-space. The ordinate in each diagram is the depth of the discontinuity (measured in surface skin-depths), the absissa is the conductivity ratio, σ_2 / σ_1 .

a. $f_{11}(\sigma, \omega)$: the region of the model space enclosed by the contour indicated $\beta_1 = 0.05$ is a part of the space where a very small model perturbation, $\delta\sigma_1$, causes $|\beta_1 f_{11}(\sigma, \omega)|$ to exceed 0.1. Thus non-linear effects may be significant in this region. In the region outside the contour $\beta_1 = 0.2$, a relatively large perturbation in σ_1 still preserves the inequality $|\beta_1 f_{11}(\sigma, \omega)| \leq 0.1$.

b. $f_{12}(\sigma, \omega)$: the effect of a perturbation $\delta\sigma_2$ to σ_1-component of the variation $\delta\gamma/\gamma$. The contours to be interpreted in the same manner as a.

c. $f_{21}(\sigma, \omega)$: the effect of a perturbation $\delta\sigma_1$ to the σ_2-component of the variation $\delta\gamma/\gamma$.

d. $f_{dd}(\sigma, \omega)$: the effect of a perturbation δd to the d-component of the variation $\delta\gamma/\gamma$.

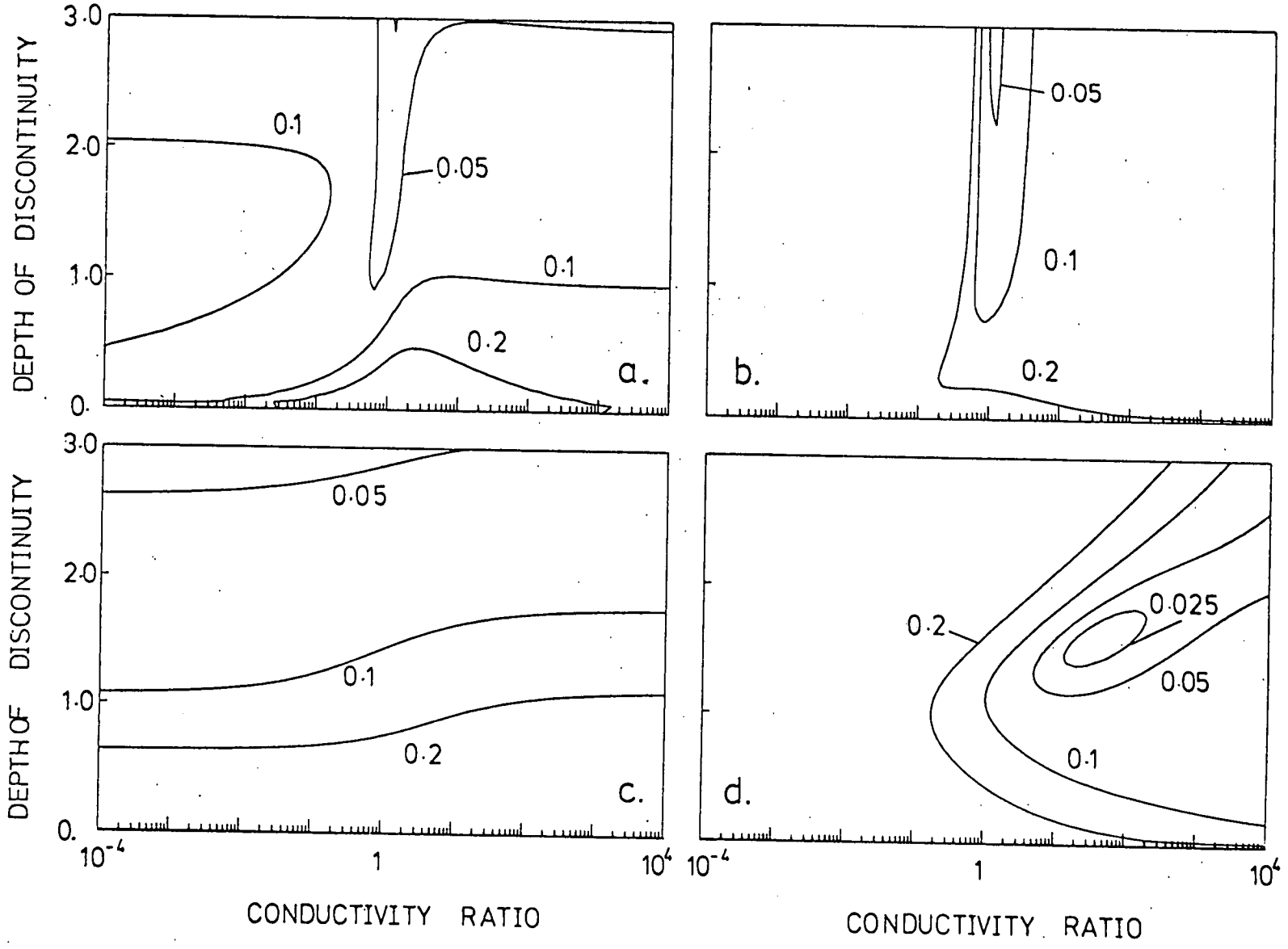
DEPTH OF DISCONTINUITY
3·0
2·0
1·0
0.
0·1
0·05
0·1
0·2
a.
0·05
0·1
0·2
b.
DEPTH OF DISCONTINUITY
3·0
2·0
1·0
0.
0·05
0·1
0·2
c.
0·2
0·025
0·05
0·1
d.
10^{-4}
1
10^{4}
CONDUCTIVITY RATIO
10^{-4}
1
10^{4}
CONDUCTIVITY RATIO

'component' of the total possible second-order contribution. Condition (3.4.16) ensures that the maximum value of the linear combination is still much less than 1. Apart from these considerations our choice of 0.1 in condition (3.4.16) is arbitrary.

Figure 3-6a displays the contours

$$\left| \beta_1 f_{11}(\sigma,\omega) \right| = 0.1$$

for the values of $\beta_1 \in \{0.025, 0.05, 0.1, 0.2\}$. The model space is characterized (in accordance with the discussion in Section 3.3) by the ratio σ_2/σ_1, and the depth of the discontinuity measured in σ_1-skin-depths. Figure 3-6a implies that, in a region enclosed by a 0.05 contour, a small perturbation of 5% in the model parameter σ_1 will be sensitive to higher order terms associated with the $\delta\sigma_1$-component; whereas in the region outside the 0.2 contour, perturbations of 20% in the $\delta\sigma_1$-component of the expansion are insensitive to the higher-order terms.

Fig. 3-6b displays the contours

$$\left| \beta_1 f_{12}(\sigma,\omega) \right| = 0.1$$

for the same values of β_1 as in the previous example.

Figure 3-6c displays the contours

$$\left| \beta_2 f_{21}(\sigma,\omega) \right| = 0.1$$

for the values of $\beta_2 \in \{0.025, 0.05, 0.1, 0.2\}$. This Figure implies that in a region enclosed by a 0.025

contour, a small perturbation in σ_1 will contribute significant higher-order terms to the $\delta\sigma_2$-component of the expansion (3.4.14).

The case of $f_{22}(\sigma,\omega)$ has not been illustrated in Fig. 3-6 since $|\beta_2 f_{22}(\sigma,\omega)| < 0.1$ throughout the model space considered in Fig. 3-6, and for the maximum β_2 we are considering (i.e. $\beta_2 = 0.2$).

Figure 3-6d illustrates the contours

$$|\beta_d f_{dd}(\sigma,\omega)| = 0.1$$

for the values of $\beta_d \in \{0.025, 0.05, 0.1, 0.2\}$. For compactness we do not display the cross-terms involving d.

c. Some specific illustrations of higher-order error

It has been our intention to achieve some qualitative view of the way higher-order terms can contribute to the inversion formalism described in Chapter 2. In this Section we consider the possible entry of this error into the least-squares procedure which has been developed. The arbitrary nature of the contours enclosed by condition (3.4.16) has already been pointed out. Also it has been suggested that the linear combination of terms (3.4.15) is related in a somewhat complicated way to its component second-order derivatives. It would therefore be reassuring to view the iterative scheme at work, and particularly to observe the paths of convergence (or otherwise) projected on the model space as it has been illustrated in Fig. 3-6. It would be interesting to try

to observe the possible effects of linearization to the procedure. To do all this a data set $\{\gamma_i\}$ is generated from a known particular model $\underset{\sim}{\sigma}^0$; various (sometimes quite remote) starting models $\underset{\sim}{\sigma}^s$ are selected, and we plot the path in the model space followed by each iteration, in a least-squares Backus-Gilbert procedure.

Figure 3-7 A involves the (error-free) synthetic data generated by the model $\underset{\sim}{\sigma}^0$: (σ_1 = 0.5 ohm^{-1} m^{-1} σ_2 = 0.05 ohm^{-1} m^{-1}; depth = 2.0 km) for ten periods over the range 1.0 sec $\leq$ T $\leq$ 100 sec. (We remark that the problem is easily scaled to embrace greater depths by considering a data set extending to greater periods. Some thought must be given to the depth of penetration of a given source frequency within any proposed model). A number of starting models are then selected -- labelled on Fig. 3-7 A as models 'a' through to 's', in order of ascending data residual -- and the various parameters are listed in Table 3.1, where we have also listed as a measure of the remoteness of the starting model from the 'true model' values for β_1 , β_2 , and β_d, defined by $\beta_1 = (\sigma_1^s - \sigma_1^0) / \sigma_1^0$, etc. Also we define, for the purposes of this table, the initial data residual to be

$$\text{Data residual} = \sum_{i=1}^{10} (\Delta g_i)^2 / 10 \; ^{\frac{1}{2}}$$

The paths traced in Fig. 3-7 A are the projections

associated with the highest frequency (recalling that the depth of the discontinuity, 'd' in equation (3.3.4) etc., is measured in skin-depths). The lower frequency paths would appear, if we chose to illustrate them, as quite similar paths arranged beneath those presented in Fig. 3-7. The inner product matrix appearing in equation (3.2.45) is inverted numerically, and directly, using partial pivotting along the diagonal. The asterisks in Fig. 3-7 A indicate those starting models which give rise to divergent paths -- this means to say the model perturbations suggested by the least-squares process resulted in negative unphysical parameters, or a hugely increased data residual.

In Fig. 3-7 B, we seek to illustrate convergence towards the model $\underset{\sim}{\sigma}^0$: ($\sigma_1 = 0.5$ ohm^{-1}m^{-1}; $\sigma_2 = 14.$ ohm^{-1}m^{-1} ; depth = 2 km) for a data set over the period range $5.0 \leq T \leq 100$ sec. This particular model is rather esoteric from the point of view of the practical magneto-telluric problem. However, it allows us to inspect convergence on the right hand side of the model space illustrated in Fig. 3-7, without the necessity of seriously reforming the range of frequencies represented in the data set. Of course, there is no difficulty in extending the procedure to more realistic models. The starting models and parameters are listed in Table 3.2. By making comparison between Fig. 3-6 and Fig. 3-7, one may be able to infer some idea of the parts

of the model space where higher-order difficulties arise.

There is, of course, the possibility that the unsuccessful starting models in Fig. 3-7 may be affected by various numerical problems related to matrix inversion on a computer. There can be round-off error generally, or instability arising from an ill-conditioned inner-product matrix (denoted in (3.2.45) as $\underline{\underline{B}}$). Gilbert has underlined the advantages to the least-squares problem afforded by orthonormalizing the set of Fréchet kernels by diagonalizing the inner product matrix. This technique was described in Section 2.2.e, and will be discussed in greater detail in Chapter 5.

However, to complete our discussion of the linearization error, we try here to 'rank and winnow' the data in the least-squares procedure, to see if we can increase our space of successful starting models. With this in mind, we repeat the same least-squares procedure applied to the same data and starting models as were illustrated in Fig. 3-7. However, we do not invert the inner product matrix directly but transform the matrix to an orthonormal frame. We then proceed to exclude those eigenvalues for which the model variance (defined in (2.2.17)) is large. Specifically, we exclude those eigenvalues which suggest unphysical models in a given iteration, or suggest model perturbations which cause the data residual to <u>increase</u> in consecutive iterations. We terminate the process when no perturbation can satisfy these criteria.

Although these criteria are crude, they possess the virtue of simplicity, and Fig. 3-8 shows that they prove effective for our chosen starting models and data (which are, after all, 'perfectly accurate' data). Our aim is to illustrate the validity, or at least the quality, of a linearization, and we do not suggest that the above-mentioned simple criteria are to be preferred in practical problems. Jupp and Vozoff (1975) describe in some detail a number of more elaborate truncation strategies to achieve stable convergence in linearized least-squares problems, the most practised of which is probably the Marquardt (1963) maximum neighbourhood method. Incidentally, Wu (1968) applied this technique successfully to the same magnetotelluric problem we are discussing here.

From Figs. 3-7 and 3-8, one might hope to determine the regions of the model space where the initial 'direction' or magnitude of the model perturbation is unhelpful to the least-squares procedure, and it would appear that these regions correspond quite well to the contours in Fig. 3-6. In Figs. 3-7 A and 3-8 A, it seems the error is associated with the $\delta\sigma_1$-higher order terms, and in Figs. 3-7 B and 3-8 B it seems the error is associated with δd-higher order terms. In this case it seems that as β_d decreases and the data residual becomes correspondingly smaller, the stability improves. This can be observed by following the path of model 'r'

FIG. 3-7 A) model $\underset{\sim}{\sigma}$: ($\sigma_1 = 0.5$, $\sigma_2 = 0.05$, d = 2 km), indicated by arrow, is used to generate data. Starting models (listed in Table 3.1 in ascending order of data residual) and the paths of the least-squares procedure projected onto the model space are also indicated.

B) model $\underset{\sim}{\sigma}$: ($\sigma_1 = 0.5$, $\sigma_2 = 14$, d = 2 km). Starting models listed in Table 3.2.

FIG. 3-8 A) The same models as Fig. 3-7 A; the procedure has been stabilized by ranking and winnowing.

B) The same models as Fig. 3-7 B; the procedure stabilized by ranking and winnowing.

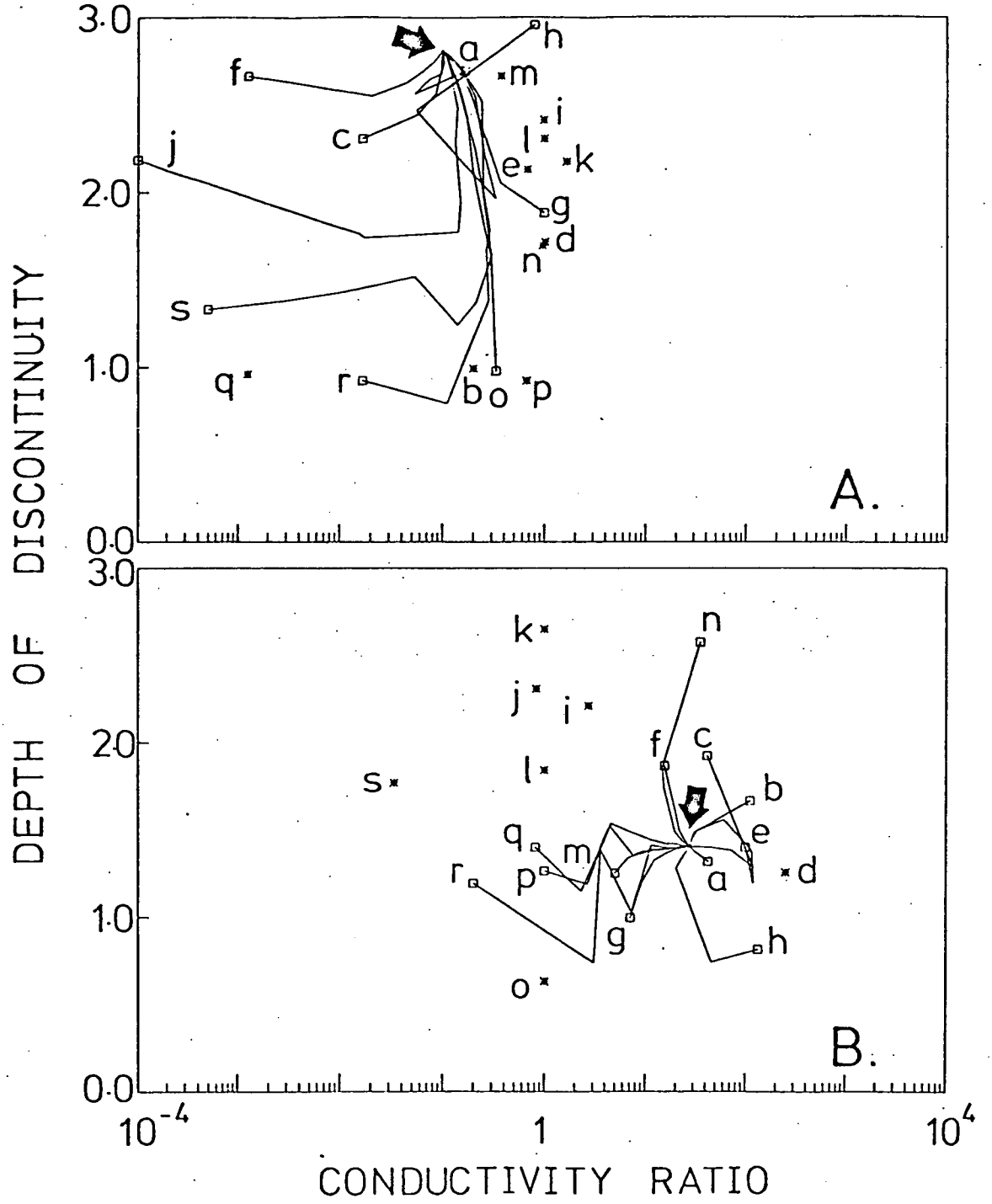
3·0
2·0
1·0
0·0
DEPTH OF DISCONTINUITY
A.
B.
10^{-4}
1
10^{4}
CONDUCTIVITY RATIO

FIG. 3-7

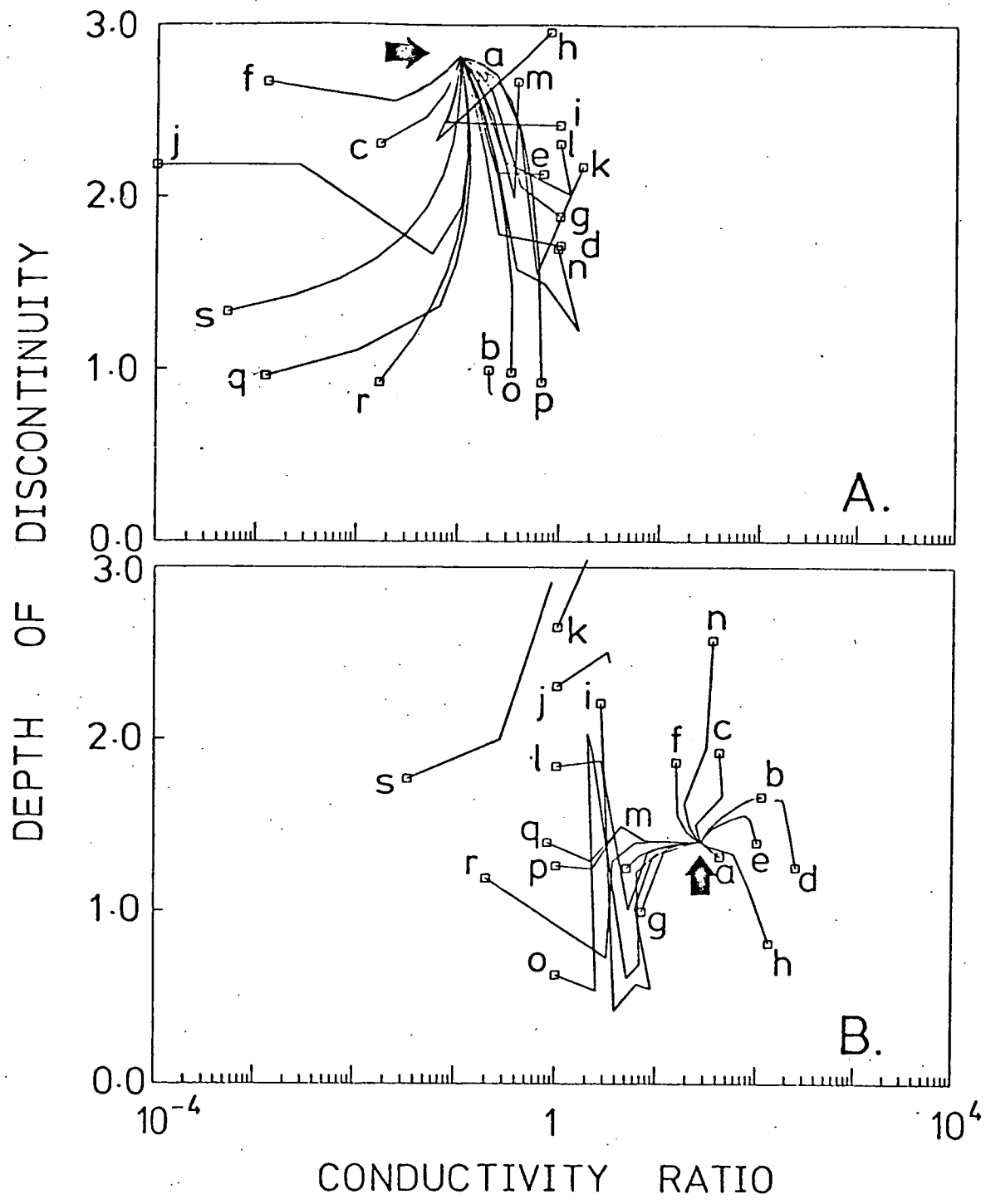
3·0
2·0
1·0
0·0
DEPTH OF DISCONTINUITY
f
a
h
m
i
j
c
l
e
k
g
d
n
s
b
q
r
o
p
A.
3·0
2·0
1·0
0·0
k
n
j
i
f
c
s
l
b
m
q
e
p
a
d
r
g
h
o
B.
10⁻⁴
1
10⁴
CONDUCTIVITY RATIO

FIG. 3-8

TABLE 3.1

Model	σ_1	β_1	σ_2	β_2	d	β_d	Residual
a	0.6	0.2	0.1	1.0	1.75	0.13	0.11
b	1.0	1.0	0.2	3.0	0.50	0.75	0.16
c	0.6	0.2	0.01	0.8	1.50	0.25	0.16
d	0.45	0.1	0.45	7.0	1.2	0.40	0.20
e	0.512	0.02	0.35	6.0	1.50	0.25	0.20
f	0.8	0.6	0.001	0.98	1.50	0.25	0.20
g	0.4	0.2	0.4	7.0	1.50	0.25	0.21
h	0.502	0.0	0.4	7.0	2.10	0.05	0.22
i	0.512	0.02	0.510	9.20	1.70	0.15	0.26
j	1.0	1.0	0.0001	1.0	1.10	0.45	0.27
k	0.3	0.4	0.5	9.0	2.0	0.00	0.28
l	0.6	0.2	0.6	1.0	1.50	0.25	0.31
m	0.8	0.6	0.3	5.0	1.50	0.25	0.32
n	0.73	0.46	0.7	13.0	1.00	0.50	0.38
o	0.3	0.4	0.1	1.0	0.90	0.55	0.40
p	0.15	0.7	0.1	1.0	1.20	0.40	0.59
q	0.65	0.3	0.0008	0.98	0.60	0.70	0.84
r	0.3	0.4	0.005	0.9	0.85	0.57	0.99
s	0.2	0.6	0.0001	1.0	1.50	0.25	1.13

TABLE 3.2

Model	σ_1	β_1	σ_2	β_2	d	β_d	Residual
a	0.4	0.2	17.0	0.21	2.10	0.05	0.08
b	0.45	0.1	50.0	2.57	2.50	0.25	0.09
c	0.60	0.2	25.0	0.79	2.50	0.25	0.10
d	0.40	0.2	100.0	6.14	2.00	0.00	0.11
e	0.55	0.1	55.0	2.93	1.90	0.05	0.11
f	0.45	0.1	7.0	0.50	2.80	0.40	0.21
g	0.70	0.4	5.0	0.64	1.20	0.40	0.22
h	0.30	0.4	40.0	1.86	1.50	0.25	0.23
i	0.55	0.10	1.50	0.89	3.0	0.50	0.29
j	0.6	0.2	0.6	0.96	3.2	0.60	0.33
k	0.55	0.10	0.55	0.96	3.60	0.80	0.35
l	0.55	0.10	0.55	0.96	2.50	0.25	0.35
m	0.3	0.4	1.50	0.89	2.30	0.15	0.35
n	0.4	0.2	14.2	0.01	4.10	1.05	0.37
o	0.5	0.0	0.50	0.96	0.90	0.55	0.38
p	0.5	0.0	0.50	0.96	1.80	0.10	0.38
q	0.55	0.10	0.45	0.97	1.90	0.05	0.38
r	1.0	1.00	0.20	0.99	1.20	0.40	0.48
s	0.6	0.20	0.02	1.00	2.30	0.15	0.60

in Fig. 3-8 B in relation to Fig. 3-6 d -- until the data residual becomes sufficiently small, the path oscillates in the 'depth'-direction.

When one considers more general classes of multi-layered models, more and more parameters are required to describe the model. Thus the number of contour curves as those illustrated in Fig. 3-6 begin to proliferate: for a three-layer model with the model parameterized as $\underset{\sim}{\sigma}: \{\sigma_1, \sigma_2, \sigma_3, d_1, d_2\}$, some twenty-five parameter curves can be constructed. It is questionable whether such a large array of diagrams can be useful for visualizing the effects of higher-order terms, and certainly the diagrams associated with a ten layered model should prove even less helpful.

However we do illustrate in Fig. 3-9 the contours

$$\left|\beta_1 f_{11}(\sigma,\omega)\right| = 0.1$$

and

$$\left|\beta_2 f_{22}(\sigma,\omega)\right| = 0.1$$

associated with a three layer model; these curves are plotted parametrically with d_1 fixed at 0.5 skin-depths, and d_2 fixed at 1.0 skin-depths. From Fig. 3-9 it appears the second-order terms may be significant for $\delta\sigma_1$-perturbations only in monotonically decreasing models, especially where $\sigma_2 \approx \sigma_3 \approx \sigma_1$.

For $\delta\sigma_2$-perturbations, there seems the possibility of error in the region $\sigma_3 \approx \sigma_2$ with σ_2 and σ_3 less

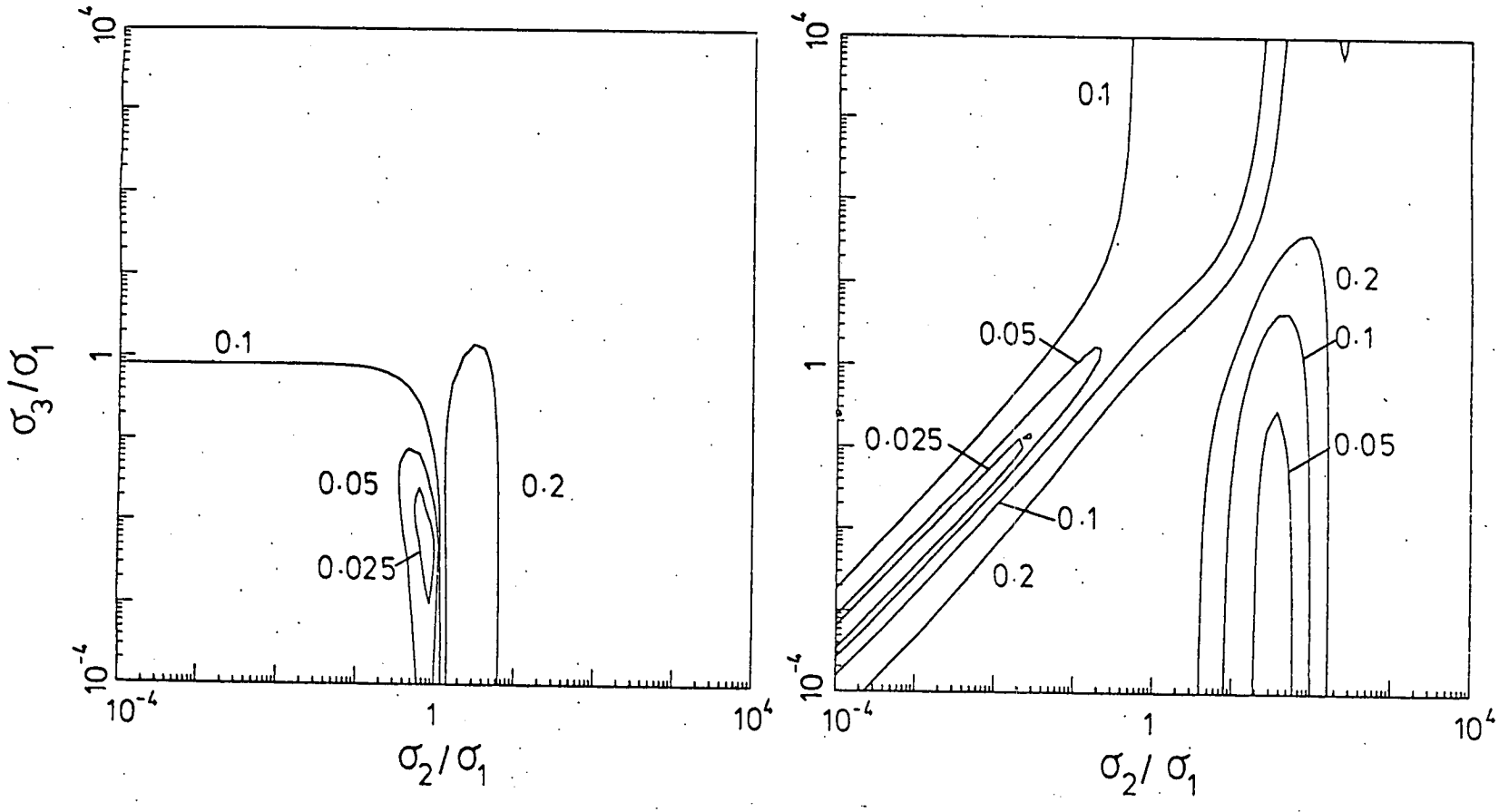

FIG. 3-9 Contours associated with $f_{11}(\sigma, \omega)$ (the diagram on the left) and $f_{22}(\sigma, \omega)$ (the diagram on the right), for a three-layer half-space with d_1 = 0.5 skin-depths, and d_2 = 1.0 skin-depths.

than σ_1. It should be pointed out that the least-squares procedure of Section 2.2.b has been applied to synthetic data for three layers (with depths allowed to vary freely) and for M layers with depths fixed. This will be described in Chapter 5.

d. Some conclusions concerning linearization error

One must not try to infer too much from an inspection of linearization error in a simple two-layer conductor. In error terms even the venture to a three layer model can be an involved step. On the other hand, although a two-layer model can be algebraically the most simple, from an inverse point of view it could prove awkward with its significant single discontinuity. For the particular data sets and starting models we have considered in Section 3.4.e, the linearization seems to have proved adequate. Indeed it has been the published experience of a number of authors that the inverse induction problem is accessible by a linear least-squares procedure.

Viewing the contours of Fig. 3-6, it would seem that some starting models are less fortunate than others from the point of view of arriving at an optimum model. When inspecting these contours one should bear in mind the greater problems associated with scattered data. Here one might hope to use some truncation strategy to minimize a data residual associated with what is really inconsistent data. One must ask whether the structure

of the higher-order contributions -- as illustrated in Fig. 3-6 -- could affect the pattern of convergence, or ultimately, the position in the model space of the local minimum that is achieved. There seems the real danger that smoothing the iterative procedure (by ranking and winnowing for example) to overcome higher-order effects, results in a degradation of resolution and information. This in turn introduces a bias into the set of acceptable models achieved by such a process. This bias is dependent upon the model one starts from -- as such it can be misleading.

It appears from Figs. 3-6 d that the quasi-linear situation is improved if one can exclude the depth of discontinuity from the parameterization -- of course this is not a very useful suggestion for the two-layer problem which is already highly constrained. However, Fig. 3-6 does suggest that the problem of locating an optimum depth of a good conductor overlain by a poor conductor is less amenable to linearization than the problem of determining the optimum conductivities themselves.

In Section 3.2.a we outlined Anderssen's criticisms: is Parker's Fréchet kernel an adequate expression of the first-order problem; and to what extent does linearizing the problem render a least-squares procedure misleading? For our simple problem we conclude that Parker's Fréchet kernel is correct; and that a linear least-squares procedure can in principle be reliable.

We have not addressed ourselves to two very important questions surrounding linearized inversion theory: how can globally distinct model solutions be explored by a theory dependent on local linearization? And how does resolution -- and the other parameters with which one tries to characterize the space of acceptable solutions -- reflect the error inherent in discarding higher-order terms from equation (2.2.3)? These rather large questions fall outwith the chosen scope of this thesis.

CHAPTER 4

DISCRETE ANALOGUES AND UNIQUENESS

4.1 Introduction

As we stated in the previous Chapter, solving for induced electromagnetic fields in conductors with one-dimensional conductivity distributions falls into the general category of classical Sturm-Liouville boundary value problems. The inverse Sturm-Liouville problem has received much attention, particularly in relation to quantum mechanics (Gel'fand and Levitan, 1954). In Chapter 1, we outlined the application of this latter inverse procedure to the induction problem as it was accomplished by Weideldt (1972). Barcilon (1974a, 1975) has also addressed the general matter of inverse eigenvalue problems which arise in geophysics, and has drawn attention to the work of Krein (1952). Barcilon has discussed particularly the question of uniqueness in inverse eigenvalue problems and has introduced, for purposes of illustration, some analogues to the general inverse problem afforded by systems of discretely specified model parameters.

Barcilon has emphasized the result proved by Borg (1946): for a unique solution $q(x)$ to the inverse Sturm-Liouville equation

$$u''(x) - (\lambda_i + q(x)) u(x) = 0 \quad , \quad x \in (0,1) \tag{4.1.1}$$

with initial conditions

$$m_1 u(0) + m_2 u'(0) = 0$$

$$n_1 u(1) + n_2 u'(1) = 0$$

it is not sufficient to have knowledge of the spectrum $\{\lambda_n\}_1^\infty$ with λ_n the eigenvalues associated with (4.1.1). In addition to this spectrum, one requires knowledge of a spectrum associated with the same equation (4.1.1), but with the eigenfunction satisfying a <u>different</u> boundary condition at one of the end-points, namely an equation

$$v''(x) - (\mu_i + q(x)) v(x) = 0 \tag{4.1.2}$$

with conditions

$$p_1 v(0) + p_2 v'(0) = 0$$

$$n_1 v(1) + n_2 v'(1) = 0 \tag{4.1.3}$$

with $p_{1,2} \neq m_{1,2}$

Borg's theorem implies that knowledge of the spectrum $\{\mu_n\}_1^\infty$ is required to find a unique solution for $q(x)$. In this Chapter we try to place the inverse induction problem within the context of Barcilon's discussion. As a preface to this, we outline Krein's results for Sturmian vibratings with distributed discrete masses. In similar fashion, we pose the problem for induction in a multi-layered conducting half-space. Then we introduce a graphical way of representing the inductive response for

a half-space as a sum of 'vectors' in the complex plane, and attempt to relate the magnitude of these vectors to energy dissipation associated with an electric and magnetic field diffusing in a conductor. Finally, we indicate the possibility of a discrete analogue to the induction problem to be found in electronic circuit theory.

4.2 The Vibrating String

Barcilon (1975) describes a discrete analogy to the general Sturm-Liouville problem, due originally to Krein (1952). The problem to be considered is that of a string consisting of N discrete masses $\{m_i\}$ separated by N lengths of string $\{\ell_i\}$. For simplicity the string is considered to be of unit length, so $\sum \ell_i = 1$; also it is considered to be under unit tension and experiencing time-harmonic vibration with frequency ω . If u_i is the vertical displacement of the string from its equilibrium position at the ith mass, m_i , (see Fig. 4-1) the Sturm-Liouville equation which must be satisfied is

$$u_i''(x) - q(x)\, u_i(x) = 0 \qquad (4.2.1)$$

the eigenvalues of which are given by

$$u_i''(x) - (\lambda_i + q(x))\, u_i(x) = 0$$

Again consulting Fig. 4-1, we find the angle θ_i between the string and the equilibrium direction (this angle is small -- consistent with the assumption of simple harmonic

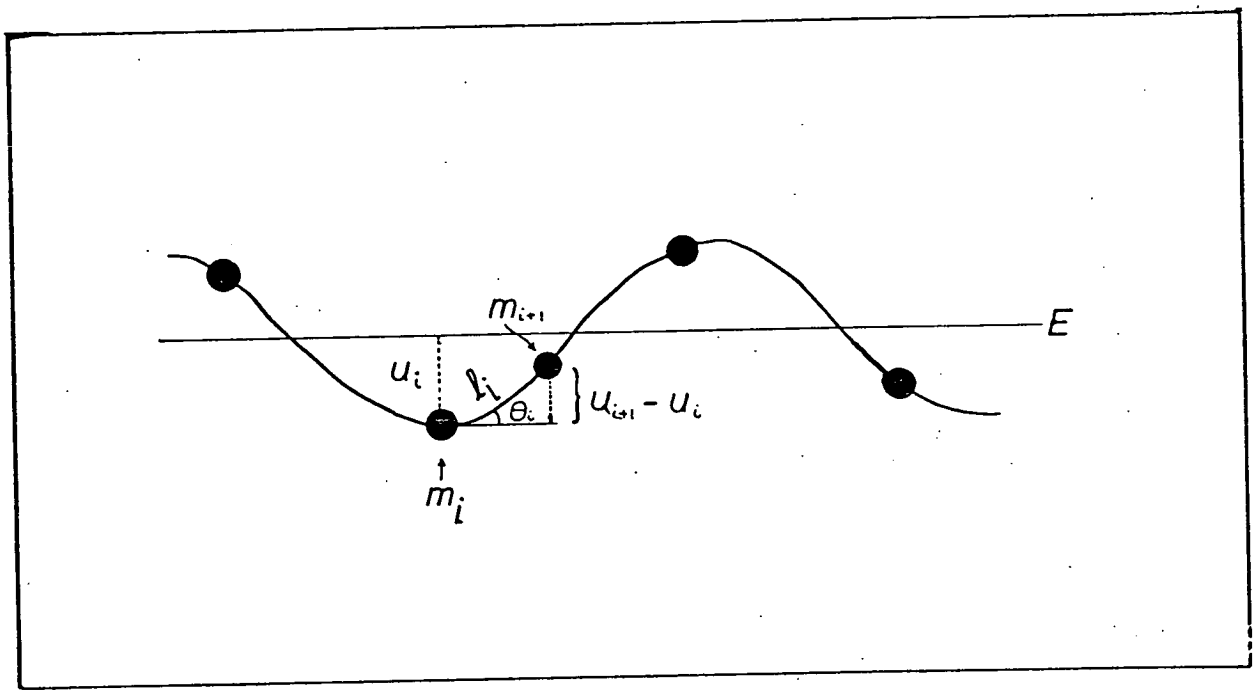

FIG. 4-1 The vibrating string with discrete masses $\{m_i\}$. The vertical displacement of the ith mass from equilibrium position E is u_i . The length of string between the ith and i + 1 th mass is ℓ_i , which makes an angle θ_i with the horizontal direction.

motion) can be expressed as

$$\theta_i \approx \frac{u_{i+1} - u_i}{\ell_i}$$

Applying Newton's Law at the ith mass by resolving forces in the vertical direction, we obtain

$$- m_i u_i \omega^2 = \theta_i - \theta_{i-1}$$

and applying this at successive points along the string, one develops a recursive relationship

$$\begin{aligned} - u_0 / \theta_0 &= \ell_0 + 1/(-\theta_0/u_1) \\ - \theta_0 / u_1 &= -m_1\omega^2 + 1/(-u_1/\theta_1) \\ - u_1 / \theta_1 &= \ell_1 + 1/(-\theta_1/u_2) \end{aligned} \qquad (4.2.2)$$

This ultimately allows the first displacement u_0/θ_0 to be expressed as a continued fraction:

$$- \frac{u_0}{\theta_0} = \ell_0 + \cfrac{1}{-m_1\omega^2 + \cfrac{1}{\ell_1 + \cdots}} \qquad (4.2.3)$$

which we express in a standard notation as

$$- \frac{u_0}{\theta_0} = \ell_0 + \frac{1}{-m_1\omega^2+} \; \frac{1}{\ell_1-} \; \frac{1}{m_2\omega^2+} \; \frac{1}{\ell_2} \cdots \frac{1}{m_N\omega^2+} \; \frac{1}{\ell_N}$$

When the terms of this fraction are reduced to a common denominator, it can be written as the following rational fraction:

$$- u_0 / \theta_0 = \prod_i \left(1 - \frac{\omega^2}{\lambda_i}\right) \Big/ \prod_i \left(1 - \frac{\omega^2}{\mu_i}\right) \qquad (4.2.4)$$

where the zeros $\{\lambda_i\}$ and poles $\{\mu_i\}$ constitute the two spectra required by the Borg theorem to ensure uniqueness in the problem. Physically the frequencies $\omega^2 = \lambda_i$ correspond to eigenfrequencies of a string with both ends fixed (since $u_0 = 0$), and the frequencies $\omega^2 = \mu_i$ to eigenfrequencies for motion with one end free ($\theta_0 = 0$). To uniquely infer the mass distribution of the string (i.e. both $\{m_i\}$ and $\{\ell_i\}$) from observations of the motion (specifically the ratio u_0/θ_0) over a complete range of frequencies, one would require knowledge of the eigenfrequencies associated with <u>two</u> modes of vibration: fixed-fixed and free-fixed.

In addition to uniqueness, it would remain to establish -- from $\{\lambda_i\}$ and $\{\mu_i\}$ -- the existence of physical solutions for $\{m_i\}$ and $\{\ell_i\}$. To this end Barcilon quotes a theorem of Stieltjes: if the spectra $\{\lambda_i\}$ and $\{\mu_i\}$ <u>interlace</u>, i.e. if $\mu_1 < \lambda_1 < \mu_2 < \cdots < \mu_N < \lambda_N$, then a solution of positive (and thus physically realizable) ℓ_i and m_i is guaranteed. By establishing (from Rayleigh's principle) this interlacing property for the string problem, <u>existence</u> of a solution to the inverse problem is assured.

4.3 <u>Uniqueness for Induction in a Stratified Half-Space</u>

In Chapter 2 we observed that our magnetotelluric response associated with a stratified conducting half-space is given by

$$H_y(0)/E_x(0) = \sigma_1 Q_1/K_1 \qquad (4.3.1)$$

where Q_1 is generated from the recursion relation (Schmucker, 1970)

$$Q_\nu = (K_{\nu+1}Q_{\nu+1} + K_\nu \tanh K_\nu d_\nu)/(K_\nu + K_{\nu+1}Q_{\nu+1} \tanh K_\nu d_\nu)$$

If we define $\alpha_\nu \equiv \tanh K_\nu d_\nu$, this can be rearranged to

$$Q_\nu = \cfrac{1}{\alpha_\nu - \cfrac{\alpha_\nu^2 - 1}{\alpha_\nu + \cfrac{K_{\nu+1}}{K_\nu} Q_{\nu+1}}} \qquad (4.3.2)$$

which gives each Q_ν associated with the layer $z_{\nu-1} < z < z_\nu$ in terms of the $Q_{\nu+1}$ associated with the deeper layer $z_\nu < z < z_{\nu+1}$ and subsequent deeper layers. We also have for the reciprocal to (4.3.1) the surface impedance

$$E_x(0)/H_y(0) = K_1 Q_1^{-1}/\sigma_1 \qquad (4.3.3)$$

where the recursion relation for Q_ν^{-1} can be written as

$$Q_\nu^{-1} = \cfrac{1}{\alpha_\nu - \cfrac{\alpha_\nu^2 - 1}{\alpha_\nu + \cfrac{K_\nu}{K_{\nu+1}} Q_{\nu+1}^{-1}}} \qquad (4.3.4)$$

The functions Q_1 in the response functions contain the boundary condition information associated with the N-1 interfaces in the conductor. Generating Q_ν

recursively, starting with $Q_N = 1$ (or $Q_N^{-1} = 1$) and terminating with Q_1 (or Q_1^{-1}), we have the following continued fraction representation for the response:

$$H_y(0)/E_x(0) = \frac{\sigma_1 K_1}{\alpha_1^-} \frac{\alpha_1^2 - 1}{\alpha_1^+} \frac{K_2/K_1}{\alpha_2^-} \frac{\alpha_2^2 - 1}{\alpha_2^+} \cdots \frac{K_N/K_{N-1}}{1} \tag{4.3.5}$$

and

$$E_x(0)/H_y(0) = \frac{K_1/\sigma_1}{\alpha_1^-} \frac{\alpha_1^2 - 1}{\alpha_1^+} \frac{K_1/K_2}{\alpha_2^-} \frac{\alpha_2^2 - 1}{\alpha_2^+} \frac{K_2/K_3}{\alpha_3^-} \cdots \frac{K_{N-1}/K_N}{1} \tag{4.3.6}$$

We are now in a position to identify the two spectra required by Borg's theorem. For this magnetotelluric problem both E_x and H_y satisfy the Sturm-Liouville equation, the eigenvalues of which are determined by

$$E_x'' - (\mu_i + K^2) E_x = 0 \tag{4.3.7}$$

with boundary conditions

$$\begin{aligned} E_x(\infty) &= 0 \\ E_x(0) &= E_0 \end{aligned} \tag{4.3.8}$$

and for the orthogonal tangential magnetic field:

$$H_y'' + (\mu_i + K^2) H_y = 0 \tag{4.3.9}$$

with the same boundary conditions as $z \to \infty$,

$$H_y(\infty) = 0$$

but the distinct condition at the surface

$$H_y(0) = H_0$$

The two quantities E_0 and H_0 correspond to the two measurements which must be performed to determine the magnetotelluric response. Thus the zeros of γ_i correspond to the eigenfrequencies of H_y, i.e. the spectrum $\{\mu_i\}_1^\infty$; and the poles of γ_i correspond to the eigenfrequencies of E_x, i.e. the spectrum $\{\lambda_i\}_1^\infty$. If the (more usual) response γ^{-1} is used, these roles are interchanged. Thus the two spectra required are implicit in the magnetotelluric response, and if a solution exists, it must be theoretically unique. To prove existence (given the response spectra $\{\lambda_i\}_1^\infty$ and $\{\mu_i\}_1^\infty$), one need only consult Weideldt's (1972) important description of the analytic properties of $E_x(z)$ and $H_y(z)$. He shows that $E_x(z)$ has simple zeros along the positive imaginary ω-axis and that these zeros interlace with the zeros of $H_y(z)$, which also lie along the positive imaginary ω-axis. Thus the zeros of $H_y(z)$ interlace with the poles of $1/E_x(z)$, and so complete knowledge of the spectra $\{\mu_i\}_1^\infty$ and $\{\lambda_i\}_1^\infty$ will ensure existence of a unique inverse solution, $\sigma(z) = (\sigma_1, \sigma_2, \sigma_3, \ldots ; d_1, d_2, \ldots)$.

For continuously defined distributions, $\sigma(z)$, uniqueness depends upon the asymptotic behaviour of the response as $\omega \to \infty$. Both Weideldt (1972) and Bailey (1970) have proved that this problem is theoretically unique and well-posed.

It is interesting to note that, for arbitrary inducing sources, the six components of $\underline{E}(0)$ and $\underline{H}(0)$

are all expressible as continued fractions. Barcilon's analysis emphasizes that uniqueness in the inverse problem depends upon two spectra being implicit in the response; each spectrum associated (in our case) with two linearly independent surface boundary conditions. Thus a response consisting of any single ratio of components of $\underline{E}(0)$ and $H(0)$ can supply spectra of which complete knowledge can ensure theoretical uniqueness.

One should also be aware that the inductive problem associated with a half-space in which the conductivity distribution is not one-dimensional does not fall into the class of inverse Sturm-Liouville problems. In this case the differential equation satisfied by $\underline{H}$ is

$$\nabla^2 \underline{H} - K^2 \underline{H} = \frac{\nabla \sigma}{\sigma} \times \text{curl } \underline{H} \qquad (4.3.10)$$

As yet, no uniqueness theorem for arbitrary conductivity distributions has been proposed.

4.4 Graphical Representation of the Response

In Chapter 3 we showed that the magnetotelluric response of a stratified half-space could be expressed in terms of a weighted average of the model parameter, i.e.

$$\gamma_i = \sum_{j=1}^{N} a_j \sigma_j \qquad (4.4.1)$$

with the weighting coefficients given by

$$\alpha_j = \int_{z_{\nu-1}}^{z_\nu} \mathcal{E}(z)^2 \, (1 + Q(z)^2) \, dz \qquad (4.4.2)$$

These coefficients themselves depend upon the model parameters, attesting to the non-linearity of the problem. Since γ is the reciprocal of the surface impedance, we can visualize the sum (4.4.1) as the result of summing the reciprocals of a set of N 'effective impedances', and the surface impedance to be the result of N such 'effective impedances' in parallel. We can illustrate the sum of complex numbers in (4.4.1) graphically in the complex plane. In Fig. 4-2 we illustrate the impedance associated with a stratified (but homogeneous) half-space. We see that the segments associated with successively deeper layers, have successively greater phases. The line which represents the vector sum of the segments has magnitude $|\gamma|$ and makes an angle ϕ (the phase of γ) with the positive real axis. In Figures 4-3a and 4-3b, we illustrate the impedance diagrams obtained for various five-layer models at various indicated periods.

4.5 Energy Dissipation and Inductive Response

In addition to equation (4.4.1) one can alternatively express the response γ as

$$= \beta \left[\int_0^\infty E(z)^2 \, dz + i\omega\mu \int_0^\infty H(z)^2 \, dz \right] \qquad (4.5.1)$$

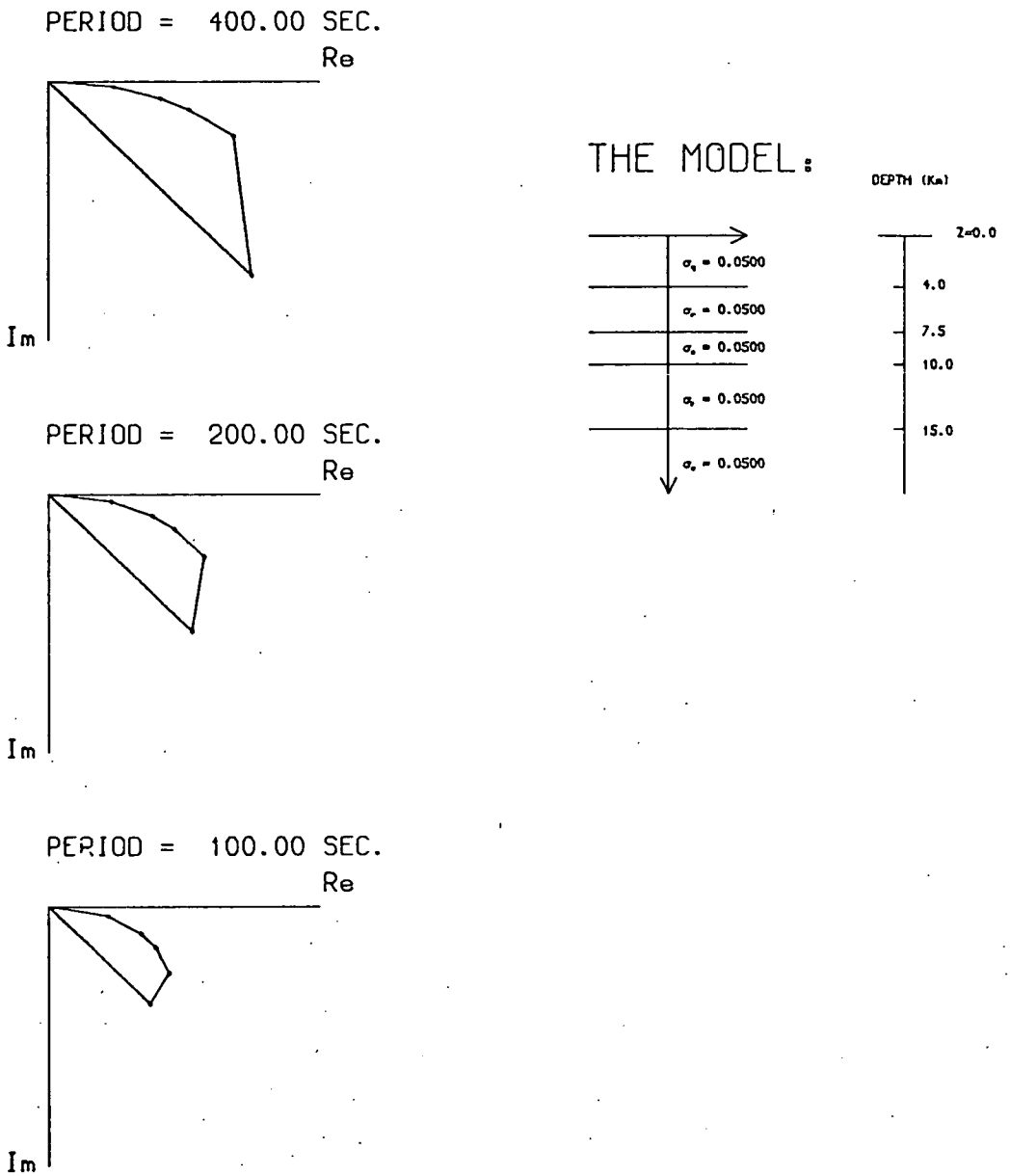

FIG. 4-2 The response Y_i plotted as a sum of 'vectors' in the complex plane for the indicated homogeneous model and for the indicated periods. The line drawn from the origin to the extremity of this sum has magnitude $|Y_i|$ and makes an angle $\arg Y_i$ with the positive real axis. For homogeneous conductors this angle is $-\frac{\pi}{4}$.

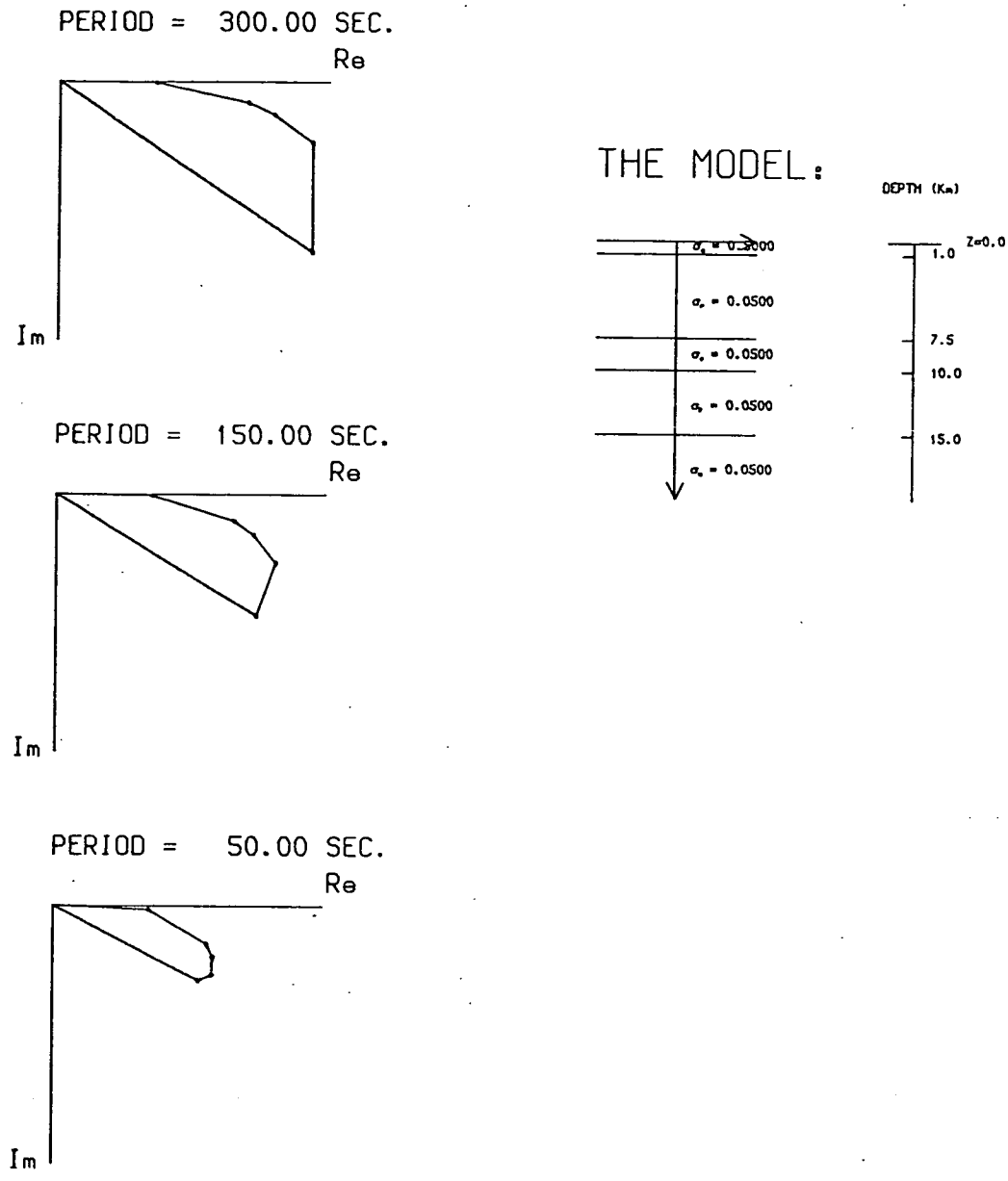

FIG. 4-3 a The complex response γ_i plotted as a vector sum for the indicated model: there is a thin (1 km) high conductivity layer near the surface. Relatively good conductivity at the surface can be associated with small phase angle.

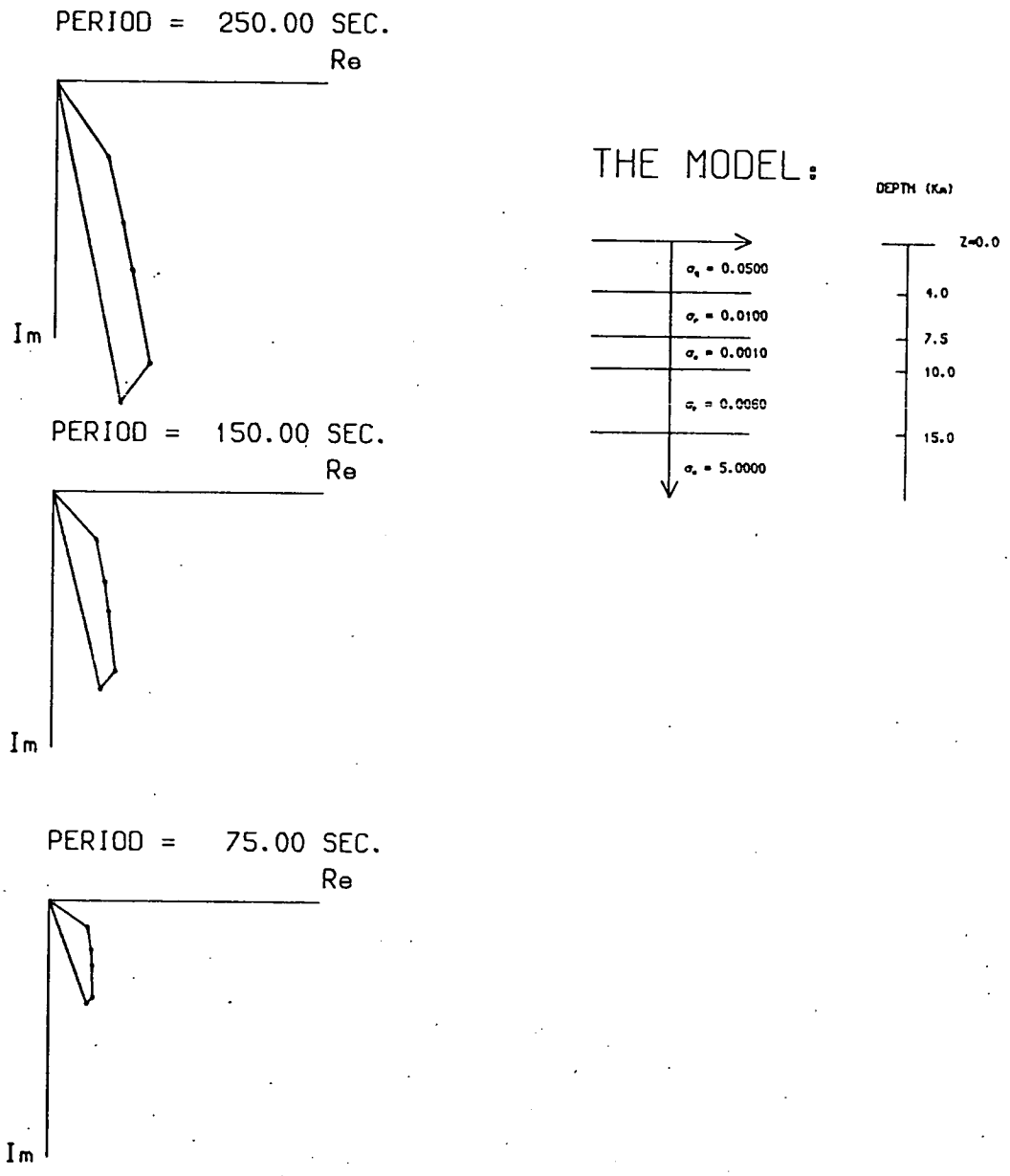

FIG. 4-3 b The complex response γ_i plotted for the model indicated: an extremely good conductor is situated at $z \geq 15$ km. Relatively poor conductivity at the surface can be associated with larger phase angles.

where $\beta = E(0)^{-2}$. Since we are considering the inducing fields to be uniform in the x - y plane, the integration in (4.5.1) may be thought of as a degenerate volume integration of an infinitely extending field as it diffuses downwards into a conductor. We seek to consider the integrand of (4.5.1) in terms of energy flux density which, when integrated over the x - y surface, provides the energy flux of the downward diffusing field. When this, in turn, is integrated over depth, z, we determine the total energy of dissipation. In these circumstances the total joule dissipation (associated with a unit surface $dA = dx\ dy$) in a conducting layer of thickness $z_{\nu-1} \leq z \leq z_{\nu}$ is

$$\widetilde{W}_E = \tfrac{1}{2} \int_{z_{\nu-1}}^{z_{\nu}} \sigma\ E\ E^*\ dz \qquad (4.5.2)$$

and the energy stored in the magnetic field is

$$\widetilde{W}_H = \tfrac{1}{2}\ \mu\omega \int_{z_{\nu-1}}^{z_{\nu}} H\ H^*\ dz \qquad (4.5.3)$$

The integrands of equation (4.5.1) can be written in terms of real and imaginary parts

$$\gamma = \beta \int \sigma\ (\ X(z) + i\ Y(z)\ )\ dz$$

with (4.5.4)

$$X(z) = \sigma(\mathrm{Re}\ E)^2 - \sigma(\mathrm{Im}\ E)^2 - 2\omega\mu\ \mathrm{Re}\ H\ \mathrm{Im}\ H$$

$$Y(z) = \mu\omega(\mathrm{Re}\ H)^2 - \mu\omega(\mathrm{Im}\ H)^2 + 2\sigma\ \mathrm{Re}\ E\ \mathrm{Im}\ E$$

Returning to our vector representation of the complex summation for γ, we can seek to relate the magnitude of in terms of energy; we define $W_E \equiv 2\widetilde{W}_E$ and $W_H \equiv 2\widetilde{W}_H$, and denote by angular brackets the integration operation over $(0,\infty)$, i.e.

$$\langle f \rangle = \int_0^\infty f(z)\, dz$$

Further we define $a \equiv \sqrt{\sigma}\,\mathrm{Re}\, E$, $b \equiv \sqrt{\sigma}\,\mathrm{Im}\, E$, $c \equiv \sqrt{\mu\omega}\,\mathrm{Re}\, H$, and $d \equiv \sqrt{\mu\omega}\,\mathrm{Im}\, H$. Hence the square of the magnitude of γ is given by

$$\beta^{-2}|\gamma|^2 = (\langle a^2\rangle + \langle b^2\rangle)^2 + (\langle c^2\rangle + \langle d^2\rangle)^2 - 2\,(\langle a^2\rangle + \langle b^2\rangle) \times (\langle c^2\rangle + \langle d^2\rangle)\cos\theta$$

which we write as

$$\beta^{-2}|\gamma|^2 = W_E^2 + W_H^2 - 2\,W_E\,W_H \cos\theta \qquad (4.5.5)$$

where

$$\cos\theta = (W_E W_H)^{-1}\Big\{ 2\langle a^2\rangle\langle b^2\rangle\left[1 - \frac{\langle ab\rangle^2}{\langle a^2\rangle\langle b^2\rangle}\right] + 2\langle c^2\rangle\langle d^2\rangle\left[1 - \frac{\langle cd\rangle^2}{\langle c^2\rangle\langle d^2\rangle}\right] - \langle cd\rangle\left[\langle a^2\rangle - \langle b^2\rangle\right] - \langle ab\rangle\left[\langle c^2\rangle - \langle d^2\rangle\right]$$

Thus we can visualize, from (4.5.5) the vector γ to be the 'vector sum' of two complex numbers, each with magnitude W_E and W_H respectively, and making an angle of θ with each other. For the case of a uniform conductor $a \equiv b$, and $c \equiv d$, and thus $\theta = \pi/2$. The vector γ can

be thought of as having an x-component (i.e. a real part) proportional to the magnetic energy dissipated in the conductor, and a y-component proportional to the joule dissipation in the conductor.

In Fig. 4-4 we show, for various non-uniform distributions of conductivity, the decomposition implicit in equation (4.5.5): in each example it would seem that the total vector can be decomposed into two orthogonal components, W_E along the y-axis, and W_H along the x-axis. Thus it seems that $\cos\theta \approx 0$ for wider classes of conductors than the homogeneous case.

It may be of interest to try to infer, from the summation diagrams, how each layer contributes to the overall energy dissipation (at least for cases where $\cos\theta \approx 0$). The projection of each vector segment on the y-axis may be interpreted as an indication of the contribution of that layer to the total joule dissipation. The projection on the real axis may be considered as the contribution of each segment to the total magnetic energy dissipated. Note that these projections are <u>not</u> proportional to the energy dissipated in the corresponding layer, but only serve to indicate the manner in which each layer contributes to the total energy dissipation. In most examples, the deeper layers contribute negatively to the total real component, i.e. the magnetic energy dissipation. This could indicate that the joule dissipation in the bottom layer is coupled to the magnetic

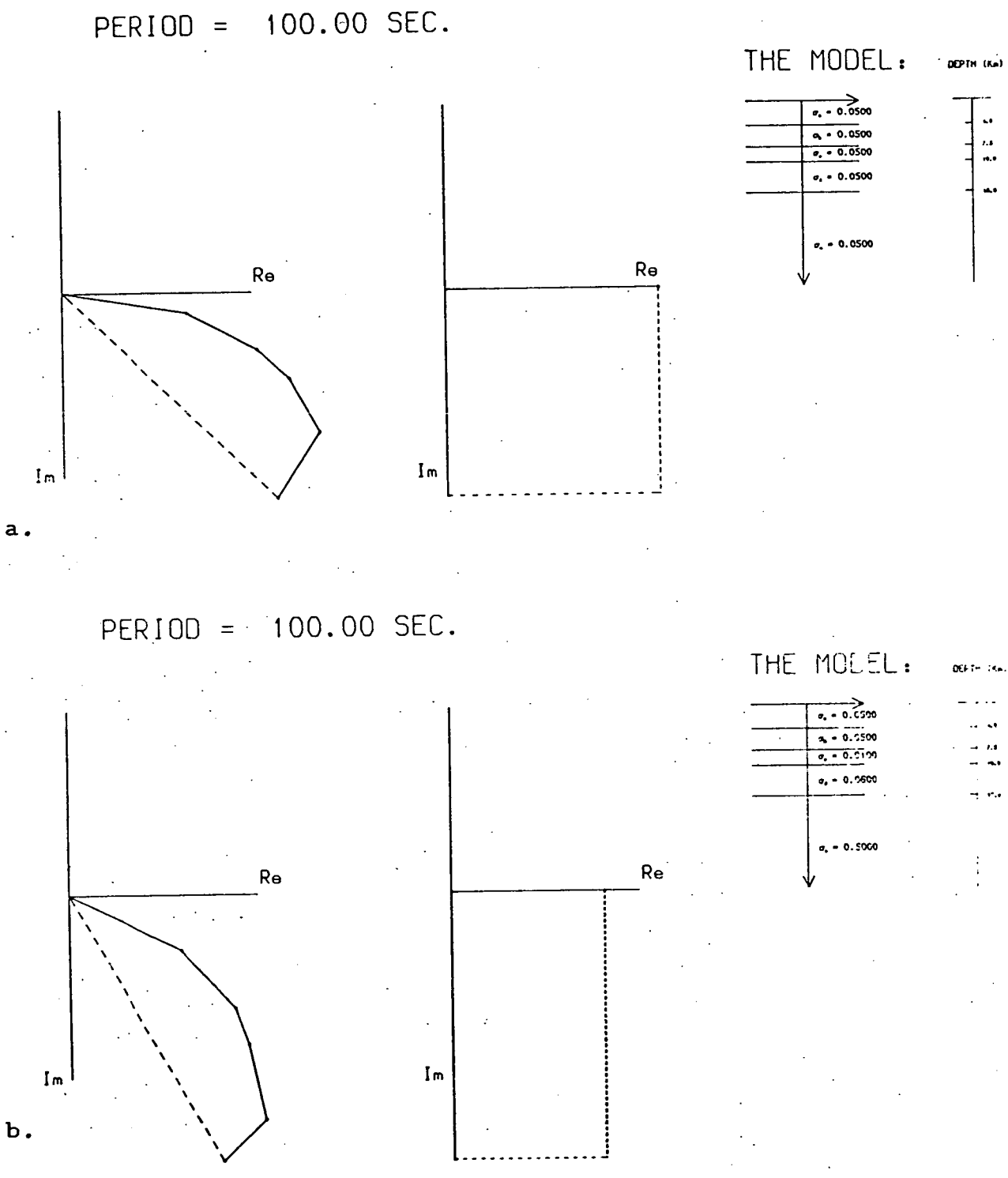

FIG. 4-4 a-d Decomposition of the summation of γ_i in the complex plane into components proportional to W_E (the fine dotted line) and W_H (the coarsely dotted line) defined in Section 4.5.. These two components are apparently orthogonal, implying $\cos\theta \approx 0$ in equation (4.5.5). The depths of the layers are the same as those in Fig. 4-2.

PERIOD = 100.00 SEC.

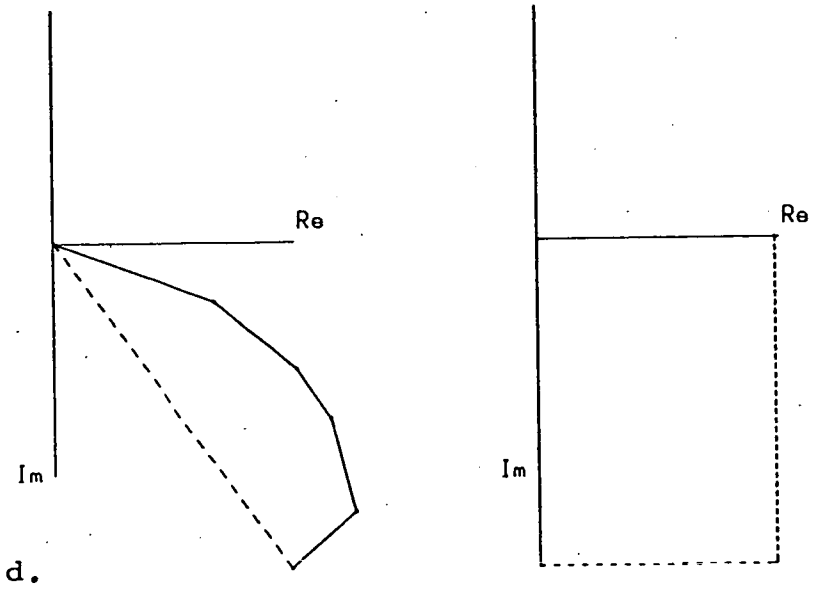

d.

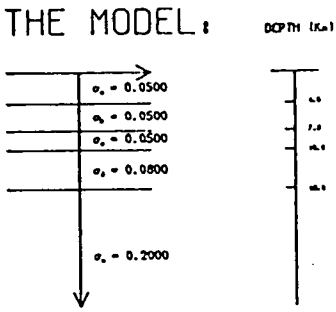

PERIOD = 100.00 SEC.

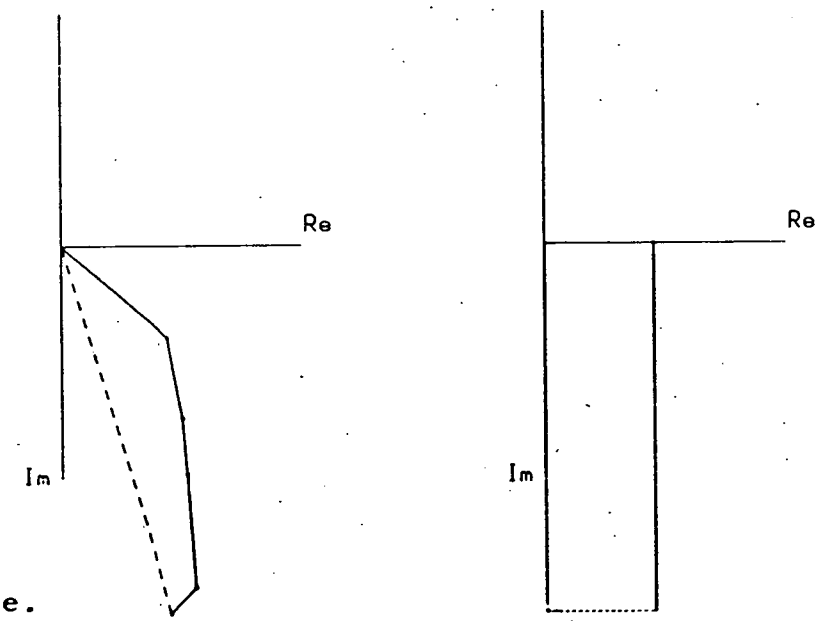

e.

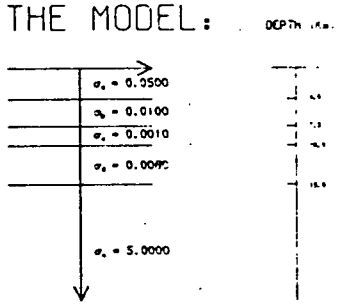

FIG. 4-4 ϕ_c, ϕ_d

energy in previous layers, and indeed these generated currents tend to reduce the overall magnetic field ... Also, in some cases, the deeper layers contribute negatively to the imaginary component as well, perhaps implying that electric energy generated in these layers exceeds the energy associated with the decaying incident field at that depth. Apart from these speculations, it is not clear whether more detailed information can be inferred from the diagrams of Section 4.4. We should note that it is not profitable to compare energies associated with different frequencies since the complex proportionality factor β is frequency dependent. However, by comparing the real and imaginary parts of δ' one can infer the relative energy dissipation in electric and magnetic fields for any given frequency.

4.6 A Discrete Circuit Analogue

In Section 4.4 we observed the similarity of the summation (4.4.1) to that one associates with the sum of reciprocal impedances for parallel circuits. We ask now whether circuit theory affords any analogue to the induction problem. Of course the sum (4.4.1) must be the sum of '*effective* impedances' in parallel, since the driving potential at depth will be smaller than at the surface. A promising circuit configuration might be that illustrated in Fig. 4-5. The effective impedance for this system is given by the continued fraction:

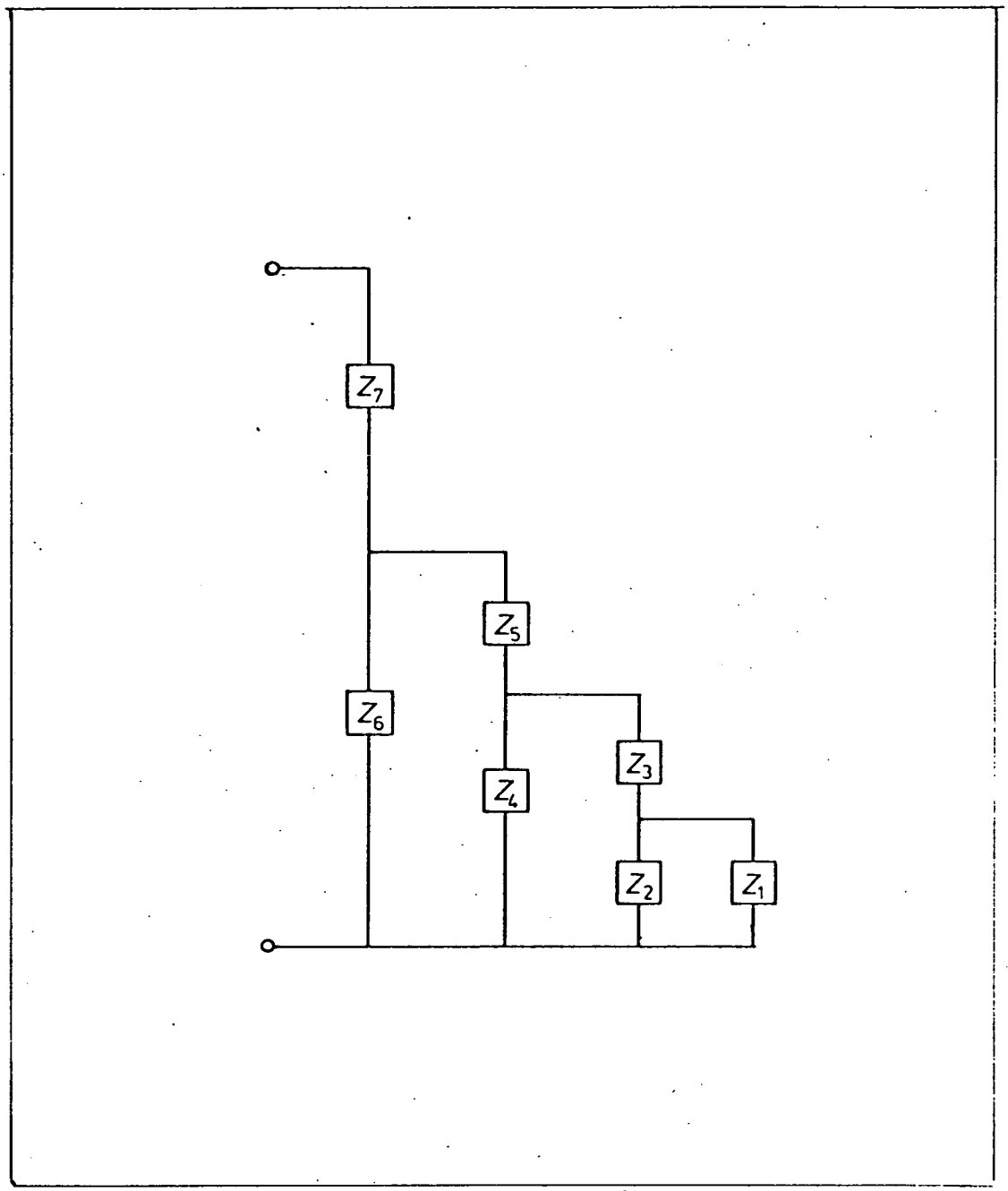

FIG. 4-5 A possible circuit analogue suggested by the vector diagrams of Fig. 4-3.

$$Z_{eff} = Z_5 + \cfrac{1}{Z_4^{-1} + \cfrac{1}{Z_3 + \cfrac{Z_1 Z_2}{Z_1 + Z_2}}}$$

where $Z_i = R_i + i\omega L_i$. If we convert this to a rational fraction, we may write its reciprocal as

$$Z_{eff}^{-1} = \sum_i Z_i^{-1}$$

and proceed to plot, in Fig. 4-6, this sum of complex numbers in the same manner as Fig. 4-3. We chose the particular values $R_i = L_i = 1$, for all i. One can at least see a resemblance of Fig. 4-6 to our previous diagrams, and can identify the curvature of the vector sum with the non-linear feed-back that we might expect as the self-inductive coupling between equivalent branches of the circuit comes into effect. Note that, in this example, we have not taken into account any possible mutual couplings which could occur.

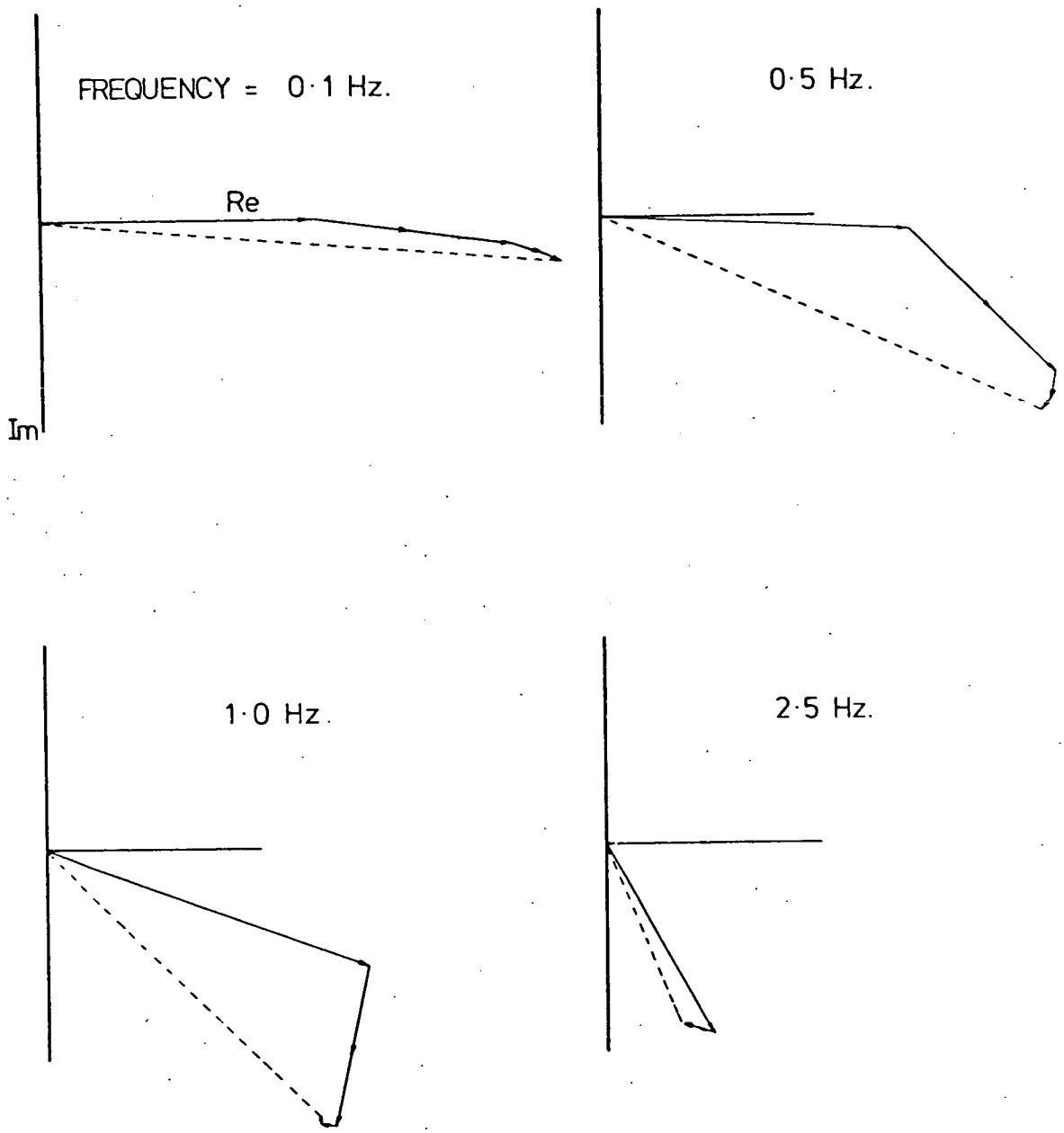

FIG. 4-6 The overall conductance (reciprocal of impedance) associated with collection of impedances as organized in Fig. 4-5. These are plotted for various frequencies as summation diagrams. Note $Z_i \equiv 1.0 + i\omega$ for this diagram.

CHAPTER 5

THE LEAST-SQUARES PROCEDURE

5.1 The Algorithm for Multilayer Conductors

In Section 3.4 it was shown that the variation $\delta\gamma_i$ for two layers is expressed by equation (3.4.1). For the case of a stratified conducting halfspace with M layers, the first order variation is given by

$$\delta\gamma_i = \int \delta\sigma(z)\, \mathcal{E}^2(z)\, dz + 0\|\delta\sigma\|^2 \qquad (5.1.1)$$

with $\delta\sigma(z)$ given by equation (3.2.31). This variation can then be expressed

$$\delta\gamma_i = \sum_j \delta\sigma_j \int_{z_{j-1}}^{z_j} \mathcal{E}^2(z)\, dz + \sum_j (\sigma_j - \sigma_{j+1})\, \mathcal{E}^2(z_j)\, \delta z_j \qquad (5.1.2)$$

From Schmucker's (1970) relationships (3.2.32) and (3.2.33), expressions for $\mathcal{E}^2(z)$ can be determined. In the layer $z_{j-1} \le z \le z_j$, $\mathcal{E}(z)$ is given by

$$\mathcal{E}(z) = \frac{E(z)}{E(z_{j-1})}\, \mathcal{E}(z_{j-1}) \qquad (5.1.3)$$

with

$$\frac{E(z)}{E(z_{j-1})} = \cosh\left[K_j(z-z_{j-1})\right] - Q_j \sinh\left[K_j(z-z_{j-1})\right] \qquad (5.1.4)$$

and

$$\mathcal{E}(z_{j-1}) = \prod_{n=1}^{j-1} \frac{E(z_n)}{E(z_{n-1})} \qquad (5.1.5)$$

With equations (5.1.3), (5.1.4), and (5.1.5), the integrations required in equation (5.1.2) can be performed analytically:

$$\int_{z_{j-1}}^{z_j} \mathcal{E}^2(z)\, dz$$

$$= \tfrac{1}{2}(1-Q_j^2)\, d_j + (1+Q_j^2)\, \frac{1}{4K_j} \sinh\left[2K_j d_j\right]$$

$$- Q_j \frac{1}{2K_j} \cosh\left[2K_j d_j\right] \qquad (5.1.6)$$

Thus the problem of computing the coefficients of equation (5.1.2) reduces to that of generating Q_j from the recursive relationship (3.2.33). The term $\mathcal{E}(z_j)$ is easily computed from (5.1.4). The computational problems associated with evaluating Q_j, $\mathcal{E}(z_j)$, and the coefficients of (5.1.2) -- and thus the inner product matrix $\underline{\underline{B}}$ defined by (3.2.46) -- are completely straightforward. There are obvious advantages offered by the present simple algorithm compared with the more arduous (and time-consuming) task of computing the actual derivatives of the response with respect to all the model parameters. The outcome of both approaches is numerically the same (cf equations (3.4.3), (3.4.4), and (3.4.5) for the two-layer case).

Our object in this present Chapter is that of illustrating the Backus Gilbert least-squares procedure for improving an initially guessed model, both with some synthetic numerical experiments, and with application to experimental data. In all the examples and experiments, the model parameters have been rendered dimensionless in a manner completely analogous to that described in Section 3.3 for the two-layer problem. Each conductivity σ_j is normalized with respect to the surface conductivity σ_1: thus the dimensionless conductivity is $\tilde{\sigma}_j = \sigma_j / \sigma_1$. The depth parameters are measured in skin-depths (evaluated using the surface conductivity). Also, the amplitude and phase of the magnetotelluric response are used as data: this is achieved by taking the natural logarithm of the complex response γ; hence

$$\ln \gamma = \ln|\gamma| + i \arg \gamma \qquad (5.1.7)$$

consists of a real part which is the logarithm of the amplitude of γ, and an imaginary part which is the phase of γ. Parker (1970) explains that the logarithm is required since the modulus of γ is not an analytic function of γ. Alternatively, one could choose as data the real and imaginary parts of γ; but it would seem that amplitude and phase are the favoured manner of expressing response data. In fact it is amplitude information alone (expressed in the form of an apparent resistivity) which is often used as the response function.

Typically, phase response curves are widely scattered and may lead to unreliable interpretation. Unless otherwise stated, the response data will be amplitude data alone. In Sections 5.3 and 5.4 the inverse least-squares formalism is used to try to determine how phase information can contribute to the interpretation of data.

We emphasize also that the least-squares inversion procedure does not require smooth data -- the procedure itself has the effect of smoothing irregular data. The error estimates which are to be associated with elements of the data set do not enter into the procedure for finding an acceptable model. The question of error is addressed when one seeks to characterize the space of acceptable models by determining the resolution of the data.

5.2 Synthetic Examples

In order to illustrate the regions of the model space where linearization error could occur, a series of numerical experiments with synthetic data were described in Section 3.4. The model space consisted of the parameters associated with a two-layer half-space. By choosing a set of ten data frequencies which penetrate some ten kilometers into the Earth, and seeking from a least-squares inverse formalism to isolate model parameters near the surface -- some two kilometers from the surface -- an underdetermined problem was posed.

The resolution of induction data deteriorates somewhat near the surface (as we shall see from Chapter 6), so we are essentially trying to optimize model parameters which are not well resolved. In the context of Chapter 3, this suits our purpose of exploring the regions where higher-order terms in equation (3.4.12) may influence the iterative scheme. An underdetermined problem will give rise to large model perturbations, and the conditions for the local linearization of equation (3.4.12) are likely to be exceeded.

We now wish to apply the algorithm described in Section 5.1 to synthetic data generated from various conductivity distributions. The following strategy will be followed. A model will be selected (for sake of nomenclature this model will be called 'the true model') and a set of synthetic data, corresponding to N distinct frequencies, will be generated from this model. We then select a different model to obtain an initial guess and compute the response to this guessed model for the same N frequencies. The term Δg_i , required in equation (3.2.44), is then computed

$$\Delta g_i = \gamma_i - g_i(\sigma^0) \qquad (5.2.1)$$

by taking the difference between the response computed from the true model (γ_i is our observed response value) and that computed from our guessed model (i.e. $g_i(\sigma^0)$). Using the algorithm described in the previous Section,

we compute the terms $\underline{b}_i$, defined by (3.2.42) with $G_i(z) = \mathcal{E}^2(z)\, H(z_1 - z)$ for the $\delta\sigma_1$-component, etc. Hence the inner product matrix $\underline{\underline{B}}$ -- the elements of which are defined by (3.2.45) -- can be formed. The vector is determined by forming the inverse of $\underline{\underline{B}}$, and operating on the vector $\underline{\Delta g}$ with $\underline{\underline{B}}^{-1}$. Hence the model perturbations $\delta\sigma_j$ and δd_j can be determined from the combinations (3.2.40) and (3.2.41).

Both stable and unstable situations will be illustrated; however at this stage no stabilizing procedures -- such as that described in Section 2.2.e -- will be introduced.

In Figs. 5-1a and 5-1b we again illustrate the application of the least-squares inverse procedure to a two-layer problem. In Fig. 5-1a a true model is chosen to be $\underline{\sigma}$: ($\sigma_1 = 0.5$ ohm^{-1}m^{-1}, $\sigma_2 = 0.05$ ohm^{-1}m^{-1}, $d = 2$ km). Ten data points are generated in a period range 1 sec. $\leq T \leq$ 100 sec. A starting model is chosen to be $\underline{\sigma}^0$: ($\sigma_1^0 = 0.667$ ohm^{-1}m^{-1}, $\sigma_2^0 = 0.025$ ohm^{-1}m^{-1}, $d = 1$ km). In a given iteration the current data residual is defined as the square root of

$$\frac{1}{N} \sum_{i}^{N} \left(\gamma_i - g_i(\sigma^0) \right)^2 \qquad (5.2.2)$$

and the current model residuals are defined by

$$\left(\sigma_1^0 - \sigma_1 \right) / \sigma_1 \qquad \text{etc.} \qquad (5.2.3)$$

An alternative situation is illustrated in Fig. 5-1b.

The period range is now chosen to be 10 sec $\leq$ T $\leq$ 100 sec. The true model and the initial guess are the same as that illustrated in Fig. 5-1a.

In Figs. 5-1a and 5-1b the instability associated with this underdetermined problem is illustrated by the data residual. In Fig. 5-1a one can see that, with the inclusion of higher frequencies, σ_2-perturbations seem to depart more strongly away from the true value whereas, if these higher frequencies are excluded (Fig. 5-1b), it is σ_1 which departs more strongly from the true value and σ_2 seems better determined. This is as one would expect from this adjustment of the period range.

During any iteration a conductivity parameter may become negative, i.e. may assume an unphysical value. In the least-squares algorithm which has been described, the model parameters have not been constrained to be non-negative. Should a model parameter become negative during an iteration, it is immediately set to the physically possible default parameter of zero. However, among the illustrations shown in this Section, only that of Fig. 5-3a involves application of this default.

Fig. 5-2 illustrates the least-squares procedure applied to a three-layer model. This constitutes a five parameter problem with the three conductivities and the two depth parameters allowed to vary during the iteration. The period range for the data is 1 sec $\leq$ T $\leq$ 100 sec and the synthetic data is generated from the true model

$\underline{\sigma}$: ($\sigma_1 = 0.6$, $\sigma_2 = 0.1$, $\sigma_3 = 1.0$; $d_1 = 1$ km, $d_2 = 2$ km). The initial guess is chosen to be $\underline{\sigma}^0$: ($\sigma_1^\circ = 0.81$, $\sigma_2^\circ = 0.085$, $\sigma_3^\circ = 0.7$; $d_1 = 0.7$ km, $d_2 = 2.6$ km). (All conductivities are measured in ohm^{-1}m^{-1}). The set of model residuals, as they are defined in equation (5.2.3), span a number of orders of magnitude. To illustrate more distinctly the model residuals in this and in subsequent examples, these residuals will be redefined by

$$\left| \ln \left(\sigma_1 / \sigma_1^{\,0} \right) \right|^{\frac{1}{2}} \qquad \text{etc.} \qquad (5.2.4)$$

Since the model residual is only defined for illustrative purposes, the form of the definition is of no material importance.

Figs. 5-3a and 5-3b illustrate the least-squares inverse procedure applied to another five-parameter problem: this time the model is parameterized with five layers located at <u>fixed</u> depths below the surface. For Fig. 5-3a data is generated from a true model chosen as $\underline{\sigma}$: ($\sigma_1 = 0.5$, $\sigma_2 = 0.001$, $\sigma_3 = 0.005$, $\sigma_4 = 0.009$, $\sigma_5 = 1.0$) over the period range 6 sec $\leq T \leq$ 100 sec. The initial guess is $\underline{\sigma}^0$: ($\sigma_1^\circ = 0.3$, $\sigma_2^\circ = 0.003$, $\sigma_3^\circ = 0.02$, $\sigma_4^\circ = 0.15$, $\sigma_5^\circ = 2.0$). The depths to the interfaces are: $d_1 = 1.0$ km, $d_2 = 2.0$ km, $d_3 = 2.4$ km, $d_4 = 2.8$ km. From Fig. 5-3a one can see that the procedure is unstable at the first iteration (resembling the situation in Fig. 3-7A). It would seem from the

FIG. 5-1 a Residuals associated with least-squares procedure for the two-layer models (true model and starting model) indicated. The period range of the data is $10 \leq T \leq 100$ sec.

FIG. 5-1 b Residuals associated with least-squares procedure for the two-layer models indicated.

FIG. 5-2 Residuals associated with the least-squares procedure for the three-layer models indicated.

FIG. 5-3 a Residuals associated with least-squares procedure for the five-layer models (with fixed depths) indicated.

FIG. 5-3 b Residuals associated with least-squares procedure for the five-layer models indicated.

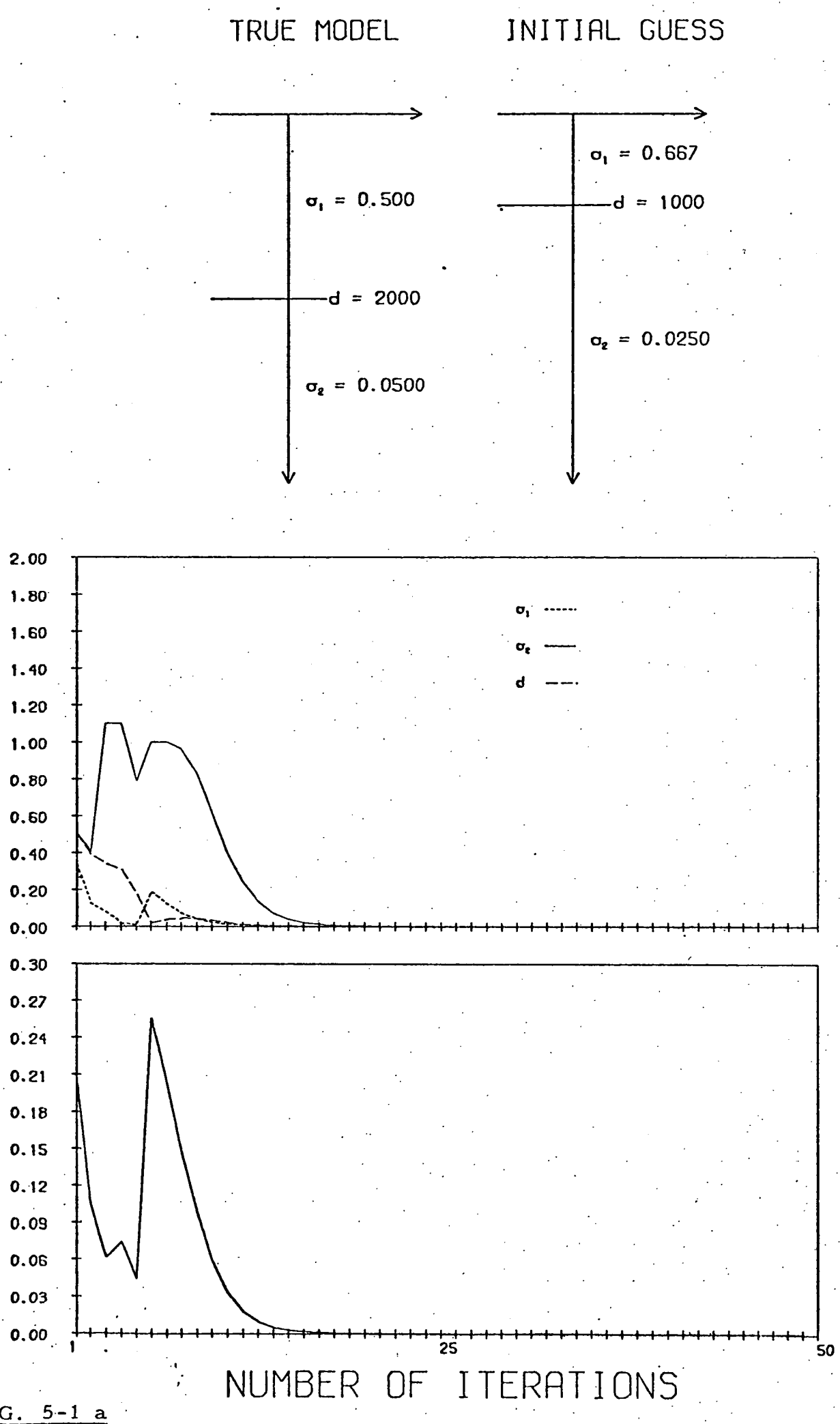
TRUE MODEL
INITIAL GUESS
σ1 = 0.500
d = 2000
σ2 = 0.0500
σ1 = 0.667
d = 1000
σ2 = 0.0250
2.00
1.80
1.60
1.40
1.20
1.00
0.80
0.60
0.40
0.20
0.00
σ1
σ2
d
0.30
0.27
0.24
0.21
0.18
0.15
0.12
0.09
0.06
0.03
0.00
1
25
50
NUMBER OF ITERATIONS

FIG. 5-1 a

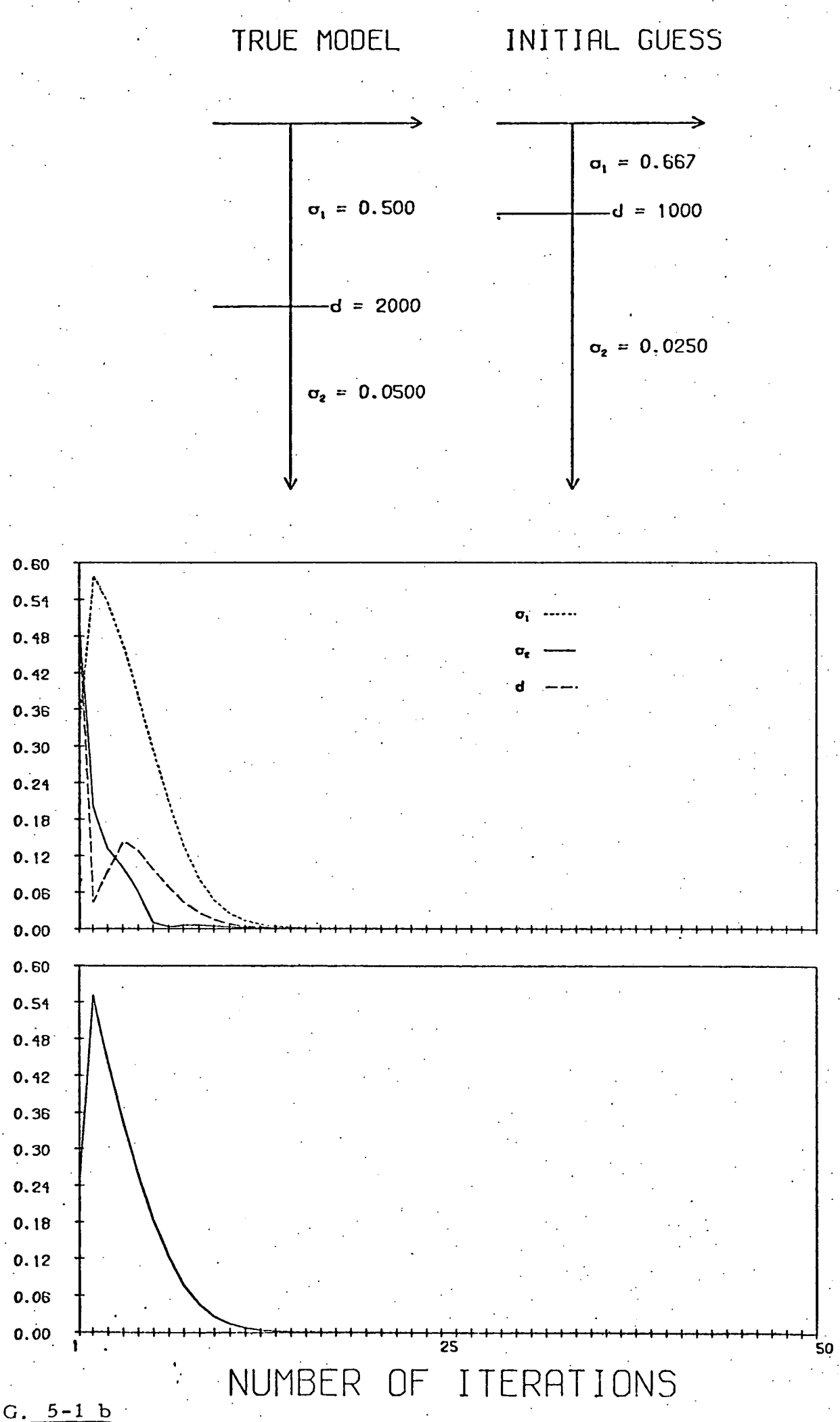
TRUE MODEL
INITIAL GUESS
σ1 = 0.500
d = 2000
σ2 = 0.0500
σ1 = 0.667
d = 1000
σ2 = 0.0250
0.60
0.54
0.48
0.42
0.36
0.30
0.24
0.18
0.12
0.06
0.00
σ1
σ2
d
1
25
50
NUMBER OF ITERATIONS

FIG. 5-1 b

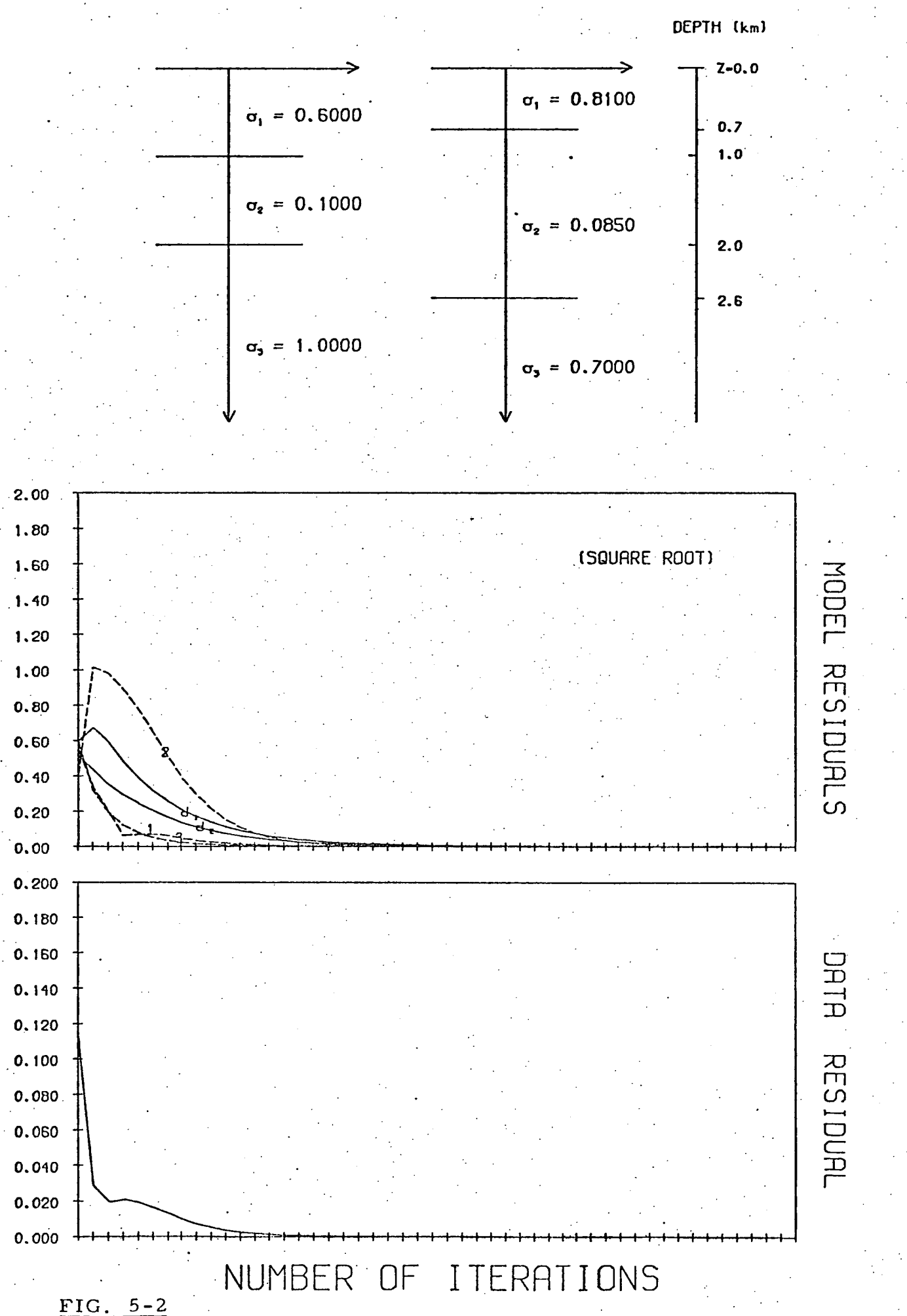
TRUE MODEL
INITIAL GUESS
DEPTH (km)
σ1 = 0.6000
σ2 = 0.1000
σ3 = 1.0000
σ1 = 0.8100
σ2 = 0.0850
σ3 = 0.7000
Z-0.0
0.7
1.0
2.0
2.6
(SQUARE ROOT)
MODEL RESIDUALS
DATA RESIDUAL
NUMBER OF ITERATIONS

FIG. 5-2

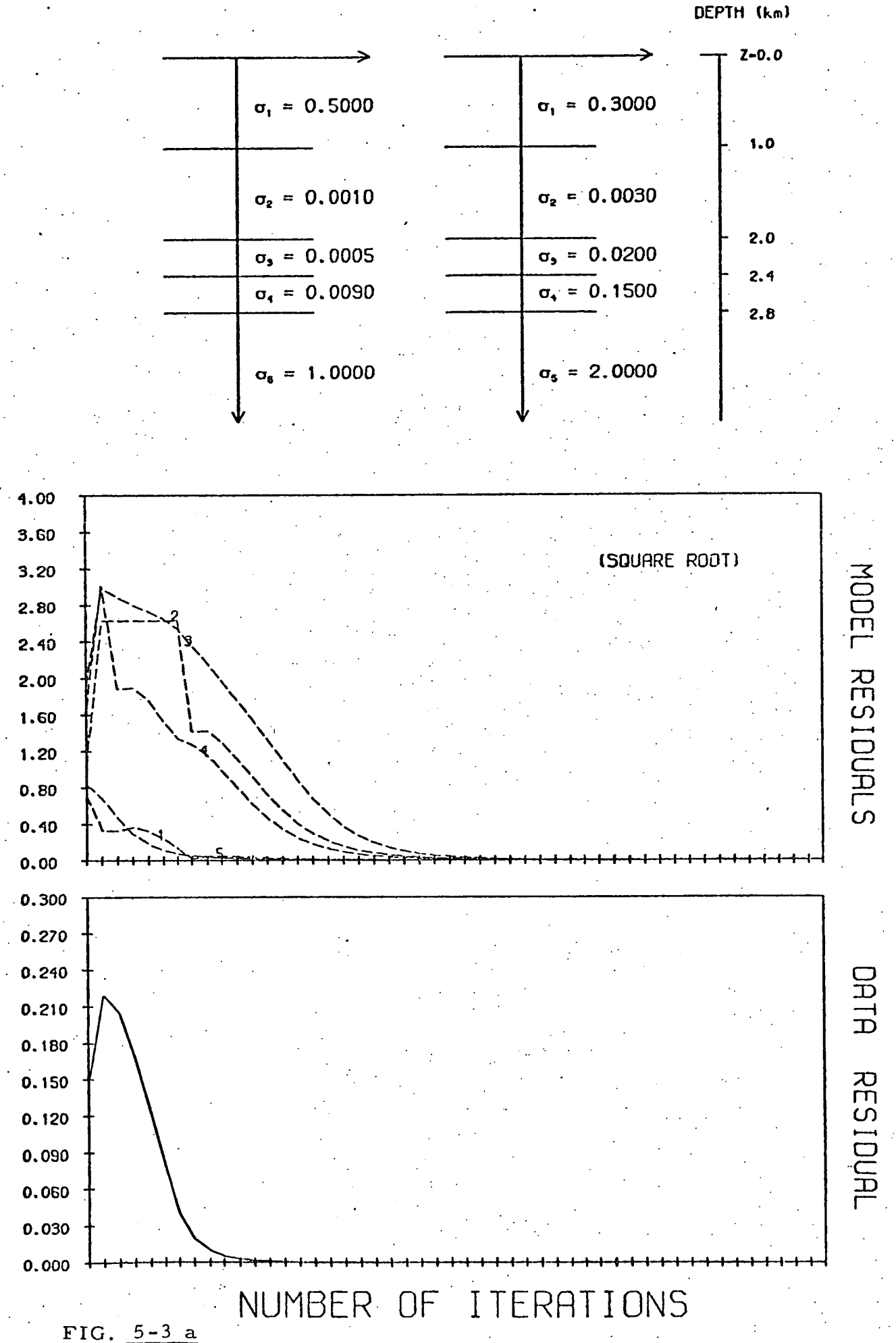
TRUE MODEL
INITIAL GUESS
DEPTH (km)
σ1 = 0.5000
σ2 = 0.0010
σ3 = 0.0005
σ4 = 0.0090
σ5 = 1.0000
σ1 = 0.3000
σ2 = 0.0030
σ3 = 0.0200
σ4 = 0.1500
σ5 = 2.0000
Z-0.0
1.0
2.0
2.4
2.8
4.00
3.60
3.20
2.80
2.40
2.00
1.60
1.20
0.80
0.40
0.00
(SQUARE ROOT)
MODEL RESIDUALS
0.300
0.270
0.240
0.210
0.180
0.150
0.120
0.090
0.060
0.030
0.000
DATA RESIDUAL
NUMBER OF ITERATIONS

FIG. 5-3 a

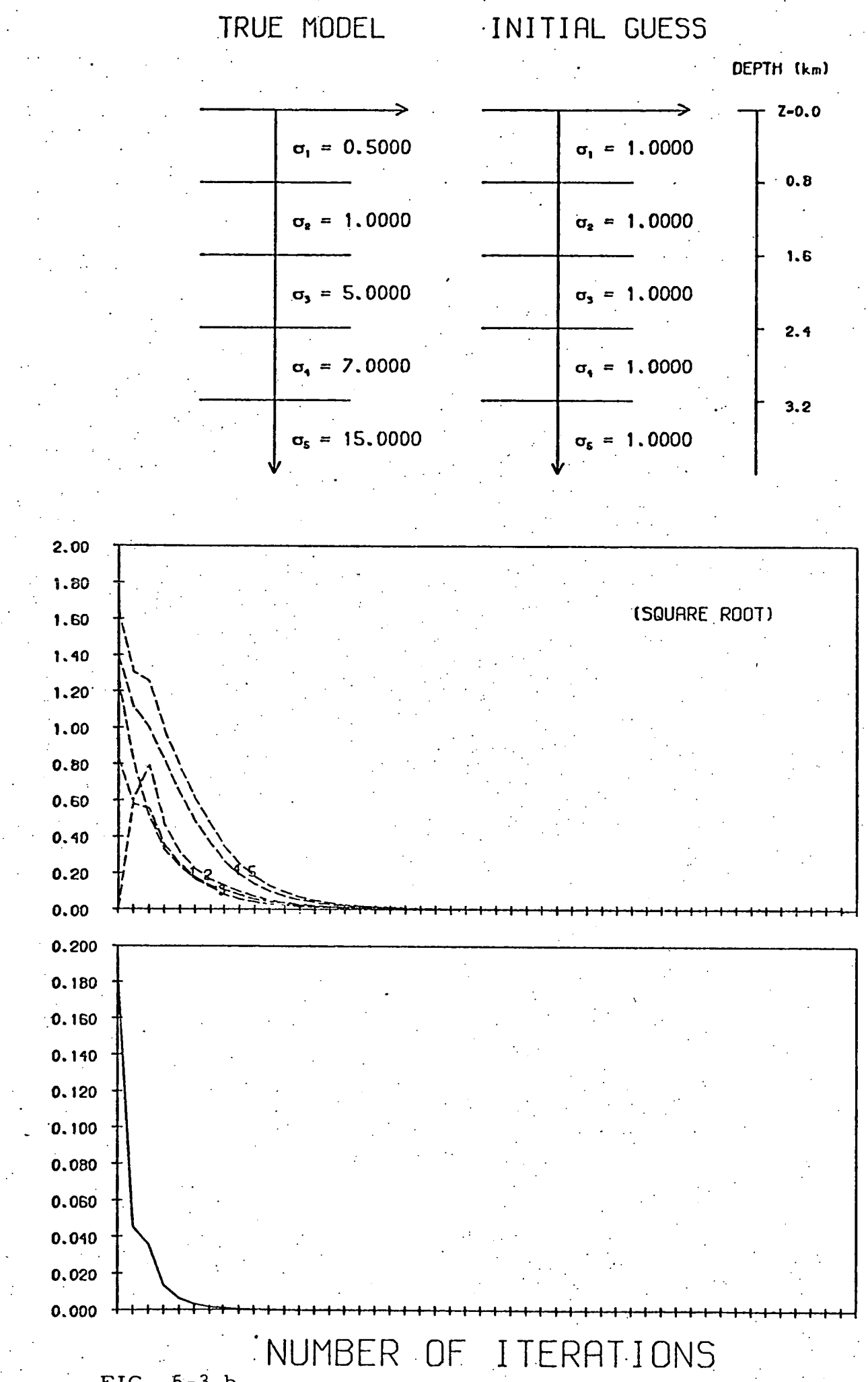
TRUE MODEL
INITIAL GUESS
DEPTH (km)
σ1 = 0.5000
σ2 = 1.0000
σ3 = 5.0000
σ4 = 7.0000
σ5 = 15.0000
σ1 = 1.0000
σ2 = 1.0000
σ3 = 1.0000
σ4 = 1.0000
σ5 = 1.0000
Z-0.0
0.8
1.6
2.4
3.2
(SQUARE ROOT)
MODEL RESIDUALS
DATA RESIDUAL
NUMBER OF ITERATIONS

FIG. 5-3 b

model residuals that the poorly conducting layers are the least well determined. Nevertheless the process converges to the true model.

Fig. 5-3b illustrates the procedure for a situation which is completely esoteric in the sense that the conductivities of the true model are an order of magnitude greater than any which might be expected in the Earth. The present example is included for purposes of comparison. The higher conductivities (and hence the relatively large induced currents) make the model well resolved, and the least-squares procedure stable and convergent. The true model is chosen as $\underline{\sigma}$: ($\sigma_1 = 0.5$, $\sigma_2 = 1.0$, $\sigma_3 = 5.0$, $\sigma_4 = 7.0$, $\sigma_5 = 15.0$). The period range is the same as for Fig. 5-3a. The depths to the interfaces are $d_1 = 0.8$ km, $d_2 = 1.6$ km, $d_3 = 2.4$ km, $d_4 = 3.2$ km. The initial guess is $\underline{\sigma}^0$: ($\sigma_1^\circ = \sigma_2^\circ = \sigma_3^\circ = \sigma_4^\circ = \sigma_5^\circ = 1.0$).

Two comments can be made concerning all the models considered so far in this Section. They are all rather esoteric from the point of view of geophysical application. Furthermore, in order to make the problem display the interesting instabilities inherent to underdetermined systems, unfortunate parameterizations are chosen. The depth of penetration of an inducing field with period 100 sec in a conductor of conductivity 0.5 $\text{ohm}^{-1}\text{m}^{-1}$ is about 100 km. Yet we seek to resolve the structure only at the top 5 km of the Earth.

Figs. 5-4a, 5-4b, and 5-4c illustrate more

geophysically appropriate parameterizations. We can see that in each case the procedure is more stable: the model perturbations are smaller and the procedure takes correspondingly longer to converge.

Fig. 5-4a illustrates the procedure associated with the three layer parameterization. A true model is chosen $\underline{\sigma}$: ($\sigma_1 = .1$, $\sigma_2 = .008$, $\sigma_3 = .1$; $d_1 = 8.$, $d_2 = 18.$) to generate ten data points in the period range 20 sec $\leq T \leq$ 300 sec. An initial model is chosen $\underline{\sigma}^0$: ($\sigma_1^\circ = .085$, $\sigma_2^\circ = .0104$, $\sigma_3^\circ = .075$; $d_1 = 7.2$, $d_2 = 21.6$). From Fig. 5-4a it can be seen -- qualitatively at least -- that, of all the model parameters, the depth parameters are among the least well resolved.

Fig. 5-4b illustrates a five layer parameterization with depths fixed. A true model is chosen $\underline{\sigma}$: ($\sigma_1 = 0.07$, $\sigma_2 = 0.05$, $\sigma_3 = 0.09$, $\sigma_4 = 0.15$, $\sigma_5 = 0.005$) to generate ten data points for the same ten periods as the previous example. The starting model is $\underline{\sigma}^0$: ($\sigma_1^\circ = \sigma_2^\circ = \sigma_3^\circ = \sigma_4^\circ = \sigma_5^\circ = 0.06$). The depths to the interfaces are $d_1 = 8$ km, $d_2 = 15$ km, $d_3 = 20$ km, $d_4 = 25$ km.

Fig. 5-4b illustrates the synthetic data generated from a true model $\underline{\sigma}$: ($\sigma_1 = .05$, $\sigma_2 = .065$, $\sigma_3 = .09$, $\sigma_4 = 0.1$, $\sigma_5 = 0.15$). The depth parameters, period range and initial guess are the same as those of the previous example.

FIG. 5-4 a Residuals associated with least-squares procedure applied to more geophysically interesting three-layer model (with floating depths) indicated. The period range is $10 \leq T \leq 300$ sec. The model residual associated with each parameter is so labelled.

FIG. 5-4 b Residuals for the five-layer model indicated.

FIG. 5-4 c Residuals for the five-layer model indicated.

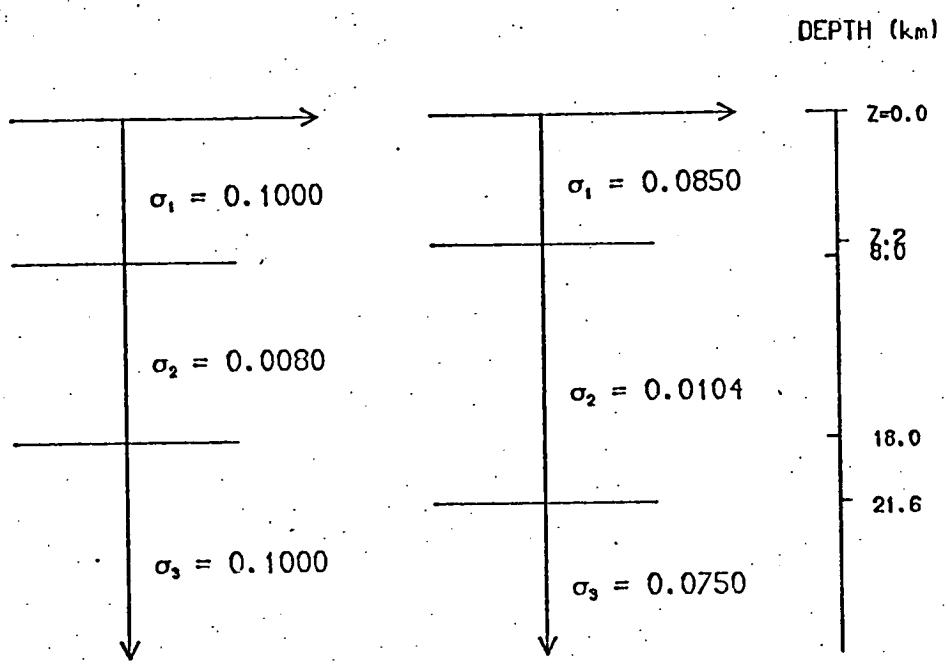

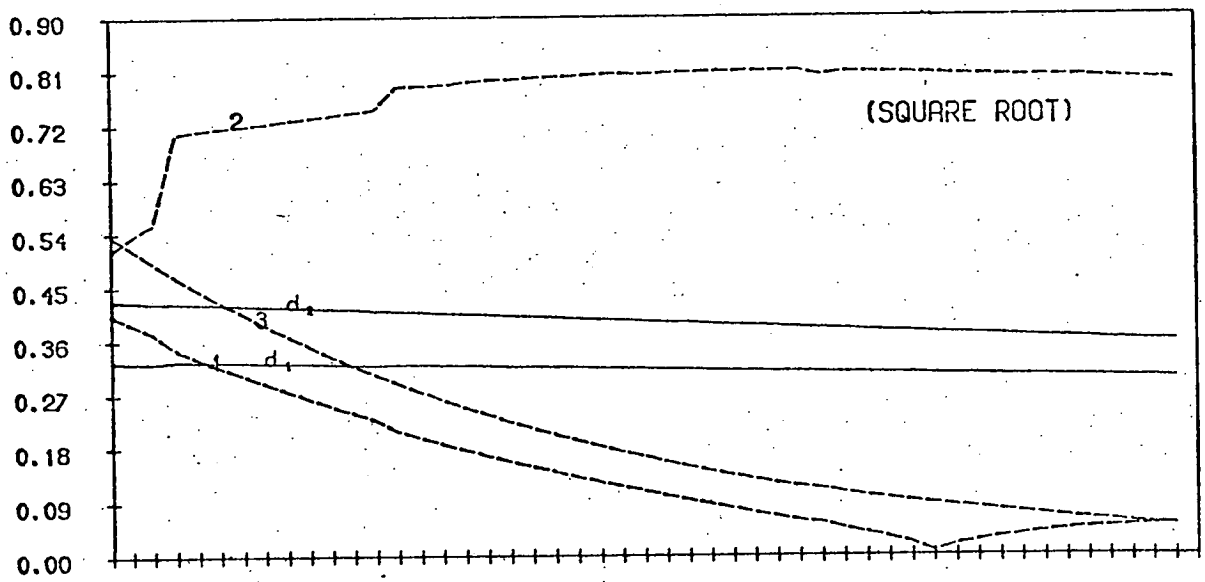

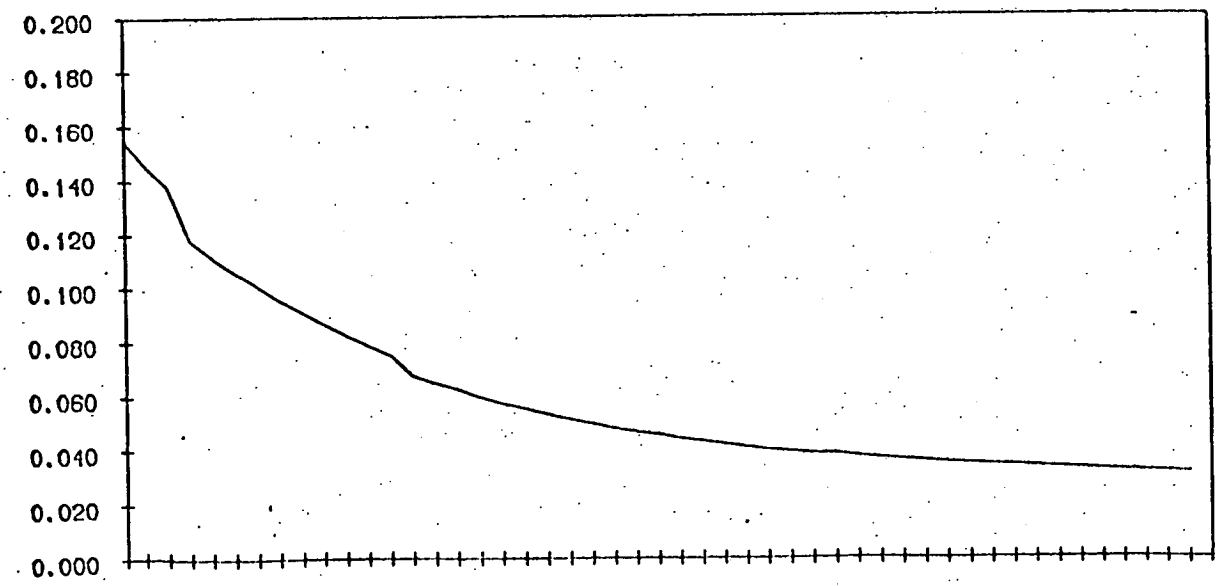

NUMBER OF ITERATIONS

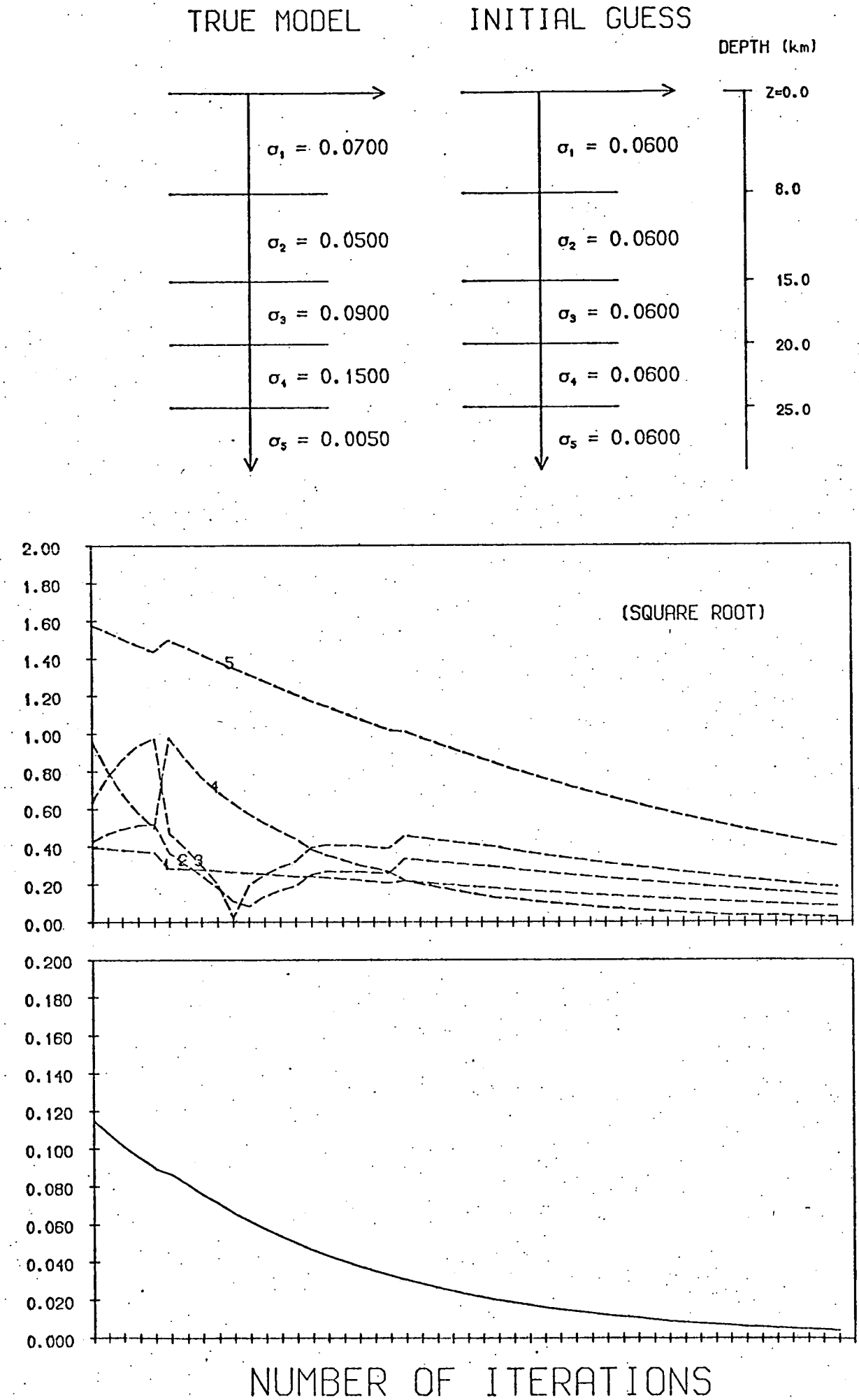
TRUE MODEL
INITIAL GUESS
DEPTH (km)
σ1 = 0.0700
σ2 = 0.0500
σ3 = 0.0900
σ4 = 0.1500
σ5 = 0.0050
σ1 = 0.0600
σ2 = 0.0600
σ3 = 0.0600
σ4 = 0.0600
σ5 = 0.0600
Z=0.0
8.0
15.0
20.0
25.0
(SQUARE ROOT)
2.00
1.80
1.60
1.40
1.20
1.00
0.80
0.60
0.40
0.20
0.00
0.200
0.180
0.160
0.140
0.120
0.100
0.080
0.060
0.040
0.020
0.000
NUMBER OF ITERATIONS

FIG. 5-4 b

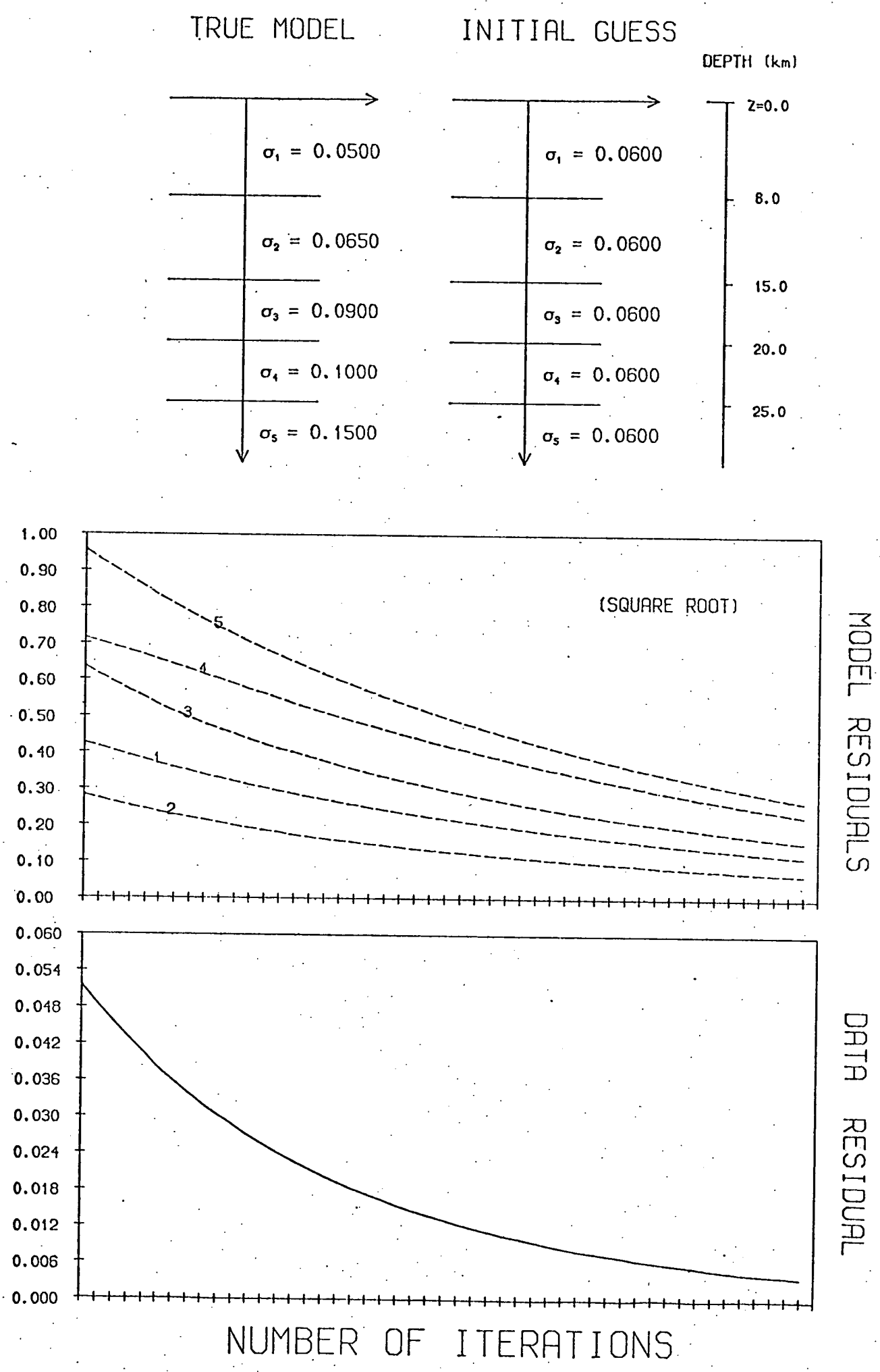
TRUE MODEL
INITIAL GUESS
DEPTH (km)
σ1 = 0.0500
σ2 = 0.0650
σ3 = 0.0900
σ4 = 0.1000
σ5 = 0.1500
σ1 = 0.0600
σ2 = 0.0600
σ3 = 0.0600
σ4 = 0.0600
σ5 = 0.0600
Z=0.0
8.0
15.0
20.0
25.0
1.00
0.90
0.80
0.70
0.60
0.50
0.40
0.30
0.20
0.10
0.00
(SQUARE ROOT)
5
4
3
1
2
MODEL RESIDUALS
0.060
0.054
0.048
0.042
0.036
0.030
0.024
0.018
0.012
0.006
0.000
DATA RESIDUAL
NUMBER OF ITERATIONS

FIG. 5-4 c

5.3 Stabilizing the Iterative Procedure

Without any *a priori* knowledge of the space of acceptable models (and without any prior understanding of the resolving power of the data), one might well parameterize the model in a way which could lead to an underdetermined inverse problem. This situation will arise if the model is so finely structured that the data set has insufficient resolution to optimize the model parameters. This failure to resolve parameters may itself arise from scatter in the data (i.e. from inconsistency in the data) or from some inadequacy in the range or density of the data. As was explained in Section 1.6a, there is difficulty in evaluating the inverse of a matrix if that matrix is associated with an underdetermined system of equations. In numerical terms, this difficulty will consist of a failure of the matrix inversion algorithm to supply an inverse; at best such an algorithm may supply a greatly inaccurate version of an inverse matrix. If an inverse of a nearly singular matrix *is* isolated numerically, the resulting model perturbations can be extreme and the conditions under which the expansion (1.6.1) was constructed may be violated. The direct implication of an underdetermined system of equations to the least-squares inversion procedure is to make the procedure unstable.

Thus a method to stabilize the procedure is required. This can be done formally by attaching additional

constraints to the minimization of U in equations (2.2.5) or (3.2.38). The additional stabilizing constraints which will be imposed are

1.) that the model perturbations give rise to physically meaningful model parameters, e.g. that the conductivity remain non-negative, and

2.) that the data residual decrease from iteration to iteration.

The method to be used to impose these constraints is that of ranking and winnowing, described in Section 2.2.e. It is this approach which is also implicit to the Lanczos formulation of the inverse problem (Jackson, 1972).

A similarity transformation is needed which will diagonalize the inner product matrix $\underline{\underline{B}}$ (using notation of Section 3.2.d). Specifically an orthonormal matrix operator $\underline{\underline{C}}$ is required such that

$$\underline{\underline{C}}^T \; \underline{\underline{B}} \; \underline{\underline{C}} = \underline{\underline{B}}' \tag{5.3.1}$$

where $\underline{\underline{B}}'$ is diagonal. Since $\underline{\underline{C}}$ is to be orthonormal, $\underline{\underline{C}}^{-1} = \underline{\underline{C}}^T$, and we can restructure this equation as

$$\underline{\underline{B}} = \underline{\underline{C}} \; \underline{\underline{B}}' \; \underline{\underline{C}}^T \tag{5.3.2}$$

and substitute this value of $\underline{\underline{B}}$ into equation (3.2.44) to obtain

$$(\underline{\underline{C}} \; \underline{\underline{B}}' \; \underline{\underline{C}}^T) \cdot \underline{\gamma} = \underline{\Delta g} \tag{5.3.3}$$

The transformations $\underline{\Delta g}' = \underline{\underline{C}}^T \underline{\Delta g}$ and $\underline{\gamma}' = \underline{\underline{C}}^T \underline{\gamma}$, reduce (5.3.3) to

$$\underline{\underline{B}}' \underline{\gamma}' = \underline{\Delta g}' \qquad (5.3.4)$$

where $\underline{\underline{B}}'$ is diagonal. (The Fréchet kernel is similarly transformed by $\underline{\underline{G}}'(z) = \underline{\underline{C}}^T \cdot \underline{\underline{G}}(z)$). Forming the inverse of a diagonal matrix is a trivial operation and so equation (5.3.4) is an extremely convenient representation for equation (3.2.44).

There are N eigenvectors and eigenvalues to be associated with a non-singular, real, symmetric matrix $\underline{\underline{B}}$ of rank N. The kth such eigenvector, $\underline{u}_k$, is defined by

$$(\underline{\underline{B}} - \lambda_k \underline{\underline{I}}) \quad \underline{u}_k = 0 \qquad (5.3.5)$$

where $\underline{\underline{I}}$ is the N x N identity matrix and λ_k is the kth eigenvalue. If the columns of the transformation matrix $\underline{\underline{C}}$ are composed of the N normalized eigenvectors of $\underline{\underline{B}}$, the matrix $\underline{\underline{C}}$ will be orthonormal. With $\underline{\underline{C}}$ chosen in this way, the matrix $\underline{\underline{B}}'$ resulting from the similarity transformation (5.3.1) will have along its diagonal the eigenvalues of $\underline{\underline{B}}$ in the same order as the corresponding columns of $\underline{\underline{C}}$, i.e.

$$\underline{\underline{B}}' = \begin{bmatrix} \lambda_1 & & & & \\ & \lambda_2 & & & \\ & & \ddots & & \\ & & & & \lambda_N \end{bmatrix} \qquad (5.3.6)$$

Unless the matrix $\underline{\underline{B}}$ is singular the elements of the set

$\{\lambda_i\}$ will all be non-zero. If these eigenvalues (and the corresponding eigenvectors in $\underline{\underline{C}}$) are ranked in descending order, the smallest eigenvalue will appear at the lower right hand corner of the matrix (5.3.6), and $\lambda_1 > \lambda_2 > \lambda_3 > \cdots > \lambda_N$. If $\underline{\underline{B}}$ is nearly singular, one should be able to identify a set of eigenvalues $\lambda_{k+1}, \lambda_{k+2}, \cdots, \lambda_N$ which are nearly zero: these can be formally separated off in (5.3.6) so that

$$\underline{\underline{B}}' = \begin{bmatrix} \lambda_1 & & & & & \\ & \lambda_2 & & & & \\ & & \ddots & & & \\ & & & \lambda_k & & \\ \hline & & & & \lambda_{k+1} & \\ & & & & & \ddots \\ & & & & & & \lambda_N \end{bmatrix} \qquad (5.3.7)$$

If only the largest k eigenvalues $\{\lambda_i\}_1^k$ are retained, the transformation $\underline{\underline{C}}$, the vectors $\underline{\gamma}'$, $\underline{\Delta g}'_i$, and $\underline{G}'$ will be correspondingly reduced in dimension. However the reduced k x k ($k < N$) matrix will be non-singular, and a well-conditioned inverse, $(\underline{\underline{B}})^{-1}$, can be constructed. Each transformed datum $\Delta g'_i$ is a (non-linear) combination of the original data $\underline{\Delta g}$, i.e.

$$\Delta g'_i = \sum_j^N C_{ij} \Delta g_j \qquad (5.3.8)$$

(C_{ij} is the ij^{th} element of $\underline{\underline{C}}$). Excluding the data

$$\Delta g'_{k+1} , \quad \Delta g'_{k+2} , \quad \cdots , \quad \Delta g'_N$$

from equation (5.3.4) effectively reduces the number of combinations of the original data represented in the inversion. This will result in some degradation of the information. However, some combinations of data may be less informative than others and the information loss from the truncation described may or may not be significant. Solving the truncated (5.3.4), one achieves the k-dimensional vector $\underline{\nu}'$ ($k < N$) with elements

$$\nu'_i = \Delta g'_i / \lambda'_i \qquad (5.3.9)$$

from which the model perturbation can be constructed

$$\delta\sigma_j = \sum_{i=1}^{k} \nu'_i G'_i{}^{(j)} \qquad (5.3.10)$$

It is to this latter equation that stability criteria can be imposed for the least-squares procedure. One simply reduces the terms in the sum (5.3.10) -- by reducing k -- until the criteria stated at the outset of this Section are satisfied.

Numerically one requires to evaluate $\underline{\underline{C}}$. This is to say one needs to evaluate the eigenvectors and eigenvalues of the inner product matrix $\underline{\underline{B}}$. Since $\underline{\underline{B}}$ is real and symmetric this is computationally a well-understood

procedure and there are a variety of well-documented methods which are suitable. One which is commonly used is that of reducing $\underline{\underline{B}}$ to tri-diagonal form using Householder's method. One then uses the L-R algorithm, or Sturm bisection to isolate the N eigenvalues; the eigenvectors are hence evaluated by back substitution. A descriptive discussion of various numerical approaches can be found in Williams (1972). The standard work on the numerical solution to algebraic eigenvalue problems is that of Wilkinson (1965). If $\underline{\underline{B}}$ is nearly singular, the isolation of the smaller eigenvalues may be very time-consuming, and inaccurate. However, one can seek to find only those eigenvalues exceeding some minimum useful value. Having found the eigenvectors, one then forms $\underline{\underline{C}}$, and operates on $\underline{\gamma}$, $\underline{\Delta g}$, and $\underline{G}$ with its transpose $\underline{\underline{C}}^T$ to obtain the transformed values $\underline{\gamma}'$, $\underline{\Delta g}'$, and $\underline{G}'$ for equations (5.3.9) and (5.3.10).

As has been stated, the exclusion of eigenvalues from (5.3.7) results in an unknown loss of information. One can examine equation (5.3.4) in the light of the discussion in Section 1.6. The transformation (5.3.8) can be described as a <u>rotation</u> of the data set $\{\Delta g_i\}$, each element of which is defined $\Delta g_i \equiv \gamma_i - g_i(\sigma^0)$. Since γ_i has itself been described as an average of the model distribution, $\sigma(z)$ (see the discussion following equation (1.6.9)), one can see how the transformation $\underline{\underline{C}}^T$ affects the weighting kernel associated with this

average. Equation (3.2.35) is restated as

$$\gamma_i = \int_0^\infty \sigma(z)\ f_i(\sigma,z)\ dz \qquad (5.3.11)$$

(with weighting function, $f_i(\sigma,z)$, given by

$$f_i(\sigma,z) = (1 + Q(z)^2)\ \ell^2(z) \qquad (5.3.12)$$

For a homogeneous conductor, $f_i(\sigma,z)$ is plotted in Fig. 5-5a for a range of frequencies. The period range corresponding to these frequencies is $6 \text{ sec} \leq T \leq 90 \text{ sec}$, and the conductivity of the half-space is taken as $0.5 \text{ ohm}^{-1}\text{m}^{-1}$. Treating $f_i(\sigma,z)$ as a weighting function, one can formally define the centre of this distribution by

$$Z_c = \int_0^\infty z\ f_i(\sigma,z)\ dz \ / \int_0^\infty f(\sigma,z)\ dz$$

and this centre is indicated in Fig. 5-5a. If γ_i is transformed by

$$\underline{\gamma}' = \underline{\underline{C}}^T \underline{\gamma} \qquad (5.3.13)$$

each γ_i' can be defined by

$$\gamma_i' = \int_0^\infty \sigma(z) \left[\sum_k C_{ki}\ f_k(\sigma,z) \right] dz \qquad (5.3.14)$$

$$= \int_0^\infty \sigma(z)\ f_i'(\sigma,z)\ dz$$

and in Fig. 5-5b the transformed weighting distributions $f'_i(\sigma,z)$ together with their respective centres are

plotted. In fact, the ten pieces of transformed data, $\{\gamma_i'\}$, are no longer to be associated with ten frequencies, since they are each comprised of a (non-linear) combination of frequencies. Instead, each one is associated with a distinct eigenvalue. The model variance (defined by equation (2.3.17) associated with each $\Delta g_i'$ is indicated. It can be seen that the centre of the transformed weighting functions distribute themselves into the conductor, until the fourth eigenvalue. Then the centre remains at depth and the amplitude of the weighting function becomes extremely small. Also, after four eigenvalues, the model variance becomes extremely large -- so those last six eigenvalues should be excluded from (5.3.7) in order to impose stability on the iterative process. The position of the centre of the six distributions with small eigenvalue is subject to great inaccuracy, as are all the characteristics of these distributions, since they are associated with the singular part of the transformation $\underline{\underline{C}}$. Of course the model variance is also dependent on the vector $\underline{\Delta g}'$, so that whether an eigenvalue is to be excluded or not cannot rest upon inspection of a diagram such as Fig. 5-5b alone.

In the discussion surrounding Fig. 3-8, ranking and winnowing had been applied to the same two-layer example which was illustrated in Fig. 3-7. We here illustrate a further example of how the stabilizing procedure which

has been described can assist one to find an adequate model when the algorithm of the previous Section is found to be non-convergent. In Fig. 5-6a and Fig. 5-6b, we illustrate the case where a synthetic data set has been generated from a true five layer model $\underline{\sigma}$: ($\sigma_1 = 0.5$, $\sigma_2 = 0.01$, $\sigma_3 = 0.005$, $\sigma_4 = 0.09$, $\sigma_5 = 1.6$) over a period range $10 \text{ sec} \leq T \leq 100 \text{ sec}$. The depths to the interfaces are $d_1 = 8$ km, $d_2 = 1.6$, $d_3 = 2.4$, $d_4 = 3.2$. The initial guess is chosen $\underline{\sigma}^0$: ($\sigma_1^\circ = \sigma_2^\circ = \sigma_3^\circ = \sigma_4^\circ = \sigma_5^\circ = 0.6$). For Fig. 5-6a the algorithm of Section 5.1 is applied directly. This results in an unstable and ultimately unsuccessful procedure. The stabilizing procedure described here has been applied, and Fig. 5-6b illustrates the result. One can see that the final data residual is much reduced, and that the iterations are very smooth and convergent. The model parameters however do not find their way to their true values, but to a final model $\underline{\sigma}^f$: ($\sigma_1 = 0.4$, $\sigma_2 = 0.085$, $\sigma_3 = 0.04$, $\sigma_4 = 0.33$, $\sigma_5 = 1.2$). By imposing stability on the procedure one has sacrificed information and resolution: although an acceptable model has been found in the sense that the data residual has been made acceptably small, the model parameters are not exactly but only approximately found. This of course demonstrates yet again the range of acceptable models which can be associated with a single set of data, especially data which is scattered and erroneous.

FIG. 5-5 a The function $f_i(\sigma, z)$ defined by equation (5.3.12) together with the centre of this distribution, Z_c, for the stated values of radial frequency, ω.

FIG. 5-5 b The function $f_i'(\sigma, z)$ appearing in the integrand of (5.3.14). These are the 'rotated' responses, γ', with their distribution centres. Also indicated is the model variance (defined by equation (2.3.17)) associated with each $\Delta g'$ for a uniform starting model $\sigma = 0.5$ ohm^{-1}m^{-1}, and a 'true' model $\underline{\sigma}$: ($\sigma_1 = 0.5$, $\sigma_2 = 0.4$, $\sigma_3 = 0.1$, $\sigma_4 = 0.01$, $\sigma_5 = 0.5$), at depths $d_1 = 1.3$, $d_2 = 1.5$, $d_3 = 2.0$, $d_4 = 3.2$ km.

FIG. 5-6 a Example of an unstable iterative least-squares procedure associated with the five-layer model shown.

FIG. 5-6 b The same data and starting model as the previous Fig. 5-6 a, however the method of ranking and winnowing has been used to stabilize the procedure. The final model which is achieved is $\underline{\sigma}$: ($\sigma_1 = 0.4$, $\sigma_2 = 0.085$, $\sigma_3 = 0.04$, $\sigma_4 = 0.33$, $\sigma_5 = 1.2$) The depths are fixed.

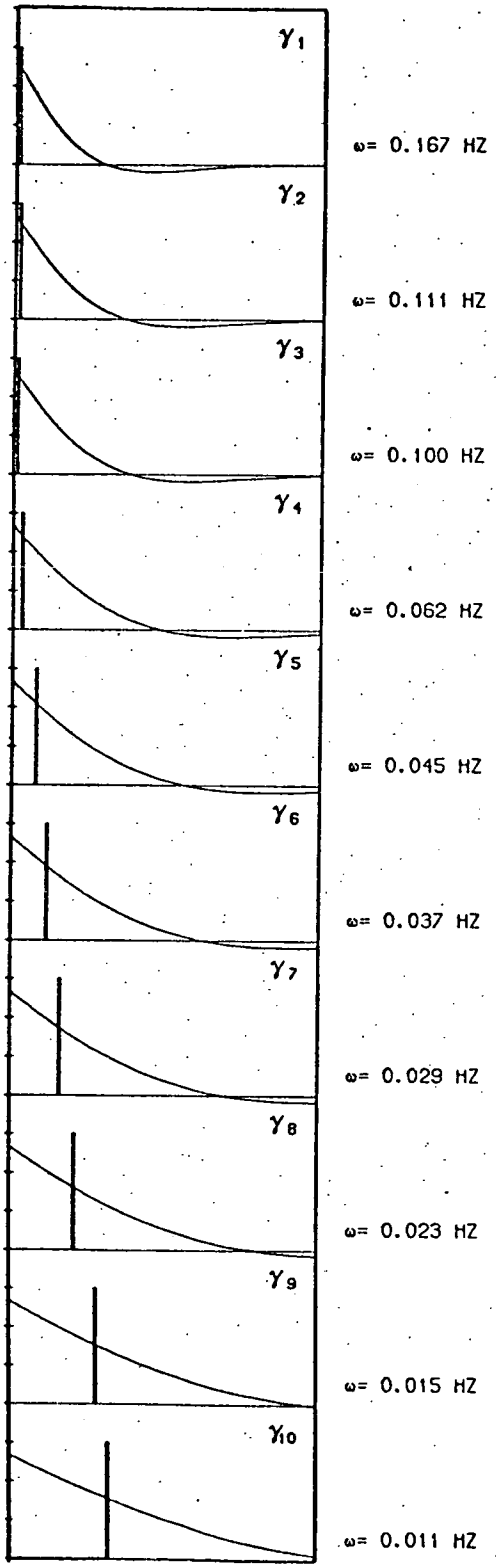

FIG. 5-5 a

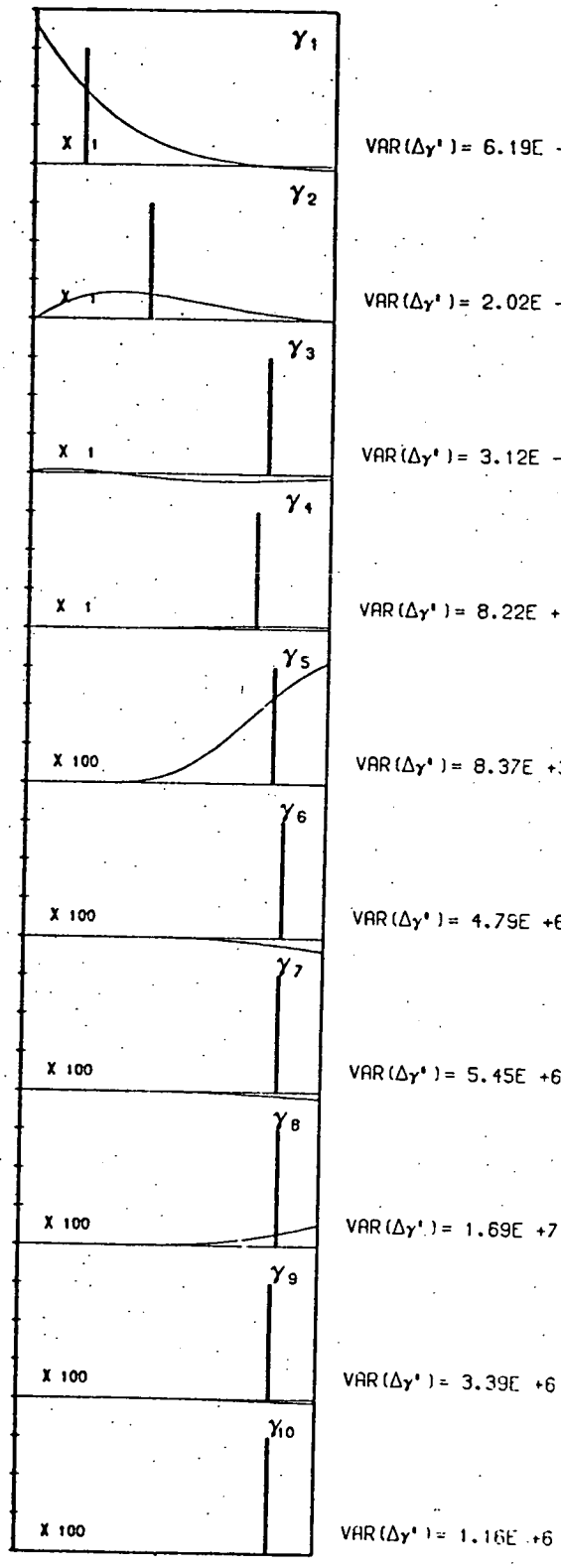

FIG. 5-5 b

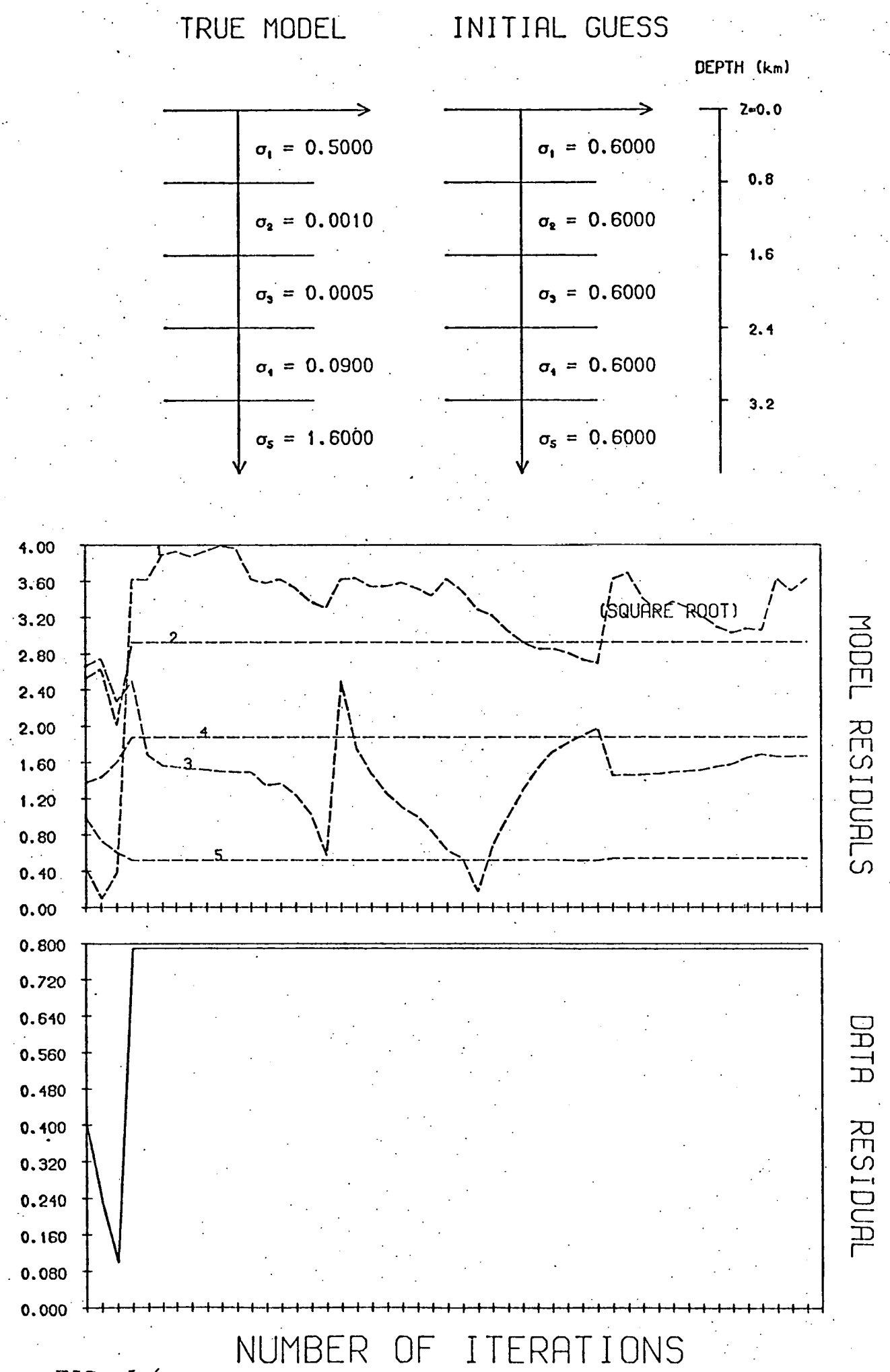
TRUE MODEL
INITIAL GUESS
DEPTH (km)
σ1 = 0.5000
σ2 = 0.0010
σ3 = 0.0005
σ4 = 0.0900
σ5 = 1.6000
σ1 = 0.6000
σ2 = 0.6000
σ3 = 0.6000
σ4 = 0.6000
σ5 = 0.6000
Z=0.0
0.8
1.6
2.4
3.2
4.00
3.60
3.20
2.80
2.40
2.00
1.60
1.20
0.80
0.40
0.00
(SQUARE ROOT)
1
2
3
4
5
MODEL RESIDUALS
0.800
0.720
0.640
0.560
0.480
0.400
0.320
0.240
0.160
0.080
0.000
DATA RESIDUAL
NUMBER OF ITERATIONS

FIG. 5-6 a

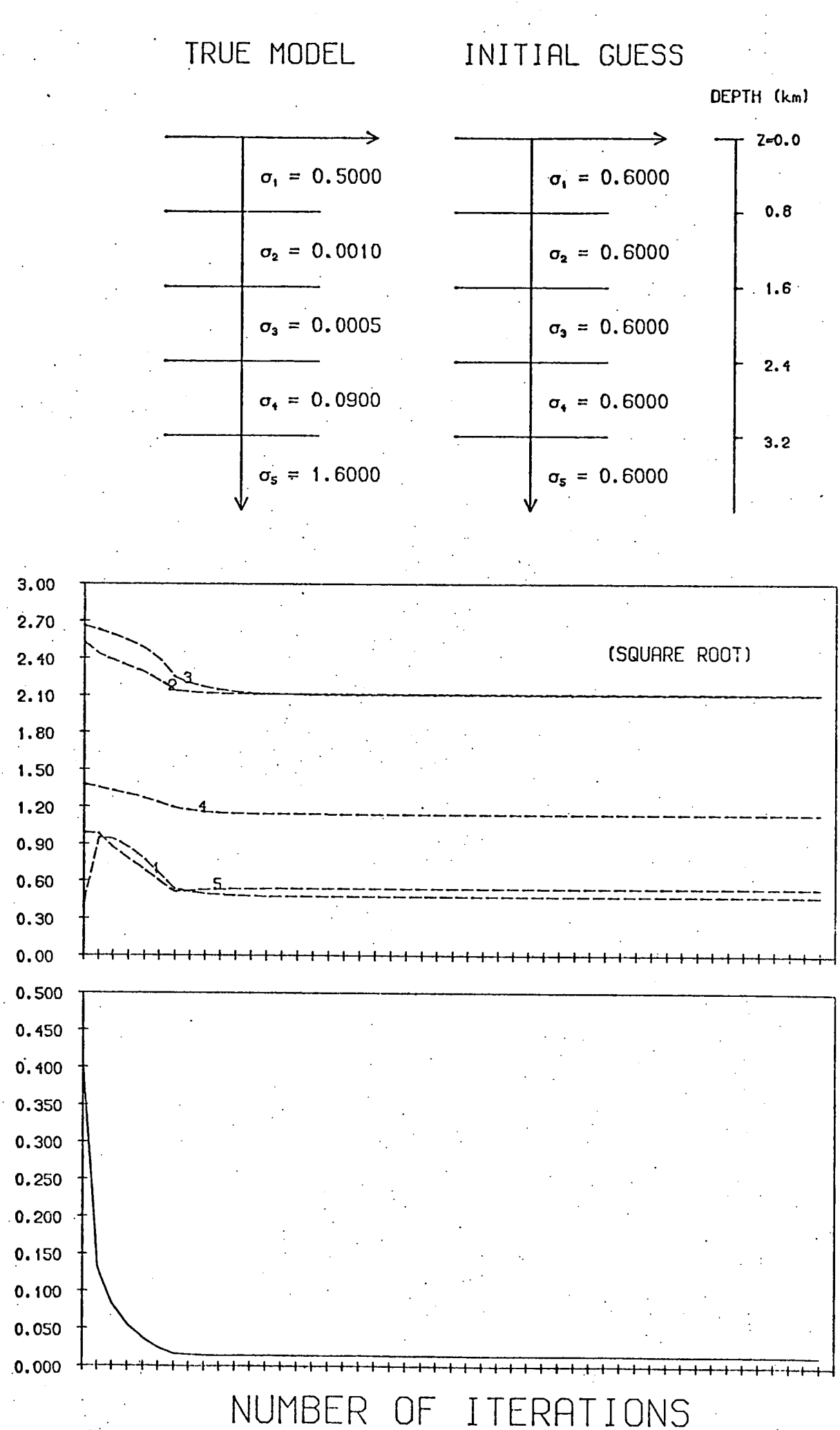
TRUE MODEL
INITIAL GUESS
DEPTH (km)
σ1 = 0.5000
σ2 = 0.0010
σ3 = 0.0005
σ4 = 0.0900
σ5 = 1.6000
σ1 = 0.6000
σ2 = 0.6000
σ3 = 0.6000
σ4 = 0.6000
σ5 = 0.6000
Z=0.0
0.8
1.6
2.4
3.2
(SQUARE ROOT)
3.00
2.70
2.40
2.10
1.80
1.50
1.20
0.90
0.60
0.30
0.00
0.500
0.450
0.400
0.350
0.300
0.250
0.200
0.150
0.100
0.050
0.000
NUMBER OF ITERATIONS

FIG. 5-6 b

5.4 Introducing Phase Into the Formalism

In the synthetic examples of Section 5.2, amplitude data alone have been used. Researchers typically use amplitude information alone because statistical estimates of the phase are often unreliable, and the plot of phase as a function of period often exhibits a large amount of scatter. From the point of view of our inverse procedure, we have been using only the real part of equation (5.1.7) as a datum and its corresponding Fréchet kernel. However, if reliable phase estimates are available to a data set, they may be able to play a decisive part in determining acceptable models.

Including other independent sets of data (which are functionals of the same model distribution) into the inversion procedure is a straightforward matter. For the problem of inferring conductivity, Vozoff and Jupp (1975b) have included direct current sounding data together with magnetotelluric sounding data in a joint inversion scheme. Müller (1976) has recently described how he has introduced phase data into a least-squares inversion, using a Marquardt non-linear algorithm. An example with relevance to the induction problem is perhaps to be found in the work of Gilbert and Dziewonski (1975) where normal mode data is inverted. Using the orthogonality properties of the eigenfunctions associated with the vibrational free modes of decay in the Earth, they form an extended inner product matrix which is block-

diagonal:

$$\underline{\underline{B}} = \begin{bmatrix} \underline{\underline{B}}_1 & & & 0 \\ & \underline{\underline{B}}_2 & & \\ & & \underline{\underline{B}}_3 & \\ 0 & & & \underline{\underline{B}}_4 \end{bmatrix} \qquad (5.4.1)$$

Each submatrix corresponds to a set of orthogonal data. Banks (1969), in his analysis of daily variation data, has assumed a P_1^0 harmonic (i.e. $\ell = 1$, $m = 0$, in equation (3.2.21)). However the orthogonality of higher spherical harmonics may be exploited in a Backus-Gilbert inversion of a more general set of response data.

Can phase be treated as an independent set of information? The statistical covariance estimates of phase and amplitude are apparently independent (Parker, 1970). Treated in an independent manner, one can form the extended inner product matrix:

$$\underline{\underline{B}} = \begin{bmatrix} \underline{\underline{B}}_1 & 0 \\ 0 & \underline{\underline{B}}_2 \end{bmatrix} \qquad (5.4.2)$$

where $\underline{\underline{B}}_1$ is the inner product matrix developed previously for amplitude data and $\underline{\underline{B}}_2$ is the inner product matrix for

phase data. However, if one were to rigorously defend this method of expressing the inner product matrix, one would need to show that the elements of $\underline{\underline{B}}$ outside the diagonal submatrices vanish. To do this one would need to show

$$\int_0^\infty \text{Re } G_k(z) \text{ Im } G_j(z) \, dz = 0 \qquad (5.4.3)$$

for all k and j. It can easily be shown that the above integral does not vanish. Since the integrals of $Z_1 Z_2$ and $Z_1^* Z_2^*$ are easily evaluated, one can use relationships such as

$$Z_1 Z_2 - Z_1^* Z_2^* = 2 i \, (\text{Re } Z_1 \text{ Im } Z_2 + \text{Re } Z_2 \text{ Im } Z_1)$$

to determine the integral over $(0,\infty)$ of the functions Re Z_1 Im Z_2 etc. For example, if $k = j$ in (5.4.3), and $G_k(z) = \mathcal{E}^2(z)$, for a homogeneous half-space we have

$$4 i \int_0^\infty \text{Re } G_k(z) \text{ Im } G_k(z) \, dz = \tfrac{1}{4} \left[\frac{1}{K} - \frac{1}{K^*} \right]$$

It can be shown also that

$$\int \text{Re } G_k(z) \text{ Im } G_k(z) \, dz \; / \; \int \text{Re } G_k(z) \text{ Re } G_k(z) \, dz = 1/3$$

Thus one must bear in mind that if a block diagonal form of the inner product matrix such as (5.4.2) is used, an element of approximation is introduced to the procedure.

5.5 Inversion of a Seventeen-Point Data Set

In both this and the following Section, we shall describe the application of the Backus-Gilbert least-squares procedure to some sets of experimental data. The application to real data of the one-dimensional procedure described in this thesis presents some problems if the data is strongly anisotropic. At a magneto-telluric station one typically measures two orthogonal components of the tangential electric field, and two orthogonal components of the tangential magnetic field. Thus, out of these components one can form two apparent resistivities,

$$\rho_{xy} = \frac{1}{\omega\mu}\left|\frac{E_x}{H_y}\right|^2 \tag{5.5.1}$$

and

$$\rho_{yx} = \frac{1}{\omega\mu}\left|\frac{E_y}{H_x}\right|^2 \tag{5.5.2}$$

If the conductivity in the Earth is a function only of depth, z, then $\rho_{xy} = \rho_{yx}$. If there is a lateral discontinuity, then the apparent resistivities will differ. Having measured the pairs (E_x,E_y) and (H_x,H_y), one can express these as tangential vectors

$$\underline{E} = E_x \hat{i} + E_y \hat{j}$$

$$\underline{H} = H_x \hat{i} + H_y \hat{j}$$

and try to find a rotation transformation, $\underline{\underline{R}}$, such that

$$\underline{E}' = \underline{\underline{R}}\,\underline{E} = E_{x'}\,\hat{i}' + E_{y'}\,\hat{j}'$$

and

$$\underline{H}' = \underline{\underline{R}}\,\underline{H} = H_{x'}\,\hat{i}' + H_{y'}\,\hat{j}'$$

and $\rho_{x'y'}$ is a maximized apparent resistivity and $\rho_{y'x'}$ is the minimum resistivity.

In terms of a 'striking' lateral discontinuity (as was discussed in Section 1.3) the minimal ρ_a can be associated with an electric field component parallel to the strike (called E-polarization) and this is less sensitive to the anomalous effects of the discontinuity. The maximum ρ_a can be associated with H-polarization, and is very strongly affected by the discontinuity. Unfortunately, it is often the major component for which the most accurate measurements are possible. The small tangential electric field appearing in the apparent resistivity ratio for the minimum, ρ_a, is subject to large signal-to-noise ratio. Rooney (1976) has presented curves to indicate how apparent resistivity can be affected by a lateral discontinuity.

If the two apparent resistivity curves for ρ_{xy} and ρ_{yx} are nearly the same, the ratio of the two resistivities will be unaffected by a rotation $\underline{\underline{R}}$. This isotropy of the apparent resistivity implies a conductor which is one-dimensional.

As a first illustration of the application of the least-squares procedure to an experimental data set, we

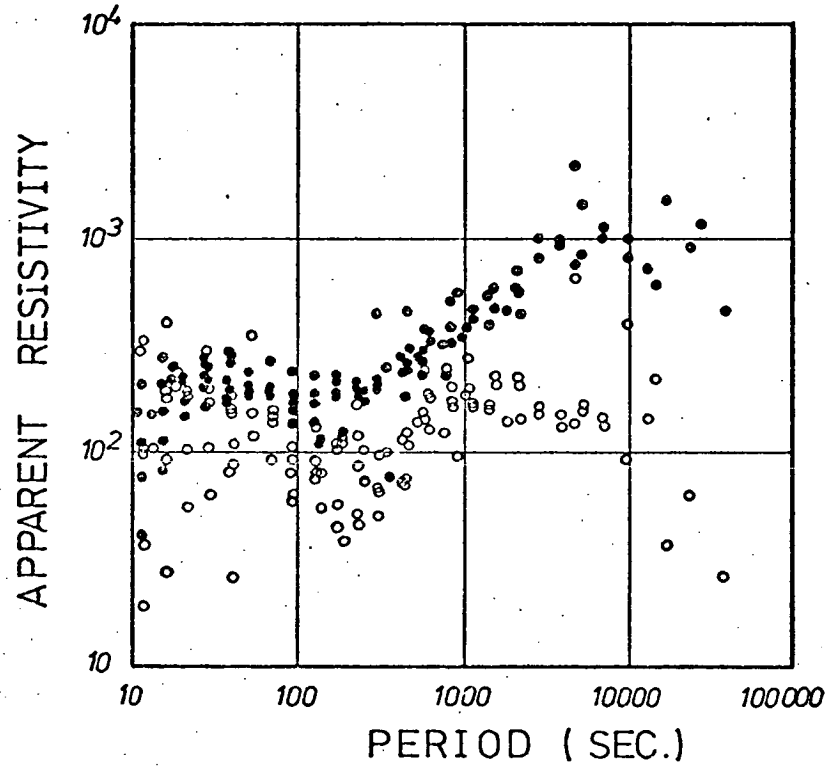

FIG. 5-7 Apparent resistivity data collected at Newcastleton site (Scotland) by Jones (1976). The open circles are the component ρ_{NS} (i.e. a North telluric field and an East magnetic field); the solid circles are ρ_{EW}. The two curves are sufficiently coincident to suggest a one-dimensional interpretation may suffice.

shall choose a set of data which shows encouraging isotropy. The data was collected and analysed by Jones (reported in Jones and Hutton, 1976), and the two orthogonal apparent resistivity curves, determined from a site at Newcastleton in the U.K., are plotted in Fig. 5-7. The solid circles correspond to a telluric field in the N-S direction; the open circles correspond to an E-W telluric field. Compared with usual magneto-telluric data, Fig. 5-7 displays considerable isotropy and this can be expressed in statistical terms: one can point to a low skew factor, and to the fact that there is little indication of a preferred direction when the response is rotated.* Jones does rotate the data to maximize the partial coherence between the North telluric and East magnetic field estimates following a practice suggested by Reddy and Rankin (1974). Also statistical acceptance criteria are applied to the data set to produce a pair of response data sets, each set consisting of about twenty amplitude and twenty phase estimates. The two apparent resistivity curves are very similar; however it is interesting to note that the curves corresponding to maximized partial coherence have an unusually smooth phase response curve. We shall consider the problem of

---

* For a thorough discussion of such statistical matters, the reader is referred to the literature, e.g. Hermance (1974).

interpreting this rotated resistivity.

Initially we invert only the amplitude (apparent resistivity) information, and at a later stage we consider phase information. A five layer parameterization -- described in Section 5.2 -- of the model was chosen, since it seems that a finer structure might be too much to ask of a 17-point data set, and less than five layers may overconstrain the problem. However these are intuitive speculations. The task is to select, by educated guess, a possible model, and then to see if the least-squares procedure (smoothed by ranking and winnowing) converges to some near-by optimum model. Table 5-1 lists the details of starting models, σ^0, labelled A to F. Fig. 5-8a illustrates by the dotted lines the response of this guessed model; the solid line indicates the response due to the hundredth iterate in a least-squares procedure. The model associated with this hundredth iterate is also enumerated in Table 5-1, and this 'optimum' model is illustrated graphically in Fig. 5-8b.

One can remark upon the similar characteristics of the models which are achieved by the procedure. Basically, there seems to be a relatively good conductor at the surface, and then another region of high conductivity at some thirty kilometers depth. Comparing Figs. 5-8a and 5-8b (bearing in mind the experimental error to be attached to the response curve) one can observe that, despite the general common features, a

FIG. 5-8 a The open circles indicate the rotated major resistivities determined from the data illustrated in Fig. 5-7. The dotted lines represent the response of starting models A to F in Table 5.1. The solid lines represent the response of the hundredth iterate in a least-squares procedure which uses only 17 amplitudes.

FIG. 5-8 b The final models achieved after one hundred iterations of the least-squares procedure applied to the data displayed by the open circles in Fig. 5-8 a.

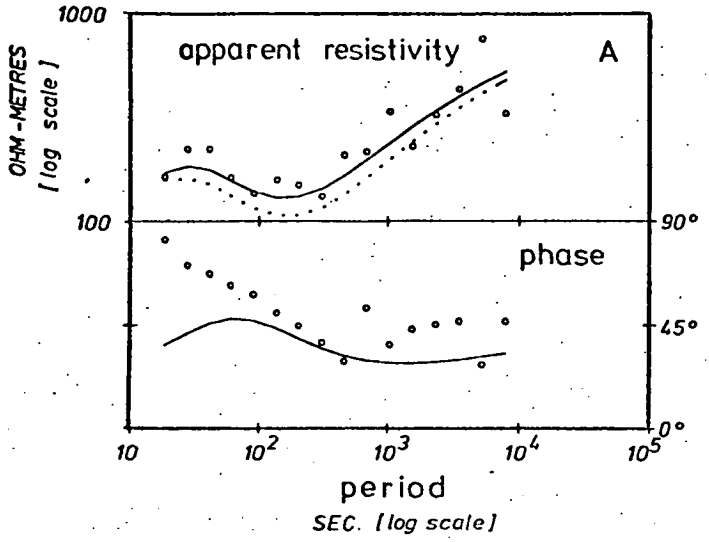
1000
OHM-METRES
[log scale]
apparent resistivity
A
100
phase
90°
45°
0°
10
10²
10³
10⁴
10⁵
period
SEC. [log scale]

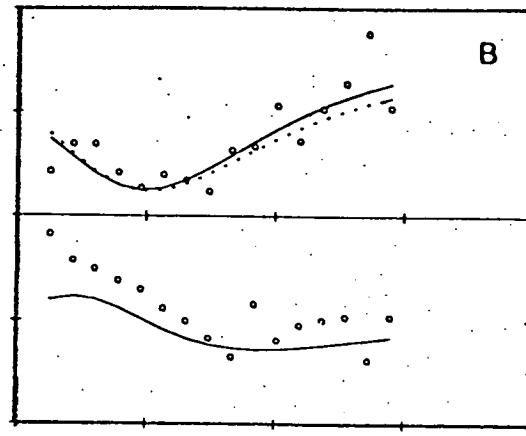
B

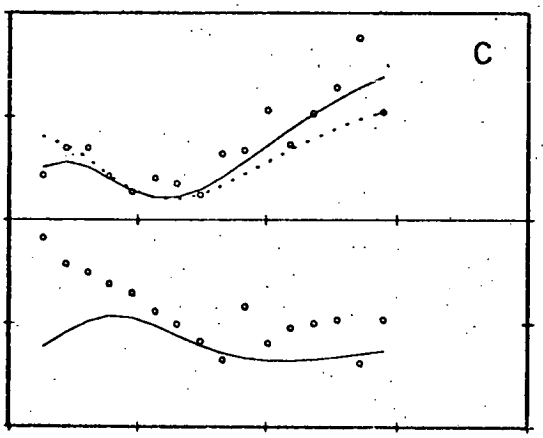
C

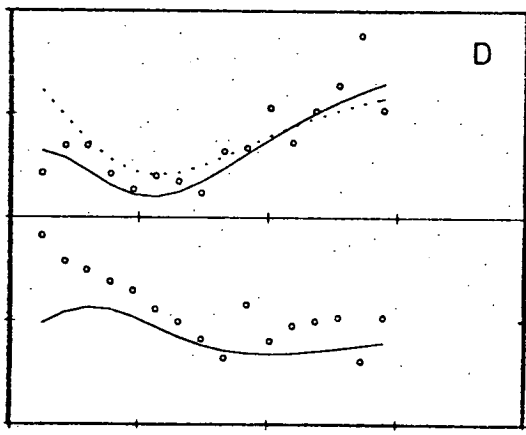
D

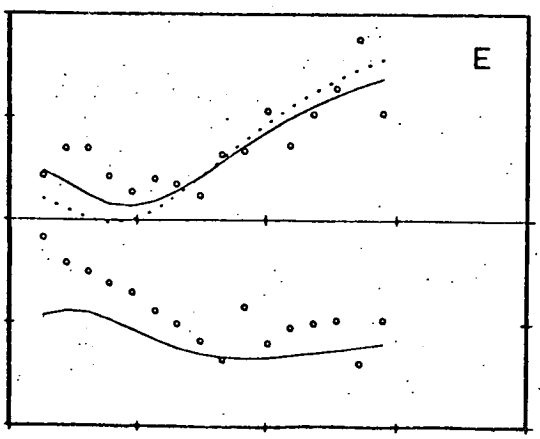
E

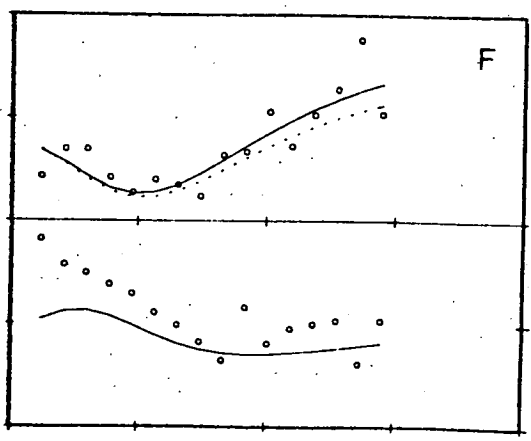
F

FIG. 5-8 a

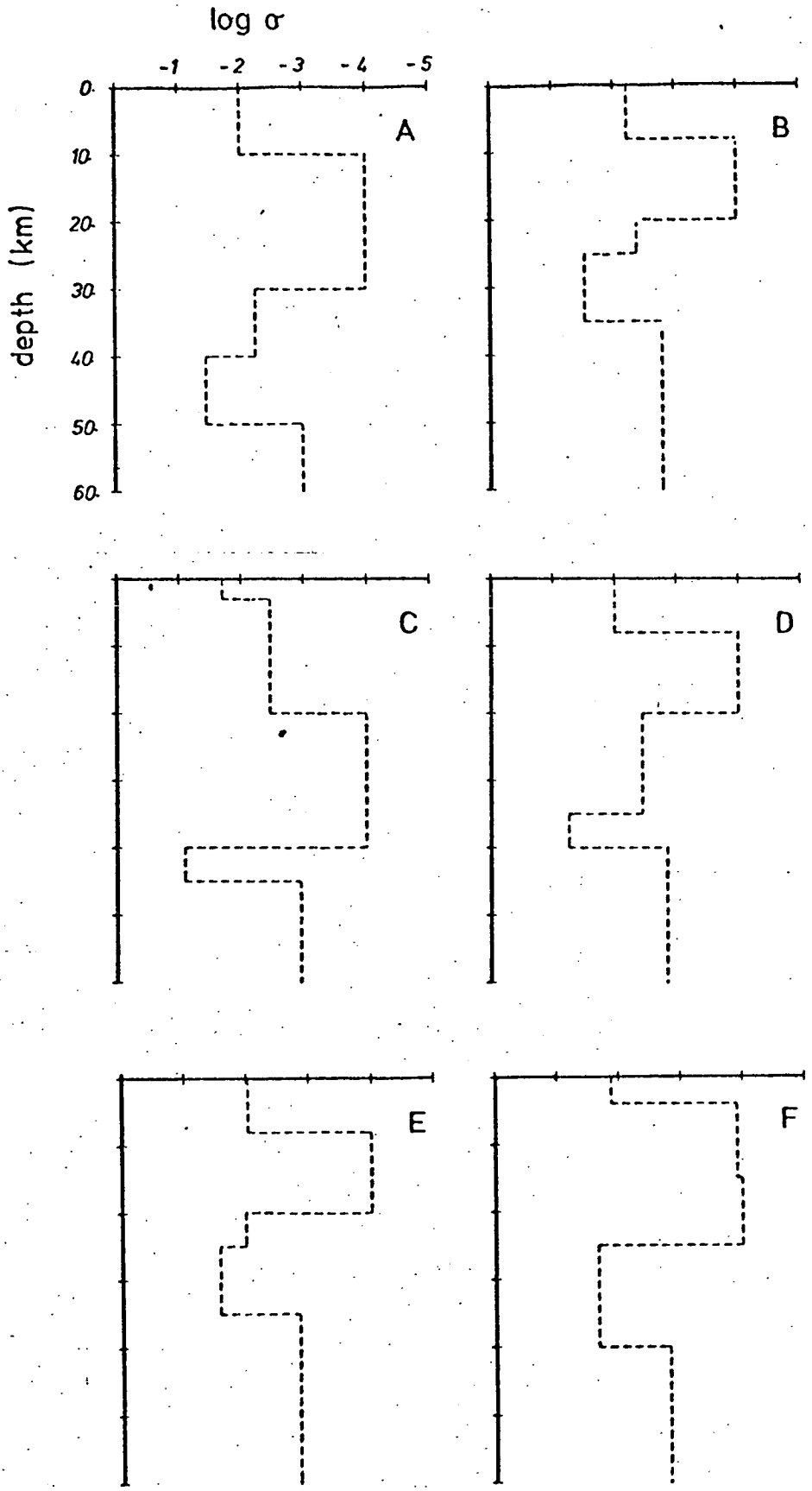

FIG. 5-8 b

TABLE 5.1

A	σ°	σ	d	B	σ°	σ	d
1	0.008	0.011		1	0.005	0.0064	
			10				8
2	0.005	0.0001		2	0.001	0.0001	
			30				20
3	0.008	0.0058		3	0.005	0.0042	
			40				25
4	0.035	0.0355		4	0.03	0.029	
			50				35
5	0.001	0.001		5	0.002	0.0016	

C	σ°	σ	d	D	σ°	σ	d
1	0.008	0.02		1	0.001	0.01	
			3				8
2	0.003	0.0034		2	0.001	0.0001	
			20				20
3	0.007	0.0001		3	0.005	0.0001	
			40				30
4	0.06	0.08		4	0.03	0.0367	
			45				40
5	0.002	0.0011		5	0.002	0.0014	

E	σ°	σ	d	F	σ°	σ	d
1	0.008	0.0093		1	0.01	0.013	
			8				4
2	0.007	0.0001		2	0.001	0.0012	
			20				15
3	0.012	0.0102		3	0.005	0.0001	
			25				25
4	0.02	0.0269		4	0.02	0.022	
			35				40
5	0.001	0.0014		5	0.002	0.0015	

variety of models can satisfy the data. It will be noticed that a good surface conductor is demanded by the data to satisfy the high-frequency data points. Also it will be seen that the phase data is not satisfied at all well (especially at high frequencies) when amplitude data alone is represented in the inversion. Fig. 5-8b is by no means an exhaustive description of the space of solutions (which may after all be infinite), nor does it pretend to be in any way representative. They are simply a few examples chosen to indicate how a variety of acceptable models can be generated by taking a variety of starting models and choosing a variety of parameterizations. This emphasizes the character of Backus-Gilbert least-squares inversion: the acceptable model closest to the starting model is located. In a least-squares procedure one might not expect to isolate bizarre acceptable models. One cannot rule out the Earth being a bizarre conductor, however whether such structure can be isolated, or resolved, is another matter.

How does the inclusion of phase information affect the procedure? If one extends the data set to include phase -- and extends the inner product matrix as described in Section 5.4 -- the inverse least-squares involves a 2N x 2N system. In this case, this is a 34 x 34 system. For such a procedure, a starting model is chosen which is known to satisfy amplitude data alone. Some idea of the influence of phase information may be obtained by

observing how the model is modified in the subsequent procedure. The result of such an experiment is shown in Fig. 5-9a. A starting model was chosen $\underline{\sigma}^0$: ($\sigma_1 = .02$, $\sigma_2 = .0001$, $\sigma_3 = .0001$, $\sigma_4 = .02$, $\sigma_5 = .001$) which is seen from the dashed line to be a good fit to amplitude data alone. After twenty iterations of a least-squares inverse procedure which includes 17 amplitude and 17 phase data points, the optimum model is found to be σ : ($\sigma_1 = .0001$, $\sigma_2 = .017$, $\sigma_3 = .0001$, $\sigma_4 = .012$, $\sigma_5 = .0025$). In Fig. 5-9a the solid line represents the fit this model makes to the data. It can be seen that phase data is more closely fitted at higher frequency (thus reducing the overall data residual), however this has resulted in some increase in the residual associated with the amplitude data alone. Specifically, one can see that the first amplitude data point -- which has entered so significantly into the least-squares procedure for amplitude data alone -- is 'overruled' by the set of ten high-frequency phase data. Thus the twentieth iterate ignores the first amplitude point, and is tending to install at the surface a relatively <u>poor</u> conductor in order to fit the phase. So it would seem including the set of phase data particularly supplies additional information relating to the structure at the surface -- this importance of phase to resolving surface structure has been suggested by Parker (1970).

FIG. 5-9 a Including phase into the data set. The dotted line is the response which fits amplitude data alone, for the model $\underline{\sigma}$: ($\sigma_1 = 0.02$, $\sigma_2 = 0.0001$, $\sigma_3 = 0.0001$, $\sigma_4 = 0.02$, $\sigma_5 = 0.001$) for depths $d_1 = 8$, $d_2 = 20$, $d_3 = 30$, $d_4 = 40$. The solid line represents the response achieved after twenty iterations of a least-squares procedure which includes 17 phase estimates. The model which is achieved is $\underline{\sigma}$: ($\sigma_1 = 0.0001$, $\sigma_2 = 0.017$, $\sigma_3 = 0.0001$, $\sigma_4 = 0.012$, $\sigma_5 = 0.0025$).

FIG. 5-9 b A starting model known to satisfy optimally phase and amplitude data (the 20th iterate of model 'A' in Table 5.2) is used as a starting model in a least-squares procedure which only involves amplitude data. The response of the starting model is the dotted lines, and the 100th iterate is the solid line. This model is $\underline{\sigma}$: ($\sigma_1 = 0.0085$, $\sigma_2 = 0.001$, $\sigma_3 = 0.0044$, $\sigma_4 = 0.033$, $\sigma_5 = 0.0014$). The phase is seen to become less well fitted.

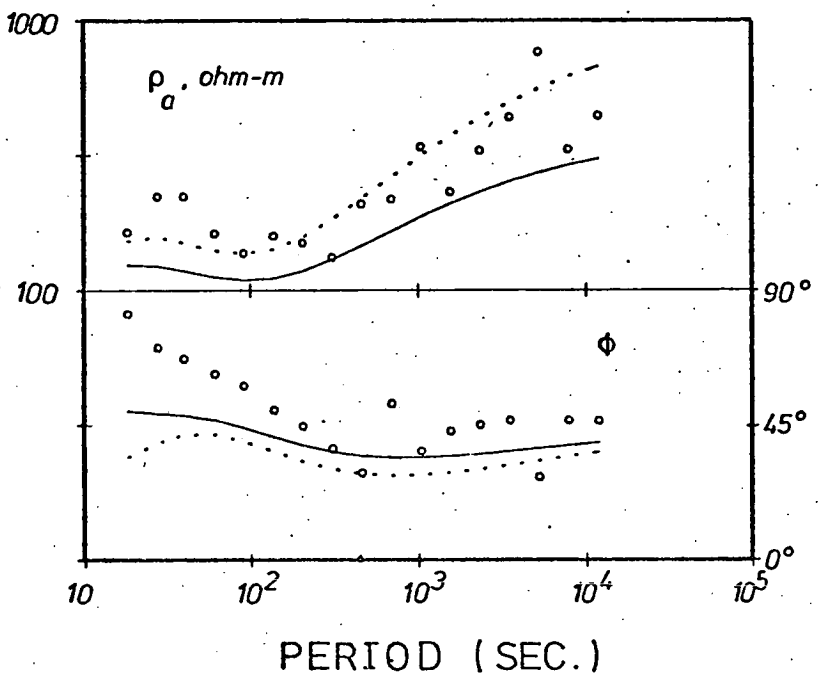
1000
ρ_a , ohm-m
100
90°
Φ
45°
0°
10
10^2
10^3
10^4
10^5
PERIOD (SEC.)

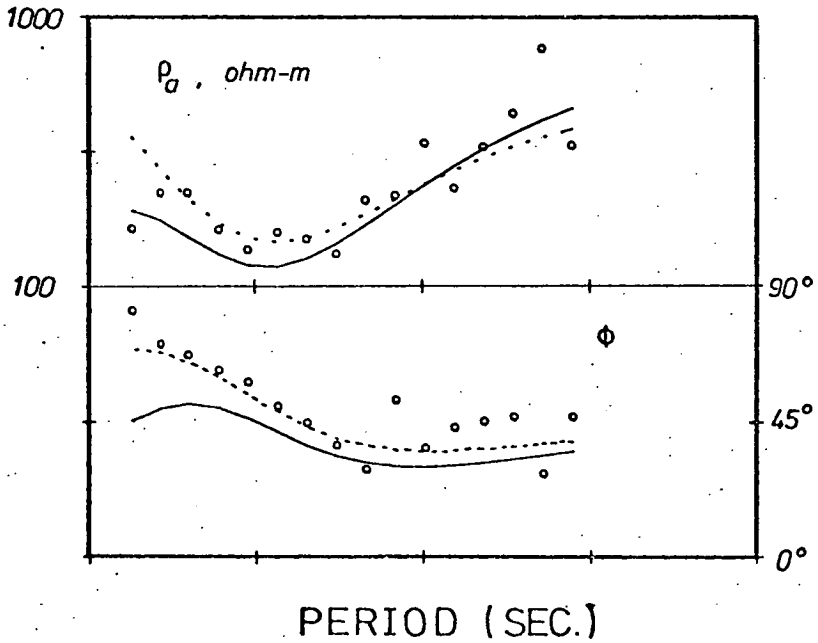
1000
ρ_a , ohm-m
100
90°
Φ
45°
0°
PERIOD (SEC.)

After twenty iterations the optimum model of Fig. 5-9a may not have been reached. Models which are more acceptable will be viewed presently, but our interest at the moment is to observe the trend established by including phase.

We attempt the reverse procedure to that illustrated in Fig. 5-9a; namely we start with a model which fits optimally the phase and amplitude together (in fact the model σ , in Table 5.2 A). We then seek to optimize the fit of the model to the amplitude data alone, and hope to see the effect on the least-squares procedure of suddenly ignoring phase information. The starting model in this case has poor surface conductivity -- the dashed line in Fig. 5-9b indicates its fit to the data points. The solid line represents the hundredth iterate in an inverse procedure involving only the amplitude. The model associated with this iterate is $\underline{\sigma}$: ($\sigma_1 = .0085$, $\sigma_2 = .0001$, $\sigma_3 = .0044$, $\sigma_4 = .033$, $\sigma_5 = .0014$), and is seen to have higher conductivity at the surface. However, from Fig. 5-9b, the phase resulting from this iterate does not fit the phase data very well.

Table 5.2 contains the model parameters for a series of starting models (along with the models for the twentieth iterates) to be used in a 34-point data inversion, involving 17 phase points and 17 amplitude points. Fig. 5-10a illustrates the response generated by the starting models A to D by the dashed lines. The

FIG. 5-10 a The responses associated with the least-squares procedure for a 34-point data set of phase and amplitude. The models involved are listed in Table 5.2. The dotted line is the response of the starting model; the solid line is the response of the 20th iterate.

FIG. 5-10 b The twentieth iterate models (A to D) associated with the least-squares procedures displayed in Fig. 5-10 a. The parameters associated with these models are contained in Table 5.2.

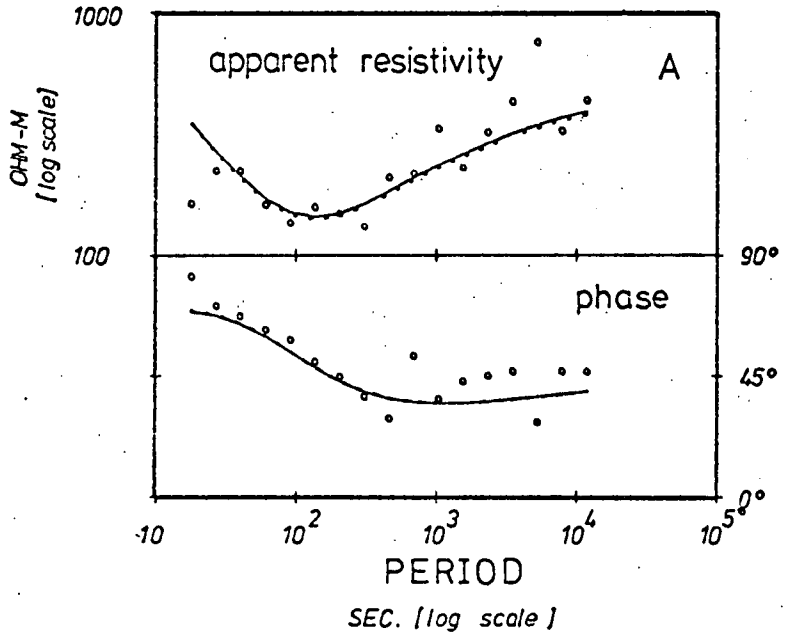
1000
100
OHM-M
[log scale]
apparent resistivity
A
phase
90°
45°
0°
10
10^2
10^3
10^4
10^5
PERIOD
SEC. [log scale]

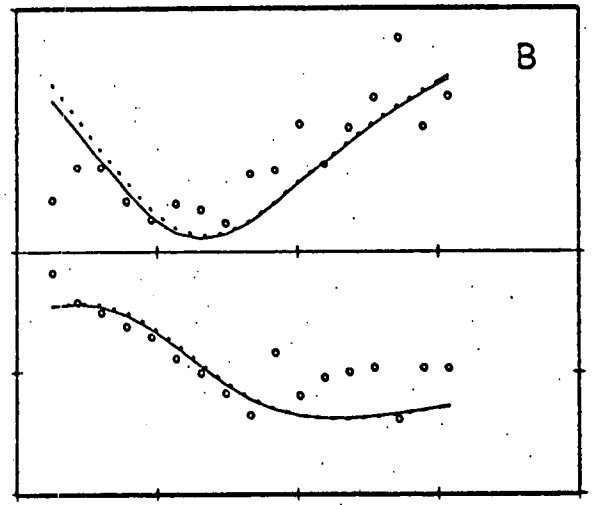
B

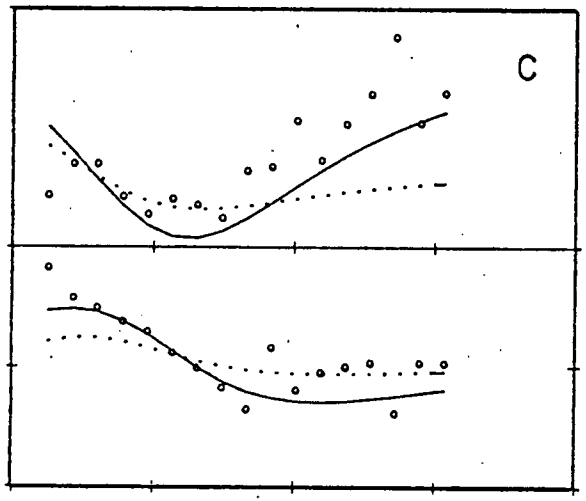
C

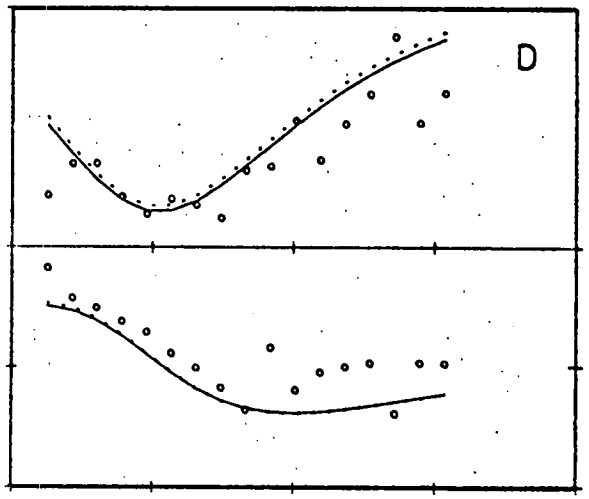
D

FIG. 5-10 a

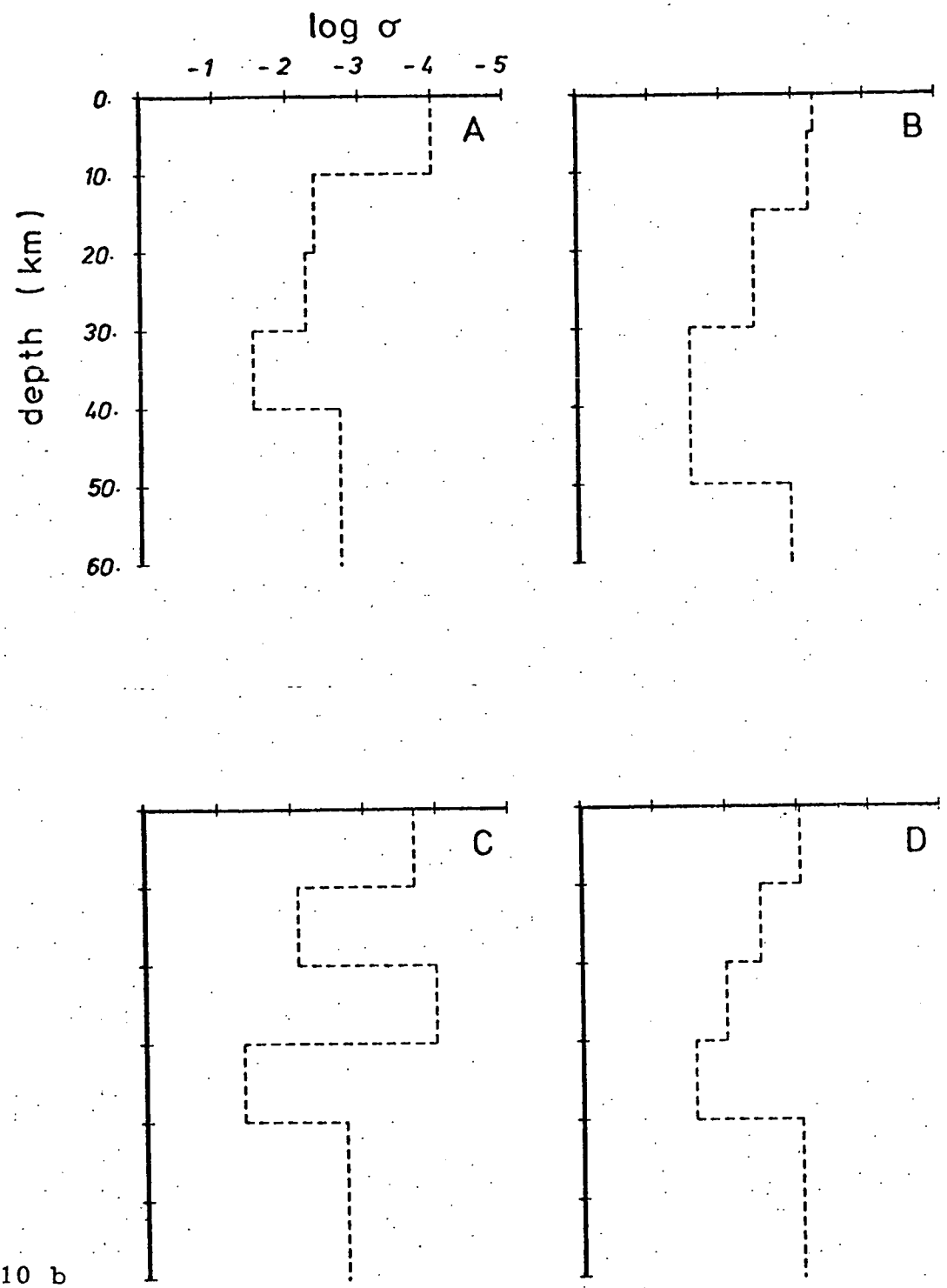

FIG. 5-10 b

TABLE 5.2

A	σ°	σ	d	B	σ°	σ	d
1	0.0006	0.0001		1	0.002	0.0005	
			10				5
2	0.002	0.0042		2	0.0007	0.0006	
			20				15
3	0.01	0.0056		3	0.0007	0.0035	
			30				30
4	0.028	0.03		4	0.03	0.027	
			40				50
5	0.002	0.0019		5	0.001	0.0011	

C	σ°	σ	d	D	σ°	σ	d
1	0.003	0.0002		1	0.0006	0.0009	
			10				10
2	0.006	0.0082		2	0.002	0.0033	
			20				20
3	0.001	0.0001		3	0.01	0.01	
			30				30
4	0.025	0.0467		4	0.027	0.0268	
			40				40
5	0.005	0.0018		5	0.0008	0.0009	

response of the twentieth iterate is indicated by the solid line. For the starting models A, B, and D, the local minimum was found to be not very far away from the starting model. The optimization associated with model C is somewhat more striking, although the twentieth iterate may not be optimum (the process is still converging after twenty iterations). It is interesting that the response for this iterate lies within the error bounds for the data. The form of the models which are isolated in this procedure is illustrated in Fig. 5-10b.

These examples of inversion of a one-dimensional data set are chosen to illustrate the procedure as it is applied to real data; the emphasis is not upon interpreting the particular data, but upon indicating how the Backus-Gilbert least-squares procedure can isolate a number of acceptable models and how phase information can serve to constrain further the space of acceptable models. The evident non-uniqueness displayed in Figs. 5-8b and 5-10b arises from the scatter in the data, the truncated nature of the data, from the variety of starting models which were arbitrarily chosen, and from the variety of model parameterizations which were also arbitrarily chosen. It is this element of choice which can make selections of models like Fig. 5-8b and Fig. 5-10b biased and incomplete.

5.6 Inversion of a Larger Data Set

In the previous Section, the generalized least-squares procedure was used as an aid for isolating individual members of the space of acceptable models. If the data set is small and if it exhibits considerable scatter, one might expect a large variety of acceptable models to exist. On the other hand, fitting a five-layer model (with fixed depths) to twenty data points might well consist of a problem both overconstrained and underdetermined. The problem may be overconstrained because the layer boundaries might not be in their optimum position; the problem may be underdetermined because the data may contain little information concerning some parameters. By choosing a wide variety of starting models, one could conceivably arrive at a wide range of acceptable models -- but a range which is by no means exhaustive or even representative. The contribution phase information can make to the demarcation of the space of acceptable models has also been investigated, and it was suggested that phase data over a fairly large range of frequency can supply information which is related to the surface conductivity.

In this Section we outline how one might apply the generalized least-squares procedure towards resolving a specific question arising out of an interpretation of a set of magnetotelluric data which includes phase estimates. The following discussion must not be considered in any

sense a conclusive answer; on the contrary, we include this as further illustration of how a systemized approach to inversion can assist our understanding of a set of data. We point out that we enter the following problem at an extremely late stage, accepting the response data per se, and without regard to the experimental details of its collection or analysis. Thus the following remarks cannot be offered as conclusive interpretation!

Weideldt (1972) illustrates his exact inversion formalism by interpreting a set of magnetotelluric data published by Wiese (1965); this data was collected at a station at Uckermunde in East Germany. The response data exhibits anisotropy, and so indicates the possible two- or three-dimensionality of the conductivity structure which must give rise to this data. A 'strike' in an East-West direction is assumed. In these circumstances, the apparent resistivity

$$\rho_a = \frac{1}{\omega\mu}\left|\frac{E_{EW}}{H_{NS}}\right|^2$$

is considered to be the most reliable response for one-dimensional interpretation. The Wiese (1965) data is illustrated in Fig. 5-11 by the discrete points. For exact inversion, one requires a smooth response function over all frequencies and such a function is illustrated by the solid line in Fig. 5-11. It is interesting to note that Weideldt does not use a 'fit' to the phase data

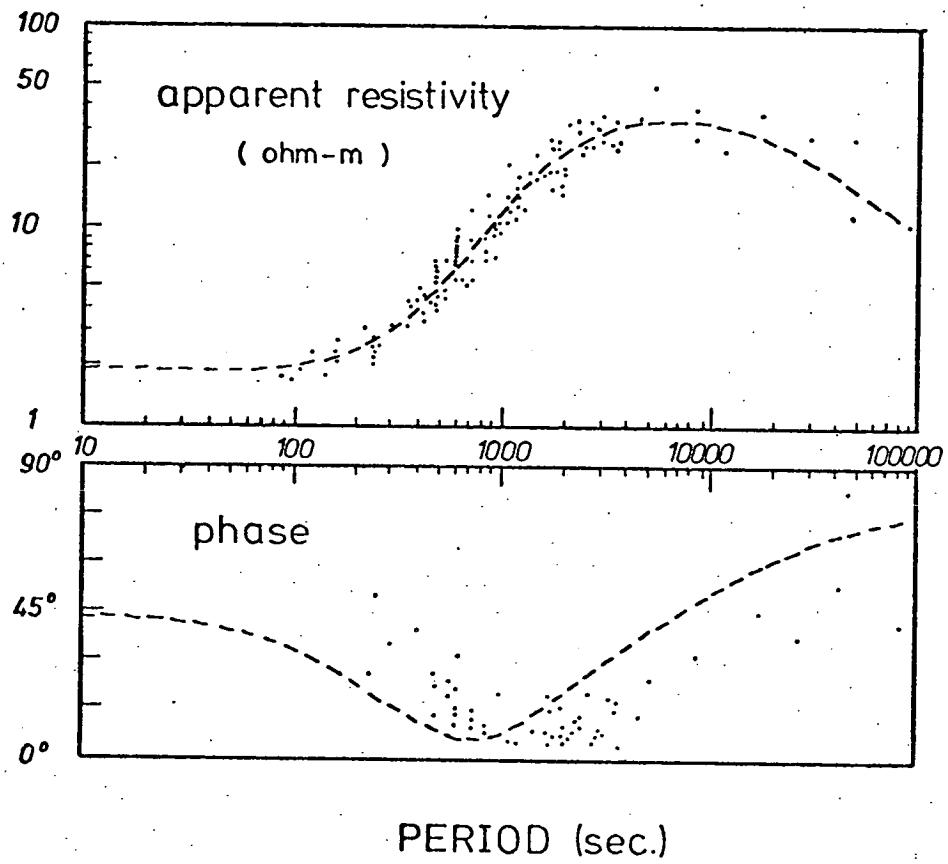

FIG. 5-11 The data set collected by Wiese (1964) and used by Weideldt (1972) to illustrate his direct inversion of induction data. The dashed line represents Weideldt's smooth, extended response for amplitude. The phase is reconstructed from the approximation (5.6.1).

for his exact inversion but uses instead a 'reconstructed phase', deduced directly from the slope of the apparent resistivity curve. This reconstructed phase is deduced from an approximate formula supplied by Weideldt (1972)

$$\phi \approx \frac{\pi}{4}\left(1 - \frac{d \ln \rho_a}{d(\ln T)}\right) \qquad (5.6.1)$$

In this way, the phase response used by Weideldt is extracted entirely from amplitude information; the measured phase estimates of Wiese are disregarded. It will be noted from Fig. 5-11 that whereas phase reconstructed from ρ_a is in qualitative agreement with the Wiese phase data, Weideldt admits a 'phase shift' between these two responses. The model achieved by exact inversion of the smooth curves in Fig. 5-11 is illustrated in Fig. 5-12. A five-layer model previously determined by Fournier (1968) is also illustrated by the dotted line in Fig. 5-12.

Within the context of Weideldt's intended illustration of the exact inverse Sturm-Liouville procedure, his use of reconstructed phase is entirely justified. However, the disparity between the reconstructed phase and measured phase estimates leads to the interesting question: can the measured phase estimates of Wiese imply in themselves some restriction to the space of acceptable models? One way to approach this question is to perform a least-squares optimization to the entire data set displayed in Fig. 5-11 -- including amplitude and phase

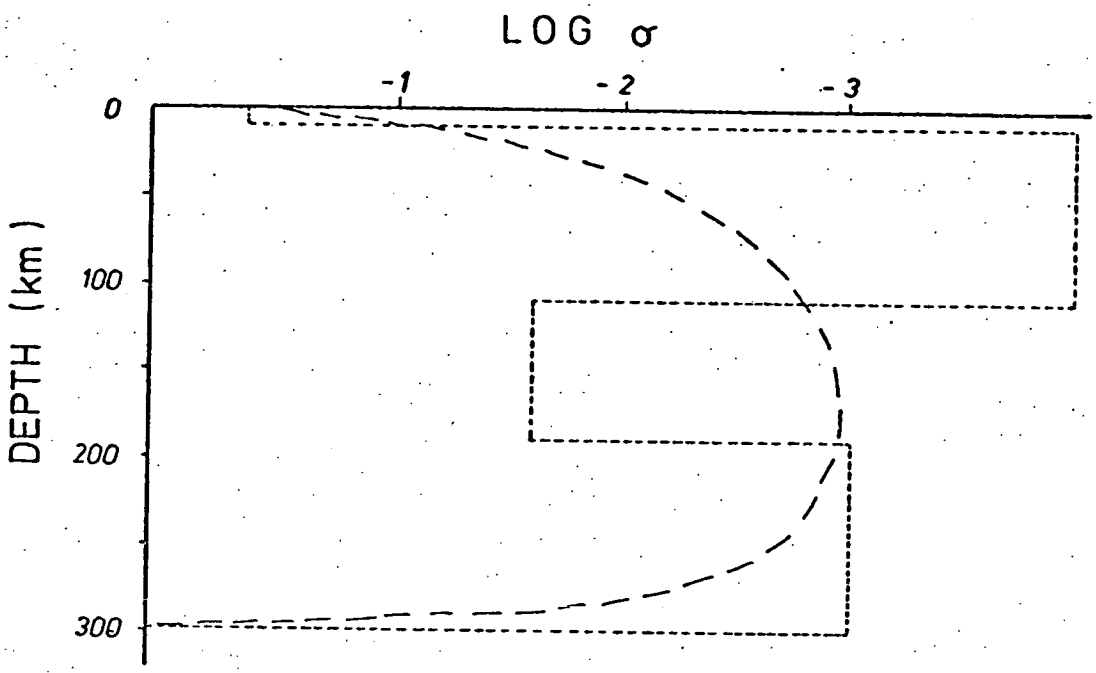

FIG. 5-12 Models proposed for the data of Fig. 5-11. The dotted line is the model of Fournier (1968). The solid line is the model determined by Weideldt by direct inversion.

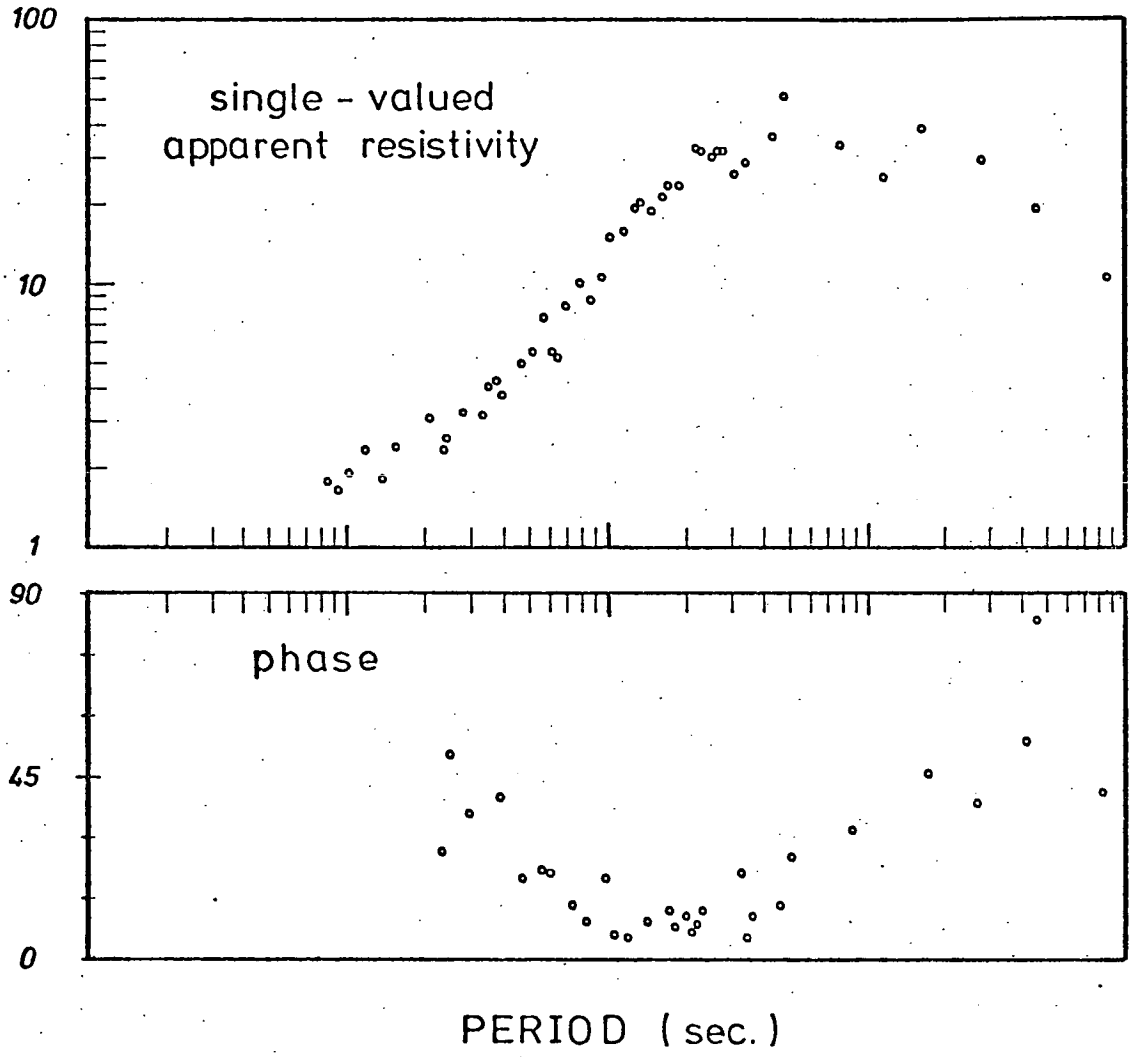

FIG. 5-13 A single-valued simulation of the data illustrated in Fig. 5-11. At each particular period where the various different response estimates appeared in Fig. 5-11, the various estimates were visually averaged to achieve a single estimate.

estimates. In this way, models may be isolated which offer a closer fit (in a least-squares sense) to the combined phase and amplitude data.

Of course, a satisfactory analysis would require some understanding of the spectral properties of the data in Fig. 5-11. For purposes of illustration, we extract from the multi-valued response in Fig. 5-11 a single-valued response which is illustrated in Fig. 5-13. (It is important that the response be single-valued. If two response estimates corresponding to the same frequency are both represented in the inverse procedure, then two rows of the inner product matrix would be identical. In these circumstances the matrix would be singular.) At each frequency where the response is multi-valued, it is made single-valued by visually averaging over the various response estimates. The resulting data set consists of forty-six amplitude estimates, and thirty phase estimates: a total of seventy-six data points altogether.

The task is to select starting models which will lead to models which are optimum in the sense that the sum of the squares of the data residuals (for phase and amplitude data) is minimized. Firstly, we illustrate the usefulness of the least-squares procedure in moving from a somewhat distant model, to a considerably more acceptable model. Fig. 5-14a illustrates with the dashed line the response due to the starting model indicated by

the letter 'A' in Table 5.3. Also illustrated in Fig. 5-14a is the response due to the first iterate (whose conductivities are also listed in Table 5.3), again this is indicated by a dashed line. The solid line in Fig. 5-14a is the response due to the twentieth iterate in the least-squares procedure. The depths have been kept fixed for this example. It may be noted that the starting model resembles somewhat the Fournier model in Fig. 5-13. It can be seen that its response is rather poorly fitted to the phase data. Also, at high frequency, the response of this starting model is a rather poor fit to the apparent resistivity data. Finding a five-layer model to fit this data is probably an overconstrained problem, and the local minimum achieved may not be a particularly good minimum in a global sense. One can visualize a local minimum existing (for this particular data) at some point where an improvement in the amplitude residuals corresponds to an equal deterioration in the residuals associated with phase data. This situation can be seen in Fig. 5-14a for the responses of low period -- the procedure tries to supply low conductivity at the surface to fit the rather large phase estimates for low period ($10^2 \leq T \leq 10^3$ sec). On the other hand, the procedure requires a large surface conductivity to satisfy the apparent resistivity data at low period. Inconsistency at low period is commonplace, since the spectral power is low, and the estimates are typically

TABLE 5.3

A. Starting Model	1st Iterate	20th Iterate	depth
0.247	0.239	0.293	
			10
0.0001	0.0025	0.006	
			100
0.001	0.0001	0.026	
			175
0.35	0.341	0.41	
			300
0.5	0.469	1.11	

B. Starting Model	1st Iterate	20th Iterate	depth
0.07	0.013	0.0125	
			0.5
0.3	0.31	0.31	
			10
0.0001	0.0019	0.0046	
			175
0.005	0.0001	0.0001	
			300
0.5	0.49	0.436	

scattered and unreliable. The interesting question is whether the least-squares procedure would help us to isolate a compromise model which corresponds to a minimum of the squares of the residuals for the extended set of phase and amplitude data.

In the previous Section, we discovered that large phase estimates associated with lower period might suggest the possibility of a more poorly conducting region near the surface. To illustrate this possibility, a very thin poorly conducting layer of 0.5 km depth is included in the parameterization of the model. A starting model, listed in Table 5.3 as model 'B', is employed. Its response is illustrated in Fig. 5-14b by a dashed line. Also illustrated in Fig. 5-14b is the first iterate of Model 'B' and the twentieth iterate, indicated by a dashed line and solid line respectively. Thus it can be seen, in Fig. 5-14b, how the phase information tends to make the surface layer less conducting, whereas the amplitude residual at the surface deteriorates. At the same time the overall phase response is much improved over that illustrated in Fig. 5-14a. Continued investigation can isolate further promising models. Despite the inclusion of phase, there is still rather poor resolution at the surface, and this can be reflected in the variety of surface conductivity profiles which lead to a more acceptable phase response. Such an example is the model $\underline{\sigma}$: $(\sigma_1 = 0.004,\ \sigma_2 = 0.55,\ \sigma_3 = 0.0015,\ \sigma_4 = 0.0001,$

FIG. 5-14 a The least-squares procedure applied to the 76-point data set in Fig. 5-13, with the (fairly remote) starting model indicated as 'A' in Table 5.3. The response of the starting model (phase and amplitude) and of the first iterate are indicated by the dashed curves; the twentieth iterate is indicated by the solid curve. The least-squares procedure adjusts the model parameters in such a way to produce successively improved model residuals.

FIG. 5-14 b The least-squares procedure applied to the data set indicated as 'B' in Table 5.3. A very thin (0.5 km) poorly conducting layer has been hypothesized for the surface. The first iterate and the starting model response are indicated by dashed lines; the 20th iterate by solid lines. The response iterates are seen to improve progressively.

FIG. 5-14 c The response due to model $\underset{\sim}{\sigma}$: ($\sigma_1 = 0.004$, $\sigma_2 = 0.55$, $\sigma_3 = 0.0015$, $\sigma_4 = 0.0001$, $\sigma_5 = 0.6$) with depths $d_1 = 4$ km, $d_2 = 10$ km, $d_3 = 35$ km, $d_4 = 300$ km.

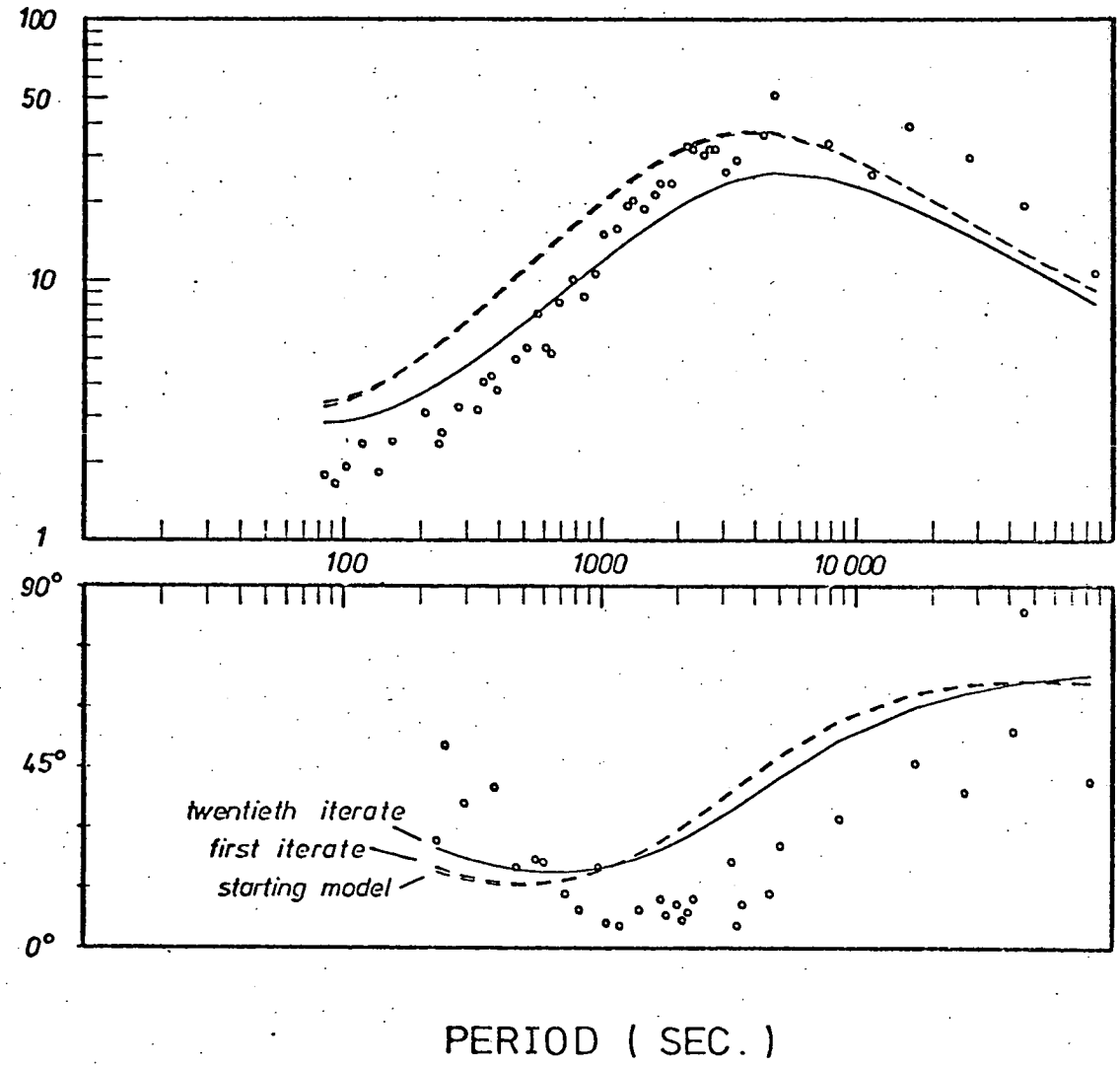
100
50
10
1
100
1000
10 000
90°
45°
0°
twentieth iterate
first iterate
starting model
PERIOD (SEC.)

FIG. 5-14 a

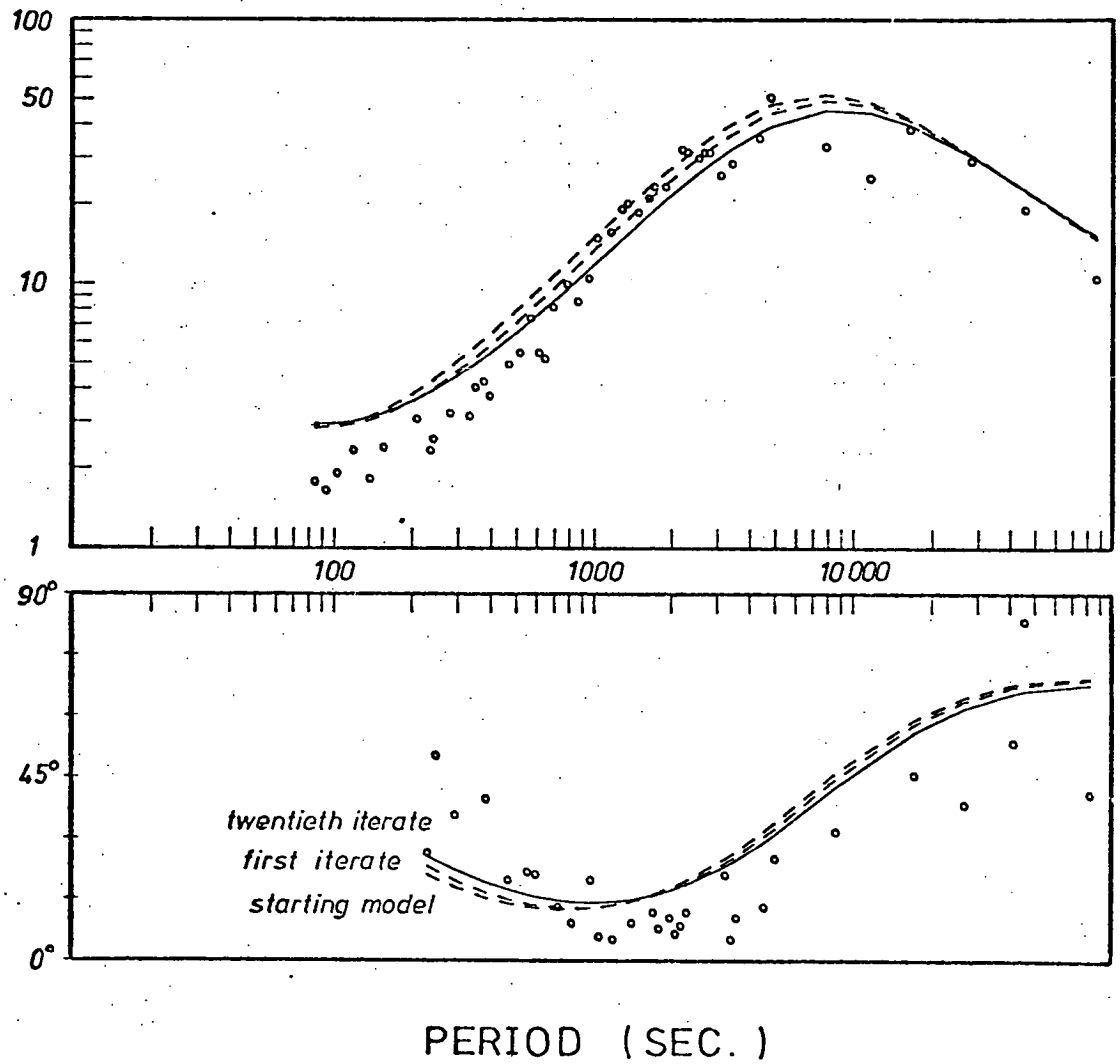
100
50
10
1
100
1000
10 000
90°
45°
0°
twentieth iterate
first iterate
starting model
PERIOD (SEC.)

FIG. 5-14 b

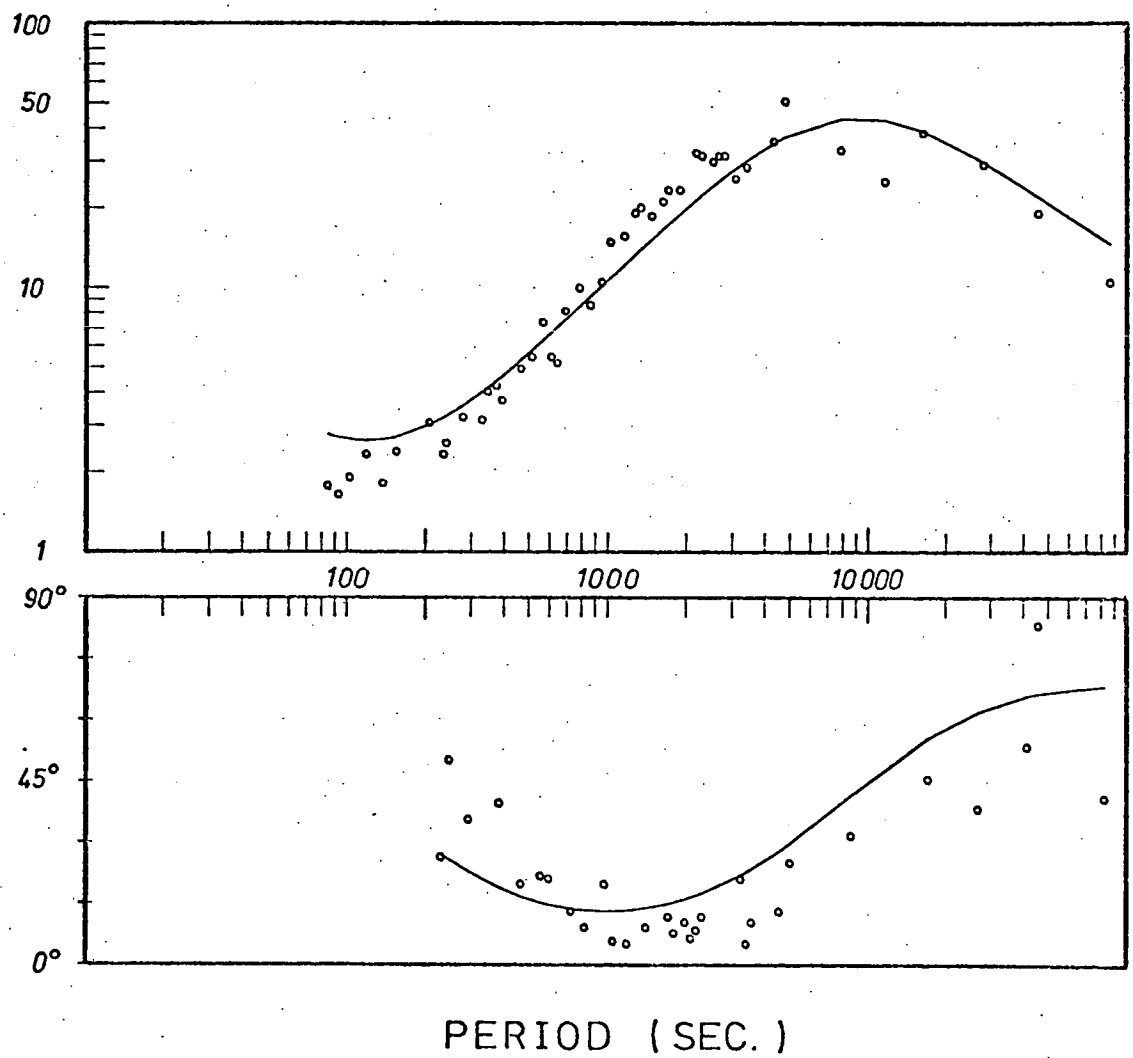

FIG. 5-14 c

$\sigma_5 = 0.6$) and depths $d_1 = 4$ km, $d_2 = 10$ km, $d_3 = 35$ km, and $d_4 = 300$ km. This model has clearly an intricate surface structure which one cannot expect the inclusion of phase information to resolve. The response due to this model is illustrated in Fig. 5-14c. In the single-valued response of Fig. 5-13, the phase data set is smaller than the amplitude data set. This will tend to weight the least-squares in favour of fitting the amplitude data -- especially as far as the higher frequencies are concerned. It would be interesting to know for this problem more phase estimates at higher frequency.

5.7 Concerning the Edgehog Procedure

Jackson (1973) has provided an additional systematic procedure for exploring a space of extremal acceptable solutions which may exist surrounding a particular acceptable solution. The procedure is really a method for displaying graphically some aspect of the non-uniqueness of an acceptable solution. Again, because the method depends upon a quasi-linear formulation of a non-linear situation, the range of models suggested by the method can not be exhaustive.

The 'Edgehog Method', as Jackson calls it, springs from the 'softness' implied by the truncation of (5.3.10) by excluding eigenvalues from the system of equations (5.3.4). The truncation associated with the exclusion

of eigenvalues is such as to reduce the model perturbations until the data residual becomes smaller than the previous data residual. To this end, all the perturbations δm_j are truncated simultaneously by each reduction in eigenvalue. For each perturbation

$$\delta\sigma_1 = \sum_{j=1}^{k} \gamma_j G_j^{(1)}$$

$$\delta\sigma_2 = \sum_{j=1}^{k} \gamma_j G_j^{(2)} \qquad (5.7.1)$$

$$\delta\sigma_3 = \sum_{j=1}^{k} \gamma_j G_j^{(2)}$$

etc.

the integer k is adjusted to satisfy the truncation criterion. This truncation may be described as 'soft' since it does not affect each perturbation in (5.7.1) individually, but in some collective sense. (The sense associated with our truncation differs from that of Jackson (1973)). After having found an acceptable solution by least-squares, one may ask whether one can hold fixed all the model parameters except one, say σ_n. Then one can proceed to <u>add</u> on perturbations

$$\delta\sigma_n = \sum_{j=k}^{k'} \gamma_j G_j^{(n)} \qquad (5.7.2)$$

where k' is made successively larger until the acceptable residual is exceeded. This supplies an extremal model

parameter σ_n^{extr}. Then one can proceed to subtract off from σ_n the perturbations (5.7.2) again until the acceptable data residual is exceeded. One can repeat the same procedure for each model parameter. An envelope can thus be constructed around the optimum model indicating some possible bounds within which each parameter (in isolation) can vary before the overall data residual exceeds its optimum value.

Although such a method can indicate something of the non-uniqueness of the inversion procedure, it cannot of course indicate models which are globally distinct from the optimum model which one is surrounding. Nevertheless it can give some idea of the parameters to which the data is most sensitive.

CHAPTER 6

RESOLUTION

6.1 Averaging Kernels

In Sections 1.6.b and 2.2.c we outlined the method of Backus and Gilbert for characterizing the space of $\mathcal{S}$-determinable models. In this present Chapter, we exclude the consideration of experimental error from the discussion and discuss the application of the Backus-Gilbert formalism to characterizing the space of acceptable conductivity models. Essentially, one tries to construct a local average of the model at some depth, z_0, by finding an optimum N-tuple $\{a_i\}$ such that the averaging kernel

$$A(z,z_0) = \sum_{i=1}^{N} a_i G_i(z)$$

resembles a Dirac delta-function centred at z_0. The quest for the optimum a_i's is posed as a problem of minimizing the spread as it is defined by equation (2.2.21). The minimization is subject to constraints, such as the unimodularity of $A(z,z_0)$. The optimal $\underline{a}$ (with N components $\{a_i\}$) is given by (2.2.27).

To calculate numerically the optimum $\underline{a}$ at each depth z_0 in a multilayered conductor, one must construct the system (2.2.26). One requires to evaluate the matrix $\underline{\underline{S}}$

with elements $S_{ij}(z_0)$ defined by (2.2.33). It can be seen that $\underline{\underline{S}}$ is expressible in terms of the three matrices $\underline{\underline{S}}^{(0)}$, $\underline{\underline{S}}^{(1)}$, and $\underline{\underline{S}}^{(2)}$ defined by (2.2.32). For the magnetotelluric amplitude data, $G_i(z) = \gamma_i^{-1} \mathcal{E}^2(z)$, and the elements of $\underline{\underline{S}}^{(0)}$ are given by

$$S_{ij}^{(0)} = \int_0^\infty \mathrm{Re}\left[G_i(z)\right] \quad \mathrm{Re}\left[G_j(z)\right] \quad dz$$

and of $\underline{\underline{S}}^{(1)}$ by

$$S_{ij}^{(1)} = \int_0^\infty z \ \mathrm{Re}\left[G_i(z)\right] \quad \mathrm{Re}\left[G_j(z)\right] \quad dz \qquad (6.1.1)$$

and of $\underline{\underline{S}}^{(2)}$ by

$$S_{ij}^{(2)} = \int_0^\infty z^2 \quad \mathrm{Re}\left[G_i(z)\right] \quad \mathrm{Re}\left[G_j(z)\right] \quad dz$$

For multilayered conductors, it is quite easy to divide up the interval of integration by layers. Since the integrals of

$$\int_0^\infty z^2 \, G_i G_j \, dz$$

are simply performed analytically, the elements of (6.1.2) can be easily determined analytically by using the simple expedient of such relationships as

$$\mathrm{Re}\, G_i(z) \ \mathrm{Re}\, G_j(z) = \tfrac{1}{4}\left[G_i G_j + G_i^* G_j^* + G_i^* G_j + G_i G_j^* \right]$$

where G_i and G_j represent the two complex Fréchet kernels,

and the asterisk denotes complex conjugates.

If an averaging kernel is indeed shaped like a delta function centred at z_0, the local average will strongly sample the model around z_0. If the kernel is broad and flat, the local average will represent a smeared average over a large expanse of the distribution. Formally the smallness of spread defined by (2.2.21) is used as a measure of the resolving power of the data. In fact, it is rather more convenient to regard spread along with the centre of the averaging kernel and its width as the parameters which characterize a $\mathcal{G}$-space of models. However, for purposes of illustration we generate a set of averaging kernels centred at depths $z_0 = 0$ km down to $z_0 = 15$ km. The half-space is uniformly conducting with conductivity $\sigma = 0.2$ ohm^{-1}m^{-1}. Ten periods are represented in the set of data; they lie in the range $5 \leq T \leq 120$ sec. This situation corresponds to some models described in Section 5.2. Fig. 6-1a illustrates a set of thirty averaging kernels corresponding to local averages to be associated with equi-spaced depths in the range $0 \leq z_0 \leq 15$ km. The data is amplitude data only. The flattening of the kernel is observed as depth increases -- this implies that the resolution declines with depth. Fig. 6-1b illustrates the same model situation, but considering only phase data. Of course one does not normally consider phase data on its own, and we include Fig. 6-1b for purposes of comparison. It will

be seen that the averaging kernels associated with phase data alone are really only delta-like near the surface. Fig. 6-1c shows the averaging kernels for a twenty-element set of phase and amplitude data. Incidentally, when making comparisons between Figs. 6-1a, 6-1b, and 6-1c, one should not compare the magnitudes of the amplitudes of the averaging kernels. These diagrams have been each normalized with respect to the maximum amplitude; thus one should only compare the shape of the kernels. In order to make a quantative comparison, we display in Fig. 6-2 the width of the kernels, the centre of the averaging kernels, and the spread of the averaging kernels associated with the Figures 6-1. The solid line indicates those characteristics for the twenty-point data set comprising amplitude and phase; the dashed line indicates the characteristics associated with phase alone; the dotted line the characteristics associated with amplitude alone. It is interesting to see that the inclusion of phase data significantly improves the spread at a depth less than 3 km. Even so, the spread does deteriorate at the surface, i.e. for $z < 3$ km. Since it was in this surface region where the models of Section 5.2 were parameterized, poor surface resolution resulted directly in the instability illustrated in Figs. 5-3 etc. Towards the surface the spread tends to increase to $\sim$20 km -- this implies a resolving length of 20 km exists in the upper 5 km of the Earth model!

FIG. 6-1 a Averaging kernel $A(z,z_0)$ for 10-dimensional set of error-free magnetotelluric amplitude data in the period range 5 sec $\leq T \leq$ 120 sec. The kernels are computed at 30 depths in the range $0 \leq z_0 \leq 15$ km for a homogeneous model $\sigma = 0.2$ ohm^{-1}m^{-1}. The curves are normalized with respect to maximum peak of the distribution.

FIG. 6-1 b Averaging kernel $A(z,z_0)$ for the same periods and model as in Fig. 6-1 a, except phase information alone is used. Again the curves are normalized with respect to maximum peak.

FIG. 6-1 c Averaging kernel $A(z,z_0)$ for a twenty-point set of data consisting of the ten amplitudes associated with Fig. 6-1 a and the ten phases of Fig. 6-1 b. The curves are normalized with respect to maximum peak.

FIG. 6-2 The three resolution characteristics associated with the kernels in Figs. 6-1 a, 6-1 b, and 6-1 c. These are the width of the kernel (defined by equations (2.2.29) and (2.2.31)), the centre of the distribution (defined by equation (2.2.30), and the spread (defined by equation (2.2.31)). The dotted line represents amplitude data only, the dashed line, phase data only; the solid line is the combination of phase and amplitude.

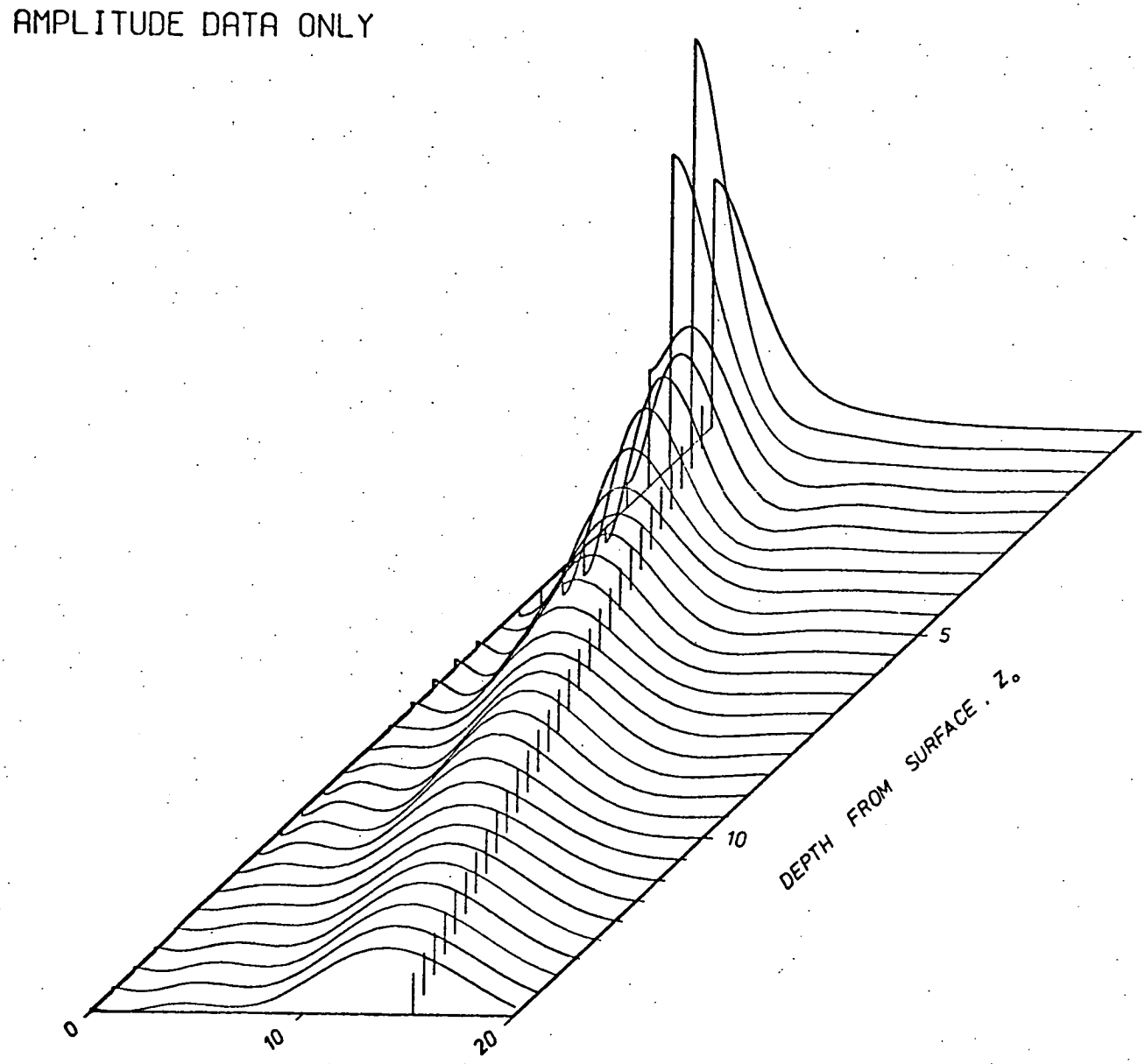

FIG. 6-1 a

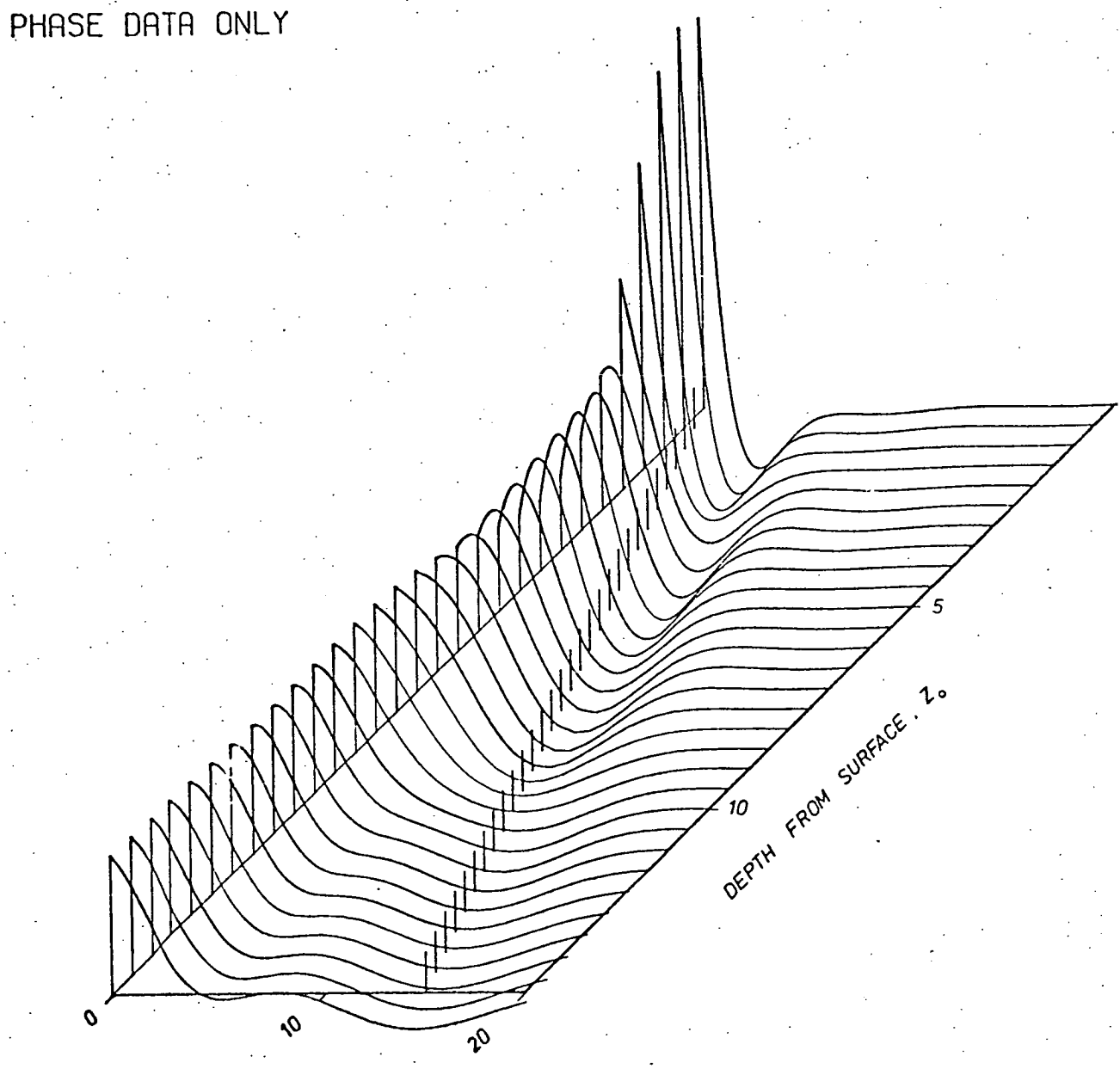

FIG. 6-1 b

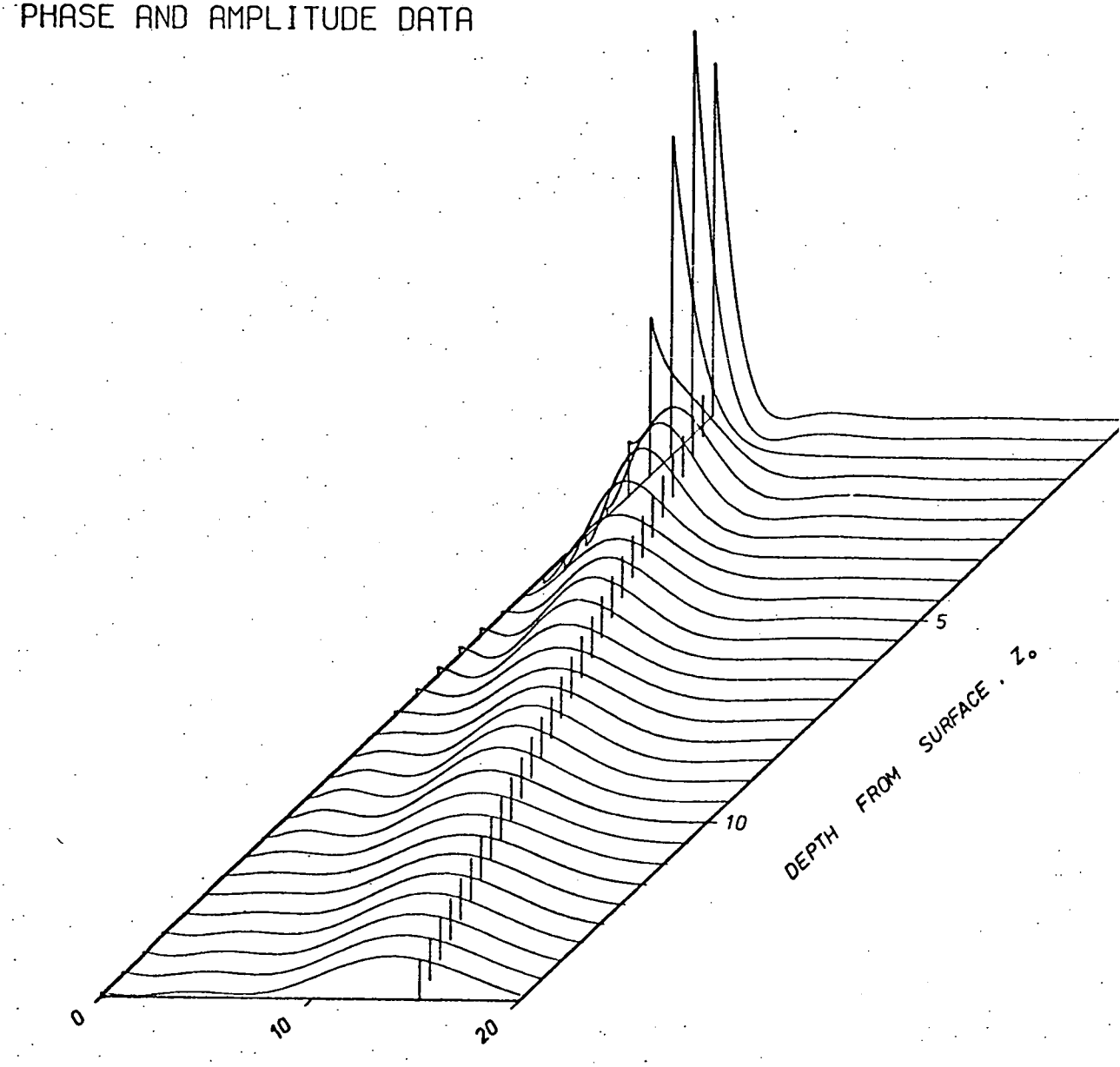

FIG. 6-1 c

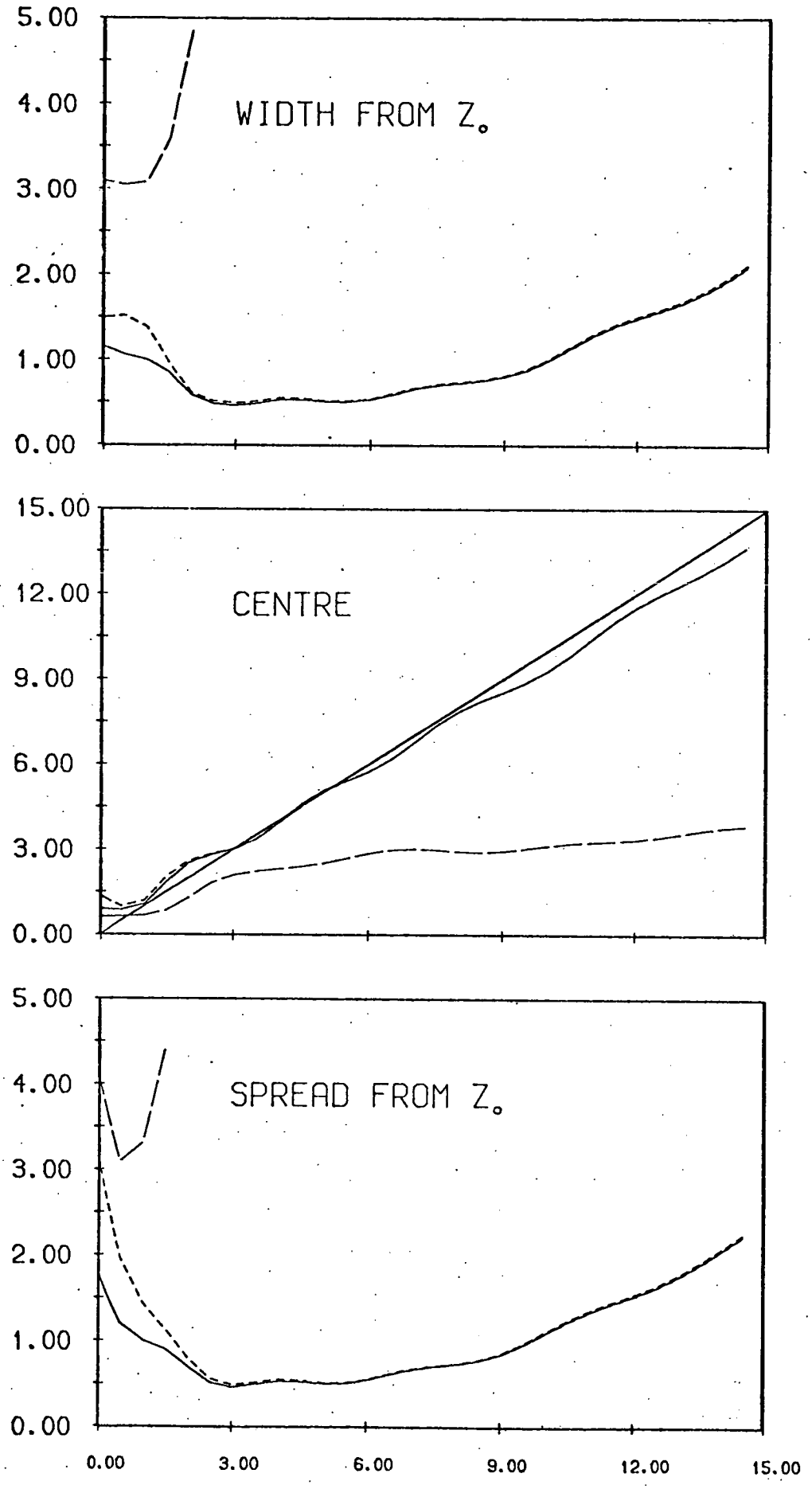
5.00
4.00
3.00
2.00
1.00
0.00
WIDTH FROM Z₀
15.00
12.00
9.00
6.00
3.00
0.00
CENTRE
5.00
4.00
3.00
2.00
1.00
0.00
SPREAD FROM Z₀
0.00
3.00
6.00
9.00
12.00
15.00
DEPTH, Z

FIG. 6-2

It should be noted that the value of the model local average is exactly the conductivity of the uniform conductor. This is a result of the unimodularity condition. The term q_i defined by equation (2.2.34), becomes for a uniform conductor

$$q_i = \sigma \int_0^\infty G_i(z)\, dz$$

and so the linear combination of q_i's are

$$\sum_i a_i q_i = \sigma \left\{ \int_0^\infty \sum_i a_i G_i(z)\, dz \right\}$$

but unimodularity implies the term in curly brackets is unity.

Fig. 6-3 illustrates thirty averaging kernels for a model that is slightly more interesting from a geophysical viewpoint. The model is of uniform conductivity 0.02 ohm^{-1}m^{-1}, and the period range is $10 \text{ sec} \leq T \leq 10000$ sec. The depths of the local averages range between $0 \leq z_0 \leq 90$ km. The resolution characteristics for this model are illustrated in Fig. 6-4. In Section 5.1 it was suggested that response data could be represented as real and imaginary parts of the complex impedance (or its reciprocal γ_i). It is interesting to view the resolution characteristics for the same model as that discussed for Fig. 6-4, but employing real and imaginary parts of the impedance rather than apparent resistivity and phase. Fig. 6-5 illustrates these characteristics:

FIG. 6-3 Averaging kernels for ten-dimensional set of error-free amplitude magnetotelluric data in the period range $10 \text{ sec} \leq T \leq 10^4 \text{ sec}$, at depths $0 \leq z_o \leq 90$ km into a conductor with $\sigma = 0.02 \text{ ohm}^{-1}\text{m}^{-1}$.

FIG. 6-4 Resolution characteristics for model and period range associated with Fig. 6-3. The solid line represents the characteristics associated with a twenty-point data set of phase and amplitude data; the dotted line is a ten-point set of amplitude data only; and the dashed line is the ten-point data set of phase only.

FIG. 6-5 Resolution characteristics for same model and period range associated with Figs. 6-3 and 6-4; however the data is now represented in terms of the real part of the complex impedance, Re γ_i, (the dotted line) and the imaginary part of γ_i (the dashed line), and the twenty-point data set consisting of both real and imaginary parts of γ_i.

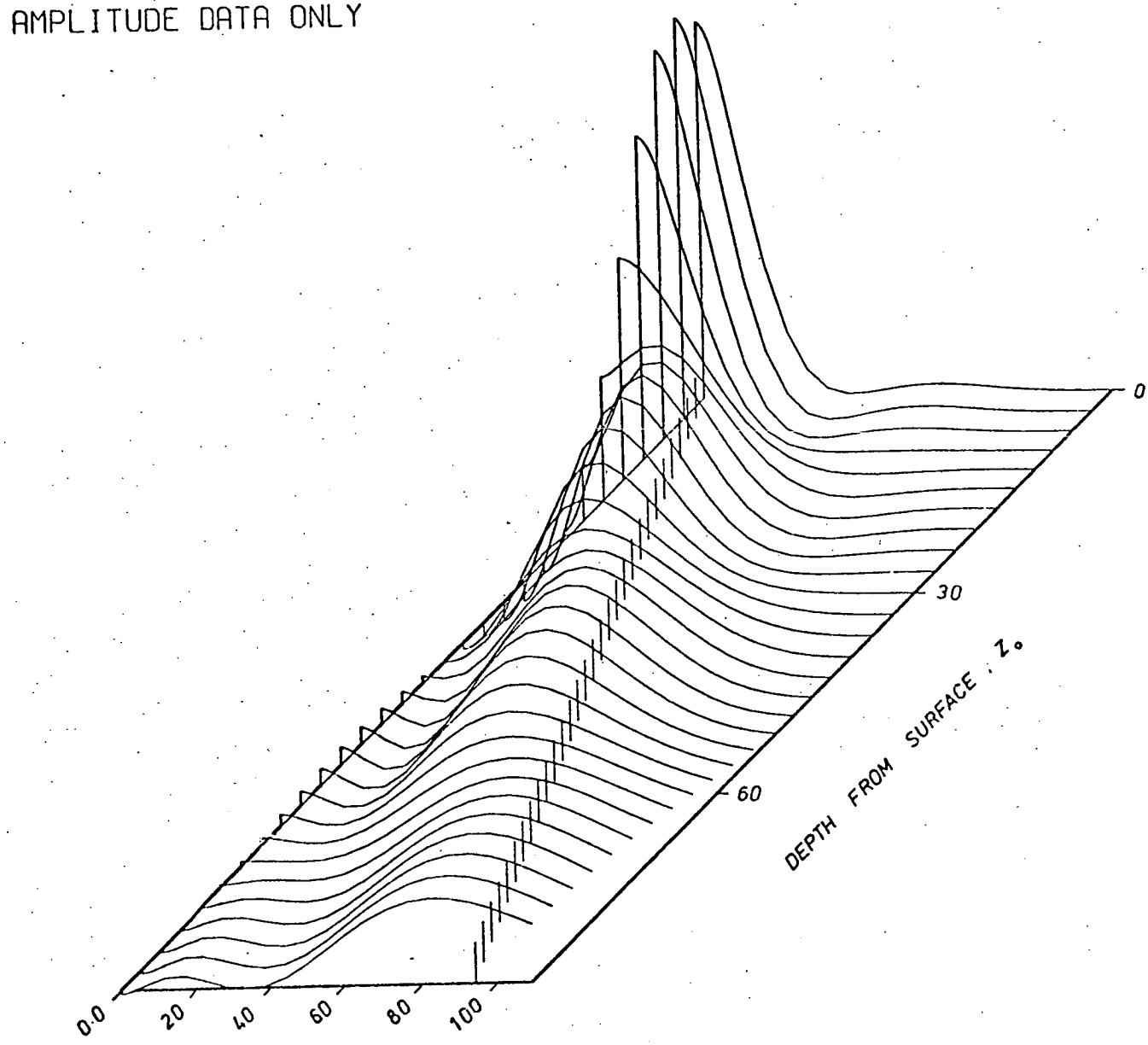
AMPLITUDE DATA ONLY
0.0
20
40
60
80
100
60
30
0
DEPTH FROM SURFACE , z.

FIG. 6-3

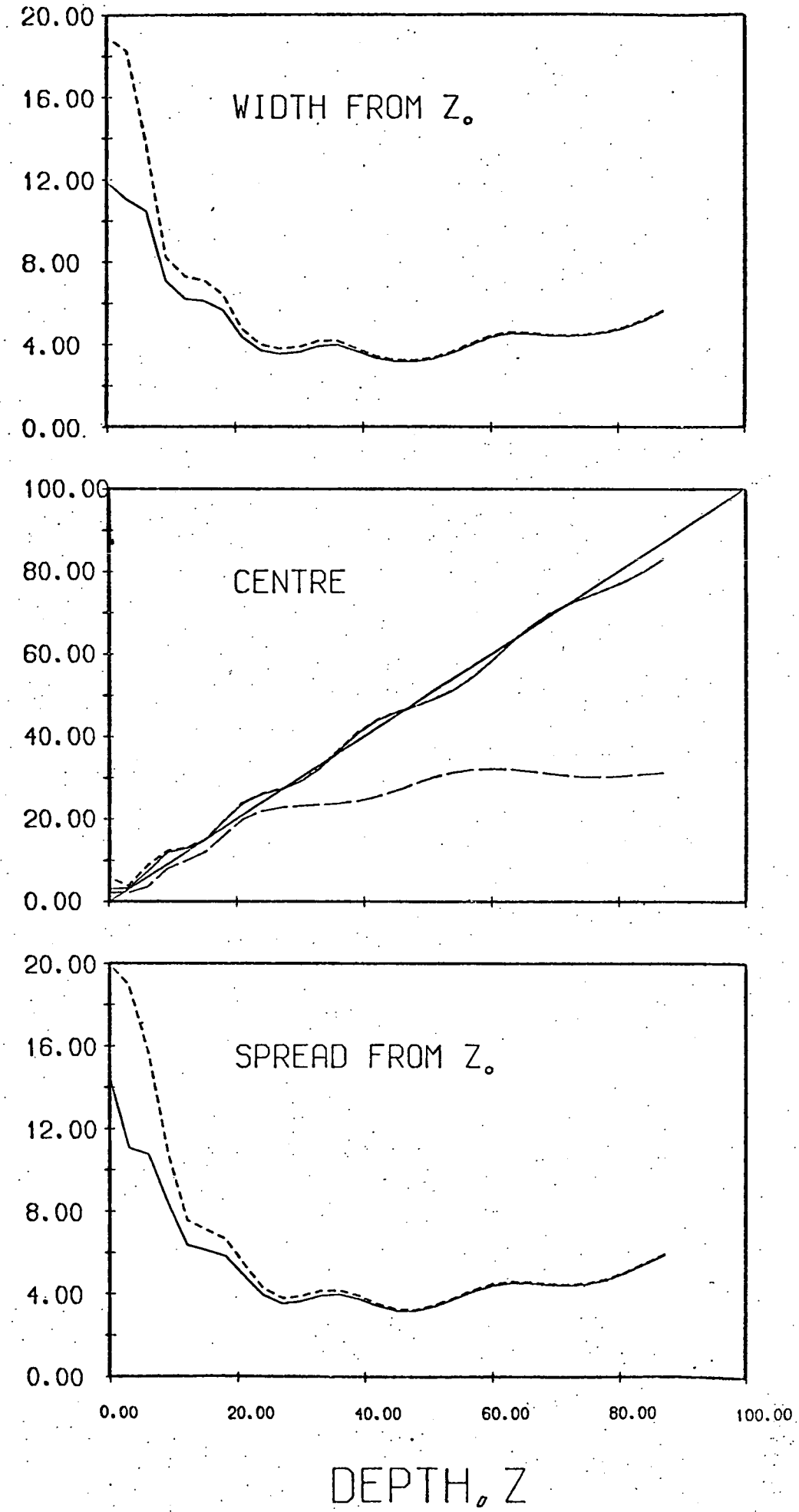
20.00
16.00
12.00
8.00
4.00
0.00
WIDTH FROM Z₀
100.00
80.00
60.00
40.00
20.00
0.00
CENTRE
20.00
16.00
12.00
8.00
4.00
0.00
SPREAD FROM Z₀
0.00
20.00
40.00
60.00
80.00
100.00
DEPTH, Z

FIG. 6-4

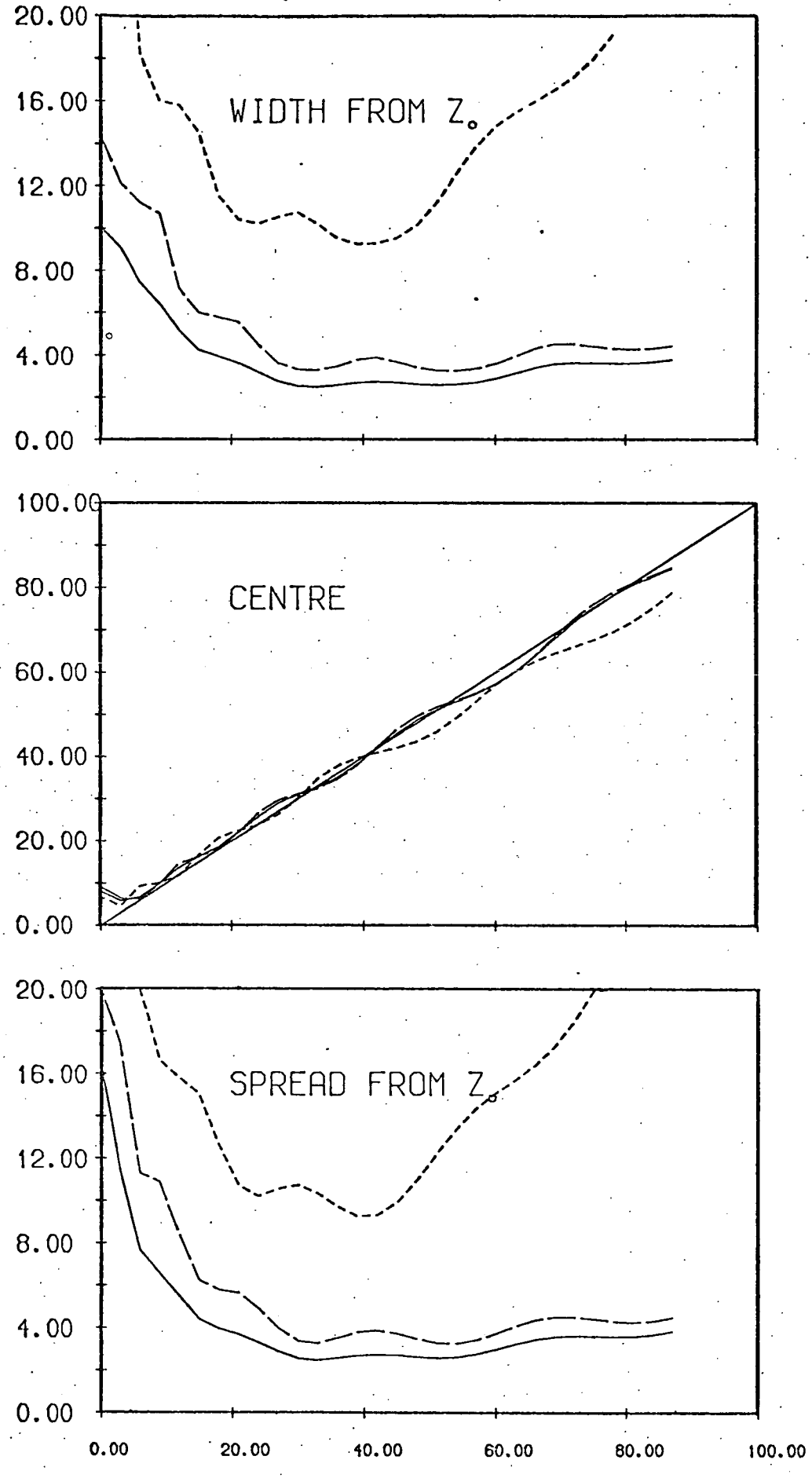
20.00
16.00
12.00
8.00
4.00
0.00
WIDTH FROM Z₀
100.00
80.00
60.00
40.00
20.00
0.00
CENTRE
20.00
16.00
12.00
8.00
4.00
0.00
SPREAD FROM Z₀
0.00
20.00
40.00
60.00
80.00
100.00
DEPTH, Z

FIG. 6-5

the dotted line represents the real part of the impedance, Re γ_i ; the imaginary part, Im γ_i , is represented by a dashed line; the solid line represents the combination of real and imaginary data sets. It can be seen that both real and imaginary parts of the impedance have associated with them a more equally-distributed resolution than was evident for amplitude and phase. One could deduce that there is less resolving power in the real part of γ_i than in the amplitude, $|\gamma_i|$, alone. It would seem that removing the imaginary part of the impedance from the data set $\{\text{Re } \gamma_i, \text{ Im } \gamma_i\}$, is a more significant omission than the exclusion of phase from the data set $\{|\gamma_i|, \arg \gamma_i\}$.

One should bear in mind that (at this stage) one is dealing with error-free data. One must consider too the possibility that differences in spread of a few kilometers need not reflect any significant difference when it comes to the real resolving power of data. It is only by considering error together with spread that a complete comparison is possible.

6.2 Resolution Characteristics

In Figs. 6-4 and 6-5, we presented the resolution characteristics for homogeneous conductors. From these diagrams, one observes relatively poor resolution at the surface and worsening resolution as depth increases. Between these two regions there lies a region of the model

which is relatively well resolved. This region probably corresponds to the 'centre of the current density distribution' which was defined in Section 1.5 (see equation (1.4.6)). The resolution characteristics associated with data represented in terms of the real and imaginary parts of the complex impedance were displayed by way of comparison. These characteristics tend to reinforce the usual preference for using amplitude data: in terms of resolution, amplitude data seems to have rather more resolving power than either real or imaginary parts of the impedance individually. Also, the contribution of phase data to the improved resolution of near-surface layers was observed. It should be remembered, from equation (2.2.3), that both the width of the kernel and the centredness of the delta-like function in relation to z_0 contribute to the spread. If the centre is severely displaced from z_0 then a meaningful model average cannot be constructed.

In this Section we look at the resolution characteristics of a few additional conductivity distributions. Of course, one must remember that these characteristics are dependent also on the range and quantity of the data. We shall confine ourselves still to data corresponding to ten periods.

Before embarking upon numerical illustration, it might be interesting to make a few order-of-magnitude arguments concerning the optimization associated with

achieving a good set of delta-like averaging kernels. The unimodularity condition (2.2.19) has rather clear implications for the N-tuple $\underline{a}$ since it implies

$$\underline{a} \cdot \underline{b} = 1 \tag{6.2.1}$$

where the components of $\underline{b}$ are defined by equation (2.2.25). For the induction problem specifically we have

$$b_i = \int_0^\infty G_i(z) \, dz \tag{6.2.2}$$

with Fréchet kernel given by

$$G_i(z) = \mathcal{E}^2(z)$$

which takes on the values

$$G_i(0) = 1$$

at the surface, and at depth

$$\lim_{z \to \infty} G_i(z) = 0$$

The kernel is a continuous function of depth with the appearance of an exponential attenuation from unity at the surface to zero as $z \to \infty$. If the conductivity of the half-space is relatively high, then the area under the function $G_i(z)$ will be correspondingly less since the normalized electric field $\mathcal{E}(z)$ will be attenuated more sharply with depth. This implies that the set $\{ b_i \}$ will contain smaller elements and, from the unimodularity condition, we can infer that the vector $\underline{a}$ must have a

larger value. If the conductivity of the half-space is relatively small, then the elements $\{b_i\}$ are large, and $\underline{a}$ is correspondingly small. Anticipating somewhat the discussion of Chapter 7, we can say immediately from the foregoing remarks that the model error is large if $\underline{a}$ is large (i.e. if the conductivity is large) since

$$\varepsilon^2 = \underline{a} \cdot \underline{\underline{E}} \cdot \underline{a}$$

and the model error becomes smaller if $\underline{a}$ is smaller. One must recall that $\underline{\underline{E}}$ is determined by experimental error exclusively. As for the spread

$$s = \underline{a} \cdot \underline{\underline{S}} \cdot \underline{a}$$

one must expect $\underline{\underline{S}}$ to be rather smaller (although $\underline{a}$ is larger) for a good conductor. Numerically (as we have seen) the spread becomes smaller as the conductivity increases.

It may be interesting to contemplate the effect a very highly conducting embedded layer might have on an attempt to find a delta-like averaging function. From equation (2.2.21), we recall that we are trying to minimize the area under $A(z,z_0)$ away from $z = z_0$. If a very good conductor is embedded in a half-space, at depth z_s say, the structure of $\mathcal{E}$ is that of a function swiftly attenuated in this layer. (In the region below the conducting slab fields may be induced by the secondary currents in the slab.) Anyway, at a very good thin conducting slab we may expect $\mathcal{E}(z_s) \approx 0$. This poses

some problem for the optimization that we are trying to undertake, since the procedure of Section 2.2.c will tend to minimize the area under $A(z,z_0)$ away from $z = z_0$, and effectively away from $z = z_s$. Thus the presence of a good conducting slab can introduce an additional 'spike' to the averaging kernel (i.e. at $z = z_s$) which makes the resolution very good at $z_0 = z_s$ but rather poor for $z_0 \neq z_s$. This results from the increasing displacement of the centre of the delta-like averaging function (which is not in fact very delta-like under the circumstances) as $|z_0 - z_s|$ becomes larger.

In Fig. 6-6a and Fig. 6-6b, we investigate a model with monotonically increasing conductivity: namely $\underline{\sigma}$: ($\sigma_1 = 0.002$, $\sigma_2 = 0.004$, $\sigma_3 = 0.01$, $\sigma_4 = 0.05$, $\sigma_5 = 0.08$ ohm^{-1}m^{-1}) with depths $d_1 = 10$, $d_2 = 20$, $d_3 = 30$, and $d_4 = 60$ km. Then periods are chosen in the range 50 sec $\leq T \leq$ 10,000 sec. One can see that for both data representations the spread is significantly less than the previous examples. One must remember that the model error of this very small spread might be unacceptably high. Again it is seen that the spread is relatively poor at the surface. Adding phase to the amplitude data does not seem to make much improvement. The departure of the centre of the distribution away from z_0 near the surface (i.e. $z_0 < 20$ km) implies that reliable model averages cannot be constructed at these shallow depths. In this example, complex impedance

FIG. 6-6 a Resolution characteristics associated with a model $\underset{\sim}{\sigma}$: ($\sigma_1 = 0.002$, $\sigma_2 = 0.004$, $\sigma_3 = 0.01$, $\sigma_4 = 0.05$, $\sigma_5 = 0.08$) with depths $d_1 = 10$, $d_2 = 20$, $d_3 = 30$, $d_4 = 60$ km, and (phase/amplitude) data for 10 periods in the range 50 sec $\leq T \leq 10^4$ sec. The solid line represents combined phase and amplitude data, the dotted line amplitude data alone; the dashed line is phase data alone.

FIG. 6-6 b Resolution characteristics associated with model and periods of Fig. 6-6 a. The data is represented as real and imaginary parts of γ_i . The solid line represents the characteristics for twenty-point data set of real and imaginary parts of γ_i ; the dotted line is for Re γ_i, and the dashed line for Im γ_i .

FIG. 6-7 a Resolution characteristics for model 'A' in Table 5.1 for ten periods in the range 50 sec $\leq T \leq 10^4$ sec. The solid line represents phase + amplitude data; the dotted line represents amplitude data alone; the dashed line represents phase alone.

FIG. 6-7 b The same model and periods as Fig. 6-7 a. The solid line represents the resolution characteristics associated with real + imaginary parts of γ_i; the dotted line with Re γ_i; the dashed line with Im γ_i .

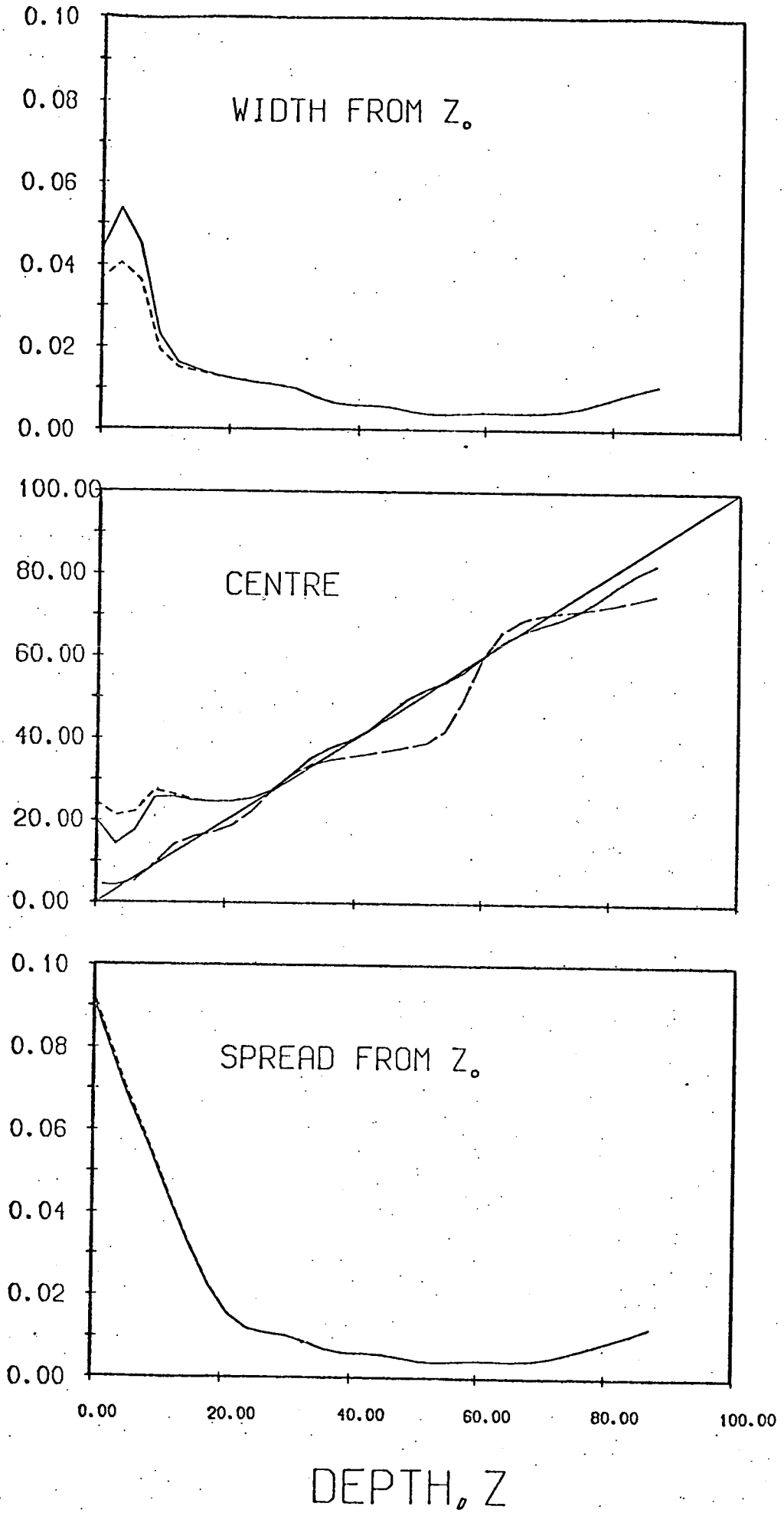
0.10
0.08
0.06
0.04
0.02
0.00
WIDTH FROM Z_o
100.00
80.00
60.00
40.00
20.00
0.00
CENTRE
0.10
0.08
0.06
0.04
0.02
0.00
SPREAD FROM Z_o
0.00
20.00
40.00
60.00
80.00
100.00
DEPTH, Z

FIG. 6-6 a

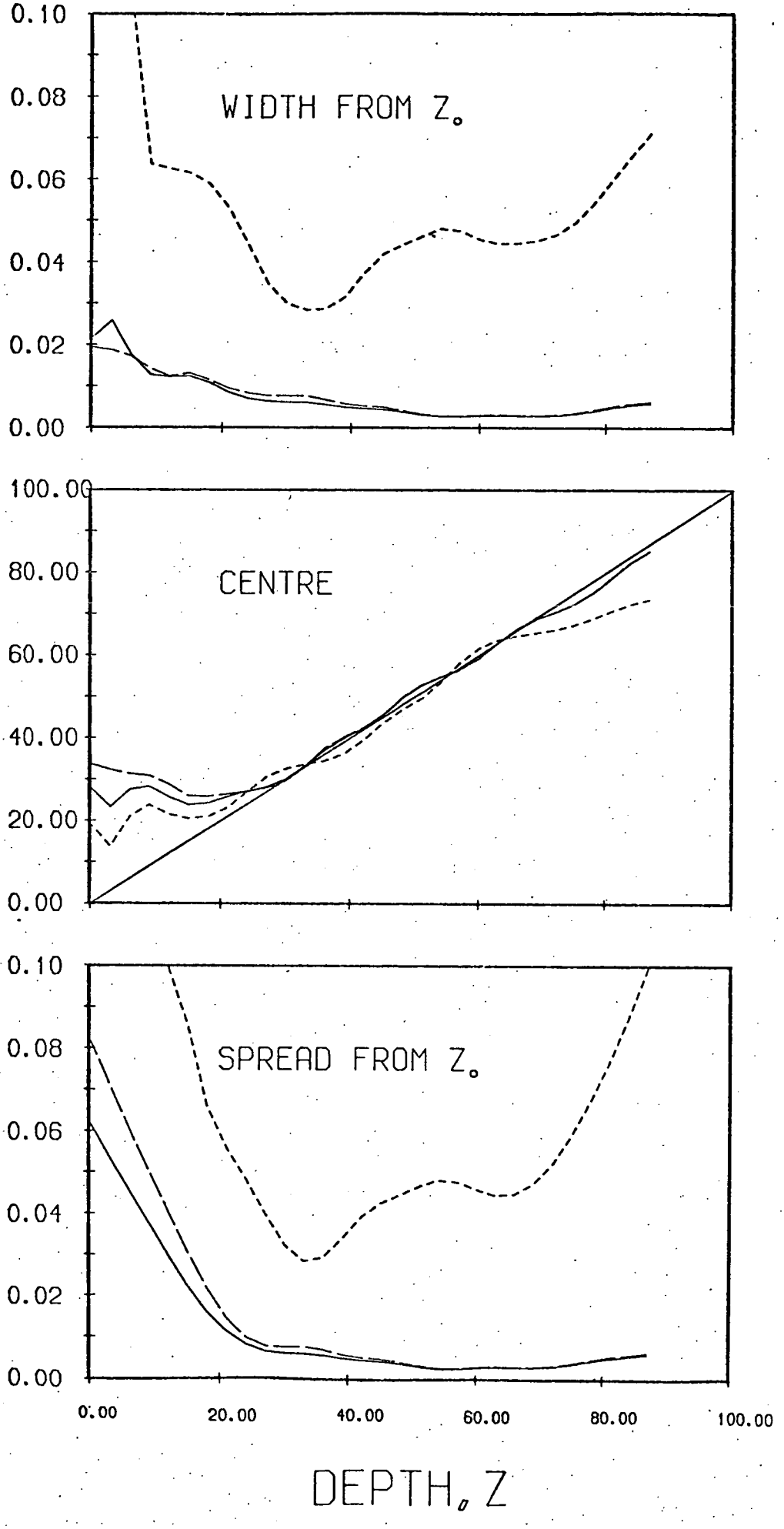
0.10
0.08
0.06
0.04
0.02
0.00
WIDTH FROM Z₀
100.00
80.00
60.00
40.00
20.00
0.00
CENTRE
0.10
0.08
0.06
0.04
0.02
0.00
SPREAD FROM Z₀
0.00
20.00
40.00
60.00
80.00
100.00
DEPTH, Z

FIG. 6-6 b

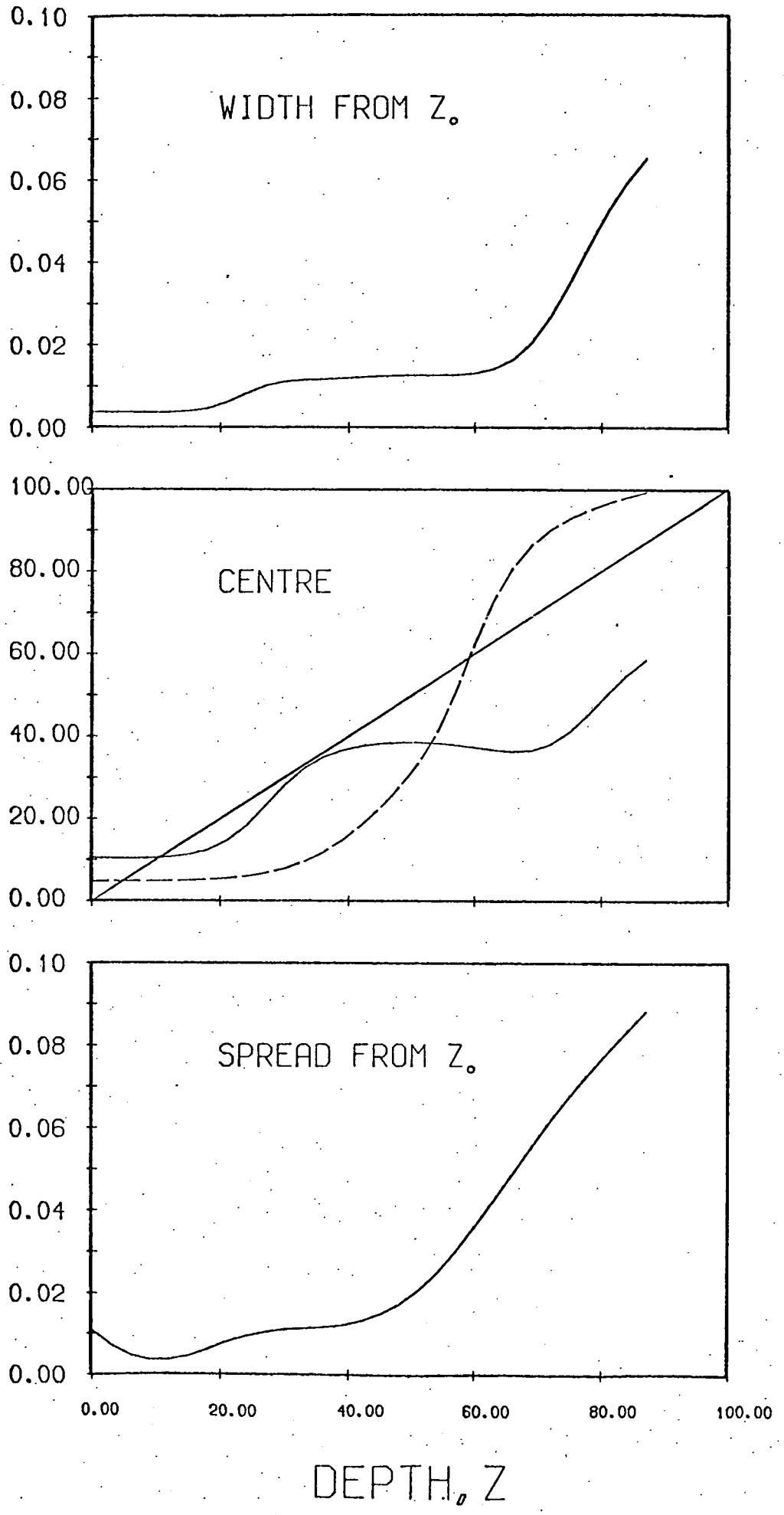
0.10
0.08
0.06
0.04
0.02
0.00
WIDTH FROM Z_o
100.00
80.00
60.00
40.00
20.00
0.00
CENTRE
0.10
0.08
0.06
0.04
0.02
0.00
SPREAD FROM Z_o
0.00
20.00
40.00
60.00
80.00
100.00
DEPTH, Z

FIG. 6-7 a

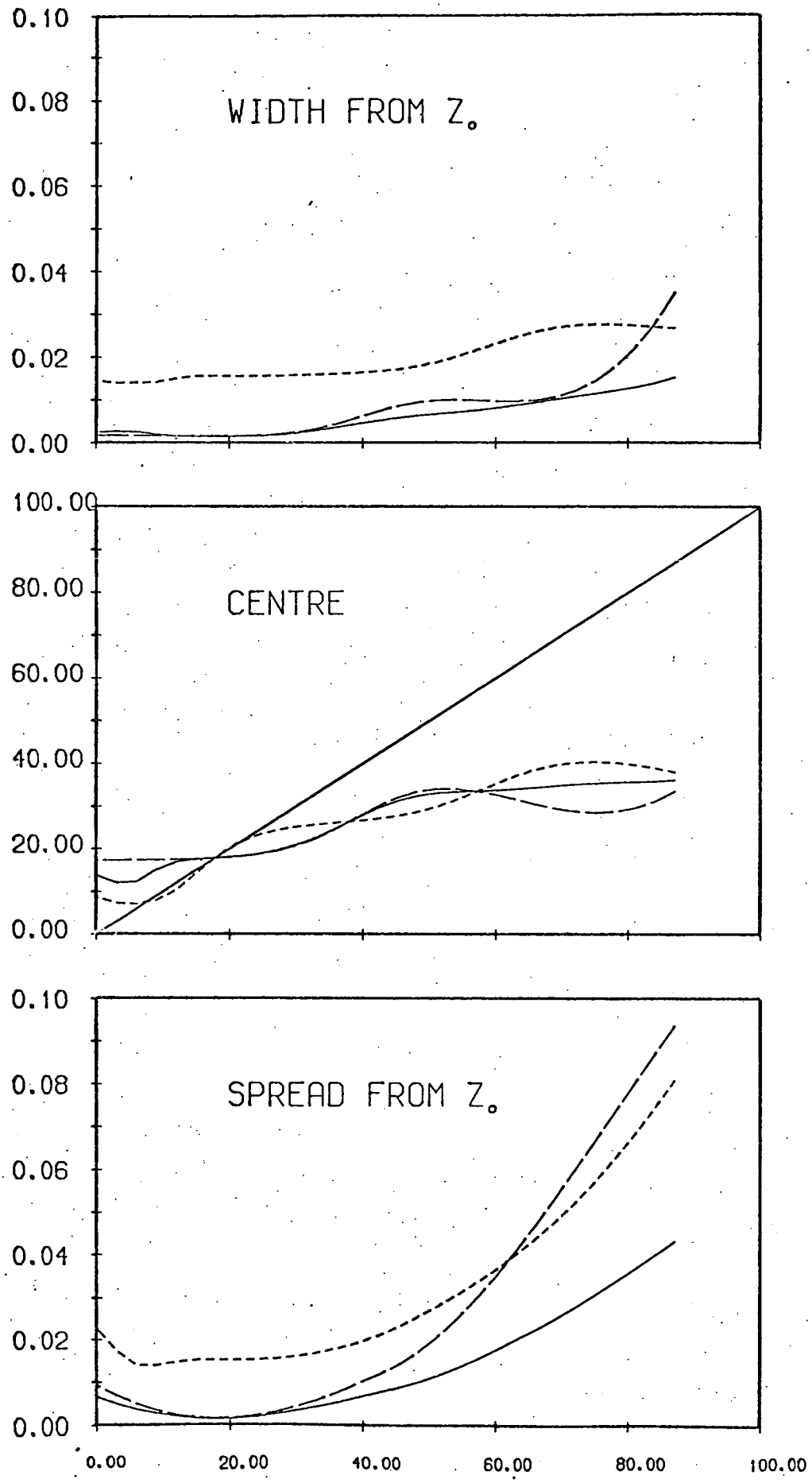
WIDTH FROM Z_o
0.10
0.08
0.06
0.04
0.02
0.00
CENTRE
100.00
80.00
60.00
40.00
20.00
0.00
SPREAD FROM Z_o
0.10
0.08
0.06
0.04
0.02
0.00
0.00
20.00
40.00
60.00
80.00
100.00
DEPTH, Z

(i.e. the twenty data points composed of the real and imaginary parts of the impedance) and apparent resistivity (i.e. the ten amplitude data points) seem to yield the same resolution characteristics.

In Fig. 6-7a and 6-7b, we investigate the model A illustrated in Fig. 5-8b. The data again reflects ten periods in the range 50 sec $\leq T \leq$ 10,000 sec. We may recall that this model has a relatively good conductor embedded at a depth more than 30 km. It is seen from Fig. 6-7b that a deterioration in the centre of the distribution occurs at $\sim$25 km, with a corresponding deterioration in resolution (i.e. an increase in spread). This sudden falling off of resolution is also observed in the amplitude/phase resolution characteristics, although it seems in this case to result from an increase in width for $z_0 > 60$ km, as well as the centre being displaced. One could infer from this that conductivity structure below 30 km is not well resolved from the data. The width and spread for phase data on its own are off the scale of Fig. 6-7a.

Fig. 6-8a and Fig. 6-8b illustrate the resolution characteristics for the model $\underline{\sigma}$: ($\sigma_1 = 0.2$, $\sigma_2 = 0.02$, $\sigma_3 = 0.01$, $\sigma_4 = 0.005$, $\sigma_5 = 0.3$ ohm^{-1}m^{-1}) with depths $d_1 = 1$ km, $d_2 = 20$, $d_3 = 30$, and $d_4 = 300$ km. This model rather resembles the models considered in Section 5.6. Fig. 6-8a illustrates the characteristics for data represented as amplitude and phase. We can make the

following observations:

1. Phase improves resolution near the surface ($z_0 < 20$ km).

2. In the region of poor conductivity (20 km $< z_0 <$ 300 km) the centre of the distribution is displaced from z_0. Thus a local average cannot be constructed at these depths. In this region the spread reaches a maximum.

3. At depth ($z_0 >$ 300 km) the distribution centre is restored to proximity with z_0. The resolution is correspondingly improved.

Although the resolution is very small (especially considering one is discussing conductivity at 300 km depth!), the corresponding model error is probably very large. We can summarize this situation as follows: a good conductor at depth has very good resolution length associated with it, although the value of the conductivity at that depth is very uncertain. On the other hand, the conductivity in the less well conducting region exhibits poor resolution, and the depth structure of the conductor is poorly determined. However, the actual conductivity magnitude at these depths has less uncertainty associated with it.

Fig. 6-8b shows the resolution characteristics for

FIG. 6-8 a Resolution characteristics associated with the model $\underset{\sim}{\sigma}$: ($\sigma_1 = 0.02$, $\sigma_2 = 0.02$, $\sigma_3 = 0.01$, $\sigma_4 = 0.005$, $\sigma_5 = 0.3$) at depths $d_1 = 1$ km, $d_2 = 20$, $d_3 = 30$, $d_4 = 300$ km. The period range of the ten data points $\{\gamma_i\}$ is again 50 sec $\leq T \leq 10^4$ sec. The solid line represents phase + amplitude data; the dotted line, amplitude data alone; the dashed line phase data alone.

FIG. 6-8 b The same model and periods as discussed in Fig. 6-8 a. The solid line represents the resolution characteristics associated with real + imaginary parts of γ_i ; the dotted lines with Re γ_i ; and the dashed lines with Im γ_i .

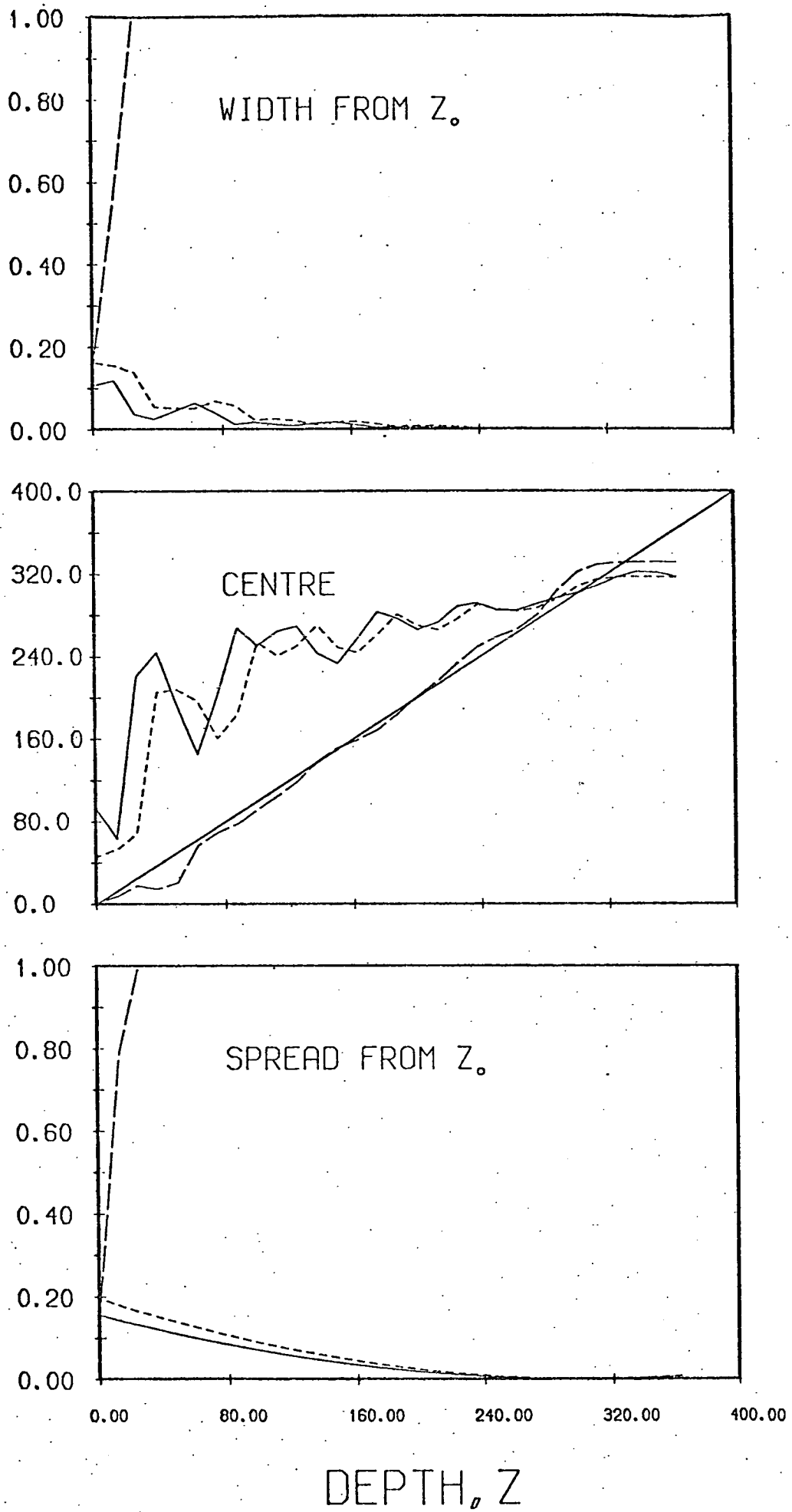
1.00
0.80
0.60
0.40
0.20
0.00
WIDTH FROM Z₀
400.0
320.0
240.0
160.0
80.0
0.0
CENTRE
1.00
0.80
0.60
0.40
0.20
0.00
SPREAD FROM Z₀
0.00
80.00
160.00
240.00
320.00
400.00
DEPTH, Z

FIG. 6-8 a

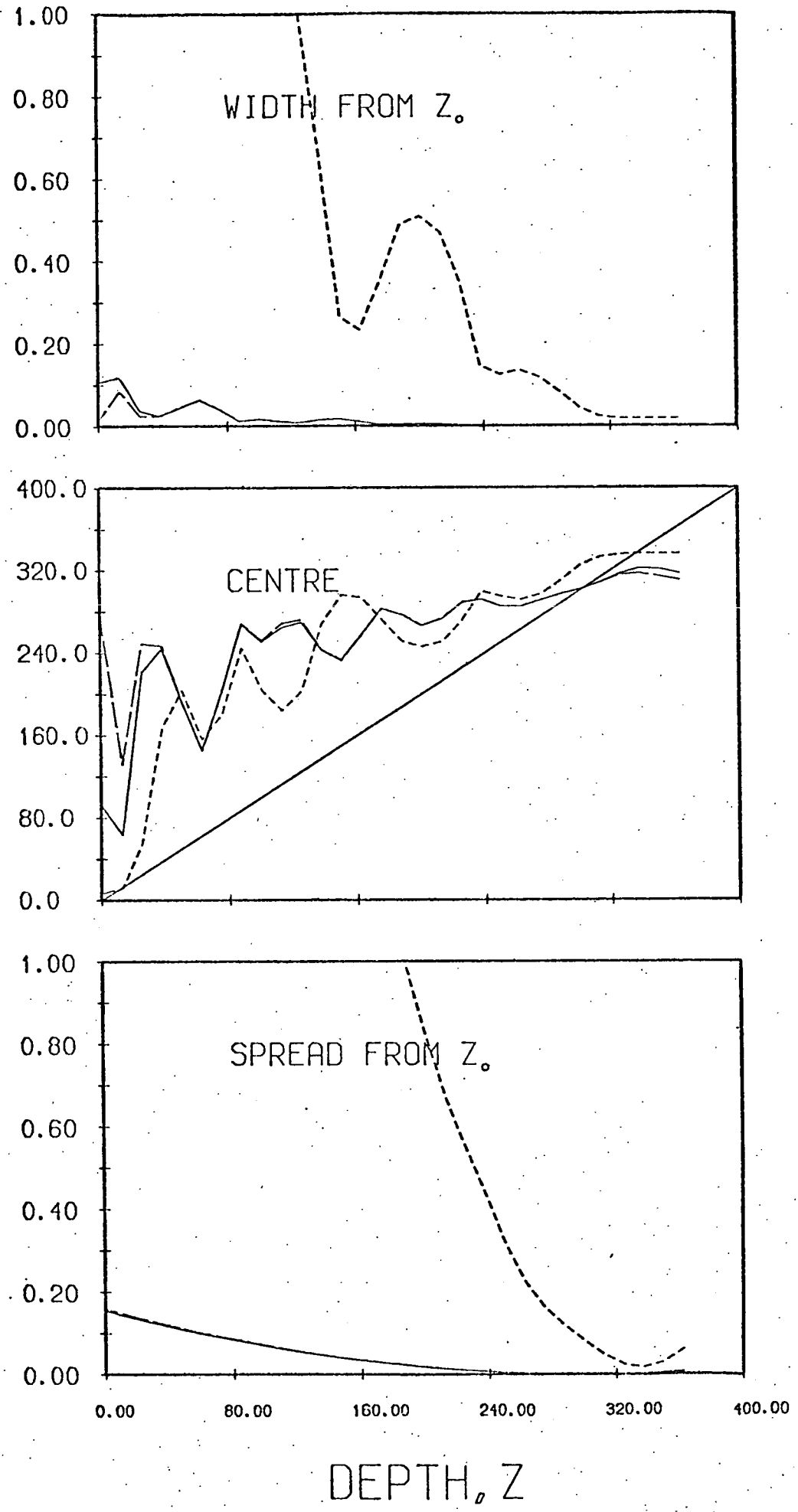
1.00
0.80
0.60
0.40
0.20
0.00
WIDTH FROM Z₀
400.0
320.0
240.0
160.0
80.0
0.0
CENTRE
1.00
0.80
0.60
0.40
0.20
0.00
SPREAD FROM Z₀
0.00
80.00
160.00
240.00
320.00
400.00
DEPTH, Z

FIG. 6-8 b

the data represented as a complex impedance.

6.3 Rotating $\underline{\underline{S}}$ into Principal Axes

In Section 2.2,e it was suggested that the search for an optimal averaging kernel can be made more simple by diagonalizing the spread matrix $\underline{\underline{S}}$. This diagonalization is accomplished with the same similarity transformation which has been described in Section 5.3. In particular, one transforms $\underline{\underline{S}}$ by

$$\underline{\underline{A}}\ \underline{\underline{S}}'\ \underline{\underline{A}}^{T} = \underline{\underline{S}} \qquad (6.3.1)$$

where $\underline{\underline{S}}'$ is diagonal. If the columns of $\underline{\underline{A}}$ contain the eigenvectors of $\underline{\underline{S}}$, then the diagonal elements of $\underline{\underline{S}}'$ will consist of its corresponding eigenvalues. By organizing these in descending order of magnitude, one can isolate the near-zero eigenvalues towards the bottom right hand corner of $\underline{\underline{S}}'$. If $\underline{\underline{S}}$ is nearly singular the prospect for finding the N x N inverse $\underline{\underline{S}}^{-1}$ may not be encouraging; however, by the rotation of $\underline{\underline{S}}$ into $\underline{\underline{S}}'$, one may be able to find a delta-like averaging kernel from a subset of the N-tuple $\{G_i'(z)\}$ corresponding to the suitably large eigenvalues of $\underline{\underline{S}}$. Thus we seek an averaging kernel

$$A(z,z_0) = \sum_{i=1}^{k} a_i'\ G_i'(z)\ , \qquad k < N \qquad (6.3.2)$$

where $\{a_i\}$ is determined from the equations

$$\underline{\underline{S}}' \quad \underline{a}' = \lambda' \quad \underline{b}'$$
$$\underline{a}' \cdot \underline{b}' = 1 \qquad (6.3.3)$$

where

$$\underline{b}' = \int_0^\infty G_i'(z) \, dz$$

and

$$\underline{G}'(z) = \underline{\underline{A}}^T \underline{G}(z)$$

Note λ' in equation (6.3.3) is the Lagrange multiplier, not to be confused with the (subscripted) λ_i which has been used previously to denote the ith eigenvalue of a matrix.

We illustrate the rotation by constructing an averaging kernel for a set of data generated by a homogeneous model with $\sigma = 0.6$ ohm^{-1}m^{-1} for a range of periods: 10 sec $< T <$ 100 sec. Upon the transformation (6.3.1) we isolate the ten eigenvalues $\{\lambda_i\}$ and rank them in descending order of magnitude. In Fig. 6-9, the uppermost curve represents the averaging kernel constructed out of the transformed Fréchet kernel corresponding to the first (and hence the largest) such eigenvalue. Since $k = 1$, there is only one element in the sum (6.3.2) and thus a delta-like kernel cannot be constructed. In the next lower diagram, the first two eigenvalues are included in the matrix $\underline{\underline{S}}'$, and an optimum kernel is constructed out of $G_1'(z)$ and $G_2'(z)$. In each

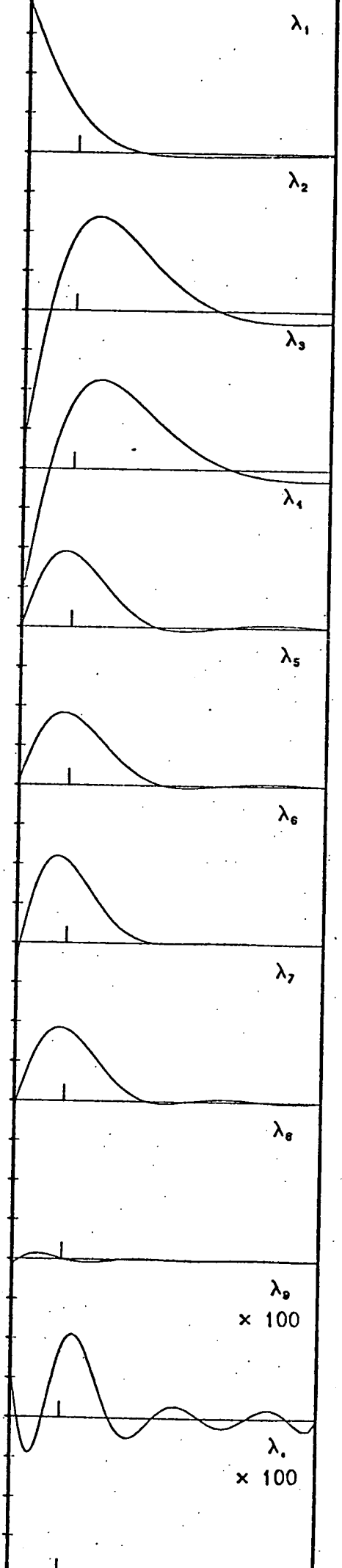

FIG. 6-9 The averaging kernels generated from increasing numbers of eigenvalues; the first frame consists of one eigenvalue, λ_1, the second of two, $\lambda_1 + \lambda_2$, the third of three, $\lambda_1 + \lambda_2 + \lambda_3$, etc. The eigenvalues have been ranked so that

$$\lambda_1 > \lambda_2 > \lambda_3 > \cdots > \lambda_{10}.$$

subsequent diagram the number of eigenvalues is increased by one over the previous. It can be seen that the delta-ness seems to improve. However when the eighth eigenvalue is included the delta-ness deteriorates. We may surmise that a meaningful inverse $\underline{\underline{S}}^{-1}$ cannot be constructed when the very small λ_k (when $k > 8$), are included in the matrix $\underline{\underline{S}}$. In these situations the optimization is not successful.

CHAPTER 7

EXPERIMENTAL ERROR

7.1 Absolute Error

The matter of incorporating the experimental error of a data set into the characterization of the space of $\mathcal{G}$-acceptable solutions was discussed in Section 2.2.d. Backus and Gilbert (1970) show in some detail how the error of surface data can directly contribute to the range of non-uniqueness of this space. In the case where one is considering absolute error, a fourth resolution characteristic is introduced in addition to the characteristics of spread, width, and centre which have already been introduced. This fourth characteristic is called the error of the model estimate and is denoted by $\mathcal{E}$. It is defined by equation (2.2.38). To include error, one needs to extend the optimization of spread (subject to the constraint of unimodularity) to the dual optimization of spread together with error (both subject to the unimodularity condition). Using the notation of Section 2.2, one wishes to find a N-tuple, $\underline{a}$, such that the following constraint is satisfied

$$\underline{a} \cdot \underline{\underline{S}} \cdot \underline{a} \leq s_t \qquad (7.1.1)$$

where s_t is some spread which is deemed acceptable. Accepting this constraint, we can proceed to minimize

the error

$$\varepsilon^2 = \underline{a} \cdot \underline{\underline{E}} \cdot \underline{a} \qquad (7.1.2)$$

subject also to the constraint of unimodularity. Alternatively, and equivalently, the problem can be posed as one of minimizing

$$s = \underline{a} \cdot \underline{\underline{S}} \cdot \underline{a}$$

subject to the constraint of unimodularity and

$$\underline{a} \cdot \underline{\underline{E}} \cdot \underline{a} \leq \varepsilon_t^2$$

where ε_t is some acceptable level of error in the model parameter.

If one considers (somewhat artificially) the case where $N = 3$, then (7.1.1) and (7.1.2) assume a significance in terms of three-dimensional geometry. In this way we may visualize the geometry of the N-dimensional problem. The space of $\underline{a}$ values satisfying the inequality

$$\underline{a} \cdot \underline{\underline{K}} \cdot \underline{a} \leq k \qquad (7.1.3)$$

where $\underline{\underline{K}}$ is any N dimensional operator and k is a scalar, constitutes a solid N-dimensional ellipsoid centred at the origin ($\underline{a} = 0$). The boundary of this ellipsoid is the surface

$$\underline{a} \cdot \underline{\underline{K}} \cdot \underline{a} = k$$

The normal (with respect to $\underline{a}$) out of this boundary is $\underline{\underline{K}} \cdot \underline{a}$. Backus and Gilbert show that, if $\underline{\underline{K}}$ is symmetric

and positive definite, then the ellipsoid is strictly convex and a straight line joining any two $\underline{a}$'s in the ellipsoid is itself confined to the ellipsoid.

In addition to this ellipsoid, one can construct an N - 1 dimensional plane defined by the condition

$$\underline{f} \cdot \underline{a} = 1 \qquad (7.1.4)$$

for any N dimensional vector $\underline{f}$. The problem discussed in the previous Chapter can now be restated as one of finding the set-intersection associated with an ellipsoid like (7.1.3) and a plane such as (7.1.4). In fact the ellipsoid is defined by

$$\underline{a} \cdot \underline{\underline{S}} \cdot \underline{a} \leq s_{min} \qquad (7.1.5)$$

and the plane is the unimodularity condition

$$\underline{a} \cdot \underline{b} = 1 \qquad (7.1.6)$$

One can imagine a very small ellipsoid associated with $s < s_{min}$, such that the ellipsoid and plane do not intersect at all. Gradually expanding the ellipsoid by increasing s, one eventually hopes to find a vector $\underline{a}$ such that the ellipsoid and the plane (7.1.6) are in contact at a single point of tangency. This is the minimum spread, s_{min}; the associate N-tuple is denoted as $\underline{a}_S$, and is given by

$$\underline{a}_S = \underline{\underline{S}}^{-1} \cdot \underline{b} \; / \; \underline{b} \cdot \underline{\underline{S}}^{-1} \cdot \underline{b} \qquad (7.1.7)$$

i.e. equation (2.2.27). The minimum spread is $s_{min} = \underline{a}_S \cdot \underline{\underline{S}} \cdot \underline{a}_S$. One can continue to increase the

ellipsoid so that its set-intersection with plane (7.1.6) consists of an increasingly larger number of elements $\underline{a}$. The situation is illustrated in Fig. 7-1.

One can consider the optimization of error (without regard to spread) in an entirely equivalent manner. In this case one seeks to find the intersection between the ellipsoid

$$\underline{a} \cdot \underline{\underline{E}} \cdot \underline{a} \leq \varepsilon_t^2$$

and the plane (7.1.6). The minimal error is given by

$$\begin{aligned} \varepsilon^2_{min} &= \underline{a}_E \cdot \underline{\underline{E}} \cdot \underline{a}_E \\ &= 1 \; / \; \underline{b} \cdot \underline{\underline{E}}^{-1} \cdot \underline{b} \end{aligned} \qquad (7.1.8)$$

where

$$\underline{a}_E = \underline{\underline{E}}^{-1} \cdot \underline{b} \; / \; \underline{b} \cdot \underline{\underline{E}}^{-1} \cdot \underline{b} \qquad (7.1.9)$$

From the convexity of the ellipsoids, Backus and Gilbert show that the maximum error is given by

$$\varepsilon^2_{max} = \underline{a}_S \cdot \underline{\underline{E}} \cdot \underline{a}_S \qquad (7.1.10)$$

and the maximum spread by

$$s_{max} = \underline{a}_E \cdot \underline{\underline{S}} \cdot \underline{a}_E \qquad (7.1.11)$$

and as s ranges from s_{min} to s_{max}, the corresponding error ranges from ε^2_{max} to ε^2_{min}. Thus one is faced with the problem of finding an optimum combination of spread and error.

The geometrical construction of Fig. 7-1 can help us to visualize the situation since we are now seeking a

FIG. 7-1 'The spread ellipsoid' (diagram after Backus and Gilbert, 1970). Three ellipsoids are drawn (for the situation $N = 3$ which can be envisaged in terms of three-dimensional geometry) in relation to the unimodularity plane $\underline{a} \cdot \underline{b} = 1$:

$$\underline{a} \cdot \underline{\underline{S}} \cdot \underline{a} \leq s_t \quad , \text{ with } \quad s_t < s_{min}$$

is an ellipsoid which does not intersect the plane.

$$\underline{a} \cdot \underline{\underline{S}} \cdot \underline{a} \leq s_{min}$$

is an ellipsoid which intersects the plane at a single point, $\underline{a}_S$

$$\underline{a} \cdot \underline{\underline{S}} \cdot \underline{a} \leq s_t \quad , \text{ with } \quad s_t > s_{min}$$

is an ellipsoid which intersects the plane at a collection of points indicated as the shaded region of the plane.

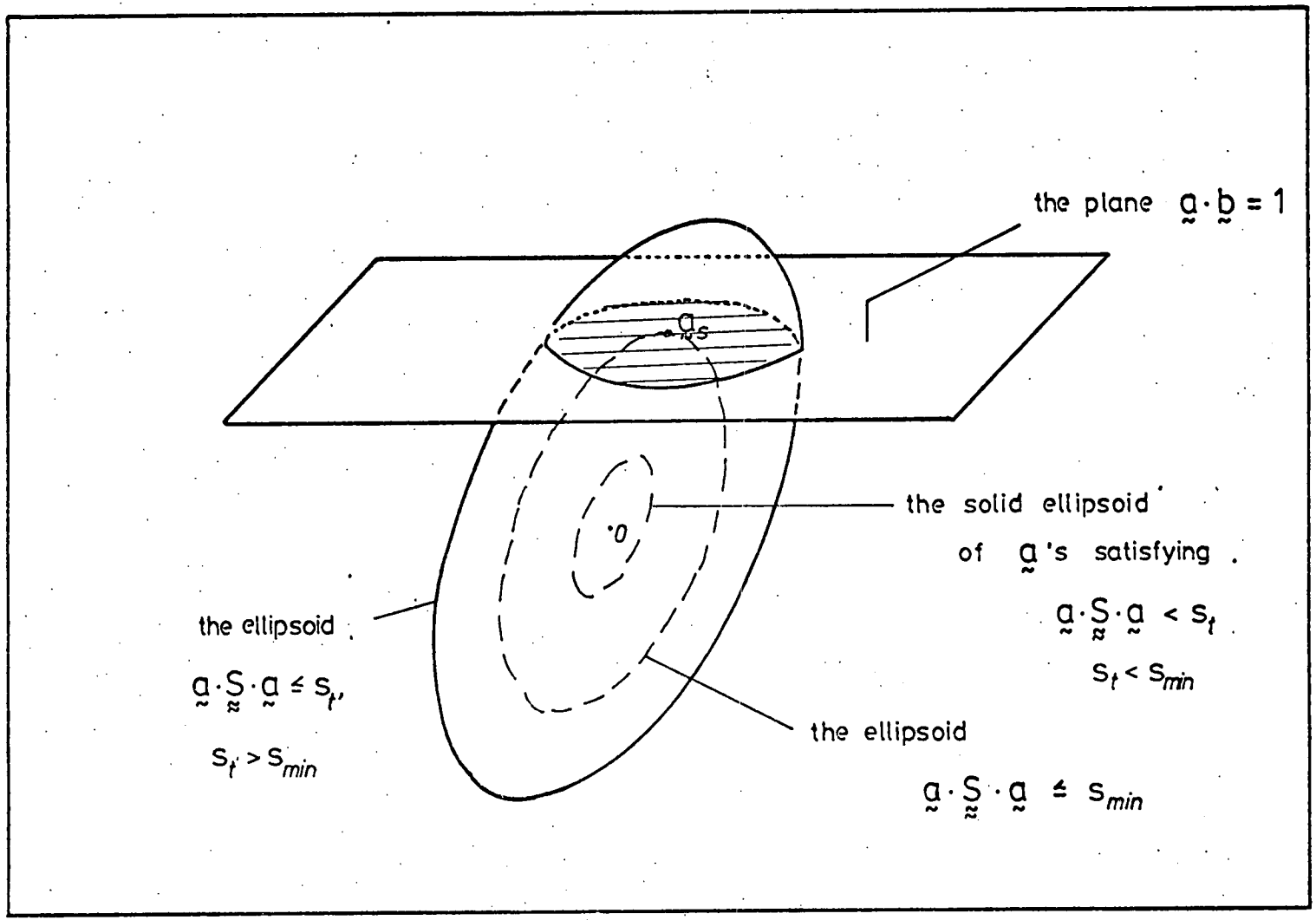
the plane $\underset{\sim}{a} \cdot \underset{\sim}{b} = 1$
$\underset{\sim}{a}_s$
0
the solid ellipsoid
of $\underset{\sim}{a}$'s satisfying
$\underset{\sim}{a} \cdot \underset{\approx}{S} \cdot \underset{\sim}{a} < s_t$
$s_t < s_{min}$
the ellipsoid
$\underset{\sim}{a} \cdot \underset{\approx}{S} \cdot \underset{\sim}{a} \leq s_{t'}$
$s_{t'} > s_{min}$
the ellipsoid
$\underset{\sim}{a} \cdot \underset{\approx}{S} \cdot \underset{\sim}{a} \leq s_{min}$

three-fold set-intersection of ellipsoid $\underline{a}\cdot\underline{\underline{E}}\cdot\underline{a} \leq \varepsilon^2$, ellipsoid $\underline{a}\cdot\underline{\underline{S}}\cdot\underline{a} \leq s_t$, and the plane (7.1.6). The solution $\underline{a}$ for (7.1.2) subject to constraints (7.1.1) and (7.1.6) is unique, since one is seeking to find N unknowns $\{a_i\}$ plus two Lagrange multipliers from N + 2 equations. Thus the set intersection of the spread ellipsoid and the error ellipsoid in the plane (7.1.6) contains a single element, the unique solution $\underline{a}$. The situation is illustrated in Fig. 7-2. If $s = s_{min}$, then $\underline{a}_S$ will coincide with point A ($\underline{a}_S$ is also indicated in the shaded region of Fig. 7-1). Although not indicated in Fig. 7-2 the error ellipsoid in this case is very large, since the boundary of its projection in the plane (7.1.6) must intersect point A. As the condition limiting the spread (7.1.1) is relaxed, the spread ellipsoid grows; conversely the error ellipsoid becomes smaller. The point of tangency of the two ellipsoids in the plane (7.1.6) moves along the path A-P-B. At point B $\varepsilon^2 = \varepsilon^2_{min}$, and $s = s_{max}$; the error ellipsoid intersects the plane (7.1.6) at a single point, $\underline{a}_E$, while the spread ellipsoid has assumed its maximum possible volume. The N-tuple $\underline{a}$ situated at point A or point B constitutes two extreme, and probably unacceptable, situations: the first corresponds to large error in the model estimate, the second to large spread and thus poor resolution. The dual optimization must seek to find an $\underline{a}$ such that the total area represented by the shaded

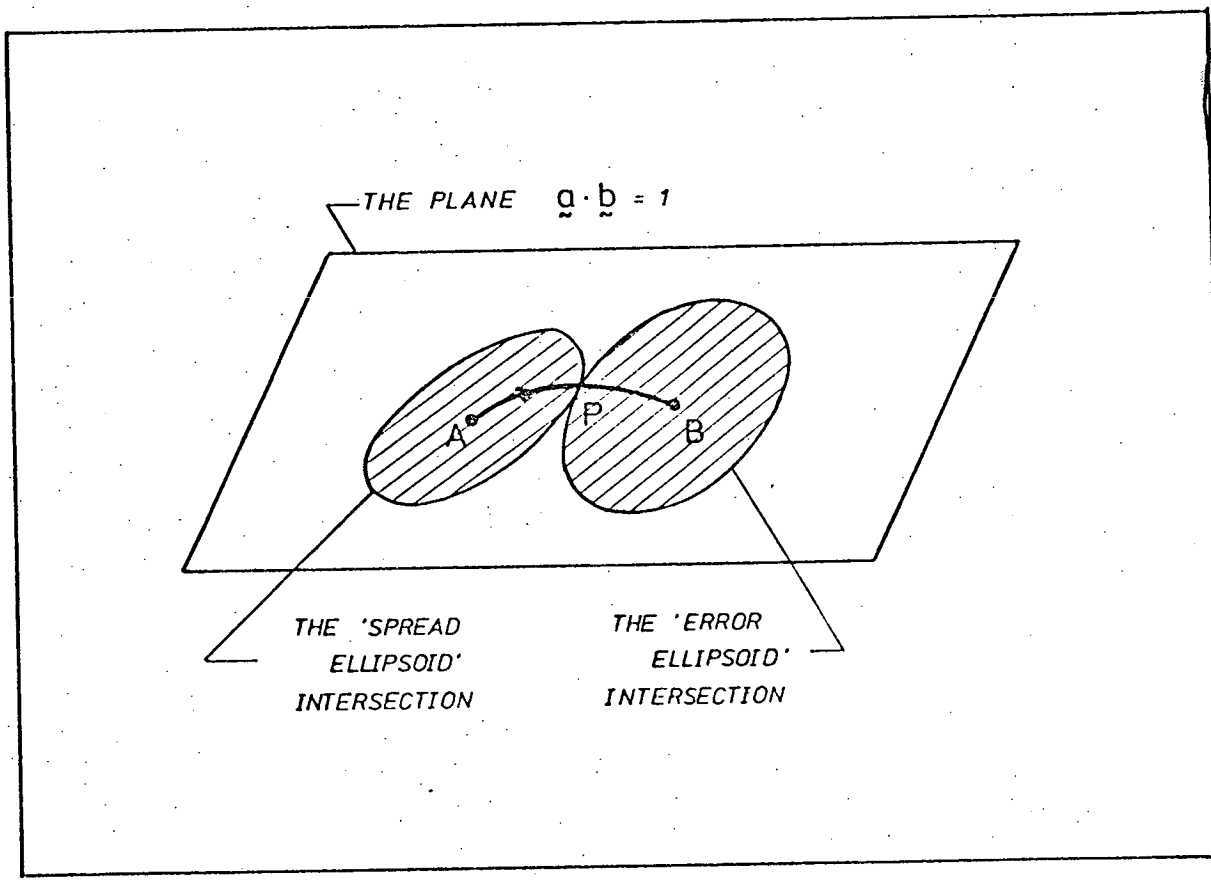

FIG. 7-2 The plane $\underline{a} \cdot \underline{b} = 1$ showing the two intersections of the spread and absolute error ellipsoids. When $s = s_{min}$, then $\varepsilon^2 = \varepsilon^2_{max}$, and the spread ellipsoid intersects $\underline{a} \cdot \underline{b} = 1$ at the single point 'A'; the error ellipsoid is maximum in this case. As the spread ellipsoid grows, the error ellipsoid diminishes, so that the mutual point of tangency of the two ellipsoids moves from 'A' to 'B'. One seeks a dual optimum of this trade-off between resolution and model error. A point such as P might constitute such an optimum.

region in Fig. 7-2 is minimal. (In fact it is the total volume of the two convex ellipsoids which should be minimized and the shaded region of the plane (7.1.6) is a projection of this volume). Let us say such an optimum N-tuple is achieved at a point P in Fig. 7-2. At the point P both the error and spread ellipsoids are mutually tangent, so the outward normals at P must be anti-parallel. The orthogonal projection of the outward normal is shown by Backus and Gilbert to be supplied by the operator $(\underline{\underline{I}} - \hat{b}\,\hat{b})$, where $\hat{b} = \underline{b}/|\underline{b}|$, $\hat{b}\,\hat{b}$ indicates the 'outer product' of these vectors, and $\underline{\underline{I}}$ is the N-dimensional identity tensor. The projection itself is given by

$$(\underline{\underline{I}} - \hat{b}\,\hat{b})\cdot\underline{\underline{E}}\cdot\underline{a}$$

for the error ellipsoid, and

$$(\underline{\underline{I}} - \hat{b}\,\hat{b})\cdot\underline{\underline{S}}\cdot\underline{a}$$

for the spread ellipsoid. Since these two are anti-parallel at P, a scalar $\propto$ can be found such that

$$\propto (\underline{\underline{I}} - \hat{b}\,\hat{b})\cdot\underline{\underline{E}}\cdot\underline{a} + (\underline{\underline{I}} - \hat{b}\,\hat{b})\cdot\underline{\underline{S}}\cdot\underline{a} = 0 \qquad (7.1.12)$$

Defining $\lambda = \underline{b}\cdot(\propto \underline{\underline{E}} + \underline{\underline{S}})\cdot\underline{a} \;/\; (\underline{b} \cdot \underline{b})$, equation (7.1.12) becomes

$$(\underline{\underline{S}} + \propto \underline{\underline{E}}) \cdot \underline{a} = \lambda \underline{b}$$

with

$$\underline{a} \cdot \underline{\underline{S}} \cdot \underline{a} = s$$

and

$$\underline{a} \cdot \underline{b} = 1$$

Thus we arrive at the optimization equations (2.2.40). The transformation $\alpha = w \tan\theta$ and the operator definition $W(\theta) = \underline{\underline{S}} \cos\theta + w \underline{\underline{E}} \sin\theta$, together with the definition $\lambda = \beta(\theta) \sec\theta$, yield the simpler form of equations (2.2.41). By solving these equations over the range $0 \leq \theta \leq \pi/2$, one can generate the trade-off curves of spread, as a function of error, for each depth z_0 at which $\langle m \rangle_{z_0}$ has been evaluated.

To illustrate these trade-off curves for magnetotelluric data, we examine the same model and data as were associated with Fig. 6-4, but now assuming the data to have a 10% experimental error. The curves are illustrated in Fig. 7-3 for various values of z_0. Backus and Gilbert (1970) proved the shape of such curves must be generally hyperbolic. For each z_0, the ideal position is that in proximity to the 'elbow' in the lower left-hand corner of Fig. 7-3 -- in this region the spread and the error is least extreme.

An alternative way of displaying this trade-off situation is to plot spread as a function of depth, z_0, plotted parametrically for various values of ε^2. Again, for the same model, it can be seen in Fig. 7-4 that the spread can be chosen to be smaller by allowing the error to become large. Solutions do not exist for $\varepsilon > \varepsilon_{max}$

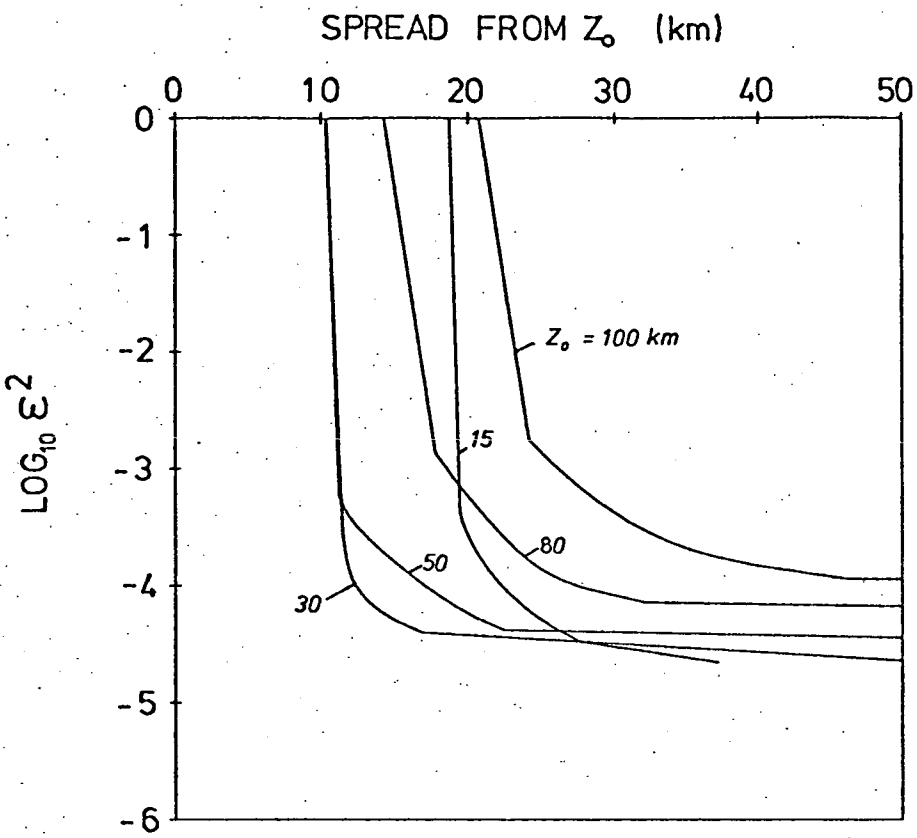

FIG. 7-3 The trade-off curves between absolute model error ε^2 and the spread from z_0, for the various indicated values of z_0. The model is a homogeneous conducting half-space with $\sigma = 0.02$ ohm^{-1}m^{-1}; the period range is 10 sec $\leq T \leq 10^4$ sec, and the ten amplitude data are assumed to have an experimental error equivalent to 10% in the logarithm of γ_i.

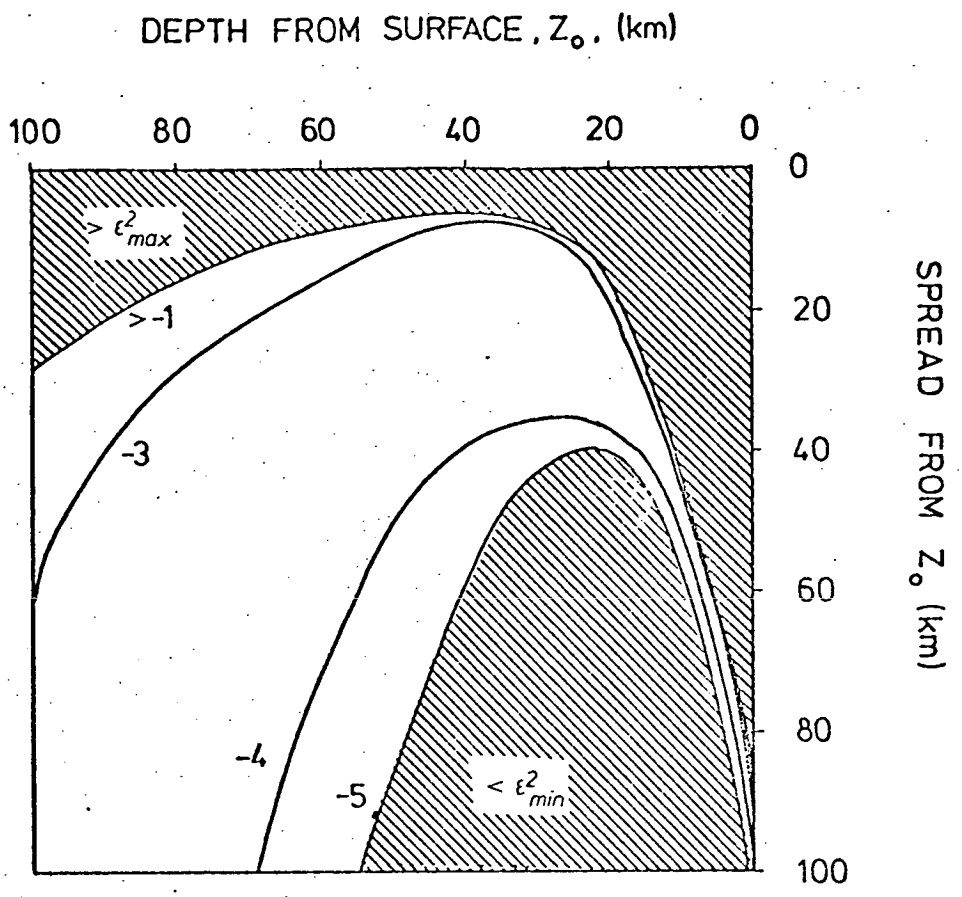

FIG. 7-4 The trade-off curves of Fig. 7-3 expressed a parametrically different way. Spread is plotted as a function of depth, z_0, for the indicated values of $\log \epsilon^2$. Although an absolute error of $\log \epsilon^2 = -5$ is extremely good, it corresponds to an extremely disappointing distribution of spread. Thus one must sacrifice error to achieve more useful spread.

and $\varepsilon < \varepsilon_{min}$, and similarly for the corresponding pairs of the spread, i.e. $s < s_{min}$ and $s > s_{max}$. At each depth z_0 the optimization is to be done anew, so a possible curve for spread as a function of z_0 can be a complicated single-valued curve between the bounds ε^2_{max} and ε^2_{min}.

One can also attempt to plot error as a function of z_0, treating spread as a set of fixed parameters. However for magnetotelluric data the useful error values (and those corresponding to useful spreads) are typically in a small range of the total range of ε^2. Difficulties arise when one attempts to plot the trade-off curves in this way. In equation (2.2.41), w is chosen in such a way that the curves of Fig. 7-3 are graphically well defined. One wishes particularly to know the structure of the elbow, rather than know a large number of points concentrated at either branch of the hyperbola. The factor w is thus chosen so that the sine and cosine terms of (2.2.41) have roughly the same order of magnitude. It seems that the interpolation associated with the numerical contouring has to contend with rather densely spaced points around the useful area of the error and a few extremal points at ε_{max} and ε_{min}. This results in a certain amount of contour structure which results from numerical interpolation rather than the actual structure of the spread. This is especially true for non-homogeneous models. The difficulty really arises

out of the unsuitability of choosing absolute error in an inversion which seeks to characterize a model (i.e. conductivity) which can range over orders of magnitude. At any rate, for purposes of illustration, Figs. 7-5a and 7-5b are supplied, but they are probably not of great value in any quantative sense. Fig. 7-5a is for the same model as was illustrated in Fig. 7-3 and Fig. 7-4. Fig. 7-5b is associated with the same model but with an additional slab of 5 km and conductivity 0.2 $\text{ohm}^{-1}\text{m}^{-1}$ located at the surface. This is a situation in which we have expressed interest previously. The solid lines in Fig. 7-5a and 7-5b represent the logarithm of the square of the conductivity at each depth of the generating model. Since the ordinate of these diagrams represents the square of the absolute error, the part of the diagram above the solid line corresponds to absolute error in the model estimate which exceeds the actual value of the model itself. This part of the space is of no practical value. In fact one would like an error somewhat below the solid line. As can be seen from the diagrams, one thus enters regions of rather larger spread. It would seem in a depth range of 15 km $\leq z_0 \leq$ 30 km for the homogeneous case one may find the model quite well-resolved. The insertion of a thin good conductor at the surface has the expected effect of worsening the spread for the corresponding useable error.

FIG. 7-5 a Spread contoured as a function of $\log \varepsilon^2$ and depth from the surface, z_0, for the same model as was discussed with Figs. 7-3 and 7-4.

FIG. 7-5 b A good conductor of depth 5 km and conductivity 0.2 $\text{ohm}^{-1}\text{m}^{-1}$ is placed at the surface of the model associated with Fig. 7-5 a. One can see the resolution below the good conductor has deteriorated. Fine-structure in such contours may be the result of numerical interpolation.

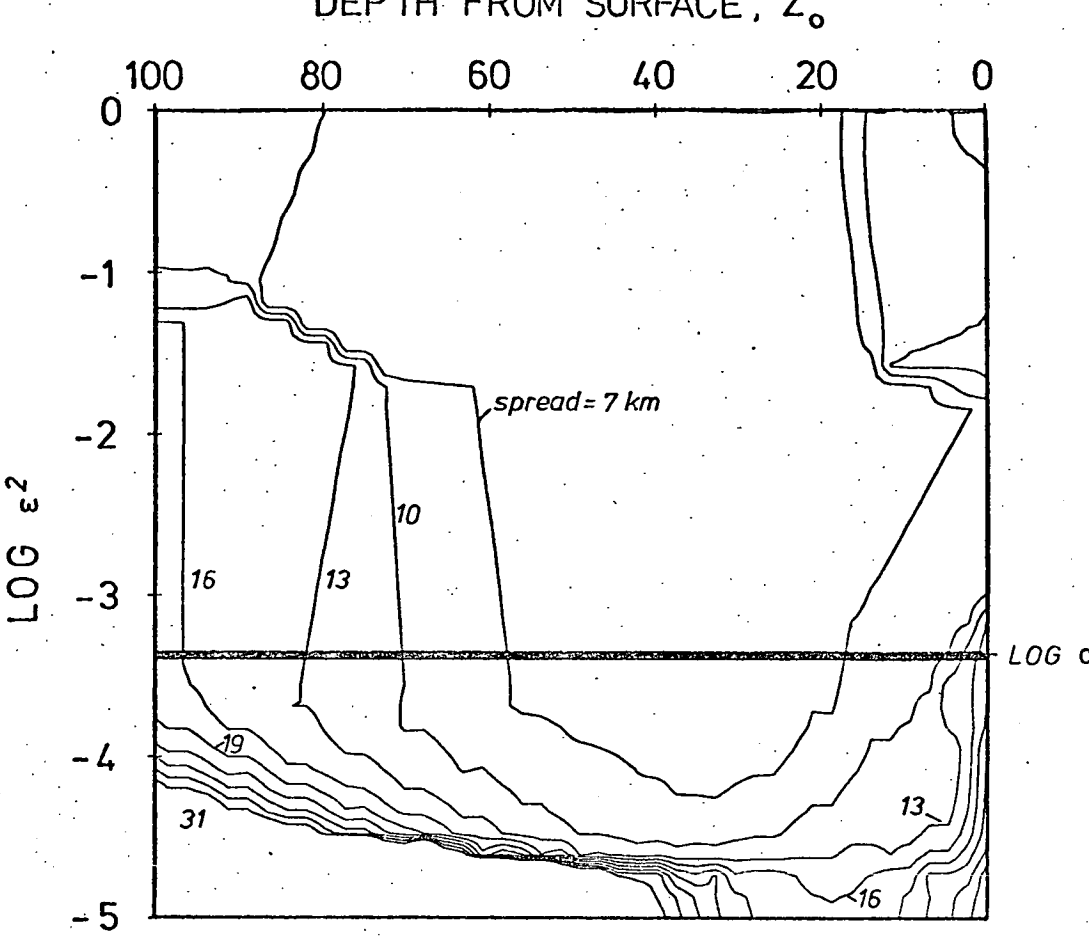
DEPTH FROM SURFACE, Z_o
100
80
60
40
20
0
0
-1
-2
-3
-4
-5
LOG ε^2
spread = 7 km
10
16
13
19
31
13
16
LOG σ

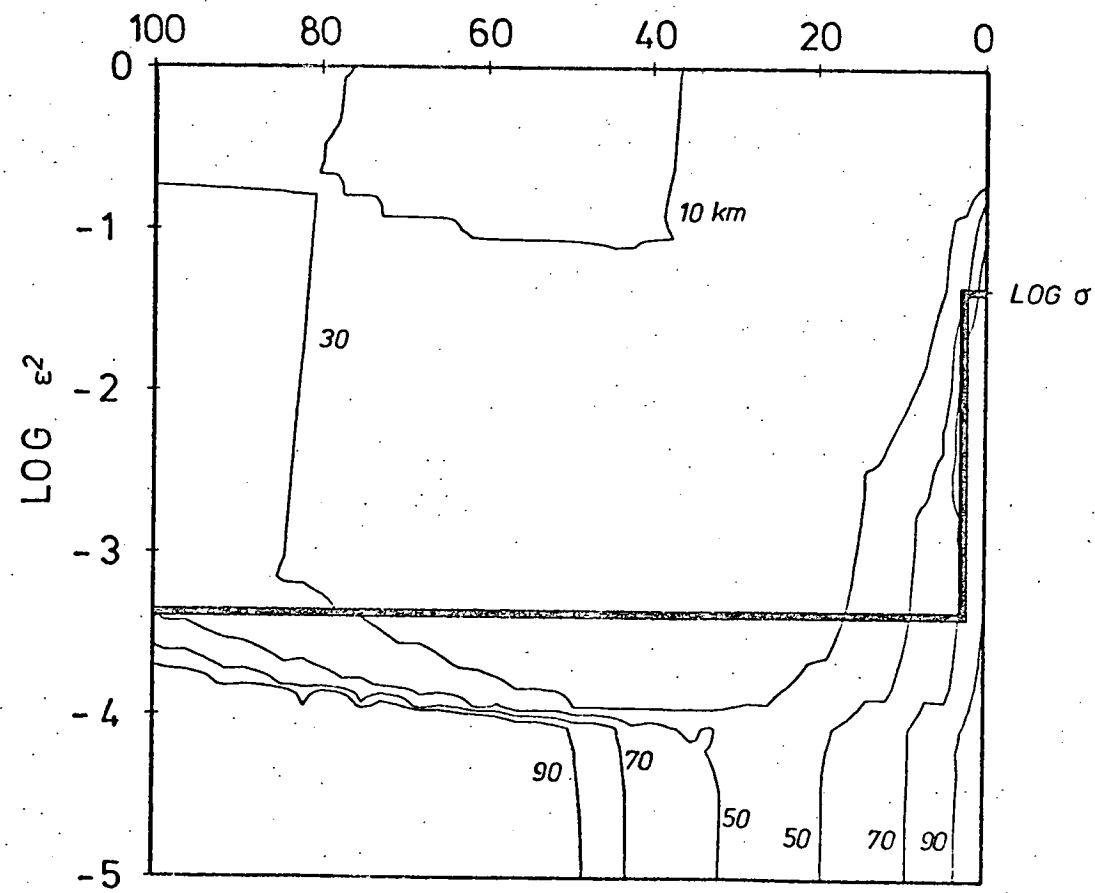
100
80
60
40
20
0
0
-1
-2
-3
-4
-5
LOG ε^2
10 km
30
90
70
50
50
70
90
LOG σ

7.2 Relative Error

We have indicated in the previous Section that it is appropriate to attach relative error to the conductivity local average rather than absolute error. This stems from the fact that electrical conductivity in the Earth may range over some five orders of magnitude. The alteration to the equations which supply a dual optimum, $\underline{a}$, i.e. equations (7.1.1) and (7.1.2), simply involves replacing absolute error ε^2 by relative error ρ^2 defined in equation (2.2.39). We rewrite this relative error in a notation consistent with the previous Section as

$$\rho^2 = \underline{a} \cdot \underline{\underline{E}} \cdot \underline{a} \; / \; (\underline{a} \cdot \underline{q})^2 \qquad (7.2.1)$$

where the elements $\underline{q}_i$ of the N-tuple $\underline{q}$ are defined by equation (2.2.34). It would seem that the problem of optimizing the error subject to a fixed spread -- or the equivalent problem of minimizing the spread subject to a fixed error -- is altered only slightly by the addition of $(\underline{a} \cdot \underline{q})^2$ in the denominator of (7.2.1). However, this addition considerably changes the geometry associated with the optimization. If ρ_t is some fixed acceptable level of relative error, the condition $\rho^2 \leq \rho_t^2$ can be expressed as

$$\underline{a} \cdot (\underline{\underline{E}} - \rho_t^2 \, \underline{q} \, \underline{q}) \cdot \underline{a} \leq 0 \qquad (7.2.2)$$

where $\underline{q} \, \underline{q}$ denotes the outer product, i.e.

$$\underline{q}\,\underline{q} = \begin{bmatrix} q_1q_1 & q_1q_2 & q_1q_3 & \cdots & \\ q_2q_1 & q_2q_2 & q_2q_3 & \cdots & \\ q_3q_1 & q_3q_2 & q_3q_3 & \cdots & \\ \vdots & \vdots & \vdots & \ddots & \\ & & & & q_Nq_N \end{bmatrix}$$

Backus and Gilbert (1970) demonstrate that (7.2.2) no longer has the geometry of a N-dimensional ellipsoid, but has rather the geometry of a double cone with junction at $\underline{a} = 0$. This is illustrated in Fig. 7-6. The two cones are associated with conditions $\underline{q} \cdot \underline{a} > 0$, and $\underline{q} \cdot \underline{a} < 0$ respectively and are designated as positive and negative cones respectively. Although the double error cone in its entirety is not convex, the positive and negative cones are individually convex. Of course the geometry of the spread ellipsoid remains unaltered.

In Section 7.1, the task of optimizing the spread and absolute error was described as one of finding the single point $\underline{a}$ contained in the set-intersection of the ellipsoids $\underline{a} \cdot \underline{\underline{S}} \cdot \underline{a} < s_t$, $\underline{a} \cdot \underline{\underline{E}} \cdot \underline{a} < \varepsilon_t^2$, and the plane $\underline{a} \cdot \underline{b} = 1$. The trade-off curves are determined by finding the ε's corresponding to a set of fixed spreads, or alternatively finding the spreads for a set of fixed absolute errors. The geometry for

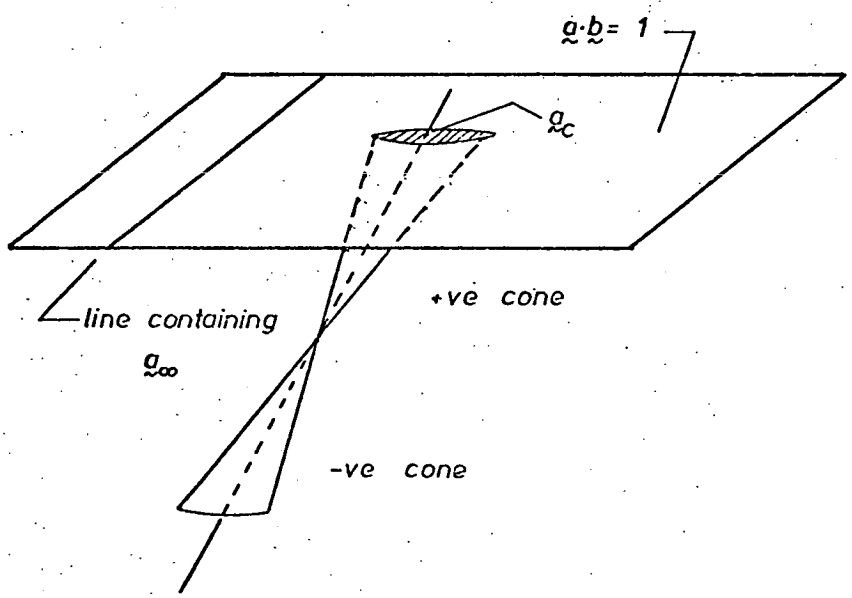

FIG. 7-6 The double error-cone (for N = 3). The shaded region represents the intersection of the positive cone to the plane $\underline{a} \cdot \underline{b} = 1$. One can visualize the situation as the axis of the double cone changes its orientation with respect to the plane. One can achieve parabolic and ellipsoidal conic-section set-intersections depending upon this orientation. If the set intersection of the error cone touches the line containing $\underline{a}_\infty$, then one may need to consider whether the negative branch of the trade-off curve can enter the problem.

relative errors requires the isolation of the set-intersection of the ellipsoid $\underline{a} \cdot \underline{\underline{S}} \cdot \underline{a} \leq s_t$, the double cone $\underline{a} \cdot (\underline{\underline{E}} - \rho^2 \underline{q}\,\underline{q}) \cdot \underline{a} \leq 0$, and the plane $\underline{a} \cdot \underline{b} = 1$.

For the moment we concentrate on the double cone. The nature of the (N-1)-dimensional sheet containing the set intersection of the double cone and $\underline{a} \cdot \underline{b} = 1$ will depend very much upon the angle made by the axis of the double cone (which is explicitly given by $\underline{\underline{E}}^{-1} \cdot \underline{q}$) and the plane. For example, if this axis is parallel to the plane, then its set-intersection will consist of two sheets bounded by two branches of a hyperbola, one in the negative cone, and one in the positive cone. By adjusting the angle of this axis, one can achieve an elliptically bounded set-intersection and a parabolically-bounded set-intersection. The angle corresponding to the parabolically-bounded sheet is important since it marks the distinction between single-valued and double-valued set-intersections. The relative error corresponding to this point is denoted as ρ_{par}, and the minimum relative error is denoted ρ_{min}. We consider the following cases:

1.) If $\rho < \rho_{min}$ then the intersection of the double cone with the plane is empty.

2.) If $\rho = \rho_{min}$ the intersection of the positive cone with the plane contains a single point, $\underline{a}_c$.

3.) In the region $\rho_{min} < \rho < \rho_{par}$ the intersection is bounded by an ellipse.

4.) For $\rho = \rho_{par}$ the intersection is bounded by a parabola.

5.) In the region $\rho_{par} < \rho < \rho_{max}$, the intersection consists of two sheets each bounded by a branch of a hyperbola.

We can now describe the trade-off between spread and relative error. If $s = s_{min}$, the spread ellipsoid intersects the plane $\underline{a} \cdot \underline{b} = 1$ at a single point $\underline{a}_s$, and the relative error achieves its maximum value ρ_{max}:

$$\rho_{max}^2 = \underline{a}_S \cdot \underline{\underline{E}} \cdot \underline{a}_S / (\underline{a}_S \cdot \underline{q})^2 \qquad (7.2.3)$$

The boundary of the error conic section may be ellipsoidal or hyperbolic depending upon the size of ρ_{max}, which in turn depends upon the separation between $\underline{a}_S$ and $\underline{a}_c$. As s increases, a value $\tilde{s}_{max}$ is reached such that the boundary of the spread ellipsoid contains $\underline{a}_c$ and

$$\tilde{s}_{max} = \underline{a}_c \cdot \underline{\underline{S}} \cdot \underline{a}_c \qquad (7.2.4)$$

with

$$\underline{a}_c = \underline{\underline{E}}^{-1} \cdot \underline{q} / (\underline{b} \cdot \underline{\underline{E}}^{-1} \cdot \underline{q}) \qquad (7.2.5)$$

This corresponds to $\rho = \rho_{min}$. The interesting domain for the spread is $s_{min} \leq s \leq \tilde{s}_{max}$, but the spread may exceed $\tilde{s}_{max}$ in some circumstances, but in this case $\rho \equiv \rho_{max}$. In addition to this consideration, one must

also take into account the relationship between ρ_{par} and ρ_{max}. Notationally, we write $s = s_\infty$ if $\rho = \rho_{par}$, and

$$s_\infty = \underline{a}_\infty \cdot \underline{\underline{S}} \cdot \underline{a}_\infty \qquad (7.2.6)$$

where $s_{min} \leq s_\infty$. However, one can have the two significant situations where either $\tilde{s}_{max} \leq s_\infty$ or alternatively $\tilde{s}_{max} \geq s_\infty$. If $\tilde{s}_{max} > s_\infty$, then one has to contend with ascertaining the error curves corresponding to two branches of the hyperbola. Backus and Gilbert (1970) show that it is appropriate in this situation to choose the minimum of the set $\{\rho_+(s), \rho_-(s)\}$, where ρ_+ is the relative error as a function of spread corresponding to the positive branch of the hyperbola and ρ_- corresponds to the negative branch. One must bear in mind that $s_\infty < \hat{s}_{max}$ may either correspond to $\underline{q} \cdot \underline{a} > 0$ or to $\underline{q} \cdot \underline{a} < 0$. However if $\underline{q} \cdot \underline{a} < 0$ then of necessity $s_\infty < \hat{s}_{max}$.

It is interesting to note that Parker (1970) does not consider the negative branch of the error hyperbolic set-intersections, arguing that a negative local average $\langle \sigma \rangle_{z_0} = \underline{q} \cdot \underline{a}$ has no meaning. However the hyperbolic set-intersection may arise when $\underline{q} \cdot \underline{a} > 0$, as we have pointed out in the preceding paragraph. Thus the conclusive test of whether $\rho_-(s)$ may enter the optimization is to be found in the relative values of s_∞ and $\tilde{s}_{max}$. If $s_\infty < \tilde{s}_{max}$ then, for those values

of spread in the range $s_\infty < s < \hat{s}_{max}$, there are two branches to be considered and one has to select the minimum of $\{\rho_-(s)\ ,\ \rho_+(s)\}$.

Using arguments similar to those preceding equation (7.1.12), Backus and Gilbert (1970) express the optimization problem associated with relative error as one of solving for $\underline{a}$ in

$$(\lambda \underline{\underline{S}} + \underline{\underline{E}}) \cdot \underline{a} = t' \underline{q} + \lambda s \underline{b}$$

where

$$\underline{a} \cdot \underline{b} = 1 \qquad (7.2.7)$$

$$s = \underline{a} \cdot \underline{\underline{S}} \cdot \underline{a}$$

and

$$t' = \rho^2 (\underline{q} \cdot \underline{a})$$

The solution to this system of equations is somewhat more daunting than for the case of absolute error. Once again $\underline{\underline{W}}$ is defined as in Section 7.1 and, defining $t = t' w \sin\theta$, we write the first equation of (7.2.7) as

$$\underline{\underline{W}} \cdot \underline{a} = t \underline{q} + s \cos\theta \underline{b} \qquad (7.2.8)$$

If we use the tilde above an arbitrary vector, say $\underline{f}$, to indicate operation by $\underline{\underline{W}}^{-1}$, i.e. $\tilde{\underline{f}} = \underline{\underline{W}}^{-1} \underline{f}$, then we can define

$$\begin{aligned} \underline{h} &= (\underline{q}\,\underline{b} - \underline{b}\,\underline{q}) \underline{b} \\ \tilde{\underline{h}} &= (\tilde{\underline{q}}\,\tilde{\underline{b}} - \tilde{\underline{b}}\,\tilde{\underline{q}}) \cdot \underline{b} \end{aligned} \qquad (7.2.9)$$

where again the products $\underline{q}\,\underline{b}$ etc. indicate the outer

product of these vectors. Hence $\underline{a}$, the solution to (7.2.8), can be expressed as

$$a = \frac{\tilde{\underline{b}} + t\,\tilde{\underline{h}}}{\underline{a} \cdot \hat{\underline{b}}}$$

and (7.2.10)

$$s \cos\theta = \frac{1 - t\,\underline{b} \cdot \hat{\underline{q}}}{\underline{b} \cdot \tilde{\underline{b}}}$$

Substituting these into (7.2.8) one obtains the quadratic

$$A\,t^2 + B\,t - C = 0 \qquad (7.2.11)$$

with

$$A = \tilde{\underline{h}} \cdot \underline{\underline{R}} \cdot \tilde{\underline{h}}$$

$$B = (\underline{b} \cdot \tilde{\underline{b}})(\underline{q} \cdot \tilde{\underline{b}}) - 2\,\tilde{\underline{b}} \cdot \underline{\underline{D}} \cdot \tilde{\underline{h}}$$

$$C = \tilde{\underline{b}} \cdot \underline{\underline{D}} \cdot \tilde{\underline{b}}$$

with $\underline{\underline{R}} = \underline{\underline{S}} \cos\theta$, and $\underline{\underline{D}} = w\,\underline{\underline{E}} \sin\theta$. It is shown by Backus and Gilbert that the positive root to (7.2.11) corresponds to the solution $\rho_+(s)$, and $\rho_-(s)$ corresponds to its negative root.

Regarding the possibility of needing to consider $\rho_-(s)$ when $s_\infty < \tilde{s}_{max}$, one can see illustration of two cases in Fig. 7-7a and 7-7b. In Fig. 7-7a we have $\rho_-(s) > \rho_+(s)$, for all s . However, in Fig. 7-7b there is a range of spread such that $\rho_-(s) < \rho_+(s)$ and in this range it is the negative branch of the trade-off curve which must be used. If $\tilde{s}_{max} < s_\infty$, it is never

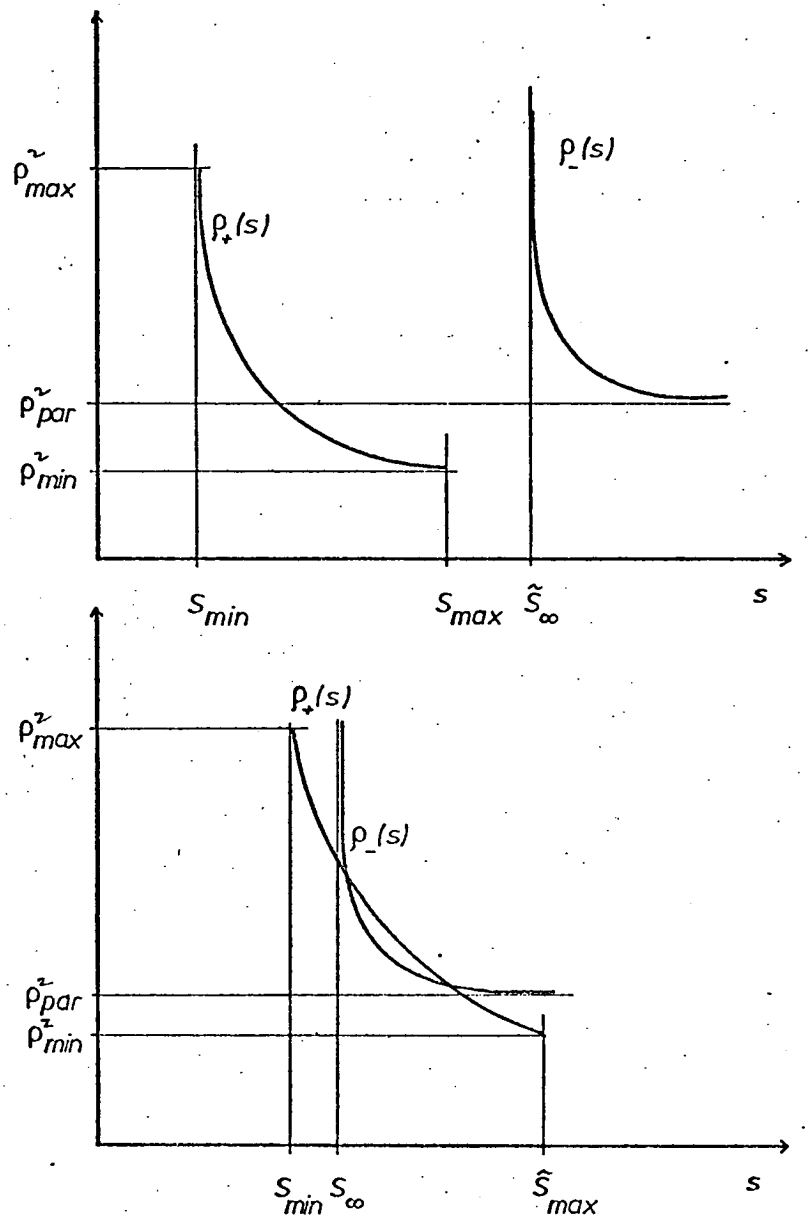

FIG. 7-7 a. Hypothetical relative error trade-off curves for the case $\rho_-(s) > \rho_+(s)$. Note that $\rho^2_{par} < \rho^2_{max}$ and $\hat{s}_{max} < s_\infty$.

b. Hypothetical relative error trade-off curves for the case where $\rho_-(s) < \rho_+(s)$ over a part of the total range of spread. Note that again $\rho^2_{par} < \rho^2_{max}$, however $s < \tilde{s}_{max}$.

appropriate to use $\rho_-(s)$. If $\tilde{s}_{max} > s_\infty$, one must consider whether $\rho_-(s)$ on the range $s_\infty < s < \hat{s}_{max}$ is larger or smaller than $\rho_+(s)$.

We now give a few illustrations of the trade-off relationship between spread and relative error as it relates to magnetotelluric data. As we have pointed out, at each depth z_0 we can select an acceptable level of spread and determine the corresponding error, and alternatively we can select acceptable error and compute the corresponding spread. For our illustrations we choose the latter alternative. Our technique will be to generate the trade-off curve between relative error and spread. This curve will be structured like those in Fig. 7-3. The curve is generated by choosing increasing values of θ in the range $(0, \frac{\pi}{2})$ in the definition of the operator $\underline{\underline{W}}(\theta)$. For $\theta = 0$, the spread is minimized irrespective of $\underline{\underline{E}}$, so the pair (s_{min}, ρ^2_{max}) is determined. The next point on the trade-off curve will supply a slightly larger spread and slightly smaller error. Thus pairs (s, ρ^2) are generated until ρ^2 falls below some preset acceptable level. One is really 'drawing a horizontal line' on Fig. 7-3 at some acceptable error level ρ_t^2 , and reading off the spread associated with the intersection of this line with the various trade-off curves. The pairs (s, ρ_t^2) achieved in this way will depend upon the value of w . Fig. 7-8a illustrates the result of this procedure to the five

layer model

	σ	d
1	0.01	1.5
2	0.001	30.
3	10.	40
4	0.0007	100.
5	0.02	

which clearly has an extremely high thin conductor embedded at a depth of 30 km. We ask how the ten-dimensional data set (of amplitude data only) comprising the periods

T_1	= 10 sec	T_6	= 60
T_2	= 15	T_7	= 80
T_3	= 20	T_8	= 100
T_4	= 30	T_9	= 200
T_5	= 40	T_{10}	= 320

is able to resolve this layer. We illustrate the relative error (truncated in the manner described previously at a level of $\rho^2 \leq 0.15$) and we consider an experimental error in the surface data of 15%. It would appear from the local averages illustrated in Fig. 7-8a, that our data set does not achieve very convincing definition of the high conductor, and the spread becomes so large that at best a very broad

averaging of the conductivity can be indicated by the data.

In Fig. 7-8b we illustrate the same situation, except for the case where the third layer conductivity has been made only 1 $ohm^{-1}m^{-1}$ instead of the previous 10 $ohm^{-1}m^{-1}$. By applying the same truncation criterion, one can see that a greatly improved model error is achieved; however, the conductivity resolution is very much reduced. The local averages after a depth of 25 km are in fact broad averages over some 50 km. In terms of the local averages, one may surmise that apart from the top twenty kilometers, the model structure is not well resolved. To resolve such structure would require better (i.e. more accurate) data, and perhaps a larger set of data extending over a larger range of periods. One can visualize the situation by consulting Fig. 6-3. The delta-like functions at depths greater than 50 km are broad and flat, and produce model averages which are in effect conductivities integrated over depths of 40 - 50 km!

Fig. 7-8c illustrates exactly the same model as Fig. 7-8b. However, in this example, we extend the data set to twenty points, at periods

T_1	= 10	T_{11}	= 125
T_2	= 15	T_{12}	= 150
T_3	= 20	T_{13}	= 175
T_4	= 25	T_{14}	= 195
T_5	= 40	T_{15}	= 200
T_6	= 50	T_{16}	= 320
T_7	= 60	T_{17}	= 420
T_8	= 80	T_{18}	= 900
T_9	= 90	T_{19}	= 1300
T_{10}	= 100	T_{20}	= 2000

It can be seen from the Figure that the spread improves considerably. In this example we record the following resolution parameters associated with depth z_0 = 100 km:

$\tilde{s}_{max}$	= 1.69×10^4	ρ^2_{max}	= 2×10^{10}
s_{min}	= 0.48	ρ^2_{min}	= 5×10^{-8}
s_∞	= 87.0	ρ^2_{par}	= 51.

We observe that $\rho^2_{par} = 51$ corresponds to a relative error of 700%. Since $\rho^2_{par} >> \rho^2_{min}$ (even though $s_\infty < \tilde{s}_{max}$), a simple sketch diagram similar to Fig. 7-7c will show that we may confidently consider only the $\rho_+(s)$ trade-off curve, since $\rho_+(s) < \rho_-(s)$ for useful values of the relative error.

FIG. 7-8 a Resolution/error characteristics are displayed for ten periods in the range 10 sec $\leq T \leq$ 320 sec, and a model $\underset{\sim}{\sigma}$: ($\sigma_1 = 0.01$, $\sigma_2 = 0.001$, $\sigma_3 = 10.00$, $\sigma_4 = 0.0007$, $\sigma_5 = 0.02$) and depths $d_1 = 1.5$ km, $d_2 = 30$ km, $d_3 = 40$ km, $d_4 = 100$ km. The trade-off curves of relative error versus spread are truncated (at each depth z_0) at the indicated level of relative error. The corresponding spread is illustrated. The local averages at ten depths into the conductor are plotted along with their corresponding relative error and spread. It will be noted that the thin 10 $ohm^{-1}m^{-1}$ conductivity layer is not really resolved.

FIG. 7-8 b The same model and periods as Fig. 7-8 a, except the 10 $ohm^{-1}m^{-1}$ layer is replaced by a 1 $ohm^{-1}m^{-1}$ layer of the same thickness. It would seem little structure is resolved at all in this case.

FIG. 7-8 c The same model as considered in Fig. 7-8 b; in this instance the data set is doubled to encompass periods in the range 10 sec $\leq T \leq$ 2000 sec. It can be seen that the conductivity at depth $z > 100$ km is much better determined ($\sigma = 0.02$ $ohm^{-1}m^{-1}$). Also some surface structure is better resolved.

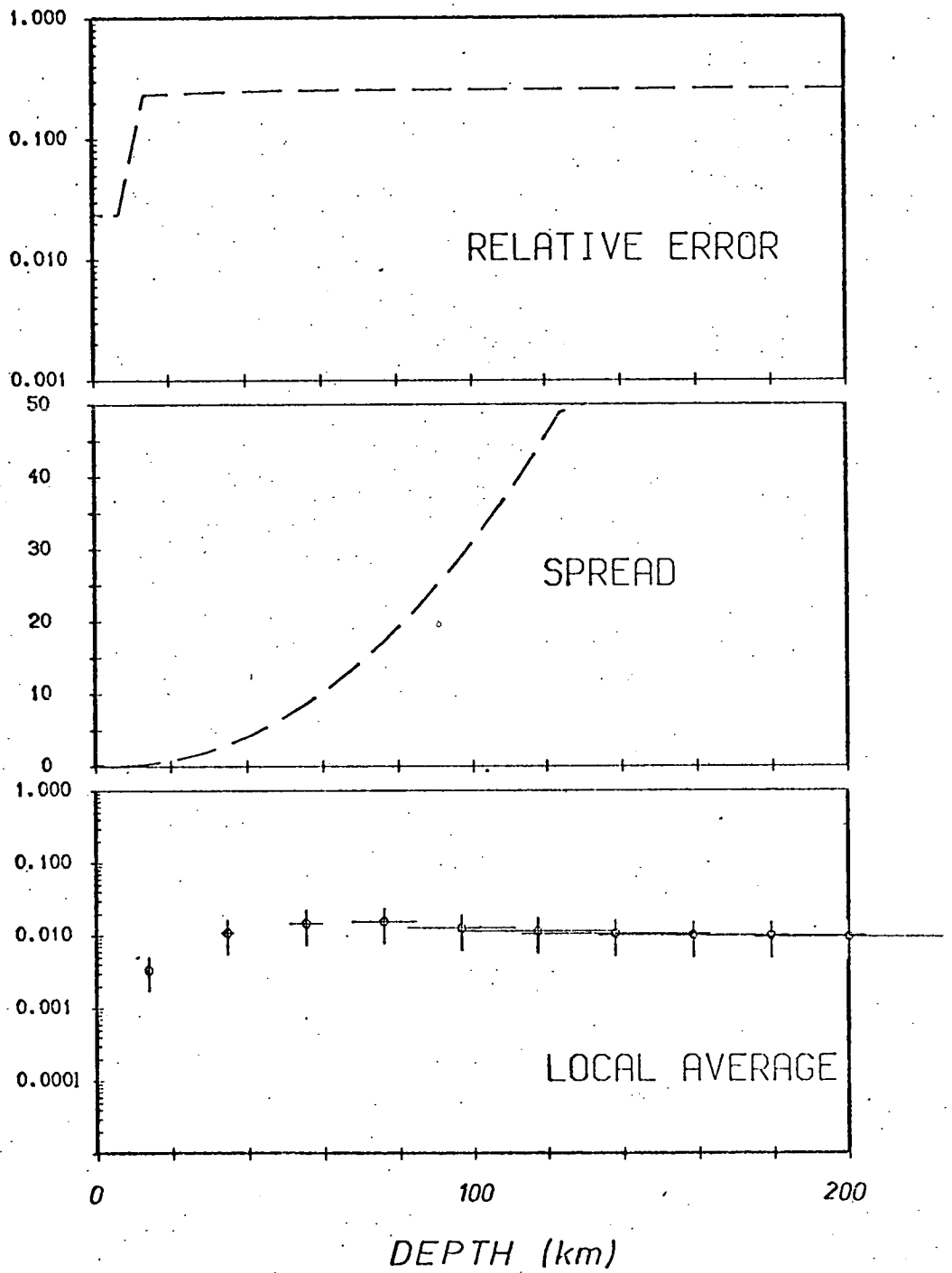
1.000
0.100
0.010
0.001
RELATIVE ERROR
50
40
30
20
10
0
SPREAD
1.000
0.100
0.010
0.001
0.0001
LOCAL AVERAGE
0
100
200
DEPTH (km)

FIG. 7-8 a

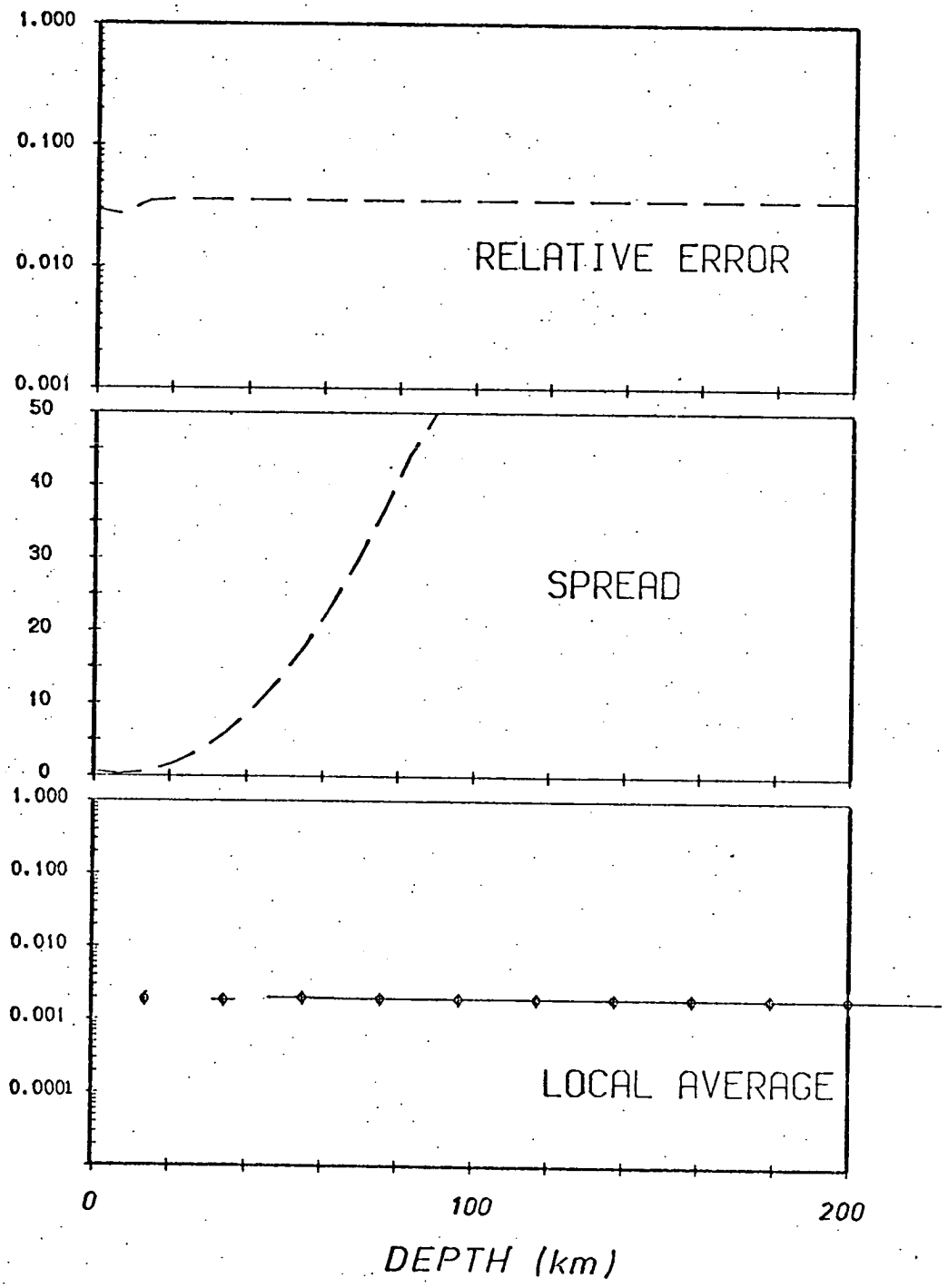
1.000
0.100
0.010
0.001
RELATIVE ERROR
50
40
30
20
10
0
SPREAD
1.000
0.100
0.010
0.001
0.0001
LOCAL AVERAGE
0
100
200
DEPTH (km)

FIG. 7-8 b

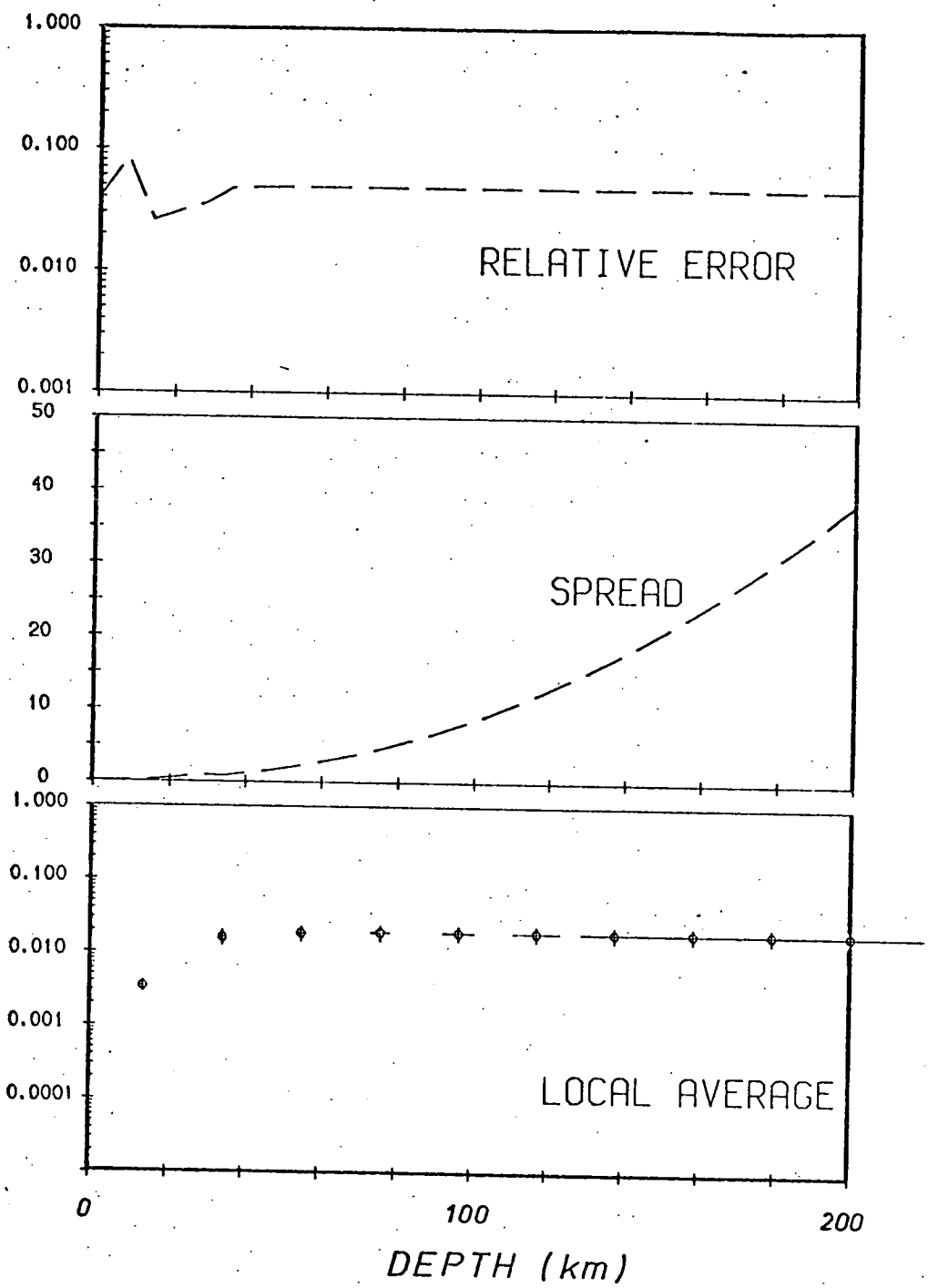
1.000
0.100
0.010
0.001
RELATIVE ERROR
50
40
30
20
10
0
SPREAD
1.000
0.100
0.010
0.001
0.0001
LOCAL AVERAGE
0
100
200
DEPTH (km)

FIG. 7-8 c

CHAPTER 8

CONCLUSIONS AND SOME REMAINING QUESTIONS

In trying to show how the formalism of Backus and Gilbert can be applied to magnetotelluric data, our motivation has been two-fold. Firstly, inverse formalisms may be of value for studying and interpreting surface data; they provide a means of assessing quantatively the resolution and non-uniqueness implied by a set of data for a particular model. Some more specific questions concerning the acceptability of models can also be posed.

Secondly, the simplicity of the inverse magneto-telluric problem allows us to study quite directly the inverse procedure itself. For example, we examine some implications of the linearization of equation (2.2.3). We have compared various representations of impedance data in terms of their inverse characteristics.

In all of this we are supposing that it is useful to study surface induction data from an inverse viewpoint. Such a study might supply a more definite understanding of what can be learned about the Earth's conductivity. Of course, the inverse formalism under investigation is based upon the quasi-linear expression of a non-linear functional, and an analysis of the formalism must involve also some attempt to assess the significance of this

linearization. Apart from Monte Carlo methods, there has as yet emerged little alternative to linearized inversion -- which incidentally enjoys the attraction over Monte Carlo procedures of a theory which seeks the solutions to the inverse problem in the physics and mathematics of induction. The question -- raised by Sabatier (1974), Anderssen (1975), and others -- is whether the linearization of (2.2.3) produces a misleading view of the character of the space of acceptable models.

We have provided here only a few illustrative examples; our aim has not been the exhaustive exploration of these problems but primarily to develop the required language. In this Chapter we summarize our work and try to indicate some possible directions for further work.

8.1 Summary

In Chapter 3 we consider as the magnetotelluric response (corresponding to the ith frequency) H_y/E_x, and this we denote by γ_i. (We point out in Chapter 4 that the expression of this surface response given by equation (3.2.35) has an interesting graphical interpretation). The variation of this response is expressed in functional form as

$$\delta\gamma_i = \int_0^\infty \delta\sigma(z)\,\mathcal{E}^2(z)\,dz + 0\|\delta\sigma\|^2 \qquad (8.1.1)$$

where $\mathcal{E}(z)$ is the ratio of the tangential electric field

$E_x(z)$, normalized with respect to its value at the surface. This is a complex continuous function with boundary values $\mathcal{E}^2(0) = 1$, and $\lim_{z \to \infty} \mathcal{E}^2(z) = 0$. The discretization of this equation (to accommodate layered half-space models) is straightforward. One has

$$\delta\gamma_i = \delta\sigma_1 \int_0^{z_1} \mathcal{E}^2(z)\, dz + \delta\sigma_2 \int_{z_1}^{z_2} \mathcal{E}^2(z)\, dz$$

$$+ \ldots + \delta\sigma_M \int_{z_{M-1}}^{\infty} \mathcal{E}^2(z)\, dz + 0\|\delta\sigma\|^2 \qquad (8.1.2)$$

Also we show

$$\frac{\partial\gamma_i}{\partial\sigma_i} = \int_0^{z_1} \mathcal{E}^2(z)\, dz \quad , \qquad \text{etc.}$$

We restate these equations here to emphasize the simple form of the inverse magnetotelluric problem. The integrals in (8.1.2) are trivial to evaluate: Schmucker (1970) provides the recursion relationship (in fact equation (3.2.32)) from which to generate the Fréchet kernel $\mathcal{E}^2(z)$. This kernel can be integrated analytically; these integrals are explicitly given in equation (5.1.6). So the Backus-Gilbert expression of the inverse problem has proved to be a very fortunate way of approaching magnetotelluric inversion. The inversion can proceed without recourse to numerical integration, not to mention the numerical differentiation often required of least-squares methods.

We have explored two inverse practices: the least-squares procedure, and the characterization of the space of acceptable models in terms of resolution. Both are posed as optimization problems which involve the solution of an N x N system of equations (for an N-dimensional data set). In either case the matrix is simply evaluated. The inner product matrix, $\underline{\underline{B}}$, (in equation (3.2.44)) is simply determined from integrated Fréchet kernels such as appear in the components of (8.1.2). Likewise the components of the spread matrix (equations (6.1.1)) are easily determined. The most time-consuming part of the inversion procedure proves to be the numerical inversion of matrices. If the inverse problem is expressed in principal axes coordinates -- such as described in Sections 5.3 and 6.3 -- then the most time-consuming numerical problem is that of isolating the eigenvalues of matrices. This is especially true for ill-conditioned matrices with very small (indeed near-zero) eigenvalues. One can improve this situation by seeking to isolate eigenvalues which lie above some reasonable minimum.

In Chapter 5, we look at the problem of finding models which are optimum in a least-squares sense. We show that the generalized least-squares procedure can be unstable, especially so if the parameterization is unfortunate. The ability of a set of data to determine a model diminishes near the surface and again at greater

depth -- this reflects the high frequency and low frequency truncation of the data set. If one seeks to determine near-surface features from such a data set, the least-squares problem can become ill-posed and instability can be the result. Stability can be enforced by reducing the number of eigenvalues represented in equations such as (3.2.44), after the problem has been transformed into a principal axes frame. However, the price to be paid for this stability is a loss in the 'exactness' of the fit that is achieved.

It is interesting to observe our synthetic examples involving a densely spaced set of data at low period (10 sec $\leq$ T $\leq$ 100 sec) associated with a model of high conductivity ($\sim$ 1 ohm^{-1}m^{-1}), parameterized at relatively shallow depth ($<$ 5 km). Such data can determine the model with some definition -- especially when compared to more sparsely distributed data at longer periods and associated with less conducting models. In these latter situations, one achieves instead a conductivity averaged over some considerable depth. In view of this contrast, it would be of great value to know whether high-frequency (e.g. T $<$ 100 sec) experimental studies can supply sufficiently reliable data to achieve good near-surface resolution.

We show how the least-squares procedure can be used as an instrument to generate acceptable models (from initial guesses). Also, we show how it can give us some

understanding of the implications associated with modifications to the data set: for example, the inclusion of phase information, or of higher frequencies, or of more closely-spaced frequencies. In this deliberate fashion we can explore the space of acceptable models.

Of course this brings us to the other useful procedure: that of characterizing the space of acceptable solutions by determining a set of local model averages each with an associated spread and error. We show that high conductivity in the Earth can be well resolved (although this deteriorates as one moves more deeply into the Earth); however, the 'model error' becomes rather larger in these cases. On the other hand, one can achieve a good model average with lower error if one is prepared to accept an average over some greater depth of conductor, i.e. an increased spread. This latter situation often corresponds to poor conductivities, although for any conductivity one can trade-off error for resolution.

In Chapter 6, we indicate how the examination of resolution characteristics can provide a quantative comparison -- in an inverse sense -- between two representations of our complex response, γ_i, namely the set $\{\mathrm{Re}\ \gamma_i\ ,\ \mathrm{Im}\ \gamma_i\}$ and the set $\{|\gamma_i|\ ,\ \arg \gamma_i\}$. By way of illustration in Chapter 7, we examine various specific models and their relationship to error and spread.

All these investigations must be considered in the light of the linearization made to equation (2.2.3). Whereas we have, in Chapter 3, taken a brief look at the structure of higher order terms, a more complicated (and interesting) question is how the linearization can effect the resolution characteristics and the local average that is achieved by an equation such as (2.2.35). It is our experience in Chapter 7 that the resolution of magnetotelluric data is somewhat disappointing, especially if one is trying to examine a conductivity contrast of only one or two orders of magnitude. Sabatier (1974) has found that the linearization of (2.2.3) can result in a resolution which may be too optimistic or too pessimistic. It would be interesting to investigate these questions for synthetic magnetotelluric data.

8.2 Some Remaining Questions

We outline here some possibilities for further research which have evolved during the course of this present work. We have already referred to some general questions; the following, however, constitute suggestions which are rather more specific.

a. Iterative direct inverse scheme

We direct attention to the iterative method developed by Barcilon (1974) for finding an optimum solution to an inverse Sturm-Liouville problem. A coupling of this

approach to the analysis of Weideldt (1972) could provide a non-linear method for optimally finding acceptable models from a guessed starting model. Barcilon suggests that his iterative method can be generalized, although in his analysis he imposes various conditions on the eigenfunctions (and on the boundary conditions) which preclude its direct application to the induction problem. One's initial guess must also satisfy various conditions if a process is to converge. Perhaps this approach to the least-squares problem would not be particularly rewarding since the prospect for finding acceptable models is anyway quite good, and another method for locating models may seem redundant. But there is the interesting prospect that an analysis of the inverse problem along these lines may lead to formulation of a non-linear method of characterizing the space of acceptable solutions. It is not clear if such an approach would admit scattered data into a direct inversion scheme.

b. Studying the significance of additional data

In Chapter 7, we pointed out how instructive it could be to ascertain how hypothetical modifications to a set of data can affect that data's resolution. In this respect, we refer to an idea of Jackson's (1972) to 'monitor' the improvement to the model variance (defined by equation (2.3.17)), when one augments the data set. One can consider the consequences of adding an additional

row and column to the inner product matrix by a first-order perturbation scheme. If we add a row $\underline{a}$ to the inner product matrix, $\underline{\underline{B}}$, corresponding to the N + 1 th datum, i.e. $\underline{a} = (B_{N+1,1} , B_{N+1,2} , \cdots B_{N+1,N+1})$, we can write the augmented matrix, $\underline{\underline{B}}^{(aug)}$, as

$$\underline{\underline{B}}^{(aug)} = \underline{\underline{B}} + \underline{a}^T \underline{a} \qquad (8.2.1)$$

(where the outer product is implied in the latter term). Similarity transformation (see equation (5.3.1)) supplies the relationship

$$\underline{\underline{C}}^T \cdot \underline{\underline{B}}^{(aug)} \cdot \underline{\underline{C}} = \underline{\underline{C}}^T \cdot \underline{\underline{B}} \cdot \underline{\underline{C}} + \underline{\underline{C}}^T \cdot \underline{a}^T \, \underline{a} \cdot \underline{\underline{C}} \qquad (8.2.2)$$

$$= \underline{\underline{\Lambda}} + \delta\underline{\underline{\Lambda}}$$

where $\underline{\underline{\Lambda}}$ is the diagonal matrix whose elements are the eigenvalues of $\underline{\underline{B}}$ and $\delta\underline{\underline{\Lambda}}$ contains the first-order perturbation to this eigenvalue (assuming a first-order change in eigenvector gives rise to a second-order change in eigenvalue). One can identify the change in eigenvalue

$$\{\delta\lambda_i\} = \{ (\underline{\underline{C}}_{(i)} \cdot \underline{a})^2 \}$$

and hence observe how the model variance improves (as long as the data set is large enough to ensure the validity of a first-order approach). A similar approach may aid an understanding of the significance of additional data to the spread and error trade-off curves.

c. Non-uniform source fields

We have only considered uniform inducing fields. It would be interesting to consider the inversion procedure applied to sources which possess spatial structure. In equation (3.1.19) we observe that the relevant equation for the Fourier transformed Hertz potential (analogous to equation (3.1.20) for E_x) is, for a one-dimensional conductivity distribution $\sigma(z)$,

$$\frac{\partial^2 P}{\partial z^2} + (k^2 + i\omega\mu\sigma) P = 0 \qquad (8.2.3)$$

where k is a two-dimensional Fourier variable, $k^2 = \xi^2 + \eta^2$. One hence pursues an analysis analogous to that surrounding equation (3.2.16) to obtain

$$\delta\gamma_i = \int_0^\infty \mathcal{P}(k, \sigma, z) \delta\sigma(z) \, dz + O\|\delta\sigma\|^2 \qquad (8.2.4)$$

where

$$\mathcal{P}(k, \sigma, z) = P(k, \sigma, z) / P(k, \sigma, 0) \qquad (8.2.5)$$

The response, $\gamma_i(k)$ is now defined by (3.1.30), i.e.

$$\gamma_i(k) \quad \frac{\mathcal{F}\{H_y\}}{\mathcal{F}\{E_x\}} \qquad (8.2.6)$$

This is the ratio of the spatial Fourier transform of the tangential magnetic field to the spatial Fourier transform of the electric tangential field, and it is a function both of period and Fourier variable. It is possible to

construct these Fourier ratios numerically from an array of simultaneously recording instruments -- however, the array would have to encompass the spatial extent of the source to avoid aliasing error in the procedure. Price (1962) has pointed out that $\mathcal{F}\{E_x\}$ can be determined from a knowledge of the field variation of H_z over the surface of the array.

The Fréchet kernel, $\mathcal{P}(k, \sigma, z)$ has an interesting form, since $P(k, \sigma, z)$ can be expressed as

$$P(k, \sigma, z) = P^s(k,0) \cdot f(k, \sigma, z) \qquad (8.2.7)$$

where $P^s(k,0)$ (used in equation (3.1.26)) is a term characteristic of the source structure. It is interesting that this term drops out when the ratio $\mathcal{P}(k, \sigma, z)$ is formed. If one assumes the conductivity to be one-dimensional beneath the array, one may be able to construct a least-squares algorithm to determine an optimal model to fit the array data. Because of the three-dimensional nature of the data ($\gamma_i \equiv \gamma(\omega, \xi, \eta)$), the inner product matrix becomes a higher-order tensor. For example, if the array is a one-dimensional traverse, the data is two-dimensional (i.e. $\gamma_i(k) \equiv \gamma(\omega, \xi)$) and the inner product tensor will have rank four. If this problem proves tractable, one can infer the conductivity distribution $\sigma(z)$ without explicit knowledge of $P^s(k,0)$. Indeed, once one has determined an acceptable $\sigma(z)$, one can hence calculate $P^s(k,0)$

from (3.1.26), and thus determine the source structure. Oldenburg (1976b) has recently developed a method to infer source current structure from magnetic array data, however he ignores induction effects as 'noise'. Perhaps it may be an informative project to incorporate induction into such a method, at least for some simple synthetic case, to see if indeed induction can be confidently ignored in such a method.

In conclusion, we remind ourselves that Price (1962) has pointed to the theoretical possibility that both source and conductivity structure may be achieved from array data.

APPENDIX I

Determination of Higher-Order Terms

In Chapter 3, the functions $f_{\nu j}(\sigma, \omega)$, with $\nu, j \in \{1, 2\}$, were stated for a two layer case: these were contoured on the model space defined by the depth (in skin-depths of the surface layer) and the conductivity ratio σ_2/σ_1. These contours are illustrated in Fig. 3-6.

For the two-layer half-space, we have

$$Q_1 = \frac{K_2 + K_1 \tanh K_1 d}{K_1 + K_2 \tanh K_1 d} \qquad (I.1)$$

One can ascertain by direct differentiation of this expression that

$$\frac{\partial Q_1}{\partial K_1} = \frac{X}{S^2} \operatorname{sech}^2 K_1 d \qquad (I.2)$$

where $S = K_1 + K_2 \tanh K_1 d$ and $X = (K_1^2 - K_2^2)\, d - K_2$. The second derivative can hence be written

$$\frac{\partial^2 Q_1}{\partial K_1^2} = \frac{2}{S^2} K_1 d \operatorname{sech}^2 K_1 d - X d \operatorname{sech}^3 K_1 d \sinh K_1 d$$

$$- \frac{X}{S} Q_1 Y \operatorname{sech}^2 K_1 d \qquad (I.3)$$

with $Y = 1 + K_2 d \operatorname{sech}^2 K_1 d$. Thus the ratio

$\frac{\partial^2 Q_1}{\partial K_1^2} \Big/ \frac{\partial Q_1}{\partial K_1}$ can be written as $2 K_1 d X^{-1} + d \tanh K_1 d - S^{-1} Y$.

Since the operator $\partial / \partial \sigma_1$ is related to the derivative with respect to K_1 by

$$\partial / \partial \sigma_1 = \frac{K_1}{2\sigma_1} \cdot \frac{\partial}{\partial K_1}$$

we can write

$$f_{11} = \frac{\partial^2 Q_1}{\partial \sigma_1^2} \Big/ \frac{\partial Q_1}{\partial \sigma_1}$$

$$= - \frac{K_1}{\sigma_1} \left\{ \frac{2K_1 d}{X} + d \tanh K_1 d - \frac{Y}{S} \right\} \qquad (I.4)$$

The derivative of Q_1 with respect to K_2 is written

$$\frac{\partial Q_1}{\partial K_2} = \frac{1 - Q_1 \tanh K_1 d}{K_1 + K_2 \tanh K_1 d} \qquad (I.5)$$

and the second derivative is

$$\frac{\partial^2 Q_1}{\partial K_2^2} = - \frac{\partial Q_1}{\partial K_2} \left[2 S^{-1} \tanh K_1 d \right] \qquad (I.6)$$

The ratio f_{22} is obtained

$$f_{22} = \frac{\partial^2 Q_1}{\partial \sigma_2^2} \Big/ \frac{\partial Q_1}{\partial \sigma_2} = \frac{K_2}{\sigma_2} S^{-1} \tanh K_1 d \qquad (I.7)$$

The cross-derivatives are given

$$\frac{\partial^2 Q_1}{\partial K_1 \partial K_2} = - S^{-1} \left(\frac{\partial Q_1}{\partial K_1} \tanh K_1 d + Q_1 d \operatorname{sech}^2 K_1 d \right) - Y \frac{\partial Q_1}{\partial K_2} \tag{I.8}$$

Hence the ratio is obtained

$$\frac{\partial^2 Q_1}{\partial \sigma_1 \partial \sigma_2} \Big/ \frac{\partial Q_1}{\partial \sigma_2} = \frac{K_1}{2\sigma_1} \left\{ \frac{\left(\frac{\partial Q_1}{\partial K_1} + Q_1 d \right)}{\coth K_1 d - Q_1} + Y S^{-1} \right\} \tag{I.9}$$

The other cross-ratio is

$$\frac{\partial Q_1}{\partial \sigma_2 \partial \sigma_1} \Big/ \frac{\partial Q_1}{\partial \sigma_1} = - \left\{ (2K_2 d + 1) X^{-1} + 2S^{-1} \tanh K_1 d \right\} \frac{K_2}{2\sigma_2} \tag{I.10}$$

For the depth component we have

$$\frac{\partial Q_1}{\partial d} = S^{-1} \left(K_1^2 - Q_1 K_1 K_2 \operatorname{sech}^2 K_1 d \right) \tag{I.11}$$

The second derivative is expressible as

$$\frac{\partial^2 Q_1}{\partial d^2} = - 2 \frac{\partial Q_1}{\partial d} S^{-1} \left(K_1 K_2 \operatorname{sech}^2 K_1 d \right) + S^{-1} Q_1 K_1 K_2 \operatorname{sech}^3 K_1 d \sinh K_1 d \tag{I.12}$$

Hence the ratio of these two terms is

$$\frac{\partial^2 Q_1}{\partial d^2} \Big/ \frac{\partial Q}{\partial d} = - \frac{2 K_1 K_2 \operatorname{sech}^2 K_1 d}{S} \times \left\{ 1 + \frac{Q_1 S \tanh K_1 d}{K_1^2 - Q_1 K_1 K_2 \operatorname{sech}^2 K_1 d} \right\} \tag{I.13}$$

The functions f_{11} and f_{22} plotted in Fig. 3-9 for the

three layer case are determined as follows: we have for the three-layer half-space

$$Q_1 = \frac{K_2 Q_2 + K_1 \cdot \tanh K_1 d_1}{K_1 + K_2 Q_2 \cdot \tanh K_1 d_1} \qquad (I.14)$$

Since Q_2 is independent of σ_1, the derivatives with respect to σ_1 may be written directly from equation (I.4) by replacing K_2 with $K_2 Q_2$. Immediately we have

$$f_{11} = -\frac{K_1}{\sigma_1}\left\{ \frac{2K_1 d_1}{X_1} + d_1 \tanh K_1 d_1 - \frac{Y_1}{S_1} \right\} \qquad (I.15)$$

where $S_1 = K_1 + K_2 Q_2 \tanh K_1 d_1$, $X_1 = (K_1^2 - Q_2^2 K_2^2)$ $d - K_2$, and $Y_1 = 1 + K_2 Q_2 d \operatorname{sech}^2 K_1 d$.

For the derivative with respect to σ_2, we can write

$$\frac{\partial Q_1}{\partial K_2} = (1 - Q_1 \tanh K_1 d) \left(\frac{Q_2 + K_2 \frac{\partial Q_2}{\partial K_2}}{S_1} \right) \qquad (I.16)$$

where

$$\frac{\partial Q_2}{\partial K_2} = (S_2^{-2} X_2^{-1} - K_3) \operatorname{sech}^2 K_2 d \qquad (I.17)$$

with $X_2 = (K_2^2 - K_3^2) d_2 - K_3$, and $S_2 = K_2 + K_3$ $\tanh K_2 d_2$. Forming the second derivative and expressing its ratio with the first derivative, we obtain

$$\frac{\partial^2 Q_1}{\partial K_2^2} \Big/ \frac{\partial Q_1}{\partial K_2} = \frac{\frac{\partial Q_2}{\partial K_2}\,(\,1 + K_2\eta\,)}{Q_2 + K_2 \frac{\partial Q_2}{\partial K_2}}$$

$$- 2(\,Q_2 + K_2 \frac{\partial Q_2}{\partial K_2}\,)\, S_1^{-1} \tanh K_1 d \qquad \text{(I.18)}$$

where $\eta = \frac{\partial^2 Q_2}{\partial K_2^2} \Big/ \frac{\partial Q_2}{\partial K_2}$, a ratio which has the same form as that associated with (I.7), namely

$$\eta = S_2^{-1} \tanh K_2 d_2 \qquad \text{(I.19)}$$

APPENDIX II

Note on Notation

In the presentation of the mathematics of generalized inverse procedures as applied to induction problems, we have tried to retain the notation of the quoted literature. However inevitable conflicts in notation have occurred. We offer the following remarks by way of clarifying the notation.

Throughout the thesis $G_i(z)$ denotes the Fréchet kernel associated with the ith frequency; $g_i[m]$ denotes the functional associated with the ith frequency; γ_i is used to denote the surface response generally in Chapter 2, and specifically the magnetotelluric response from Section 3.2.b onwards; V_i denotes the response for the spherical induction problem in Section 3.2.b.

In Chapter 2 λ is the Lagrange multiplier associated with the optimization of averaging kernels. In Chapters 5 and 6 the set $\{\lambda_i\}$ denotes the N-tuple of eigenvalues associated with various operators. In Chapter 2 $\underline{\underline{\Gamma}}$ denotes the inner product matrix generally. For discretized magnetotelluric problems this matrix is defined in (3.2.45) and is denoted subsequently as $\underline{\underline{B}}$.

Throughout the text a subscripted ρ has denoted apparent resistivity. In Chapter 7 ρ^2 denotes the square of the relative error. Also in Chapter 7 ε^2

denotes the square of the absolute error, whereas in Chapter 3 ε is used to denote electrical permittivity.

There are a number of such inconsistencies in the text; it is hoped that the context will suffice to clarify each situation.

REFERENCES

Abramovici, F., Landisman, M., and Shoham, Y., 1976. Partial derivatives for the one-dimensional magnetotelluric problem, Geophys. J. R. astr. Soc., 44, 359 - 378.

Anderssen, R. S., 1968. Note on conductivity models for the Earth, J. Geophys. Res., 13, 6535 -

Anderssen, R. S., 1970. Bounds for conductivity modelling, Earth Planet. Sci. Lett., 7, 314 - 316.

Anderssen, R. S., 1974. On the linearization of geophysical inversion problems, Personal Communication.

Anderssen, R. S., 1975. On the inversion of global electromagnetic induction data, Phys. Earth Planet. Inter., 10, 250 - 261.

Backus, G., and Gilbert, F., 1967. Numerical application of a formalism for geophysical inverse problems, Geophys. J. R. astr. Soc., 13, 247 - 276.

Backus, G., and Gilbert, F., 1968. The resolving power of gross Earth data, Geophys. J. R. astr. Soc., 16, 169 - 205.

Backus, G., and Gilbert, F., 1970. Uniqueness in the inversion of inaccurate gross Earth data, Phil. Trans. R. Soc., A266, 123 - 192.

Bailey, R. C., 1970. Inversion of the geomagnetic induction problem, Proc. R. Soc. Lond., A315, 185 - 194.

Bailey, R. C., 1973. Global geomagnetic sounding, methods and results, Phys. Earth Planet. Inter., 7, 234 - 244.

Bailey, R. C., Edwards, R. N., Garland, G. D., Kurtz, R. D., and Pitcher, D., 1974. Electrical conductivity studies over a tectonically active area in Eastern Canada, J. Geomagn. Geoelectr., 26, 125 - 146.

Banks, R. J., 1969. Geomagnetic variations and the electrical conductivity of the upper mantle, Geophys. J. R. astr. Soc., 17, 457 - 487.

Barcilon, V., 1974a. On the uniqueness of inverse eigenvalue problems, Geophys. J. R. astr. Soc., 38, 287 - 298.

Barcilon, V., 1974b. Iterative solution of the inverse Sturm-Liouville problem, J. Math. Phys., 15 429 - 436.

Barcilon, V., 1975. Well-posed inverse eigenvalue problems, Geophys. J. R. astr. Soc., 42, 357 - 383.

Borg, G., 1946. Eine Umkehrung der Sturm-Liouvilleschen Eigenwertaufgabe, Acta Math., 78, 1 - 96.

Cagnaird, L., 1953. Basic theory of the magnetotelluric method, Geophysics, 18, 605 - 635.

Caner, B., and Auld, D. R., 1968. Magnetotelluric determination of upper mantle conductivity structure at Victoria, British Columbia, Can. J. Earth Sci., 5, 1209 - 1220.

Chapman, S., 1919. The solar and lunar diurnal variation of the Earth's magnetism, Phil. Trans. Roy. Soc., A218, 1 - 118.

Chapman, S., and Price, A. T., 1930. The electric and magnetic state of the interior of the Earth as inferred from terrestrial magnetic variations, Phil. Trans. Roy. Soc., A229, 427 - 460.

Chapman, S., and Whitehead, T. T., 1923. The influence of electrically conducting material within the earth on various phenomena of terrestrial magnetism, Trans. Cambridge Phil. Soc., 22, 463 - 482.

Coggan, J. H., 1971. Electromagnetic and electrical modelling by the finite element method, Geophysics, 36, 132 - 155.

Courtillot, V., Ducruix, J., and LeMouel, J.-L., 1974. A solution of some inverse problems in geomagnetism and gravimetry, J. Geophys. Res., 79, 4933 - 4940.

Dorman, L. M., and Lewis, B. T. R., 1970. Theory of the determination of the Earth's isostatic response to a concentrated load (Parts I and II), J. Geophys. Res., 75, 3357 - 3386.

Dorman, L. M., and Lewis, B. T. R., 1972. Inversion of the Isostatic Green function and lateral density changes, J. Geophys. Res., 77, 3068 - 3077.

Duba, A., 1976. Are laboratory electrical conductivity data relevant to the Earth?, Review paper presented at 3rd IAGA Workshop on E.M. induction in the Earth, Sopron, Hungary.

Dziewonski, A. M., Hales, A. L., and Lapwood, E. R., 1975. Parametrically simple Earth models consistent with geophysical data, Phys. Earth Planet. Inter., 10, 12 - 48.

*

Edwards, R. N., Law, L. K., and White, A., 1972. Geomagnetic variations in the British Isles and their relation to electrical currents in the ocean and shallow seas, Phil. Trans. Roy. Soc., A270, 289 - 323.

Fournier, H. G., 1968. Proposition d'une methode pour determiner la structure du premier millier de kilometres de la terre d'apres la resistivite apparente, Acta Geophys. Polonica, 16, 215 - 248.

Gel'fand, I. M., and Levitan, B. M., 1955. On the determination of a differential equation from its spectral function, Am. Math. Soc. Transl., 1, 253 - 304.

Gel'fand, I. M., and Fomin, S. V., 1963. Calculus of Variations, trans. R. A. Silverman, Prentice-Hall, N. J., pp. 232.

Gilbert, F., 1971. Ranking and winnowing gross Earth data for inversion and resolution, Geophys. J. R. astr. Soc., 23, 125 - 128.

Gilbert, F., 1973. Inverse problems for the Earth's normal modes, in Lectures in Applied Mathematics, Vol. 14, 107 - 127, A. M. S., Providence, R. I.

Gilbert, F., and Dziewonski, A. M., 1975. An application of normal mode theory to the retrieval of structural parameters and source mechanisms from seismic spectra, Phil. Trans. Roy. Soc., A278, 187 - 269.

Hermance, J. F., 1973. Processing of magnetotelluric data, Phys. Earth Planet. Inter., 7, 349 - 364.

Hewson-Browne, R. C., and Kendal, P. C., 1976. Magneto-telluric modelling and inversion in three-dimensions, Review paper presented at 3rd IAGA Workshop on E.M. induction in the Earth, Sopron, Hungary.

*

Eckhardt, D. H., 1963. Geomagnetic induction in a concentrically stratified Earth, J. geophys. Res., 68, 6273-6278.

Hibbs, R. D., and Jones, F. W., 1972. Electromagnetic induction in the Earth by a symmetric non-uniform source, Geophys. J. R. astr. Soc., 32, 269 - 277.

Hildebrand, F. B., 1965. Methods of Applied Mathematics, Prentice-Hall, N. J., pp. 362.

Hobbs, B. A., 1972. The inverse problem of the moon's electrical conductivity, Earth Planet. Sci. Lett., 17, 380 - 384.

Householder, A. S., 1964. The Theory of Matrices in Numerical Analysis, Blaisdell, New York, pp. 257.

Hutton, V. R. S., 1976. Induction studies in rifts and other active regions, Review paper presented at 3rd IAGA Workshop on E.M. induction in the Earth, Sopron, Hungary.

Hutton, V. R. S., 1976. The electrical conductivity of the Earth and planets, Rep. Prog. Phys., 39, 487 - 572.

Jackson, D. D., 1972. Interpretation of inaccurate, insufficient, and inconsistent data, Geophys. J. R. astr. Soc., 28, 97 - 109.

Jackson, D. D., 1973. Marginal solutions to quasi-linear inverse problems in geophysics: the Edgehog Method Geophys. J. R. astr. Soc., 35, 1 - 16.

Jady, R. J., 1974a. The conductivity of spherically symmetric layered Earth models determined by Sq and longer period magnetic variations, Geophys. J. R. astr. Soc., 36, 399 - 410.

Jady, R. J., 1974b. Conductivity models and Banks' Data, Geophys. J. R. astr. Soc., 37, 447 - 452.

Jones, A. G., and Hutton, V. R. S., 1976. Magneto-telluric investigation of the Eskdalemuir Anomaly, contributed paper, 3rd IAGA Workshop on E.M. induction in the Earth, Sopron, Hungary.

Jones, F. W., 1972. The electromagnetic perturbation fields of conductivity anomalies within the Earth, Geophys. J. R. astr. Soc., 30, 211 - 228.

Jones, F. W., and Price, A. T., 1970. The perturbations of alternating geomagnetic fields by conductivity anomalies, Geophys. J. R. astr. Soc., 20, 317 - 334.

Jupp, D. L. B., and Vozoff, K., 1975. Stable iterative methods for the inversion of geophysical data, Geophys. J. R. astr. Soc., 42, 957 - 976.

Kennett, B. L. N., 1976. A comparison of travel-time inversions, Geophys. J. R. astr. Soc., 44, 517 - 536.

Krein, M. G., 1952. On inverse problems for inhomogeneous strings (Russian), Dokl. Akad. Nauk SSSR, 82, 669 - 672.

Kuckes, A. F., 1973a. Relations between electrical conductivity of a mantle and fluctuating magnetic fields, 32, 119 - 131.

Kuckes, A. F., 1973b. Correspondence between the magnetotelluric and field penetration depth analyses for measuring electrical conductivity, Geophys. J. R. astr. Soc., 32, 381 - 385.

Kunetz, G., 1972. Processing and interpretation of magnetotelluric soundings, Geophysics, 37, 1005 - 1021.

Lahiri, B. N., and Price, A. T., 1939. Electromagnetic induction in non-uniform conductors and the determination of the conductivity of the Earth from terrestrial magnetic variations, Phil. Trans. Roy. Soc., A237, 509 - 540.

Lamb, H., 1883. On the electrical motions in a spherical conductor, Phil. Trans. Roy. Soc., A174, 519 - 549.

Lanczos, C., 1961. Linear Differential Operators, D. Van Nostrand, London, pp. 564.

Larsen, J. C., 1975. Low frequency (0.1 - 6.0 cpd) electromagnetic study of deep mantle electrical conductivity beneath the Hawaiian Island, Geophys. J. R. astr. Soc., 43, 17 - 46.

Le Mouel, J.-L., Courtillot, V., and Ducruix, J., 1975. A solution of some inverse problems in potential theory, Geophys. J. R. astr. Soc., 42, 251 - 272.

Lighthill, M. J., 1958. Introduction to Fourier analysis and Generalized Functions, Cambridge University Press, Cambridge, pp. 79.

Loewenthal, D., 1975. Theoretical uniqueness of the magnetotelluric inverse problem for equal penetration discretizable models, Geophys. J. R. astr. Soc., 43, 897 - 903.

Loewenthal, D., 1975. On the phase constraint of the magnetotelluric impedance, Geophysics, 40, 325 - 330.

Madden, T. R., 1972. Transmission systems and network analogies to geophysical forward and inverse problems, Tech. Rept. No. 72-3, Dept. of Earth and Planetary Sciences, M.I.T.

Madden, T. R., and Swift, C. M., 1969. Magnetotelluric studies of the electrical conductivity structure of the crust and upper mantle, in The Earth's Crust and Upper Mantle (ed. P. J. Hort), AGU Monograph 13, p. 469.

Marquardt, D. W., 1963. An algorithm for least-squares estimation of non-linear parameters, J. SIAM, 11, 431 - 441.

Maxwell, J. C., 1873. A Treatise on Electricity and Magnetism. Oxford University Press, Oxford.

Muller, W., 1976. Inversion by simultaneous fitting of apparent resistivity and phase angle, contributed paper at 3rd IAGA Workshop on E.M. induction in the Earth, Sopron, Hungary.

Oldenburg, D. W., 1974. The inversion and interpretation of gravity anomalies, Geophysics, 39, 526 - 536.

Oldenburg, D. W., 1976a. Calculation of Fourier transforms by the Backus-Gilbert method, Geophys. J. R. astr. Soc., 44, 413 - 431.

Oldenburg, D. W., 1976b. Ionospheric current structure as determined from ground-based magnetometer data, Geophys. J. R. astr. Soc., 46, 41 - 66.

Parker, R. L., 1970. The inverse problem of electrical conductivity in the mantle, Geophys. J. R. astr. Soc., 22, 121 - 138.

Parker, R. L., 1972. Inverse theory with grossly inadequate data, Geophys. J. R. astr. Soc., 29, 123 - 138.

Parker, R. L., and Huestis, S. P., 1974. The inversion of magnetic anomalies in the presence of topography, J. Geophys. Res., 79, 1587 - 1593.

Parsons, B. E., 1972. Changes in the Earth's Shape, Ph.D. Thesis, University of Cambridge, pp. 200.

Patrick, F. W., and Bostick, F. X., 1969. Magneto-telluric modelling techniques, Electrical Geophysics Research Laboratory Technical Report 59, University of Texas at Austin.

Porstendorfer, G., 1975. Principles of Magnetotelluric Prospecting, Geoexploration Monograph Series 1 No.5, Gebruder Borntraeger, W. Berlin, pp. 118.

Price, A. T., 1950. Electromagnetic induction in a semi-infinite conductor with a plane boundary, Quart. J. Mech. Appl. Math., 3, 385 - 410.

Price, A. T., 1962. The theory of magnetotelluric methods when the source field is considered, J. Geophys. Res., 67, 1907 - 1918.

Price, A. T., 1970. The electrical conductivity of the Earth, Q. Jl. R. astr. Soc., 11, 23 - 42.

Price, A. T., 1973. The theory of geomagnetic induction, Phys. Earth Planet. Inter., 7, 227 - 233.

Price, A. T., and Wilkins, G. A., 1963. New methods of analysis of geomagnetic fields and their application to the Sq field of 1932 - 1933, Phil. Trans. Roy. Soc., A256, 31 - 98.

Reddy, I. K., and Rankin, D., 1971. Magnetotelluric measurements in Central Alberta, Geophysics, 36, 739 - 753.

Reddy, I. K., and Rankin, D., 1972. On the inter-pretation of magnetotelluric data in the plains of Alberta, Can. J. Earth Sci., 9, 514 - 527.

Reddy, I. K., and Rankin, D., 1973. Magnetotelluric response of a two-dimensional sloping contact by the finite element method, Pure App. Geophys., 105, 847 - 857.

Reddy, I. K., and Rankin, D., 1974. Coherence functions for magnetotelluric analysis, Geophysics, 39, 312 - 320.

Reitmayr, G., 1975. An anomaly of the upper mantle below the Rhine Graben studied by the inductive response of natural electromagnetic fields, J. Geophys., 41, 651 - 658.

Rikitake, T., 1950. Electromagnetic induction within the Earth and its relation to the electrical state of the Earth's interior, Bull. Earthquake Res. Inst. Tokyo Univ., 28, 45 - 100.

Rikitake, T., 1966. Electromagnetism and the Earth's Interior, Elsevier, Amsterdam, pp. 308.

Rikitake, T., and Honkura, Y., 1973. Recent Japanese studies on conductivity anomalies, Phys. Earth Planet. Inter., 7, 203 - 212.

Rooney, D., 1976. Magnetotelluric measurements across the Kenyan Rift valley, Ph.D. Thesis, University of Edinburgh, pp. 206.

Sabatier, P. C., 1974. Remarks on approximate methods in geophysical inverse problems, Proc. R. Soc., A337, 49 - 71.

Schmucker, U., 1970. Anomalies of geomagnetic variations in the Southwestern United States, Scripps Institution Bulletin, Vol. 13, pp. 165.

Schmucker, U., 1976. Geomagnetic induction studies with individual storms, contributed paper, 3rd IAGA Workshop on E.M. induction in the Earth, Sopron, Hungary.

Schuster, A., 1889. The diurnal variations of terrestrial magnetism, Phil. Trans. Roy. Soc., A208, 163 - 204.

Sims, W. E., Bostick, F. X., and Smith, H. W., 1971. The estimation of magnetotelluric impedance tensor elements from measured data, Geophysics, 36, 938 - 942.

Srivastava, S. P., 1966. Theory of the magnetotelluric method for a spherical conductor, Geophys. J. R. astr. Soc., 11, 373 - 387.

Srivastava, S. P., Douglass, J. L., and Ward, S. H., 1963. The application of magnetotelluric and telluric methods in Central Alberta, Geophysics, 28, 426 - 446.

Stratton, J. A., 1941. Electromagnetic Theory, McGraw Hill, London, pp. 615.

Summers, D. M., 1971. Electromagnetic Induction in a Stratified Conducting Half-space, M.Sc. Thesis, University of Victoria, Canada.

Summers, D. M., and Weaver, J. T., 1973. Electromagnetic induction in a stratified conducting half-space by an arbitrary periodic source, Can. J. Phys., 51, 1064 - 1074.

Swift, C. M., 1967. A magnetotelluric investigation of an electrical conductivity anomaly in the South-western United States, Ph.D. Thesis, M.I.T.

Thomson, D. J., and Weaver, J. T., 1975. The complex image approximation for induction in a multilayered Earth, J. Geophys. Res., 80, 123 - 129.

Tozer, D. C., 1959. The electrical properties of the Earth's interior, in Physics and Chemistry of the Earth, (eds. Rankama and Runcorn), Pergamon Press, London, 3, 414 - 436.

Vozoff, K., 1972. The magnetotelluric method in the exploration of sedimentary basins, Geophysics, 37, 98 - 141.

Vozoff, K., and Jupp, D. L. B., 1975. Joint inversion of geophysical data, Geophys. J. R. astr. Soc., 42, 977 - 999.

Wait, J. R., 1954. On the relation between telluric currents and the Earth's magnetic field, Geophysics, 19, 281 - 289.

Wait, J. R., 1962. Theory of magnetotelluric fields, J. res. Natl. Bur. Std., D66, 509 - 541.

Wait, J. R., 1962. Electromagnetic Waves in Stratified Media (1st Ed.) Pergamon Press, London.

Ward, S. H., Peeples, W. J., and Ryu, J., 1974. Analysis of geoelectromagnetic data, in Methods in Computational Physics, Vol. 13 (Geophysics), Academic Press, New York, pp. 473.

Weaver, J. T., 1971. The general theory of electro-magnetic induction in a conducting half-space, Geophys. J. R. astr. Soc., 22, 83 - 100.

Weaver, J. T., 1973. Induction in a layered plane earth by uniform and non-uniform source fields, Phys. Earth Planet. Inter., 7, 266 - 281.

Weideldt, P., 1970. Die Umkehraufgabe der erd-magnetischen Tiefensondierung fur horizontal geschichtete Leiter, Diss. Math.-Naturw. Fak. Univ. Gottingen.

Weideldt, P., 1972. The inverse problem of geomagnetic induction, Z. fur Geophys., 38, 257 - 289.

Weideldt, P., 1975. Inversion of two-dimensional conductivity structures, Phys. Earth Planet. Inter., 10, 282 - 291.

Weideldt, P., 1975. Electromagnetic induction in three-dimensional structures, J. Geophys., 41, 85 - 109.

Wiese, H., 1963. Geomagnetische Tiefentellurik, Dt. Akad. Wiss. Berlin, Geomagn. Inst. Potsdam, 36.

Wiggins, R. A., 1972. The general linear inverse problem: implication of surface waves and free oscillations for Earth structure, Rev. Geophys. Space Phys., 10, 251 - 285.

Wiggins, R. A., McMechan, G. A., and Toksoz, M. N., 1973. Range of Earth structure non-uniqueness implied by body wave observations, Rev. Geophys. Space Phys., 11, 87 - 113.

Wilkinson, J. H., 1965. The Algebraic Eigenvalue Problem, Oxford University Press, London, pp. 662.

Williams, P. W., 1972. Numerical Computation, Nelson, London, pp. 191.

Wu, F. T., 1968. The inverse problem of magnetotelluric sounding, Geophysics, 33, 972 - 979.

Yukutake, T., 1959. Attenuation of geomagnetic secular variation through the conducting mantle of the Earth, Bull. Earthquake Res. Inst., Tokyo Univ., 37, 13 - 32.